Hydrogeological Considerations for Landscape Reconstruction and Wetland Reclamation in the Sub-humid Climate of Northeastern Alberta, Canada

by

Pamela Twerdy

A thesis submitted in partial fulfillment of the requirements for the degree of

Master of Science

Department of Earth and Atmospheric Sciences
University of Alberta

Abstract

Oil sands mining companies must reclaim tailings deposits to equivalent land capability in Alberta's boreal forest. Post-mining landscapes should be reconstructed to promote the development of hydrologic systems that can sustain reclaimed ecosystems in a sub-humid climate, while limiting migration of salts from underlying waste materials. However, landform design requirements that foster the development of appropriate near-surface hydrologic flow systems are poorly understood. Syncrude Canada Ltd. constructed Sandhill Watershed (SHW), a 52 ha coarse-textured upland/lowland complex overlying a deep tailings deposit, to explore the influence of landform characteristics, reclamation cover choices and vegetation densities on reclamation performance.

This study examines the hydrogeologic characteristics of SHW and explores the resulting groundwater flow system in the years following its construction. Field measurements collected from May to October (2015 to 2017), from 230 shallow piezometers, including groundwater measurements (water level, temperature, and electrical conductivity), water samples and soil saturation maps were used to characterize the hydrogeology. A subset of data, including stable water isotopes and elemental chemistry, were collected during 2017 to resolve the mechanisms leading to observed solute distributions. Field observations were used to calibrate a three-dimensional steady-state numerical groundwater flow model to evaluate present and possible future hydrologic systems.

A shallow groundwater system dominated by lateral flow developed within SHW. The flow system is strongly influenced by hydraulic conductivity and appears to have negligible inputs from deeper groundwater. Most recharge originates from a laterally extensive upland feature coinciding with the adjacent groundwater divide, beyond the southern extent of the study area. Shallow water tables near, and standing water in, the lowlands are most sensitive to precipitation. Overall, solute

concentrations increase with depth in the watershed; however, areas with shallow water tables and shallow slopes are prone to developing elevated solute concentrations following precipitation events. Analyses indicate water table configurations responded dynamically to variable recharge rates associated with the depth to water table, and reclamation prescriptions for soil and vegetation.

These results indicate fresh shallow groundwater systems can develop for wetland reclamation in post-mining reconstructed landscapes. By appropriately sculpting coarse-textured construction materials during landform design, a freshwater lens developed at the water table beneath hummocks where groundwater is approximately 2 m below ground surface; here, the vertical geochemical gradient transitions from mixed-fresh groundwater to Na^+ Cl^-/SO_4^{2-}-enriched groundwater approximately 1.8 m below water level. Sloped areas with shallower water tables that fluctuate within the rooting zone tend to have elevated solute concentrations near the water table, especially following precipitation influxes, due to lateral groundwater seepage, groundwater ridging and evapoconcentration. These results provide guidance for designing future coarse-textured landforms and developing hydrologic systems for boreal forest reclamation. In particular, designers should reconstruct watersheds that promote groundwater recharge in upland areas by building lower and more laterally expansive hummocks than those in SHW to support water tables approximately 2 m BGS. Furthermore, the interface between the uplands and lowlands should be abrupt, to limit the extent of seepage faces. With these slight landform modifications, recharge and solutes can be better managed to allow the shallow groundwater system to remain fresh, while sustainably sourcing water to down gradient environments.

Acknowledgements

Foremost, I would like to express my sincere gratitude to my advisor, Dr. Carl Mendoza, for his patience, guidance and encouragement throughout my Masters program. I am beyond grateful to have been afforded the opportunity to work on such a meaningful and applied project with someone who is as kind, humble, and willing to teach as him. I will forever appreciate having such a wonderful mentor. I would also like to thank Dr. Dan Alessi, for his wisdom and guidance when helping me navigate my sodium-enriched waters, Dr. Ben Rostron, who took the time to help me incorporate isotopes into my site conceptual model, and Dr. Kevin Devito, for enlightening discussions about reclamation and ecohydrology in the Boreal Plains.

I would like to acknowledge and thank the funding bodies that made this research possible. Student support was provided by a Natural Sciences and Engineering Research Council (NSERC) CGS M scholarship, Walter H. Johns graduate fellowships, Alberta's Scholarship for Graduate Students, Queen Elizabeth II Graduate Scholarship and Teaching Assistantships from the Department of Earth and Atmospheric Sciences. Syncrude Canada Ltd. provided funding and logistical support for field activities, preformed geochemical analyses, and contributed to student support and conference presentations. I would like to thank Carla Wytrykush, Jessica Piercey, Dallas Heisler, Lori Cyprien, Mohammed Salem, among others, in Syncrude's Research & Development offices who have contributed time to solving this piece of the reclamation puzzle.

Colleagues from the Ecohydrology Research group and lab mates from the Hydrogeology Research group, I am so thankful for the friendship, camaraderie, and support you have shown me during this endeavor. Kelly, Mika, Max, Judit, Alex and Emily, thank you. Mika Little-Devito, your assistance with field work, data management and data analysis were truly invaluable. Nicole Brazzoni, thank you for your efforts with saturation mapping (they are beautiful!). Jordan Pearson, thank you for the wild field season; I will never forget it!

I would like to thank each of the graduate students in the department who have helped build up the community that I have come to cherish. You have contributed to some of my fondest memories, and for that, I am beyond thankful.

There are no words to express my gratitude for the kindness, love, patience and encouragement that my family, and lifelong friends have shown me during my academic pursuits. I'd like to extend a heartfelt thank you to the Ingrams, my parents Lori and Dwayne, and my grandmother Lucy; I simply could not have done this without your unwavering love and support.

Contents

List of Tables

List of Figures

List of Abbreviations & Acronyms

σ	Standard deviation
AAS	Above acceptable standard deviation
AET	Actual Evapotranspiration
AOSR	Athabasca Oil Sands Region
BC	Boundary condition, or base case
BDL	Below detection limits
C	Conductance (m^2/d)
CBE	Charge balance error
CT	Composite tailings
EC	Electrical Conductivity (µS/cm)
EIP	East In-Pit
Fm	Formation
GHB	General Head boundary condition
ha	hectare (1 ha = 10000 m^2)
Δh	Change in hydraulic head
HRA	Hydrologic Response Areas
HU	Hydrologic Unit
i	Hydraulic gradient
i_h	Horizontal hydraulic gradient
i_v	Vertical hydraulic gradient
K	Hydraulic conductivity (m/s)
K_v	Vertical hydraulic conductivity (m/s)
K_h	Horizontal hydraulic conductivity (m/s)
KFW	Kingfisher Watershed
LEL	Local Evaporation Line
LFH	Litter-Fibric-Humic soil horizon
LMWL	Local Meteoric Water Line
m AGS	metres above ground surface
m ASL	metres above sea level
m BGS	metres below ground surface

m BWL	metres below water level
MLR	Mildred Lake Reservoir
MS	Midscreen
n	Porosity, or number of samples
NEP	North East Pond
OSPW	Oil Sands Process-affected Water
P	Precipitation
PET	Potential Evapotranspiration
Pf	Pleistocene-fluvial
PMM	Peat-Mineral-Mix
SCL	Syncrude Canada Ltd.
SHW	Sandhill Fen Watershed
SW	Surface water/standing water
SWM	Soil Wetness Map
TS	Tailings sand
TLC	Temperature, conductivity, water level meter
uLMWL	Unweighted Local Meteoric Water Line
WL	Water level (m)
wLMWL	Weighted Local Meteoric Water Line
WSP	Water Storage Pond

Chapter 1: Introduction & Background

1.1. Introduction

Anthropogenic activities, including oil and gas development, coal mining, forest harvesting and wildfire, have led to large-scale land disturbance in Alberta's boreal forest. Most of these activities can drastically alter the ecology, pedology, and hydrology of natural boreal environments (Buttle et al., 2000), but surface mining also disrupts the geology of the area, thereby completely transforming the landscape. Mining companies in the Athabasca Oil Sands Region (AOSR) are obligated to reclaim heavily disturbed landscapes, providing opportunities for Alberta's boreal forest to recover once these anthropogenic activities cease. As of 2016, the total active footprint for surface oil sands mining disturbance was approximately 953 km^2, which is 20% of the total mineable area (4800 km^2; Figure 1; CAPP, 2018). Given the continued demand for oil sands products in the global market (CAPP, 2018), and that only 11% of the total active footprint has been or is being reclaimed (AEP, 2017), the amount of disturbed land that must be reclaimed due to bitumen surface mining will only increase over the coming decades.

Open-pit mining requires a balance between water, ore, and waste management to limit the overall impact of the mine on the current and future environment (Mikula et al., 1996). Bitumen mining uses large, heavy machinery to remove overlying, non-economic rock (quaternary deposits, shale or lean oil sands) to access underlying bitumen-laden sands (ore), sometimes mining up to 75 m below ground surface (Government of Alberta, 2019). This process disrupts the natural environment in the affected area and creates waste rock that must be stored in on-site overburden dumps. The ore is then hauled to crushers and sent for extraction, which requires using water, steam, mechanical conditioning, and caustic (NaOH) to separate bitumen from sand/sediments (Mikula et al., 1996).

Tailings are a by-product of bitumen extraction. Tailings have various proportions of sediments (sand, silt, clay), process-affected water (ubiquitously termed oil sands process water, OSPW, in AOSR), and residual, unrecovered bitumen (Mikula et al., 1996). Different types of tailings are produced at various points in the extraction process, some of which include composite tailings (predominantly sand mixed with clays, silts, and gypsum, $CaSO_4$), and coarse sand tailings (mostly sand with some fines). Composite tailings are transported by pipeline to tailings deposits where they are stored permanently and left to consolidate before landscape reconstruction and reclamation can begin (Johnson & Miyanishi, 2008). Tailings sand can then be placed on the surface of composite tailings and be used to reconstruct landforms and provide substrate for sub- and topsoil reclamation materials prior to revegetation (Daly et al., 2012).

There are many challenges associated with landscape reconstruction and reclamation in the AOSR. Adding caustic (NaOH) during bitumen processing increases the overall bitumen recovery; however, it also elevates the salinity of OSPW in tailings (~4,000 µS/cm; BGC, 2008), which has been shown to negatively impact aquatic and terrestrial biota (Apostol et al., 2004; Jacobs & Timmer, 2005; Mackinnon et al., 2001; Renault et al., 1998, 1999; Scott et al., 2005; Timmer & Teng, 2004). Further increases in salinity results from recycling of process water. This becomes an issue where tailings are used as watershed construction materials during landscape reconstruction (Daly et al., 2012; Ketcheson et al., 2016; Pollard et al., 2012). Given that topography, lithology, and climate affect groundwater movement in natural landscapes (Devito et al., 2005a; Haitjema & Mitchell-Brucker, 2005; Hokanson et al., 2019; Schoeneberger & Wysocki, 2005; Tóth, 1963; Winter, 2001; Winter et al., 2003), oil sands companies must ensure proper material placement occurs during landscape reconstruction such that the subsequent hydrologic system that develops can sustain reclamation vegetation. This may mean designing coarse-textured watersheds to create groundwater flow systems that minimize OSPW movement, thereby limiting its effects on the reclaimed environments, and to provide adequate water supply and quality to sustain the hydrological, biogeochemical and ecological processes of reclamation vegetation (Daly et al., 2012).

1.2. Background

1.2.1. Water Movement in Alberta's Boreal Landscapes

Climate & Groundwater Movement

Groundwater movement in northern Alberta is complicated by the sub-humid climate, shallow surficial and bedrock geology, topography (regional to local), and ecohydrology of boreal environments (Devito et al., 2000, 2005a, 2012; ESWG, 1995). Groundwater recharge is limited, given that historic annual potential evapotranspiration (PET, 517 mm; Bothe & Abraham, 1993) often exceeds historic average annual precipitation (P, 456 mm; Environment Canada, 2019). This sub-humid climate can result in 10- to 15-year cycles of mesic conditions punctuated with higher than- and lower than-average moisture conditions (Devito et al., 2005a, 2012). Moisture availability is further restricted by intra-annual variability in P and actual evapotranspiration (AET), where the largest precipitation events often coincide with the peak of vegetation water demand during the growing season (Devito et al., 2005a). These climate moisture conditions affect groundwater recharge, water table configurations, and the overall availability of groundwater in a given landscape (Devito et al., 2012; Hokanson et al., 2019; Lukenbach et al., 2019; Schoeneberger & Wysocki, 2005; Smerdon et al., 2008).

Utilizing a Tóthian approach for conceptualizing shallow groundwater flow in the Boreal Plain of Alberta may not be suitable for adequately predicting water tables and groundwater movement through landscapes associated with sub-humid climates in this region (Hokanson et al., 2019). This is, in part, because the Tóthian conceptual framework inherently assumes abundant groundwater recharge, comparable to more humid climates, and regional-scale aquifers (length and depth). While regional groundwater flow systems have been characterized in the Boreal Plain utilizing Tóth's hydrogeological framework of nested flow systems (Tóth 1978), catchments at local- and intermediate-scale are more likely to be influenced by climate, local and intermediate topography, and stratigraphy (*i.e.*, aquifer transmissivity), rather than regional topography and relief alone (Devito et al., 2005a; Haitjema & Mitchell-Bruker, 2005; Hokanson et al., 2019; Winter et al., 2003).

Hydrogeological conceptual frameworks that emphasize the influence of groundwater recharge have demonstrated that water tables may or may not develop as subdued replicas of topography in areas with limited recharge (*i.e.*, sub-humid climates; Haitjema & Mitchell-Bruker, 2005). These water tables are more responsive to shifts in inter- and intra-annual water variability in local- and intermediate-scale topographic features (Schoeneberger & Wysocki, 2005) which can shift hydrologic sources/sinks in a given boreal environment between wetlands and forests depending on the climate cycles. Over time, climate cycles can create moisture surplus or moisture deficits in boreal landscapes, which can impact landscape connectivity and ecosystem services to down-gradient environments (Devito et al., 2012).

Geology & Groundwater Movement

The landscape in northeastern Alberta has subtle regional topographic relief (400-800 m), with stream courses, depressions, and ridgelines with hillslopes between them, as well as numerous lakes, ponds, and peatlands (Johnson & Miyanishi, 2008). The surficial geology is moderate to thick (30-200 m) and comprised of glaciolacustrine tills or glaciofluvial sands, or a combination thereof near transition areas (Andriashek & Atkinson, 2007; Atkinson et al., 2014; Johnson & Miyanishi, 2008). The sediments that make up landforms in the boreal have been grouped conceptually into three types of hydrologic response areas (HRAs) based on similar water storage and transmission properties: coarse-textured (*e.g.,* glaciofluvial sand), fine-textured (*e.g.,* glaciolacustrine clay or moraine deposits), and veneer (*e.g.,* 2 metres of sand layered over fines or fines layered over sands; Devito et al., 2012).

Substrate texture, permeability, and stratigraphy affect the scale and nature of groundwater movement that develops within a given HRA landform; this is particularly evident in areas with low regional relief and locally hummocky topography (Figure 2; Devito et al., 2012). Coarse-textured HRA landforms have higher hydraulic conductivity (sediments ranging from gravel, sand, sandy-gravel, silty-sand, and silty-gravel textures) with high specific yield compared to other HRAs, generally making them moisture sources over the long term (Devito et al., 2017). In moisture-limited climates, water tables in coarse-textured HRAs tend to be relatively flat, found further below ground surface, and experience high net-recharge (Devito et al., 2017). These characteristics develop regional groundwater flow systems that cut across landscapes and discharge in topographic lows, where favorable hydrologic conditions for wetlands are created (Devito et al., 2012, 2017; Winter et al., 2003). Then, within these landforms, local hummocks, forestlands or lithological heterogeneities may facilitate the development of nested, local flow systems. Coarse-textured HRAs with regional groundwater flow systems, and some nested, local flow systems, have been observed in natural boreal environments situated on glaciofluvial outwash plains at Utikuma Research Study Area (Devito et al., 2017; Hokanson et al., 2019; Smerdon et al., 2005).

Fine-textured HRAs differ, in that they have low hydraulic conductivity (ranging from silt, clay, sand-silt-clay, and sandy-silt textures) with lower specific yield compared to coarse-textured HRAs. These characteristics limit net-recharge by increasing water losses via AET (Devito et al., 2017). Given that fine-textured HRAs tend to function as long-term water sinks in sub-humid climates, the low regional topographic relief and hummocky topography tend to develop depressed water table configurations below uplands, where vertical atmospheric fluxes dominate, and focus discharge to landscape depressions. This can result in limited regional groundwater connectivity in fine-texture HRAs and may preferentially develop localized flow systems or perched water tables that source water between forestlands and wetlands (Devito & Mendoza, 2006; Schoeneberger & Wysocki, 2005; Tóth, 1963; Winter et al., 2003). Natural boreal environments with clay-rich till deposits (hummocky moraines) have been shown to preferentially develop these localized flow systems between upland and lowlands, controlled by vertical fluxes and, to a limited degree, horizontal fluxes beyond the transition zones during drier years (Ferone & Devito, 2004; Thompson et al., 2015).

Finally, veneer HRAs with thin layers (approximately 2 m) of permeable coarse sediments overlying fine-textured sediments, develop shallow groundwater systems that are highly responsive to precipitation (Devito & Mendoza, 2006). Similarly, high hydraulic conductivities associated with organic soils (*i.e.*, shallow peat) situated atop clayey tills have also demonstrated this type of responsive groundwater system in areas near Fort McMurray (Wells & Price, 2015). Veneers with fine sediments overlying coarse sediments tend to behave as fine-textured deposits, by developing perched groundwater systems above, and limiting recharge to, the deeper groundwater system (Devito et al., 2012; Riddell, 2008; Winter et al., 2003).

Boreal Hydrologic Units

Forests and wetlands are distinct hydrologic units (HUs) in the Boreal Plain (Devito et al., 2017), each with unique soil-vegetation-atmosphere interactions that are complicated by the groundwater availability of the given HRA upon which they are located. The type of boreal environment that develops in a given landscape is influenced, in part, by the availability of groundwater within the HRA. Forestland HUs tend to form in areas that have drained soils with deeper water tables compared to wetlands; therefore, have a greater potential for deeper groundwater storage. Forestland HUs that develop on coarse-textured deposits have the greater propensity for recharge, limiting losses to AET, locally reducing overland flow, and ensures water availability over the longer term for regional runoff (Devito et al., 2017). This differs from forestland HUs on fine-textured deposits, where water that would otherwise recharge groundwater is lost to soil-water storage, runoff, and ET (Devito et al., 2017; Redding & Devito 2008). In general, wetland HUs have limited water storage capacity compared to forestland HUs and develop shallower flow systems with water tables that fluctuate near or above the ground surface. Wetlands tend to be water sources to landscapes because soils and vegetation limit water losses through a series of complex feedback mechanisms, which shed or conserve water availability through wet and dry climate cycles, respectively (Waddington et al., 2015). Exceptions to this include wetlands with semi-permanent and permanent standing water, which have the potential to create net moisture deficit conditions (Devito et al., 2017; Smerdon et al., 2005).

Together, HUs and HRAs form a gradient of hydrogeologic landscapes where the proportion of each HU is dependent on the type of HRA (*i.e.*, groundwater system), its surficial topography and climate (Devito et al., 2017). In general, topographic highs are primarily dominated by forestland HUs, and wetlands tend to form in depressions and topographic lows (Devito et al., 2012). For fine-textured HRAs, the local topography determines the proportion of wetlands in the landscape; flatter areas are predominantly comprised of wetlands with forest stands on local topographic highs, whereas hummocky areas are dominated by forestlands interspersed with wetlands in depressions (Devito et al., 2012). With coarse-textured HRAs, the regional topographic position influences proportions of forests to wetlands; regional topographic highs are dominated by forests with wetlands in local depressions which transitions to wetland-dominated topography in regional lows, where patches of forest stands are scattered on local topographic highs (Devito et al., 2012). Veneer HRAs, often found in transition zones between coarse- and fine-textured HRAs, are also dominated by wetlands and have forest stands scattered throughout local topographic highs.

The proportion of each HU in a given landscape influences the availability of groundwater within an HRA, as well as the connectivity to adjacent HRAs and, subsequently, the ability to redistribute water to down-gradient ecosystems. Given that wetlands have lower storage potential and are water sources over shorter time scales compared to forestlands, a greater abundance of connected wetland HUs would increase the availability of water to adjacent, down-gradient HRAs (Devito et al., 2012). Conversely, HRAs with a higher proportion of forests have the potential to store large amounts of water during years of moisture surplus, while contributing to regional groundwater flow, but also have the potential to reduce the connectivity to down-gradient HRAs during years of moisture deficit. It is the distribution and proportion of these HUs across the boreal that collectively manage the limited moisture that is available from the sub-humid climate (Devito et al., 2012). Groundwater movement in and between HUs and HRAs is further complicated by the ecohydrological characteristics within each type of forestland (mixed wood, conifer, deciduous) or wetland (fen, bog, marsh, swamp) found in the boreal (Devito et al., 2017).

Boreal Forest Ecology

The AOSR is primarily located in the Central Mixedwood Boreal Subregion in the Western Boreal Plain Ecozone in northern Alberta (ESWG, 1995; NRC, 2006). The subregion is comprised of a mosaic of wetland and forestland complexes situated atop thick heterogeneous glacial deposits in a sub-humid climate (NRC, 2006). Over half of the area is covered by wetlands, while the remainder is a mix of deciduous and conifer stands. Forestlands, where fine-textured soils exist, are a mix of closed-canopy aspen-dominated deciduous stands, aspen-white spruce stands, and white spruce-dominated stands, while jack pine tends to prefer coarser, drier substrates (NRC, 2006). In the boreal, forestland ecosystems have the potential to source water to down-gradient environments during wetter climate cycles; however, they can also behave as moisture sinks during drier climate cycles (Schoeneberger & Wysocki, 2005).

Wetlands are highly valued in the boreal primarily due to the ecosystem services they provide to surrounding landscapes, including carbon storage, water conservation, and biodiversity (Waddington et al., 2016). They are commonly found with an underlying confining layer (*e.g.,* clay), variable depths of undecomposed or partially decomposed organic mater, and an actively growing layer of organic materials at the surface (Wylynko & Hrynyshyn, 2014). In Alberta, wetlands are classified as peat-forming (peatland) or non-peat-forming (mineral wetlands), which are further subdivided based on vegetation, and biological, hydrological and chemical attributes (ESRD, 2015). Peatlands have at least 40 cm of peat, or unconsolidated, partially decomposed organic matter and are found in frequently or permanently saturated areas (ESRD, 2015). Peatlands include fens and bogs which differ by their hydrology, in addition to their geochemistry and vegetation; fens are primarily minerogeneous with abundant nutrients delivered to vegetation by groundwater located at or just below ground surface (up to 20 cm), while bogs are primarily ombrogeneous (water sourced primarily from precipitation, isolated from groundwater) and have less nutrients available for vegetation when compared to minerogeneous wetlands (ESRD, 2015). Mineral wetlands differ from these peatlands because they have less than 40 cm of peat accumulation and have predominantly mineral (clay or silt) soils. Types of mineral wetlands include swamps, marshes and shallow open water; these wetlands have water tables near, at, or above ground surface which may be flooded permanently, repeatedly, or infrequently throughout the year (ESRD, 2015).

Boreal peatlands, predominantly comprised of fens (Rooney et al., 2012), may be surrounded by wooded, coniferous trees (*e.g.,* black spruce, tamarack), shrubby vegetation or graminoids (ESRD, 2015). Fen and bog wetland vegetation thrive in conditions where the water table is relatively stable, and water is slow moving, which promote anaerobic conditions that slow decomposition and encourage peat accumulation (ESRD, 2015). Bog vegetation prefer more acidic (pH <4.5) and fresher water (electrical conductivity <500 μS/cm; EC) and do not tolerate elevated salinity. Conversely, fen vegetation prefers acidic to alkaline water (pH ranges <5.5 to >7) that can be fresh to slightly saline (EC <500 μS/cm to 2000 μS/cm; ESRD 2015). However, fens with water that exceed these salinity ranges have been observed elsewhere in the boreal (Purdy et al., 2005; Wells & Price, 2015). Vitt & Chee (1990) discuss fen geochemistry in further detail, and Alberta's wetland classification guidelines (ESRD, 2015) provide a thorough description of the types of vegetation commonly found these wetlands.

1.2.2. Oil Sands Mine Reclamation

Given that the mineable land in the AOSR falls within the greater Western Boreal Plain (Figure 1), there is a desire and regulatory requirement for the post-mining landscape to be comprised of reclaimed environments equivalent to those naturally observed in the area, including both wetlands and forestlands (Rooney et al., 2012; Wylynko & Hrynyshyn, 2014). However, most previous surface mining reclamation efforts in the AOSR have been focused on developing forests, or upland landforms (Rooney et al., 2012). Given that wetlands are also a critical component of the boreal (Raine et al., 2002, as discussed in Rooney et al., 2012), provincial directives have been recently amended to encourage oil sands mining companies to incorporate both wetlands and forestlands in their mine closure plans. More specifically, due to their prevalence in the boreal (Rooney et al., 2012), there is an emphasis on including peat-forming wetlands (bogs or fens) in final mine-closure landscapes.

The primary challenge regarding the modified directive is that current reclamation summary guidance documents (Devito et al., 2012; Wylynko & Hrynyshyn, 2014; Wytrykush et al., 2012) provide recommendations for designing and reclaiming peatlands on post disturbance landscapes, but they do not provide design guidelines specifically for reconstructing landforms that create hydrologic systems to support wetlands. Smaller wetlands have been restored but have not been reclaimed at an industrial-scale before (BGC, 2015). Therefore, oil sands mining companies are also required to demonstrate their research and methods used to develop watersheds for self-sustaining wetland-forest ecosystems that realize equivalent land capability.

Oil sands mining companies in the AOSR anticipate that watersheds can be designed and reconstructed to develop desirable hydrologic systems for boreal environments on tailings deposits while simultaneously protecting them from OSPW in waste materials (used for landform reconstruction). They anticipate this can be done by developing hydrogeologic systems that utilize groundwater recharge to dilute, flush or isolate saline water entirely (McKenna, 2002). Since limited knowledge exists for the design specifications of reconstructed watersheds that are needed to create the requisite hydrologic systems to sustain boreal environments, watershed managers and engineers have used natural analogue study sites also within the Western Boreal Plain to develop hydrogeological conceptual models and guide the designs for one of the first industrial-scale reconstructed watersheds in the AOSR (Devito et al., 2012; Ketcheson et al., 2016; Pollard et al., 2012; Price et al., 2010).

Sandhill Watershed Hydrogeological Conceptual Model

Syncrude Canada Ltd. (SCL) designed, reconstructed, and instrumented Sandhill Watershed (SHW), a 52 ha fine-grained sand watershed overlying a soft composite tailings deposit to research the design specifications needed to construct landscapes that promote groundwater systems for wetland development (BGC, 2014). The watershed's hydrogeological design was intended to control vertical movement of groundwater, limit the presence and impact of OSPW in the surficial groundwater system, and ensure long-term water availability and quality for the reclaimed upland forest and wetland ecosystems in the watershed. The ultimate goal is to demonstrate that watersheds that facilitate wetland development for reclamation can be reconstructed in post-mining landscapes and to provide science-based recommendations for improved reclamation techniques and future watershed designs.

The hydrogeological conceptual model for the watershed design was primarily based on coarse-textured HRAs in the boreal forest, by using sculpted tailings sand hummocks (*i.e.*, hills) of various sizes to develop a fresh, shallow, localized groundwater flow systems for a centralized wetland in the lowlands. Designers anticipated local flow systems could preferentially develop over intermediate flow systems using hummocks as local recharge areas, to limit the vertical migration and discharge of OSPW from deeper zones into the wetland (Figure 3). Shallow groundwater flow paths associated with local flow systems (*i.e.*, recharge areas are located immediately adjacent to discharge areas; Tóth, 1963), which have smaller vertical hydraulic gradients and would be more likely to maintain freshwater near the water table while reducing pore water mixing with underlying process water. Intermediate groundwater flow paths (*i.e.*, recharge areas are not located immediately adjacent to discharge areas) would likely result in deeper flow paths causing vertical migration of OSPW to discharge in the wetland, essentially losing incoming freshwater to pore water mixing with the tailings process water. Therefore, designers utilized the relationships between recharge, hydraulic conductivity, length and depth of aquifer, and topography from Devito et al., (2012), Haitjema & Mitchell-Bruker (2005), and Winter et al., (2003) to assist in estimating water levels and predicting groundwater flow paths in the reconstructed watershed using a combination of field measurements and observations from boreal forest analogue study areas.

The resulting design was a watershed constructed from fine-grained tailings sand sculpted into hummocky terrain surrounding a central wetland, with the reclaimed surface situated 10 to 15 m above the consolidated, composite tailings in the lowlands (Figure 4; BGC, 2014a). The hummock heights were moderate, to allow the water table to be close enough to ground surface without intersecting the rooting zone and to facilitate groundwater mounding. Furthermore, the areal coverage of the uplands ensured adequate recharge potential, given the various soil prescriptions (BGC, 2015). Prescribed thicknesses of topsoil and subsoil were limited to reduce excessive soil moisture storage and to conserve reclamation materials. Finally, the overall length of potential flowpaths in the watershed were short (hundreds of metres), given the overall area of the watershed, in its entirety, is 52 ha. With these features in mind, designers anticipated a shallow groundwater system would develop, where freshwater inputs would gradually flush and dilute residual OSPW from the unsaturated and shallow saturated pores of the surficial tailings sand, while isolating concentrated OSPW stored in deeper underlying tailings sand and consolidated composite tailings.

Sandhill Watershed was designed to provide water to other down-gradient reconstructed watersheds in the final mine-closure landscape that will eventually be released to the greater environment; therefore, the water quality in SHW should fall within recommended targets (*e.g.*, less than 2000 μS/cm; Howat, 2000) to sustain reclaimed boreal vegetation not only within it, but downstream as well. SHW is isolated from the surrounding natural regional hydrogeological system; therefore, freshwater inputs are limited to recharge from snowmelt and precipitation. Given the potential for a water deficit, designers predicted that additional freshwater might be needed to assist in initially freshening the watershed post-construction to buffer water quality while vegetation became established (BGC, 2008). Therefore, groundwater management infrastructure, a pump and water storage pond with a "leaky" dam, were included in the watershed's design to provide freshwater to SHW, should it be required. Other infrastructure was installed to remove water if the water levels rose too high, or water quality exceeded acceptable standards including four drains running the length of the lowlands, a sump and weir (BGC, 2008).

Freshwater was initially pumped from Mildred Lake Reservoir (MLR; Figure 1), the freshwater reservoir on SCL's Mildred Lake Lease (sourced from Athabasca River and precipitation; Baer et al., 2016), into SHW water storage pond (WSP; BGC, 2008; Nicholls et al., 2016; Wytrykush et al., 2012). The WSP was engineered to gradually release freshwater to the down-gradient wetland; some water was also pumped from the WSP and discharged to the "perched fens" on the south side of Hummock 7 (BGC, 2008; Wytrykush et al., 2012). While human intervention was planned to initiate favorable initial watershed conditions, the watershed was designed to be unmanaged and self-sustaining over the long term. Freshwater inputs from MLR ceased after 2014 (Nicholls et al., 2016). Output events have been reduced in recent years; the watershed's groundwater has been largely unmanaged since 2015.

1.3. Research Goals & Objectives

This study fits into a greater research framework for watershed/wetland reclamation with SCL by expanding on previous hydrological work conducted at Sandhill Watershed (Baer, 2016; Biagi et al., 2018; Ketcheson et al., 2016; Nicholls et al., 2016; Spennato et al., 2018; Vessey et al., 2018) and refining hydrogeological conceptual models for reconstructed watersheds. This work evaluates how the design of the watershed has influenced groundwater movement in Sandhill Watershed 3 to 5 years after reconstruction and reclamation was completed. The overall purpose of this study is to characterize the hydrogeology of Sandhill Watershed using data from 2015 to 2017 (3 to 5 years post-construction and after active water management ceased) to better understand the influence of the watershed's design on groundwater availability and chemistry. The objectives of the study were to analyze a) the short- and long-term dynamics of the shallow flow system in the watershed utilizing groundwater data and numerical modelling, and b) the spatio-temporal evolution of solute concentrations utilizing geochemistry and isotopes. These analyses are subsequently used to c) evaluate the influence of the watershed's design and hydrogeological characteristics on the current, and potentially future, groundwater system with the intent of optimizing future reconstructed watershed designs in post-mining landscapes.

A comprehensive approach was taken for characterizing the hydrogeology of the reconstructed watershed. Spatial and temporal data were collected for both water level and geochemical data to assess the progression of the groundwater system in SHW. The influence of the watershed's design (hydrostratigraphy and topography), and atmospheric and managed water fluxes, on the resulting groundwater system were evaluated using a combination of hydrological data, geochemical plots, and water table, EC and soil wetness maps to assess the spatio-temporal evolution of the groundwater system. Geochemical data, including EC, major ions and stable water isotopes (δ^2H and $\delta^{18}O$) were plotted to understand sources and elucidate causes of solute distributions within the watershed. Finally, a three-dimensional numerical model was developed to integrate the physical hydrogeology observations and to assess the influence of the watersheds hydrostratigraphy and design (topography) on the resulting groundwater system and used to perform scenario testing for potential climate change trajectories.

Chapter 2: Study Area & Methods

2.1. Sandhill Watershed

2.1.1. Location, Regional Context & Design

This study was conducted on Sandhill Watershed (SHW), a reconstructed landscape approximately 40 km north of Fort McMurray, at Syncrude Canada Ltd.'s (SCL) Mildred Lake Lease (MLL; 57°02' N, 111°35' W) in the AOSR (Figure 1). The AOSR is located within the Boreal Plains ecozone (ESWG, 1995), where the climate is characterized as sub-humid (potential evapotranspiration often exceeds average annual precipitation). Average annual precipitation is 419 mm and average annual temperature is 1°C (1981-2010; Environment Canada 2017). Temperatures, on average, range from -17.4°C to 17.1°C (January and July, respectively), but can reach to extremes of -50.6°C in the winter to 37°C in the summer (1947 and 1991, respectively; Environment Canada, 2017).

The Western Canadian Sedimentary Basin outcrops in the Athabasca Oil Sands Region, with shallow bitumen reservoirs that are accessible through surface mining or in-situ methods. Mildred Lake Lease is located within the Athabasca River lowland, where the bituminous McMurray Formation (Fm) sandstone underlies Cretaceous Clearwater Fm shales, and surficial quaternary deposits. These surficial deposits include glaciolacustrine and glaciofluvial sediments from glacial outwash lakes and subglacial channels. Buried gravel channels incise quaternary deposits in the area (Andriashek and Atkinson 2007). Overall, local topographic relief is subtle (up to tens of metres), with rolling hummocky terrain interspersed among plains and deep river valleys.

2.1.2. Reconstructed Watershed Lithology & Topography

SHW was constructed from fine-grained tailings sand on top of consolidated composite tailings. More specifically, the tailings deposit is contained within a former in-pit mine (East In-Pit; EIP) that was backfilled with (in ascending order): an average of 29 m of hydraulically-placed composite tailings (sand, silt, clay, OSPW, residual bitumen; typical horizontal hydraulic conductivity, K_h = 1.7E-7 m/s; vertical hydraulic conductivity, K_v = 1.7E-8; Thompson et al., 2011), approximately 10 m of hydraulically-placed (*i.e.*, by slurry via a pipeline) tailings sand cap (sand, OSPW and residual bitumen; typical K_h = 4.4E-6 m/s, K_v = 7.3E-7 m/s; BGC; Thompson et al., 2011) and mechanically-placed (*i.e.,* by heavy machinery), sculpted tailings sand hummocks (sand, residual OSPW and bitumen; K_{hv} = 2.6E-5 m/s; Benyon, 2014).

The overall study area is approximately 1000 m long (E-W direction) and 500 m wide (N-S direction; Figure 1). The northern and western boundaries of SHW coincide with the northern-most and western-most extent of EIP; the low hydraulic conductivity of the original bedrock (Cretaceous McMurray and Clearwater Formations; $K_h = 1.6E\text{-}7$ m/s, $K_v = 1.0E\text{-}9$ m/s; Thompson et al., 2011) limits seepage of OSPW from tailings into adjacent units (BGC, 2015). The southern extent of the study area coincides with an east-west trending tailings sand dyke, 318 Berm, which is the most laterally extensive upland feature in the tailings deposit (approximately 318 m ASL and >30 ha, respectively), and served as the southernmost boundary for North East Pond (NEP), the north-draining portion of EIP (Figure 1; BGC, 2008). NEP was subsequently reclaimed into two watersheds, SHW and Kingfisher Watershed (KFW), which are separated by a tailings sand berm, Sandhill Berm, designed to permit groundwater flow (Figure 4; BGC, 2014a). KFW is designed to function in tandem with, and receive water from, SHW as part of a mosaic of lowlands and uplands planned for the final mine closure landscape (BGC, 2015).

The topography of SHW was sculpted by heavy machinery to simulate upland/lowland landforms similar to those found in the boreal (Ketcheson et al., 2016; Pollard et al., 2012; BGC, 2008). The uplands (*i.e.*, hummocks, swales and slopes) are located on the northern and southern areas of the watershed, surrounding the central lowlands (Figure 4). Hummocks range in height and areal extent (~3 to 8 m and ~0.25 to 3.5 ha, respectively), covering 55% of the upland area. The remaining 45% of the upland areas are either slopes (laterally expansive areas with shallow gradients gently extending from 318 Berm to the lowlands), or swales (small, narrow draws with shallow gradients located between two adjacent hummocks). The uplands cover ~67% of the 52 ha watershed; the remaining 33% are topographically defined lowlands intended to develop into wetlands. The lowlands are approximately 700 m long and 250 m wide (17 ha), oriented east-west between the east-west rows of hummocks in the north and the south (Figure 4; BGC 2008, 2015).

2.1.3. Reclamation Materials

SHW was designed to investigate the designs necessary for the development of wetland/forestland complexes in a reconstructed watershed; therefore, the placement of subsoil, topsoil and vegetation was well-documented and surveyed. In general, subsoil in the uplands consists of approximately 0.5 m of Pleistocene-fluvial (Pf) sand on Hummocks 2, 4, 5, 7, and 8, and approximately 0.3 to 0.5 m of clay till everywhere else (including Hummocks 6 and 9). The topsoil covering Hummocks 2, 4, 5, 7, and 8 was a xeric (*i.e.*, coarse) litter-fibric-humic A/B ecotype soil (LFH-A/B, average thickness = 0.2 m), and Hummocks 6 and 9 have mesic to sub-xeric (*i.e.*, fine) litter-fibric-humic D ecotype soil (LFH-D, average thickness = 0.2 m). Peat-mineral-mix (PMM) topsoil was spread across the remaining areas in the uplands with an average thickness of 0.3 m. In the lowlands, the subsoil is clay till, approximately 0.5 m thick, that was roughly compacted prior to topsoil placement. The topsoil in the lowlands is approximately 1.0 m thick PMM. Detailed soil placement and thickness maps are provided in Appendix A (modified from BGC, 2014b). The hydraulic properties for each reclamation material are summarized in Benyon (2014), Longval & Mendoza (2014), and Lukenbach et al., (2019).

Revegetation in the lowlands included spreading seeds harvested from natural fens in the Fort McMurray area to develop targeted plant communities that represent wetland vegetation otherwise found in the Central Mixedwood natural sub-region (BGC, 2008). Hummocks had a more rigid structure for revegetation for research purposes; trees were planted at variable and predetermined densities (0, 5,000, 10,000 stems/ha) where the prescribed ecosite soils of each hummock influenced the proportion of each tree species that were planted (*Populus tremuloides, Picea glauca,* and *Pinus banksiana*). The remaining areas between study plots were prescribed equal proportions of tree species (*Populus tremuloides, Picea glauca, Pinus banksiana, Picea mariana* and *Betula papyrifera*), at a density of 2,000 stems/ha. Further information regarding vegetation prescriptions can be found in Merlin et al., (2018).

Other constructed elements included features that were designed to potentially develop into perched wetlands on the south side of Hummock 7. These ‘perched wetlands’ were underlain by 0.3 m of clay that was poorly compacted during construction; then, 0.5 m of flushed tailings sand and PMM (each) were placed as sub and topsoil in the west ‘perched wetland’, whereas only 1.0 m of PMM and no subsoil was placed in the east ‘perched wetland’ (BGC, 2014a). The soil placements were intended to encourage the development of upland perched wetlands similar to those found in natural Boreal Plains environments (BGC, 2014a); however, the ‘perched wetlands’ did not develop hydrologically perched water tables and will not be discussed further.

Water management infrastructure was installed, as discussed previously, to manage groundwater quality and water levels in the event of low water quality or excess water (Figure 4). Three coarse woody debris berms were installed across the lowlands to reduce erosion (should appreciable surface water movement occur). Three boardwalks were installed in the lowlands to assist in watershed monitoring (BW1 to BW3, west to east; Figure 4). Watershed reconstruction concluded in 2011. Final soil placements and planting occurred in 2012. Hydrological monitoring began toward the end of 2012. Groundwater management (inputs and outputs) occurred from 2013 to 2015 (Biagi et al., 2018; Nicholls et al., 2016; Spennato et al., 2018); only occasional groundwater management activities have occurred since.

2.2. Field Methods

Most data were collected from May 2013 to October 2017 and are discussed below; however, only data from May 2015 to October 2017 are reported in the results sections. All the data discussed in the methods (2013 to 2017) are available in an electronic appendix.

2.2.1. Field Monitoring Installations

A comprehensive network of piezometers was installed across the uplands and lowlands to spatially monitor the entire groundwater system in SHW following reconstruction (Figure 5). A total of 223 piezometers, organized into 85 nests (*i.e.*, monitoring points), were installed in the tailings sand and surficial reclamation materials throughout 2012 and 2013, with supplemental piezometers installed in 2014 and 2017. Piezometer nest locations were chosen based on anticipated groundwater flowpaths; nests were oriented parallel to flow along transects (whenever possible), as well as to integrate with soil moisture and vegetation plots. A piezometer nest may consist of one to six piezometers screened between 1 and 11 metres below ground surface (m BGS) to capture the vertical hydraulic head dynamics at a given location. At any nest, piezometers are separated laterally by approximately 1 m and vertically by 1 to 4 m intervals. Piezometers are constructed from threaded polyvinyl chloride (PVC) pipe (inner diameter = 0.0254 m) with a 0.30 m screen and PVC drive point tip at the bottom, though selected few piezometers have modified screen lengths (Longval & Mendoza, 2014). Piezometers were generally installed in augered holes and pushed through caved sand below the water table. Piezometers completed in the tailings sand and reclamation materials have the following naming convention: SH-GW-##-##, where SH-GW-nest ID - piezometer ID (*e.g.*, SH-GW-75-02. Nests with multiple piezometers are indicated as follows: SH-GW-##-##/## (*e.g.*, SH-GW-41-03/05). Surveys were performed using differential GPS in 2013, 2014 and 2017 (± 0.01 m) to update, track, and correct piezometer elevations throughout annual freeze/thaw cycles; this was done by measuring elevation of top of casing to accurately calculate hydraulic head values through time. Installation information is thoroughly detailed in Longval & Mendoza (2014) and is summarized in Appendix A.

Some deeper (7 to 74 m deep) piezometers were installed in the composite tailings prior to SHW construction. These piezometers were installed for geotechnical purposes; here they are used to monitor groundwater conditions (*i.e.*, chemistry) in the composite tailings below the watershed. These piezometers follow a different naming convention than those in the tailings sand: BGC-08-##-##, where BGC-08-nest ID-piezometer ID (*e.g.*, BGC-08-10-C).

2.2.2. Groundwater & Surface Water Measurements

Manual groundwater measurements were collected from shallow piezometers biweekly to monthly during the field season (May-October; Figure 5) from 2013 to 2017 with a temperature, level, and conductivity meter (TLC; Solinst, Canada). When standing water was present adjacent to a piezometer, surface water elevations relative to the top of the piezometer were collected. Deep piezometers were measured once per year in 2013, 2014 and 2017. The TLC was quality checked before and after each sampling campaign; a three-point calibration was performed on the TLC as needed due to drift.

Automated water level measurements were recorded hourly, ranging from intermittently to year-round, from 44 pressure transducers located in representative piezometer locations over 5 years (2013 to 2017; Figure 5). Data were logged by a pressure transducer (Solinst Levelogger-Edge or Solinst-Levelogger) and were compensated with barometric data collected on-site (Solinst Barologger-Edge). Representative daily water level data were obtained by averaging three hourly measurements: before, at, and after noon (*i.e.*, 11:00, 12:00, 13:00). Water level data and EC data are discussed further in Appendices B and C, respectively.

2.2.3. Soil Saturation & Wetness Mapping

Soil saturation and wetness mapping required delineating the extent of standing water, saturated soil and unsaturated soil intermittently throughout the field seasons (May-October) utilizing the squishy-boot method (Devito et al., 2005b). Mapping was done manually, with a map and a GPS receiver in 2013-2015, and digitally, on an Apple iPad with Bluetooth-enabled GPS (BadElf) and mapping software (ArcGIS) in 2016 and 2017. Soil wetness maps (SWMs) are discussed further in Appendix D.

2.2.4. Measuring Meteorological Variables

Three meteorological (MET) towers were equipped with a Campbell Scientific Model CS700 tipping bucket rain gauge (rainfall), and Model HC2 sensor (air temperature) to measure corresponding parameters hourly and daily from 2013 to 2017 (Figure 5). Due to lack of data continuity, data from only one MET tower were used for rainfall and temperature (Station 1 on Hummock 6). These data were collected and managed by a third party (O'Kane Consultants Inc).

Daily snowmelt was estimated from snow surveys completed by O'Kane Consultants along transects throughout the watershed in March each year and daily temperatures from the MET towers. Details about snow surveys are outlined in O'Kane's Annual Performance Monitoring Reports (2015, 2016, 2017).

Three eddy covariance towers were used to determine actual evapotranspiration (AET) values in the watershed (Figure 5), though only lowland AET values are presented for the study period (*i.e.*, Fen_S). These data were collected, analyzed and managed by McMaster University (Carey, S.). Details about the MET and eddy covariance towers are outlined in Nicholls et al., (2016).

2.2.5. Geochemical & Stable Water Isotope Sampling

Geochemical sampling for major and minor ions, EC, and pH occurred midsummer, once per year, from 2013 to 2017, from all SH-GW piezometers when enough water was available. Samples of surface water were obtained adjacent to any pipe when standing water was observed (except for 2016). Samples from BGC piezometers were only collected in 2013, 2014 and 2017. All piezometers and wells were purged approximately two weeks prior to sampling. Samples were obtained using a 1" rolling ball bailer attached to a string; the lowermost portion of the bailer was used to acclimate the sample bottle and the remainder was collected as the sample. The bailer was rinsed between samples. Water samples were collected in 250 mL poly sample bottles, filled to zero headspace, and filtered upon returning to the lab (via vacuum filtration with a 0.45 μm filter). Samples were refrigerated until analyses were performed by SCL, in Edmonton, AB. A charge balance error (CBE) was calculated to assess sample analysis quality; samples exceeding 10% CBE were excluded from the results. Analyses and instrumentation are summarized in Table E-1. These data are discussed further in Appendix E.

A subset of groundwater samples was collected six times over the 2017 summer field season, every 2-4 weeks, from piezometers located along two transects in SHW (Figure F-1). These samples were used specifically for a detailed, spatio-temporal analysis of sodium concentrations and stable water isotopes. Sampling and collection methods for this subset of data were identical to annual chemistry sampling methods (described above), except samples were stored and filled to zero head space in 15 mL polystyrene conical tubes. Samples were stored at room temperature at the University of Alberta until they were filtered and analyzed for stable water isotopes (Isobrine Solutions Inc.) followed by common metals (Alessi Research Group). Oxygen and hydrogen stable isotope compositions were determined from mechanically and chemically cleaned samples using IRMS; standard deviations (σ) for $\delta^{18}O$ and $\delta^{2}H$ were equal to or better than 0.2 ‰ and 2.0 ‰, respectively ($\pm 1\sigma$). The elemental composition of groundwater samples (B, Na, Mg, Al, Si, K, S, Ca, Mn, Fe, Ni, Cu, Zn, Br, Sr, Ba) was determined by inductively coupled plasma mass spectrometry (ICP-MS) using an Agilent 8800 ICP-MS/MS (Agilent Technologies, Mississauga, ON). Raw and diluted (10x) samples were analyzed to reduce risk of errors from common metal interference. Data below sample-specific detection limits (BDL), or above an acceptable relative standard deviation (RSD >10% = AAS) were not used. These data are elaborated upon and synthesized in Appendix G.

Rain water isotope samples were collected intermittently during the 2017 field season. Precipitation was collected using the method of Gröning et al., (2011). Single rain events were collected when possible; however, multiple small rain events were often captured within one sample and total event volumes were not recorded. Consequently, precipitation samples could not be volume weighted by event. Samples were analyzed for stable water isotopes (Isobrine Solutions Inc), where oxygen and hydrogen stable isotope compositions were determined from mechanically and chemically cleaned samples using IRMS, in the same manner as the groundwater samples (described above). The standard deviations for $\delta^{18}O$ and $\delta^{2}H$ were equal to or better than 0.2 ‰ and 2.0 ‰, respectively ($\pm 1\sigma$).

2.2.6. Tailings Sand & Peat Hydraulic Conductivity

Slug tests were performed at five locations in 2017 to supplement historical tailings sand hydraulic conductivity values, and at three locations to assess the hydraulic conductivity of the peat in the wetland (Figure 5; Hvorslev, 1951). A 0.5 to 1 L freshwater slug was added to upland piezometers and a Solinst Levelogger-Edge was used to capture the initial rise in water level and subsequent recovery. The transducer was set to record at 1 second intervals. In the wetland, surface water immediately adjacent to the piezometer was used as the slug. Analysis involved using the methods of Hvorslev (1951), which complement historical hydraulic conductivity analyses of the tailings sand, including bail tests (Longval & Mendoza, 2014) and Guelph Permeameter tests to asses in situ saturated hydraulic conductivity (Benyon, 2014). These data are further discussed in Appendix G and applied in Appendix H.

2.3. Analytical Methods

Groundwater and geochemical data were analyzed to evaluate the short-term (single events) to seasonal and long-term (year to year) influences of climate and hydrostratigraphy on the groundwater system dynamics. Water table maps were developed to illustrate the progression of the water table configuration three to five years after watershed construction ceased. Hyetographs (P vs t) were paired with hydrographs (h vs t) that were developed from manual and automated water level data to determine the influence of precipitation on the water table at various points along two transects (*e.g.*, spring freshet or large precipitation events), and to examine long-term water table dynamics (>1 year). These data were paired with temporal plots of manual electrical conductivity data (EC vs t) to evaluate the spatial and temporal influence of groundwater inputs and outputs on relative solute distributions throughout the watershed. EC maps were also developed to compare spatial and temporal solute distributions. Finally, soil wetness maps were developed to evaluate the catchment area in the lowlands and to assist in evaluating the responsiveness of the wetland to large precipitation events and how solutes (EC maps) change in relation to precipitation events.

Two detailed transects were chosen to evaluate groundwater and geochemical dynamics in different landform configurations (Transect 1 and Transect 2; Figure 5). Transect 1 intersects Hummock 7 that extends from the southern boundary of the watershed (318.5 m ASL) for approximately 320 m before transitioning into the lowlands (*i.e.*, wetland, 313.3 m ASL). Transect 2 intersects a slope that extends from the southern topographic high (318.2 m ASL) for 140 m as it transitions into the lowlands (313.3 m ASL).

A major challenge when analyzing the geochemical, EC and stable water isotope data was accounting for fluctuations in the water levels (WL) relative to ground surface and the position of the midscreen (MS) relative to the water level. That is, the position of a piezometer screen remains constant in space while the sampling depth within a water column changes with water level fluctuations. Furthermore, not all nests have a piezometer that consistently samples the same depth within the column of water as surrounding nests. To overcome this problem, piezometers were assigned one of six groundwater classes based first on the average depth of the water level relative to ground surface, and second the average depth of the midscreen relative to the water level observed in the piezometer. The classification is outlined in Figure 6 and explained in detail in Appendix F.

A groundwater mixing model was developed for SHW by qualitatively defining endmember compositions from known major inputs to the groundwater system (*i.e.,* OSPW and Mildred Lake Reservoir, MLR). Stable water isotopes, EC, and chemistry were used to characterize the surface water, and shallow and deep groundwater in piezometers across SHW. These endmembers were used to determine the sources of groundwater at various locations in the watershed and elucidate mechanisms of solute movement along two specific transects in the watershed corresponding to different topographic configurations. Endmember compositions were obtained from the literature where the data record is incomplete. Eighteen groundwater samples collected from BGC piezometers in SHW during 2013 and 2014 were averaged to define the major ions of OSPW geochemistry and were paired with the average OSPW isotope composition from Baer et al., (2016) to collectively represent the OSPW endmember composition in SHW following land reconstruction. Only one geochemical sample was collected and analyzed from MLR during the study period, in 2015 (Vessey et al., 2018); this data point was paired with the average isotope endmember composition for MLR presented in Baer (2014), both of which are considered to adequately represent the 2013 and 2014 MLR water added to SHW. Isotope data were plotted in dual isotope space using site specific weighted and unweighted Local Meteoric Water Lines (wLMWL and uLMWL, respectively; Baer et al., 2016) and Local Evaporation Lines (LEL; Biagi et al., 2018) obtained from the literature. These data are further discussed and summarized in Appendix F.

2.4. Numerical Modelling

To assist in conceptualizing groundwater movement through the reconstructed watershed, a three-dimensional groundwater flow model was developed utilizing a digital elevation model (DEM; D. Heisler, SCL, pers. com.) and reported reconstructed hydrostratigraphy of the watershed, as well as recent climatic fluxes, to simulate steady-state conditions (Figure 7). The goal of the model was to reproduce the average water table configuration observed in SHW to quantify the volumetric flows through the watershed and evaluate the sensitivity of the calibration parameters (*i.e.,* hydraulic conductivity and recharge) on the flow system. The calibrated model was also used to explore potential scenarios, such as changes in climate or evapotranspiration, that may affect the water table in the study area.

2.4.1. Model Design

The three-dimensional, finite-difference groundwater model was developed using Visual MODFLOW (Figure 7; Waterloo Hydrogeologic, 2018). The steady-state model was calibrated to 22 monitoring points in the watershed, using automated water level data from 20 piezometers that had annual continuous data (time gaps were less than one month) from mid-September 2016 to mid-September 2017, and interpolated data at the remaining 2 locations (nest 15 and 25; Figure H-1; Appendix H). Data from automated measurements, rather than manual measurements, were used as calibration points to minimize the bias toward summer water levels that would otherwise be introduced by solely relying on manual measurements. Water table maps (Appendix B) and soil wetness maps (Appendix D) were referenced for the general water table configuration within the watershed. These field observations were compared to the simulated hydraulic heads, water table elevation and configuration, and volumetric flows during model calibration.

Recharge rates used in this model were taken from values derived from Lukenbach et al., (2019). They estimated recharge rates by using HYDRUS modelling software to simulate flow through the unsaturated hummocks at SHW. The simulations were calibrated to three years of data collected from 126 soil moisture access tubes, 9 soil pits, and three meteorological and eddy covariance towers in SHW (discussed previously; Figure 5). Hydrostratigraphic properties used by Lukenbach et al., (2019) were based on field measurements and observations when available (Appendix G; Benyon, 2014), or were otherwise approximated from engineering designs (BGC, 2014a; BGC, 2015). Simulated hydraulic conductivities from Lukenbach et al., (2019) were referenced as needed when developing the groundwater model. Unsaturated flow modelling methods from SHW are discussed further in Lukenbach et al., (2019).

2.4.2. Model Domain

The model domain is 990 m by 1180 m, discretized to a 10 m x 10 m grid horizontally and extends beyond the southern extent of the study site to encompass 318 Berm; the most laterally extensive upland feature (>30 ha) in the tailings deposit and an interpreted major source of groundwater recharge to the watershed (Figure 7). Areas extending beyond the northern, eastern and western boundaries of the watershed were defined as inactive (*i.e.*, beyond the perimeter of the watershed; Figure 7). The surface of the model corresponds to the topographic surface defined by the LiDAR (Figure 7; D. Heisler, SCL, pers. com.), and the entire base of the model was set to 304 m ASL, the approximate elevation of the interface between the top of the composite tailings and the bottom of the hydraulically-placed tailings sand cap. This interface is approximately 10 m thick below the lowlands and up to 18 m thick below the upland hummocks. Three hydrostratigraphic units were defined vertically downwards from ground surface: topsoil (layer 1 = 0.50 m thick) and subsoil (layer 2 = 0.5 m thick) overly the tailings sand that was equally discretized into three sublayers between the subsoil and base of the model (layers 3 to 5). All layers were defined as variably confined/unconfined layers.

2.4.3. Hydrogeological Parameters

The topsoil and subsoil hydraulic properties observed in the watershed were incorporated into the upper two layers of the groundwater model based on the observed areal coverage of each soil type (Appendix A). The remaining layers are comprised of tailings sand (Appendix H). These parameters were calibrated through trial and error based on field data (Appendix G) or literature values; these data are provided in the next chapter.

2.4.4. Boundary Conditions & Initial Conditions

The inflows and outflows of the groundwater model are represented by specified flux (net-recharge and no-flow) boundary conditions (BCs), and head-dependent flux BCs (general head boundary condition, GHB). No specified head BCs were used in the model (Appendix H).

Recharge BC

A net-recharge flux was applied to the uppermost active layer, lumping evapotranspiration (AET) and groundwater recharge into one value (Figure H-4; Appendix H). Net-recharge zones were defined by the hydraulic properties of the soil (topsoil and subsoil transmissivity) and vegetation, which were independently simulated by Lukenbach et al., (2019) to provide reasonable recharge rates for each type of reclamation material in SHW. Negative net-recharge rates in the lowlands reflect excess AET losses to the atmosphere due to vegetation and permanent surface water in the wetland. It also accounts for annual average ‘managed’ outflows that occurred from the lowlands, calculated from the three years detailed in this study.

Watershed Perimeter

The perimeter of the active cells in the model represents the interface between the tailings sand and surrounding geology (Clearwater Formation; K_h = 1E-8 m/s, K_v = 1E-10 m/s, n = 0.20; BGC, 2015). Because of the low hydraulic conductivity of these surrounding materials, this interface was represented as a no-flow boundary condition.

Base of Model

The base of the model was assigned a no-flow boundary condition due to differences in hydraulic conductivity between the overlying sand cap and underling composite tailings (K_h = 1.7E-7 m/s, K_v = 1.7E-8 m/s; Thompson et al., 2011). Groundwater was expected to preferentially flow through the sand cap due to differences in hydraulic conductivity of approximately three orders of magnitude with the CT.

General Head BC

Two GHBs, to the east and to the north, were used represent lateral outflows from the watershed (Figure H-4). The eastern GHB was split into two zones, one to represent seepage under Hummock 6 in the north, through the Sandhill Berm (East GHB-1) and the other to represent seepage through Sandhill Berm, spanning the topographic low between the easternmost hummocks (East GHB-2). For both eastern GHBs, hydraulic heads were assigned to 311 m ASL, the approximate elevation of standing water in the down gradient Kingfisher Watershed. Eastward flow appeared to be constrained by the topography and hydraulic conductivity of the materials in Sandhill adjacent to the berm. More specifically, standing water is often observed in the lowlands immediately adjacent to Sandhill Berm. Therefore, these observations were modelled using different conductance values (C) in the East GHB-1 and East GHB-2 boundaries (C = 0.03 m^2/d, and 1.4 m^2/d, respectively).

The northern GHB was constructed to represent groundwater that is diverted from the primary flow path, flowing north, likely through buried gravel channels beyond the northern extent of SHW boundary. No standing water was observed within the topographic lows in the area 200 m north of the watershed during the summer of 2017; therefore, the hydraulic head for that boundary was interpreted as 310.85 m ASL, below the lowest part of the drainage ditch adjacent to the highway located approximately 70 m north of the watershed's northern boundary. The boundary spanned from the western wetland to Hummock 4 (C = 0.33 m^2/d).

2.4.5. Calibration

Annual recharge fluxes were determined for each soil type (LFH-A/B, LFH-D, and upland PMM) in SHW independently by Lukenbach et al., (2019). The values specified in this model were for the annual recharge values from 2015 (M. Lukenbach, unpublished data). The values for cumulative recharge from 2015 were below (LFH-A/B, PMM) or identical (LFH-D) to the average annual recharge values simulated in Lukenbach et al., (2019).

Calibration involved individually adjusting hydraulic parameters (hydraulic conductivity, and GHB conductance) by performing multiple simulations through trial and error until the simulated hydraulic heads adequately represented the water table configurations observed during summer months of 2017. Calibrated hydraulic parameters were compared to values obtained from the field (*e.g.,* tailings sand and PMM hydraulic conductivities; Appendix G) or the literature where field data were unavailable (Lukenbach et al., 2019). Calibrated hydraulic parameters were maintained within half an order of magnitude of previously estimated values wherever possible and are presented in the Results.

As previously mentioned, calibrating the model required comparing average observed heads measured in SHW during the study period to simulated heads from the model at 22 calibration points (Figure H-1). The data were analyzed using statistical analyses within the software to evaluate whether the model produced an adequate representation of the observed conditions following simulations.

2.4.6. Scenario Analyses

As vegetation grows and becomes established, the water available for recharge will likely decline due to decreases in soil moisture (increased rooting depth and above ground interception) and increased AET (increased leaf area index; Lukenbach et al., 2019). Furthermore, while boreal wetlands can naturally self-regulate water resources in a moisture-limited climate (Waddington et al., 2015), the province's climate will likely become drier overall in the coming decades (Keshta et al., 2011; Schneider, 2013). In northern Alberta, the distribution of precipitation throughout the year is expected to decrease during the growing season and increase during the winter months (Schneider, 2013). There is also expected to be an increase in mean annual temperatures, which will result in longer growing seasons, thereby increasing mean annual AET and reducing groundwater recharge.

Forecasting the availability of groundwater for possible future scenarios helps to elucidate the trajectory of reconstructed landscapes. Therefore, the calibrated steady-state model was used to test potential changes in recharge (including ET) that the watershed might encounter. Specifically, scenario testing was conducted by reducing the base case recharge values in the upland areas by 5%, 10% and 25%, and by increasing the base case recharge by 5%. Comparisons are made by evaluating the differences from the water levels predicted for the base case at observation points along Transect 1 and Transect 2.

Chapter 3: Results

3.1. Hydrometric Data

Variability in climatic and managed fluxes in the watershed created dynamic hydrological conditions during the study period. Total annual precipitation (P; rainfall and snowmelt) increased by 156 cm between 2015 (306 mm) and 2016 (462 mm), then decreased by 133 mm in 2017 (329 mm; Figure 8). Total rainfall for 2016 was much higher compared to rainfall climate norms from 1981-2010 in Fort McMurray (417 mm and 316 mm, respectively; Environment Canada 2017), whereas 2015 and 2017 were drier than average (254 mm and 289 mm, respectively). The estimated snowmelt decreased each year, from 52 mm in 2015 to 40 mm in 2017 (Figure 8). Daily rainfall values in 2016 were much larger than the other years; four major events (>30 mm/d) contributed to 40% of total P (177 mm total from events on Jun 9, Jul 31, Aug 27 and Sept 3; Figure 9); all rain events in 2015 and 2017 were <30 mm/d. Most precipitation fell consistently in July and August each year, although in 2016 and 2017 rain continued later into the year compared to 2015.

Total annual AET in the lowlands was greatest in 2015 (392 mm) and decreased through 2016 (310 mm) and 2017 (298 mm) (Figure 8; Lukenbach et al., 2019; S. Carey, unpublished data). During 2015, AET exceeded P (-91 mm), and during 2016 and 2017, P exceeded AET (152 mm and 31 mm, respectively). PET values decreased from 2015 (659 mm) to 2016 (583 mm; Lukenbach et al., 2019) then increased in 2017 (602 mm; M. Lukenbach, unpublished data). No AET data are available for the uplands during this time. The average daily temperatures for each month ranged from -21.2 ºC to 20.9 ºC consistently from 2015 to 2017; temperatures were overall warmer than climate norms during the study period (Figure 9; Environment Canada, 2017).

Managed outflow events occurred in 2015 and 2017 from the sump located at the eastern end of the wetland (Figure 8). In 2015, a 56-hour pumping event from Jun 3 to 5 removed 9,334 m^3 of water, an equivalent of 55 mm from the 17 ha lowland (Spennato et al., 2018). In 2017, a 5-day pumping event from July 8 to 13 removed 17,129 m^3 of water, or 101 mm, from the lowland. No managed inflow events occurred during the study period.

3.2. Groundwater Movement

3.2.1. Shallow Groundwater Flow System

Following construction, a shallow groundwater flow system developed in the upper surficial reconstructed tailings sand of SHW. Groundwater flowed from the southern boundary of the watershed and diverged to the north (S-N flow path) and east (S-E flow path) consistently throughout the study period (2015 to 2017; Figure 10; Appendix B). The water table configuration indicates groundwater does not mound beneath individually constructed hummocks (Figure 10). Instead, the horizontal hydraulic gradients originate from 318 Berm, which is the most laterally extensive upland feature (>30 ha) in EIP and is immediately south of SHW. The S-E flow path was engineered to source water to KFW, down-gradient from SHW, whereas the S-N flow path was not engineered; groundwater flows through the northern boundary of the watershed were unexpected.

During the summer field seasons (May to October), depth to groundwater below the uplands ranged (spatially) from 8.7 metres below ground surface (m BGS; average WL depth at nest 11, below Hummock 7; Figure 5), to fluctuating immediately below ground surface, near areas transitioning into lowlands (*e.g.*, nests 75 and 76; Figure 11). In the uplands, the hummocks tend to have deeper water levels relative to ground surface ("deep", WL >1.8 m BGS), compared to the slopes where the water level is shallower relative to ground surface ("shallow", WL <1.8 m BGS) over larger areas (Figure 11). Maximum and minimum water levels manually measured in hummocks showed relatively subdued water level changes through time relative to the notable changes in water levels observed in the slopes (Figure 11). Overall, water levels in piezometers on the southern uplands of Transect 1 (nest 29-32) were lower in 2016 and 2017 compared to 2015; the water levels in the remaining piezometers fluctuated within the same range year to year (Figure 11a). Water levels in piezometers along Transect 2 all fluctuate within the same range, year to year (Figure 11b).

In general, the lowlands have shallow groundwater levels relative to land surface, but some areas have an average standing water level 0.7 metres above ground surface (m AGS; "surface/standing water", WL >0 m AGS; Figure 11). Standing water appears to persist throughout the summer, year to year, in two areas (east and west wetlands herein; Figure 12; Appendix D). The wetlands are more responsive to snowmelt than areas where the water table is further below ground surface (Figure 11). The seasonal maximum areal extent of the standing water and saturated areas in the lowlands may occur early in the field season following snowmelt, although the watershed may wet up appreciably after several sequential large rain events (*e.g.*, in 2016; Appendix D). The smallest standing water and saturated areas generally occur later in the field season (*i.e.*, October; Appendix D), except in years with late summer, large precipitation events (*i.e.*, September 2016). Based on soil wetness maps, the wettest days in the lowlands during the study period, correspond to saturated and standing water areas of 17.0 ha and 13.1 ha, respectively, on June 3, 2017 and the driest days in the lowlands during the study period correspond to saturated and standing water areas of 4.9 ha and 1.3 ha on October 25, 2015 (Appendix D).

3.2.2. Hydraulic Gradients

Horizontal hydraulic gradients (i_h) are greatest below southern Hummocks 7 to 9 ($i_h = 0.01$) and decrease as the topography transitions into lowlands ($i_h << 0.01$; Figure 10); i_h remain consistent through the study period (Appendix B). In the uplands, vertical hydraulic gradients (i_v) range from -0.08 to 0.1 (up and downward flow, respectively) and are intermittent; upland vertical gradients are short lived and overall negligible, on average 0.009 ± 0.02 (downward flow). Wetland vertical gradients are slightly larger, ranging from -0.3 to 0.5 (up and downward flow, respectively) and have greater temporal variability (Appendix B).

Determination of vertical hydraulic gradients at the toes of hummocks using E/F/G nested piezometers completed in tailings sand was complicated by the short distance between piezometers screens; therefore, they are not included. In upland/lowland transition areas adjacent to the toes of hummocks, vertical hydraulic gradients were evaluated using A/B/C/D nested piezometers. Small vertical gradients (upward flow) exist between piezometers completed across the compacted clay layer (*e.g.*, 23-A and 23-C); however, both downward and upward flow may occur between nested piezometers completed in the underlying tailings sand in these areas (*e.g.*, 23-C and 23-D) during the study period indicating the presence of locally confined conditions (Appendix B).

3.2.3. Event-based Responses

Notable examples of watershed response to input (precipitation) or output (pumping) events can be observed in the early spring every year (snowmelt events), late in the summer of 2016 (multiple consecutive large precipitation events) and midsummer of 2017 (the 5-day outflow event in July; Figure 11). Spring melt influx is observed every year in the continuous water level data from piezometers screened in areas with shallow water tables (WL <1.8 m BGS), or piezometers in standing water in the lowlands. Effects of spring melt were notably less prominent in upland piezometers where the water table was >1.8 m BGS (Figure 11).

The overall response of the groundwater system to precipitation events is best demonstrated in 2016, where two major precipitation days (>30 mm/d) occurred late summer (Aug 27 and Sept 3) between two soil wetness mapping events (Aug 21, pre-event, and Sep 15, post-event; Appendix C). Over the 25-day period between mapping events, 126 mm of rain fell in the watershed, causing a 0.16 m increase in standing water levels (Δh, captured by loggers at nests 65 and 69) on boardwalk 3 (S. Carey, unpublished data). This expanded the standing water area by approximately 79% (pre-event = 45,017 m^2, post-event = 80,399 m^2), and the overall saturated/standing water areas increased by 33% (pre-event = 87,353 m^2, post-event = 115,995 m^2). In the uplands, the greatest increases in water levels were recorded from piezometers along Transect 2 (Figure 11b), on the slopes (Δh = 0.30 m in 41-3 and 42-03; Δh = 0.50 m in 75-02 and 76-02). Water level responses recorded from piezometers on the hummock along Transect 1 were varied (Figure 11a); the southernmost piezometers had a subdued response (*i.e.*, Δh = 0.06 m in nests 32, 31, 30, and 29) whereas water level changes closer to the wetland were similar to changes observed in the wetland itself (*i.e.*, Δh = 0.22 m in nests 27, 26, 24 and 23).

In 2017, a 5-day pumping event (Jul 8 to 13) removed 17,129 m^3 of water, or 101 mm, from the watershed at the sump on the eastern edge of the lowlands (Figure 12). Compared to water levels prior to the pumping event, water levels in the eastern wetland decreased by 0.22 m approximately one week following the pumping event, and by 0.32 m approximately one month after the pumping event (loggers at nests 65 and 69; S. Carey, unpublished data) (Figure 11). Observed decreases in standing water and saturated/standing water areas were 18% and 11% in the week after pumping (-19,931 m^2 and -15,209 m^2, respectively), and 50% and 41% in the month after pumping (-55,410 m^2 and -56,119 m^2, respectively; Figure 12). In the uplands, water levels in Transect 2 responded immediately to the pumping event, decreasing by a maximum of 0.45 m in the month after pumping ceased (nest 76), whereas the water level response in all upland piezometers along Transect 1 were subdued, decreasing by a maximum of 0.11 m (nest 32) over that time.

3.3. Groundwater Chemistry

3.3.1. Electrical Conductivity

Electrical conductivity (EC; µS/cm) is used to generalize solute distribution and movement in the watershed. Available manual surface water EC measurements adjacent to piezometers in the wetlands ranged from 600 to 3200 µS/cm in the 2016 and 2017 summer field season (*e.g.*, nests 15 and 16 along BW1, and nests 65 to 71 along BW3, respectively; Appendix C). The average EC of surface water in the wetlands from the 2016 and 2017 field seasons was 1600 ± 500 µS/cm (n = 50) and 1400 ± 500 µS/cm (n = 89), respectively, which is lower than the range of average EC values for water measured in 2015 from wetland wells that were screened to surface (1785 ± 929 µS/cm; Biagi et al., 2018). Spatially, ECs were lower in the east wetland (1300 ± 400 µS/cm, n = 98) than the west wetland (1800 ± 600 µS/cm, n = 41) during the 2016 and 2017 field seasons. A small, isolated permanent surface water body (2 m by 1 m), located in a low spot adjacent to Hummock 7 (and nest 38), had an average EC of 2300 ± 500 µS/cm over 2016 and 2017, with minimum and maximum values of 1800 µS/cm to 3400 µS/cm, respectively.

Groundwater manual EC measurements range from 100 µS/cm to 5700 µS/cm during the summer field seasons of 2015 to 2017 (Appendix C). The lowest EC values correspond to piezometers installed in the wetlands, whereas higher ECs are associated with lowland areas along the periphery of the uplands and beneath the uplands themselves (Figure 11). In the uplands, EC distributions were more variable than those in the wetlands, as depths to the water table are less consistent, and the piezometers may be screened deeper into the water column.

In general, EC increases with depth, through the water column; values from piezometers installed in areas with shallow or deep water tables (relative to ground surface) and deeper midscreens (relative to the water level), have high EC values (shallow/deep and deep/deep piezometers, respectively; Figure 11). Piezometers located in areas with deep water tables relative to ground surface, and shallow midscreens relative to the water table (deep/shallow piezometers tend to have lower EC values, compared to piezometers located in areas with shallow water tables and shallow midscreens relative to the water table (shallow/shallow piezometers). The latter tend to have higher ECs and larger ranges in ECs overall.

Measured ECs fluctuate throughout each field season (Figure 11), regardless of water table depth and sampling location (collectively, the piezometer's water class; Figure 6). The EC fluctuations align with inflow/outflow events; unfortunately, the summer field seasons did not capture EC responses to spring melt. In 2015, the ECs in the watershed slowly freshened throughout the summer, following a 55 mm outflow event, with temporary increases to several small subsequent rainfall events (Figure 11). In 2016, the watershed received more precipitation and larger individual rain events compared to 2015; overall, EC values were elevated throughout the 2016 field season compared to 2015. In particular, in the 25 days between Aug 21 and Sept 15, during which time 126 mm of rain fell, upland EC values in Transect 1 piezometers increased in most sampling locations (*e.g.*, up to 1300 μS/cm in nest 30, a shallow/shallow piezometer), but decreased in others (*e.g.*, down 700 μS/cm in nest 29, a deep/deep piezometer). In Transect 2, all upland piezometers increased ECs during this time period (200 to 500 μS/cm; Figure 11). These trends were also observed spatially in EC maps, beyond the transects (Appendix C). In 2017, a 101 mm pumping event (nearly double the 2015 outflow event), resulted in an average decrease of 400 μS/cm in all upland nests along Transect 1, whereas Transect 2 upland piezometers ranged from a 400 μS/cm increase (nest 75, a shallow/shallow piezometer) to a 400 μS/cm decrease (nest 42, a shallow/deep piezometer) in the week following pumping. In the month following pumping EC values rebounded to be greater than pre-event conditions, increasing up to 1700 μS/cm in Transect 1 (nest 23, shallow/deep), and greater than 2000 μS/cm in Transect 2 (nest 42; shallow/deep)

3.3.2. Annual Chemistry

The annual geochemical sampling (major and minor ions) provide a general characterization for groundwater and surface waters located within the watershed across three years, though it is difficult to evaluate year to year trends given the overall temporal resolution of the data (Figure 13; Appendix E). Major ions are therefore compared spatially instead (horizontally and vertically) by grouping piezometers based on their water classes (defined in Figure 6) relative to the groundwater endmember, Mildred Lake Reservoir (MLR) and OSPW (Appendix E).

Groundwater measured from artesian piezometers (artesian/shallow and artesian/deep piezos) plot similarly to surface waters as well-mixed water, regardless of the midscreen/sampling depth (relative to the water level; Figure 13, Appendix B). All surface water and artesian water classes correspond to piezometers in the wetlands along BW1 (nests 15 and 16) and BW3 (nests 64 to 71), and are overall enriched with sulphate and calcium, and depleted in sodium compared to endmember compositions. Groundwater sampled from shallow water tables with shallow midscreens (shallow/shallow pipes) ranges from a mixed-cation and chloride-sulphate-enriched water-type (Cl^-/SO_4^{2-}) to a sodium-chloride-sulphate enriched water-type (Na^+ Cl^-/SO_4^{2-}). Groundwater samples from piezometers in areas with shallow water tables and deeper midscreens (shallow/deep pipes) plot almost exclusively as sodium-chloride-sulphate-enriched water (Na^+ Cl^- $/SO_4^2$), overlapping with OSPW endmember compositions. Groundwater sampled from piezometers located in areas with deep water tables and shallow midscreens (deep/shallow pipes) have a similar range of mixed chemistries compared to water from shallow/shallow piezometers. Samples from deeper water tables yield similar chemistries as shallow/deep piezometers, with few exceptions, overlapping in chemistry with the OSPW endmember. Groundwater samples from BGC piezometers collected in 2017 plot in the immediate vicinity of OSPW endmember (averaged from the same piezometers, using 2013 and 2014 data), especially for cation proportions (Na^+ enriched; Figure 13; Appendix E).

3.3.3. Stable Water Isotopes, Sodium & EC

Of the endmembers that exist within SHW, OSPW was the most isotopically enriched endmember, plotting above the LEL, and had the highest concentration of sodium (Figure 14). MLR is more isotopically depleted than OSPW, plotting closer to the intersection of the LEL and wLMWL, and has very low sodium concentrations (Appendix F).

Groundwater samples collected from piezometers completed in the tailings sand (SH-GW piezometers) predominantly plot along a line between OSPW and MLR $\delta^2H/\delta^{18}O$ endmember signatures, and between the wLMWL and LEL for both Transect 1 and Transect 2 (Figure 14a and 14b, respectively). Groundwater samples with depleted $\delta^2H/\delta^{18}O$ values fall near the wLMWL/LEL intersection, closer to P and MLR isotope endmember compositions. These samples also tend to have lower sodium concentrations, plotting near the MLR Na^+ endmember composition (Figure 14). Groundwater samples that are more isotopically-enriched plot closer to the OSPW isotope endmember composition, and have higher concentrations of sodium, plotting near the OSPW Na^+ endmember composition. The most isotopically depleted groundwater samples plot below the LEL adjacent to the wLMWL, not between the MLR/OSPW endmembers (Figure 14b).

In Transect 1, where the water level is deeper below ground surface (WL >1.8 m BGS), groundwater isotope signatures tend to plot very close to the MLR endmember and up to halfway between MLR and OSPW (deep/shallow or deep/deep; Figure 14a). Samples that have freshest water compositions, closest to precipitation, are obtained within 1.8 m of the water level (MS <1.8

m BWL; shallow/shallow and deep/shallow pipes). The groundwater samples that plot closest to OSPW endmembers (δ^2H, $\delta^{18}O$ and Na^+) were from nest 23, located in the lowlands at the toe of Hummock 7 (Figure 14a). Samples from nest 23 also have the greatest variability, compared to the other nests along the transect. Samples collected in the wetland both plot near the LEL moderately between MLR and OSPW endmember isotope compositions (nests 66 and 69; artesian/deep); the Na^+ values indicate nest 66 has less sodium than nest 69, which plots along the theoretical mixing line between MLR and OSPW Na^+ endmembers (Figure 14a). Overall, stable water isotope values obtained along Transect 1 fall neatly along a line between OSPW and MLR endmember compositions; however, the Na^+ data do not.

Most groundwater samples collected along Transect 2 are more isotopically enriched compared to samples from Transect 1, plotting towards the OSPW isotope endmember composition (Figure 14b). Samples that are isotopically enriched also have higher concentrations of Na^+ and subsequently plot near the OSPW Na^+ endmember. These enriched samples were all collected from piezometers in areas with shallow water levels (WL <1.8 m BGS), sampled from anywhere within the water column (shallow/shallow and shallow/deep pipes; Figure 14b). The exception is the nest installed at the top of the slope, near 318 Berm, where the groundwater is further from ground surface (*i.e.,* nest 41; deep/shallow pipe); samples plot below the LEL, near the wLMWL (not between OSPW and MLR endmembers), and have very low sodium values compared to the rest of the data collected along Transect 2. Overall, the isotope and Na^+ data from Transect 2 plot between the OSPW and MLR endmember compositions (except nest 41). Relationships between δ^2H, $\delta^{18}O$, EC and Na^+ are discussed further in Appendix G.

3.4. Groundwater Modelling

3.4.1. Model Calibration

Calibrating the steady-state groundwater model involved manually adjusting hydraulic conductivity to within half an order of magnitude of calculated observed or modelled values from the literature (Table 1; Appendices F and H), while simultaneously adjusting GHBs to manage the water balance. This required performing multiple simulations through trial and error to develop a water table configuration that simulated hydraulic heads observed in SHW with realistic volumetric flow rates. Recharge values were specified throughout the calibration process (Table 2).

Table 1: Hydrostratigraphic parameters in base case model compared to literature values

Hydro-stratigraphic Zone	**Depth Range (m BGS)**	**Material**	**Calibrated Parameters**			**Literature K (m/s)**	**Literature Source**
			Kx (m/s)	**Ky (m/s)**	**Kz (m/s)**		
Topsoil	0.0-0.5	PMM[1]	0.01	0.01	0.004	2.8E-04	Lukenbach et al., (2019)
		PMM[2]	4.0E-6	4.0E-6	4.0E-6	1.5E-05	Benyon (2014)
		LFH-A/B	0.02	0.02	0.0002	6.1E-05	Lukenbach et al., (2019)
		LFH-D	4.3E-6	4.3E-6	4.3E-6	1.3E-05	Lukenbach et al., (2019)
Subsoil	0.5-1.0	Clay Till[1]	4.0E-6	4.0E-6	4.0E-6	1.0E-07	Lukenbach et al., (2019)
		Clay Till[2]	1.0E-6	1.0E-6	1.0E-6	1.5E-05	Lukenbach et al., (2019)
		PMM[2]	4.0E-6	4.0E-6	4.0E-6	1.5E-05	Benyon (2014)
		Pf Sand	1.0E-4	1.0E-4	1.0E-4	5.1E-05	Benyon (2014)
		Tailings Sand	1.3E-5	1.3E-5	1.3E-5	2.6E-05	Benyon (2014), Appendix F
Tailings Sand	>1.0	Tailings Sand	1.3E-5	1.3E-5	1.3E-5	2.6E-05	Benyon (2014), Appendix F

[1] Lowlands: regularly experiences standing water and permanently saturated soils in some areas. Subsoil was compacted during initial placement.

[2] Uplands: topsoil and subsoils do not experience lowland saturated hydrologic conditions.

Calculated hydraulic heads were compared to observed average water levels from the 22 piezometers across SHW (calibration points; Figure H-1; Appendix H). The goodness-of-fit

Table 2: Recharge parameters/zones in base case model

Recharge Zone	**Areal Coverage (m^2)**	**Rate (mm/y)**	**Ponding Depth (m AGS)**
LFH-A/B	81,293	88	0
LFH-D	115,179	40	0
PMM - Lowlands	162,309	-50	1.5
PMM - Uplands	160,144	41	1
PMM[1] - 318 Berm	331,932	88	1

[1] 318 Berm did not have PMM placed until winter 2016-2017, or vegetation until summer 2017; less soil moisture storage and ET demand meant more recharge available.

Table 3: Calibration statistics from base case model

Calibration Statistics	**Base Case Results**
Min. Residual	-0.0045 m (SH-GW-39)
Max. Residual	-0.4 m (SH-GW-05)
Residual Mean	-0.013 m
Abs Residual Mean	0.13 m
Standard Error of the Estimate	0.035 m
Root Mean Squared	0.16 m
Normalized Root Mean Square	5.05 %
Correlation Coefficient	0.99

Determined from data in Figure H-5

between calculated and observed hydraulic heads were quantified using the software's performance indicators, which demonstrated the model achieved a statistically acceptable representation of the groundwater flow system in SHW (Table 3; Figure 15). The Normalized Root Mean Square error for the calibrated parameters was 5.05% (obtained from data in Figure H-5).

Given that a) the calibrated hydraulic conductivity values fall within an acceptable range of the literature values (Table 1), b) the simulated water table resembles the water table configuration observed during summer field seasons (Figure 15; Appendix B) and c) the calibration statistics indicate calculated heads adequately represent field conditions (Table 3), the model provides a reasonable representation of the groundwater system in SHW. The largest residuals were observed at calibration points along the southern boundary of the watershed, where the simulated water table was slightly lower than observed in the field (-0.4 m). The heads in the wetland were most sensitive to small adjustments in the GHBs during calibration; hydraulic heads in the uplands were the least responsive. Raising hydraulic heads in the uplands to observed values required raising recharge values beyond an acceptable range and led to large water level rises elsewhere in the model.

The water table mounded below 318 Berm, extending into the study watershed below the southern hummocks (Figure 15). As the topography flattens to the lowland, the hydraulic gradient also flattens as flow is diverted through the wetland to the north and east GHBs. Maintaining realistic volumetric flows and out of the model required adjusting the areal extent of 318 Berm, thereby affecting effective recharge area, by gradually deactivating cells, since the area of 318 Berm contributing recharge is relatively poorly constrained and the watershed's range of recharge are limited (M. Lukenbach, University of Alberta, pers. Com.). Given that SHW loses an unknown amount of groundwater through the northern boundary and Sandhill Berm was constructed to permit groundwater flow to KFW, the volumetric flows out the GHBs were constrained by modifying the conductance terms (a model parameter used to represent resistance to flow) within reasonable limits to ensure flow occurred predominantly through the eastern boundary (Appendix H; Table H-4).

While comparing the elevation of the simulated water table relative to topographic surface was considered, the LiDAR that was used to produce the digital elevation model (DEM) did not account for standing bodies of water in the lowlands; consequently, the DEM over-estimates the topographic elevation in these areas. This made it impossible to generate accurate soil wetness maps within the model, as the water table is near and above ground surface throughout the lowlands in the model.

3.4.2. Scenario Analyses

The calibrated steady-state model (base case herein), was subsequently modified to simulate decreasing and increasing recharge rates associated with climate change, wetland vegetation growth or extreme climate conditions. More specifically, the base case recharge values were reduced in the upland areas by 5%, 10%, and 25%, and subsequently increased by 5% (Figure 16; Table 2). Observation points along Transect 1 and 2 were used to evaluate the response of the groundwater system by calculating the difference between the hydraulic heads from the base case to the observed heads simulated in each scenario.

In general, the water table elevation decreases as recharge decreases and increases as recharge increases. Overall, areas in the watershed that have previously been described as having shallow water tables (*i.e.,* upland areas adjacent to and transitioning into lowlands), also have the greatest capacity to buffer the water level changes through different recharge scenarios (Figure 16). The hydraulic heads in these areas consistently have the least fluctuations (*e.g.*, nests 23, 24, 26, 27, 75, 76). Upland areas adjacent to and including 318 Berm have some of the largest changes in water levels through different recharge scenarios. This follows from the steady-state calibration; the groundwater mound below 318 Berm is sensitive to changes in recharge. Large changes in hydraulic heads are also observed in lowland areas across different recharge scenarios (*e.g.*, nests 66 and 69; Figure 16).

Chapter 4: Discussion

One of the overarching goals for reconstructing and reclaiming SHW was to construct a landscape that could develop a groundwater flow system to support the hydrologic needs of wetland vegetation. Because the tailings sand used to construct SHW contains OSPW (up to ~4,000 µS/cm; BGC, 2008), which exceeds the EC tolerance thresholds for natural boreal wetland vegetation (<2,000 µS/cm; Howat, 2000), the watershed was designed to promote groundwater recharge to dilute and flush the surficial tailings sand, thereby reducing the deleterious effects of concentrated OSPW on overlying reclaimed vegetation. To achieve this, designers constructed a coarse-textured watershed analogous to those observed elsewhere in the Boreal Plain with extensive uplands for forestland development and greater recharge potential to supply groundwater to wetlands in the central lowlands (Figure 4). A major concern was that concentrated OSPW from tailings at depth could be mobilized and discharge in the wetland if vertical hydraulic gradients and deeper groundwater flow paths developed. Reclamation designers anticipated they could mitigate these less desirable flow systems from developing by constructing hummocks to preferentially develop localized groundwater mounds, through recharge, for shallow flow systems (BGC, 2015); the hummocks were thereby constructed out of tailings sand. Given that most boreal wetlands are predominantly comprised of fens (Rooney et al., 2012), which require water tables that fluctuate at or near ground surface and prefer groundwater that is fresh to slightly saline (<2000 µS/cm; ESRD, 2015), constructing such a shallow groundwater flow system would be ideal for maintaining freshwater near ground surface for wetland vegetation (Daly et al., 2012; Ketcheson et al., 2016; Pollard et al., 2012).

In the years following landscape reconstruction and reclamation, SHW has developed a somewhat intermediate groundwater flow system (discussed previously; Figure 3), with shallow flow paths and only temporary, intermittent vertical hydraulic gradients. The water table is laterally planar beneath the southern hummocks where no localized groundwater mounds were observed. Instead, a flow-through system has developed with a water table that fluctuates at, or rises above, ground surface in the wetlands consistently throughout the study period (Figure 12; Appendix B). The groundwater flow system is largely driven by horizontal hydraulic gradients that likely originate from a groundwater divide below 318 Berm, south of the study area, contributing to predominantly horizontal groundwater flow; this indicates the true extent of the watershed extends slightly beyond the boundary of the study area formally defined as Sandhill Watershed. Given that vertical hydraulic gradients are intermittent and variable, vertical flow is likely to be negligible when hydraulic conductivities are also considered (Appendix B).

In general, the surface water quality in the lowlands is within tolerable ranges for natural boreal vegetation (<2,000 μS/cm; Howat, 2000). The groundwater in the east wetland stays below 2000 μS/cm, except following short periods of influx or outflux (*e.g.,* nests 66 and 69; Figure 11); the groundwater in the west wetland has elevated EC more often (*e.g.,* nest 15; Appendix C). Areas with shallow water tables below ground surface (WL <1.8 m BGS) are generally found along the periphery of the lowlands, as well as sloping topography in the uplands, all of which tend to have higher ECs throughout the water column (Figure 12; Appendix C). By comparison, the water column in upland areas with deeper water tables (WL >1.8 m BGS) tends to have a vertical geochemical gradient of freshwater (*i.e.*, derived from recharge) mixing downward into underlying OSPW (Figure 14). This freshwater lens is particularly evident in the southern uplands, adjacent to 318 Berm on sloping terrain, and below larger hummocks and tend to coincide with the coarse topsoil and subsoil prescriptions (Appendix C). Inflows and outflows to the groundwater flow system temporarily affect the water quality (*i.e.*, as indicated by EC) in the watershed (Figure 12); however, the water quality returns to pre-event levels shortly thereafter (Figure 11).

Given the current availability of fresh groundwater in the lowlands of SHW, watershed designers have successfully created a watershed that developed a shallow, freshwater flow system (albeit without localized mounding) that can provide an adequate supply of fresh groundwater and surface water to the reclaimed environment. The broader goal for SHW was to develop an understanding of the physical processes that have influenced the resulting hydrogeology of the watershed, and evaluate their relative importance, such that conceptual models could be developed for anthropogenic watersheds reconstructed from coarse-textured materials. In order to provide recommendations for future reclamation in post-mining landscapes, it necessitates a thorough understanding of the drivers and mechanisms that have caused the groundwater system to develop in the manner it has.

4.1. Groundwater Flow System

Based on the observed field conditions and simulated groundwater flow system, the horizontal hydraulic gradients in SHW appear to be driven by the up-gradient topographic high, 318 Berm, south of the study area, which is likely coincident with a groundwater divide (*i.e.*, divide axis oriented parallel to southern boundary of SHW). The primary groundwater flow path (S-E) was engineered to curve through SHW from Hummocks 7 and 8 towards KFW by utilizing differences in hydraulic conductivities between the watershed's tailings sand and the adjacent shale along the western and northern edges of the former mine (EIP). The groundwater flowing through the northern boundary (S-N flow path) is likely being diverted through high K materials (*i.e.*, buried gravel channels) located beyond the northern extent of the former mine. Limited borehole data are available beyond the extent northern extent of EIP; those that are available suggest there may be localized gravel channels into which shallow groundwater from the former mine flows (D. Heisler, SCL, pers. com.). The groundwater system is therefore influenced by the broader, intermediate topography (318 Berm), rather than local hummocks, in conjunction with contrasting hydraulic conductivities between watershed tailings sand and surrounding geology.

The hydraulic gradients in the watershed vary between the uplands and lowlands, both horizontally and vertically (Figure 10). The horizontal gradients in the uplands are laterally planar and steep, relative to the subtle gradients observed in the lowlands. The abrupt break in the steep slope of the water table in the southern uplands coincides with the topographic transition from uplands into the lowlands (Figure 10). The water table fluctuates near ground surface in this transitional zone throughout the study period, at times intersecting ground surface (Figure 11). These areas are essentially seepage faces (*i.e.*, discharge areas) across which horizontal hydraulic gradients drive groundwater movement. In hummocky terrain, the extent of these discharge areas is limited to where the water table coincides with the toe of the hummock. The water table is shallow below ground surface and fluctuates the most in these areas. In areas with gently sloping topography, the seepage faces are more diffuse; the water table fluctuates near ground surface over a more extensive area.

Overall, the watershed is an unconfined aquifer, aside from discrete areas that exhibit temporary confining, or perched, conditions around the perimeter of the lowland (*i.e.*, nest 23 and nest 60, respectively). Nests at the toes of hummocks (nests with A/B/C/D piezometers) were completed in the lowlands, and have piezometers screened above the clay (A piezometers), in the clay (B piezometers) and below the clay in tailings sand (C/D piezometers). Some areas demonstrated vertical hydraulic gradients indicative of confining conditions across the clay layer (*e.g.,* nest 23; Appendix B); in other areas, the water table does not contact the clay layer, remaining in the tailings sand, creating unconfined conditions (*e.g.*, nest 14). Therefore, while vertical gradients exist, the overall flow across the clay is considered negligible when the duration of the gradients and the hydraulic conductivity of the compacted clay along the periphery of the watershed are considered. Furthermore, these transition areas may have lower hydraulic conductivities than the more central lowland areas where the clay is permanently saturated (Benyon, 2014).

Although the entire lowland was intended to develop into a wetland, small-scale variations in topography, and potentially outflows through the northern boundary, resulted in two persistent standing bodies of water (east and west wetlands); the areas between and adjacent to these wetlands may develop into terrestrial environments (Vitt et al., 2016). Overall, throughout the study period, the lowlands tended to have highest annual water levels occurring early in the field season, which then declined progressively through October (Figure 11a). Of the 17 ha lowlands, the maximum and minimum extent of the standing water/saturated soils during the study period was 17.0 and 4.9 ha (June 3, 2017 and October 25, 2015, respectively), while the maximum and minimum extent of standing water in the lowlands was 13.1 and 1.3 ha (same dates, respectively; Appendix D).

The influence of atmospheric and managed fluxes on the water table configuration was observed through the study period. In 2015, outfluxes were dominated from by AET and groundwater pumping (ignoring groundwater inflows and outflows), resulting in a gradual decline in water levels through fall and the lowest water levels observed in the watershed throughout the study period. During 2016, influxes due to snowmelt and rainfall dominated, leading to higher water levels than the year previous; water levels at the end of the 2016 field season were approximately the same as at the start of the field season. This led to particularly high water levels for the start of the 2017 field season. While outfluxes (*i.e.,* pumping) were greater than influxes in 2017, the fluxes were more balanced than previous years; therefore, water level changes due to pumping were likely buffered by incoming precipitation. Regardless, following pumping, water levels gradually declined, responding similarly to the pumping event in 2015.

Groundwater recharge values demonstrated higher recharge rates in areas with coarse-textured top/subsoils than areas with fine-textured top/subsoils, ranging from 40 to 88 mm/y in the upland areas for 2015 (Table 2; M. Lukenbach, unpublished data.). Given that the groundwater system is driven by hydraulic gradients originating from the groundwater divide below 318 Berm, the magnitude of recharge contributed within SHW is smaller than what is contributed by the greater area of 318 Berm (Table 2; Table H-4). The groundwater model indicates 20% of the total water budget inputs are attributed to net-recharge across the entirety of SHW. Because these are net-recharge values (*i.e.*, recharge minus AET), actual recharge in SHW is under-represented here due to AET losses in the wetland being included. Furthermore, because all groundwater is sourced from recharge, the watershed is highly responsive to changes in recharge, as is evident from sensitivity analyses where the uplands (below hummocks) and the wetlands are most sensitive to changes in atmospheric fluxes (Figure 16).

4.2. Solute Distributions & Dynamics

The groundwater flow system in SHW is dynamic, rising and falling in response to daily and seasonal fluxes into and out of the watershed, which directly influences the spatial and temporal distribution of solutes in groundwater and surface water (Figure 11). Understanding what causes solute distributions in the landscape is difficult, given that the existing installations do not consistently sample at the same depth into the water column. This becomes especially problematic where a vertical geochemical gradient exists. Thus, to adequately characterize the observations, each piezometer was assigned to one of six groundwater classes based on the average depth of the water level relative to ground surface, and the average midscreen depth of the piezometer relative to the water level observed in the piezometer. This classification is outlined in Figure 6 and explained in detail in Appendix G.

Since 2012, the groundwater system has been exposed to recharge via rainfall and snowmelt and, to a lesser degree, managed freshwater influxes (*i.e.,* pumping). These influences led to the development of a shallow groundwater system with a thin freshwater lens overlying, and gradually mixing into, the underlying concentrated OSPW. In general, electrical conductivity increases with depth in the groundwater column, and tends to be higher in uplands compared to the wetlands throughout the study period (Figure 12).

The wetlands in the central lowlands are frequently wetted due to daily and seasonal precipitation; therefore, total dissolved solids (*i.e.,* electrical conductivity) are likely diluted and buffered by rising water levels that frequently result in standing water and saturated soil conditions (Appendix C). This differs from the periphery of the lowlands, where the lowlands transition to the uplands, and upland areas with shallow water tables (WL <1.8 m BGS); the water tables do not frequently rise above ground surface, if at all. Consequently, these peripheral soils are not flushed during rain events like those soils in the centralized areas of the wetlands. Instead, the soil in these areas gradually accumulate solutes, likely through cycles of evapoconcentration due to shallow water table fluctuations, which may be entrained in stagnant pore water during periodically high water levels and mobilized to down gradient areas in the watershed. Finally, in the uplands, where water tables are generally deeper below ground surface (WL >1.8 m BGS), the groundwater at the water table is likely freshened by recharge (Appendix C).

The geochemistry was used to elucidate the causes of the distribution of solutes associated with shallow/deep water levels relative to ground surface and shallow/deep midscreen locations relative to the water level (Appendix E). Temporally, groundwater chemistry (*i.e.*, major ion proportions) remains generally consistent at each location in a given area, across annual sampling campaigns (Figure 13a/b). Spatially, the proportion of major ions varies across sampling locations, ranging from OSPW dominant (Na^+ Cl^-/SO_4^{2-} groundwater), to a mixed water type plotting away from the MLR and OSPW endmembers. Samples from surface water and artesian piezometers (exclusively located in the wetland) have a mixed groundwater composition. Samples from the deepest groundwater relative to the water table indicates the highest proportion of OSPW in the watershed (*i.e.*, MS >1.8 m BWL), regardless of the water level position relative to ground surface (*i.e.*, shallow/deep and deep/deep groundwater); though, some deep/deep groundwater indicates mixing away from OSPW endmember. The shallowest water sampled relative to the water table (*i.e.*, MS <1.8 m BWL) tends to have the highest variability in ion proportions; shallow groundwater (relative to the water table) ranges from OSPW dominant to mixed water, regardless of the depth of the water table below ground surface (*i.e.*, shallow/shallow, deep/shallow).

Given that water sampled near the water table (MS <1.8 m BWL) shows variably mixed water chemistry with OSPW and can have elevated ECs, stable water isotopes were used to determine whether the concentrated solutes in the shallow water table were truly mixed with OSPW, or if solute distributions were being influenced by other factors (*e.g.,* soil storage, attenuation, transformations). Stable water isotopes indicate water sampled from the water column, just below the water table (shallow/shallow and deep/shallow), in hummocks is predominantly comprised of rain water and is, at most, moderately mixed with OSPW (Figure 14a; Appendix F). This is likely the result of gradually diluting residual OSPW pore water with incoming recharge from precipitation. In the slopes, shallow groundwater is predominantly comprised of OSPW (shallow/shallow) with far less recharge than hummocks (except for the water sampled from deeper water tables; deep/shallow). Pairing these data with the Na^+ mixing line, groundwater in the slopes is predominantly comprised of OSPW mixed water, and groundwater in the hummocks do not mix linearly between OSPW and MLR, likely attributable to the incoming recharge (Figure 14b).

Areas with elevated EC and Na^+ have previously been described as "hot spots" attributed to upwelling of OSPW (Biagi et al., 2018); however, vertical gradients appear to be negligible overall. The groundwater flow system is predominantly driven by horizontal gradients, as confirmed by the groundwater simulations, which integrates physical processes across the site; therefore, it follows that groundwater with elevated EC, Na^+ and $\delta^{18}O$ compositions (indicating OSPW endmember mixing), are primarily associated with residual OSPW that was stored in the tailings sand and now discharges laterally across the seepage face. Given that the water table fluctuates within/across these seepage faces, and slowly declines (in general) through the field season, solutes could potentially accumulate in the pore spaces of the intermittently saturated zone through cycles of evapoconcentration. Then, during periods of rain water influx, rapid water table rises associated with groundwater ridging may force out pre-event water (Gillham, 1984), leading to elevated EC "slugs" moving through the system, entraining concentrated pore water solutes once again through subsequent dissolution. The larger groundwater system will continue to laterally discharge residual OSPW (solutes) from the tailings sand to these seepage faces, with negligible relief from incoming recharge due to the rooting zone intersecting the water table in these areas (Lukenbach et al., 2019).

The effect of different recharge rates on EC distributions in the uplands, due to various soil prescriptions, was evident when comparing groundwater quality below Hummock 7 and Hummock 9; both of which have water tables further below ground surface over larger areas and similar flow paths, but have different cover prescriptions (*i.e.*, coarse- and fine-textured soils, respectively). Groundwater below Hummock 7 has some of the lowest EC values of the upland areas in the south, whereas Hummock 9 consistently has some of the highest EC values in the entire watershed (Appendix C). This indicates the watershed is sensitive to recharge, given that EC distributions in shallow groundwater are very dynamic throughout the field seasons and across the study period.

The lowlands were specifically developed to have shallow water tables (or standing water) relative to land surface; however, EC, Na^+ or $\delta^{18}O$ values indicate OSPW is not concentrating in any location specifically within in the wetlands, or at depth; this is only occurring along the periphery of the lowlands (*i.e.*, nests with A/B/C/D piezometers). Given that the extent of the standing water and saturated areas in the watershed are highly variable within a single field season (Figure 12) and highly responsive to fluxes in and out of the watershed (Appendix D), the soils in the lowland show greater potential for dilution and flushing than upland soils that will never be saturated.

4.3. Watershed Design

SHW is one of the first permanent reconstructed watersheds built at the industrial scale, with the greater intent to test and evaluate the influence of landform designs and materials on the subsequent groundwater system. The landscape design, construction materials and location within the regional climate were all instrumental in facilitating the development of the groundwater flow system and geochemical distributions within SHW. Hummocky terrain surrounding the lowlands promoted recharge to freshen and source water for the wetlands in the lowlands, which would eventually grow to buffer groundwater availability in the sub-humid climate. While constructing an unmanaged, self-sustaining watershed would be ideal, water management infrastructure was necessary to ensure this watershed would progress beyond initial reclamation so that the influence of the watershed's design on the groundwater flow system and the overlying reclaimed environment could truly be evaluated.

Hummocks were constructed at various heights and areal extents to assess their potential for groundwater recharge and were intended to develop local mounded flow systems with the adjacent lowlands (Figure 3). The primary material used to construct the watershed and hummocks was fine-grained tailings sand, which is relatively homogeneous, and ranges from isotropic to anisotropic between the mechanically-placed and hydraulically-placed materials, respectively (Benyon, 2014; Longval and Mendoza, 2014; Thompson et al., 2011). Between the moisture limited climate, various hummock heights and areal extents, and the hydraulic conductivity of the tailings sand (and thin veneer of top and subsoils; Table H-1), the hummocks appear to recharge groundwater (*e.g.*, evidence from precipitation isotope signatures below uplands; Figure 14) but does not appear to be in sufficient quantity to support local, mounded flow systems (Figure 10). Instead, groundwater predominantly flows horizontally along longer, intermediate flow paths driven by the groundwater mound below 318 Berm through the north and east boundaries of the watershed (Figure 10; Appendix B).

Given the variability in the water levels, geochemistry and topography along the southern uplands, the implications of developing hummocks of various sizes, with various slopes, should be addressed. The upland areas that appear to have the greatest potential for recharge are associated with deeper water tables (Figure 14). A freshwater lens has developed in these areas, although it appears to be thin and grade steeply into OSPW dominant groundwater within the first 1.8 m (*e.g.*, nests 31 and 41; Figure G-6). Other hummocks do not demonstrate this gradient; instead, OSPW is mixed throughout the water column (*e.g.*, nest 39; Figure G-6). In these areas, the areal extent and height of the hummock are much smaller and the hummocks are surrounded by large areas with shallow water tables (*e.g.*, Hummock 8 adjacent to sloping terrain; Figure G-6). Finally, upland areas without hummocks (*i.e.*, slopes) demonstrate a much higher degree of freshwater mixing with OSPW, particularly where the water table is shallow or along seepage faces (Figure 14b).

Overall, broader hummocks that are laterally extensive, low to moderate in height (scaling to ensure water table is approximately 2 m BGS) and with steep slopes near the transition to lowlands, appear to be an idealized design for developing fresher, shallow groundwater systems (Figure 17). Broad hummocks are better suited for recharging reclaimed landscapes compared to smaller hummocks and sloping terrain, given that broad hummocks have greater potential for recharge, by limiting root water uptake, and limiting the areal extent of "hotspots" or seepage faces to the toe of the slope. By applying this information and using concepts from Haitjema & Michell-Bruker (2005), that incorporate hydraulic conductivity, recharge, and extent of upland areas, reclamation designers can develop idealized hummocks that manage atmospheric fluxes and solutes in boreal reclaimed environments simply by design.

Beyond the hydrogeological challenges of properly placing tailings sand in a watershed, designing and constructing watersheds requires vast volumes of materials which may be expensive to place and contour; over 430,000 m^3 of tailings sand were used to construct SHW. Therefore, the volumes of materials used in landscape reconstruction must be optimized from both reclamation and financial standpoints. From this, the concept of "goldilocks" hummocks emerges, where hummock height and areal extent are balanced to promote recharge (*i.e.,* reducing losses to vegetation through root water uptake), thereby also reducing excess placement of materials that would otherwise reduce groundwater recharge (*i.e.*, increase distance to water table and increase soil storage; Lukenbach et al., 2019). Hummock 7 has a freshwater lens near 318 Berm with water tables as deep as 8 metres below ground surface; decreasing the height of this hummock by a few metres would shorten the travel time of recharge through the unsaturated zone, and allow longer, broader hummocks to be placed with the excess materials and increasing the area contributing to groundwater recharge. In summary, developing watersheds with broad “goldilocks” hummocks with steep slopes at the upland-wetland interface, where the wetland occupies all of the lowland, increases groundwater recharge, thereby minimizing the concentration of OSPW solutes at the water table, while reducing the areal extent of seepage faces that concentrate OSPW near land surface.

Chapter 5: Conclusions

A primary purpose of this study was to perform a full hydrogeological characterization of a reconstructed watershed for the 3- to 5-year period following construction, reclamation and revegetation. This work complements and expands upon previous studies on surface water dynamics in SHW by providing insights into how the groundwater system has developed over the years following reconstruction and reclamation. A comprehensive field monitoring program was used to assess groundwater and solute movement through the landscape during the years 2015 to 2017.

Following reclamation, SHW developed a shallow groundwater flow system that flows northward into the study area, from a groundwater divide in 318 Berm, through to Sandhill Berm and KFW in the East, with some flow diverging north. The difference between hydraulic heads in 318 Berm and the lowlands of SHW results in a groundwater flow system dominated by horizontal hydraulic gradients. Average vertical hydraulic gradients were generally weak throughout the watershed, including discharge areas, because their directions often fluctuated and were temporary. Consequently, the horizontal groundwater flow often leads to discharge to the lowlands though seepage faces.

Geochemical, EC and stable water isotope data consistently show that groundwater deeper than 1.8 m below the water table is predominantly comprised of OSPW. In areas where the water table is regularly found at depth (deep WL; WL >1.8 m BGS), the chemistry of the groundwater within 1.8 m of the water table has a higher proportion of freshwater, indicative of groundwater recharge and the development of a freshwater lens. The chemistry of the groundwater within 1.8 m of the water table becomes more mixed with OSPW solutes as the water table transitions from deep (WL >1.8 m BGS) to shallow (WL <1.8 m BGS). However, once the water table regularly fluctuates at, or above, ground surface (resulting in intermittent standing water), the water becomes fresher, regardless of the depth at which it is sampled.

Transition areas from uplands to lowlands are not always directly adjacent to wetland areas, (*i.e.,* they are on the perimeter of the lowlands). Water discharging through seepage faces in these areas may be subject to evapoconcentration during dry periods, leading to an accumulation of water with elevated solute concentrations. The groundwater is highly responsive to influxes and outfluxes of water (natural and managed fluxes), particularly in areas with shallow water tables or standing water; therefore, solutes that concentrate in the pore spaces of sediments with shallow water tables may be easily mobilized during and following precipitation or snowmelt events, affecting newly reclaimed wetland vegetation. This phenomenon may explain previous observations of hot spots of high solute concentrations within the wetlands.

The greater research purpose for the design and development of SHW was to evaluate how the materials and landscape design affect the resulting groundwater system, and how to improve future designs; therefore, understanding how solutes move and accumulate in the watershed through groundwater movement is paramount. Since hotspots are associated with areas that have shallow water tables relative to ground surface that do not experience frequent flooding (Appendix D), it would follow that, when developing a fresh groundwater system intended to support boreal wetland vegetation, the landscape design should reduce the overall areal extent of topography with shallow water tables (WL <1.8 m BGS). Furthermore, if the distance between the water table and land surface (*i.e.,* vegetation rooting zone) is great enough, losses to AET could be reduced such that influxes can supply more freshwater to the groundwater system.

Where tailings sand, which contains residual OPSW, is used as the primary construction material, future reclamation planners and watershed designers could develop watersheds that promote groundwater recharge by constructing hummocks that are broader in areal extent and are more moderate in height (relative to the anticipated water table) than those in SHW. Hummocks should also have steep slopes at the upland-lowland transition, and wetlands should occupy most of, if not all of, the lowlands to reduce the area exposed to shallow fluctuating water tables, thereby further reducing movement of OSPW.

SHW is slowly becoming established with taller wetland and forestland vegetation each year. The shallow groundwater and surface water are within an acceptable EC range for reclaimed vegetation and is in adequate supply in the lowlands throughout the study period. While the watershed becomes enriched with solutes during major flux events (*e.g.*, extreme rainfall in 2016 or pumping in 2017), the groundwater quality returns to background solute conditions soon thereafter.

In subsequent years following this study, evapotranspiration demands will likely increase as vegetation continues to develop. This has the potential to reduce recharge in the watershed (at minimum, assuming incoming precipitation remains similar), which has been shown via groundwater modelling to lower water table elevations in higher, upland positions and the lowlands throughout the watershed. While the deeper groundwater in the uplands has the potential to remain fresh, as beneath Hummock 7, lower water tables in the wetlands may result in solutes concentrating through evapoconcentration if the soils are not regularly inundated with standing water. As a result, the wetlands could begin to develop EC concentrations similar to those currently observed in slopes.

While SHW currently has a water table that fluctuates near ground surface in the lowlands, the successional trajectory of wetland may be at the mercy of future weather and climate. Within the period of study, the lowlands could be almost entirely covered with standing water during wet periods (June 2017; Appendix D), but during dry periods the standing water was almost gone (October 2015; Appendix D). If dry conditions persisted, the wetlands would likely gradually become enriched with OSPW. Therefore, ensuring that reclaimed wetlands are frequently wetted will help to mitigate the concentration of solutes in the lowlands. Watershed managers may achieve this using a weir, with a spill point at which water will be removed from the watershed during periods of moisture surplus. Alternatively, managers may construct a dyke similar to Sandhill Berm, but with lower hydraulic conductivities to reduce overall losses from the watershed.

This work has been invaluable in testing hydrogeological conceptual models for coarse-textured hydrologic response areas that were developed from studying natural boreal analogues (Devito et al., 2012, 2017; Hokanson et al., 2019). Oil sands mining companies have demonstrated that watersheds can be constructed to develop favorable groundwater flow systems to support wetland vegetation; however, the effects of long-term cycles of moisture surplus/deficit associated with the sub-humid climate may affect the trajectories of these reclaimed landscapes, particularly due to their sensitivity to recharge. Therefore, future watersheds should be designed to include broad, steeply sloped hummocks of moderate heights to balance atmospheric influxes and outfluxes through periods of moisture excess or deficit, without sacrificing the quality of groundwater available to the reclaimed wetlands. Steep interfaces with lowlands should be constructed such that seepage faces over broad slopes are avoided to minimize evapoconcentration effects.

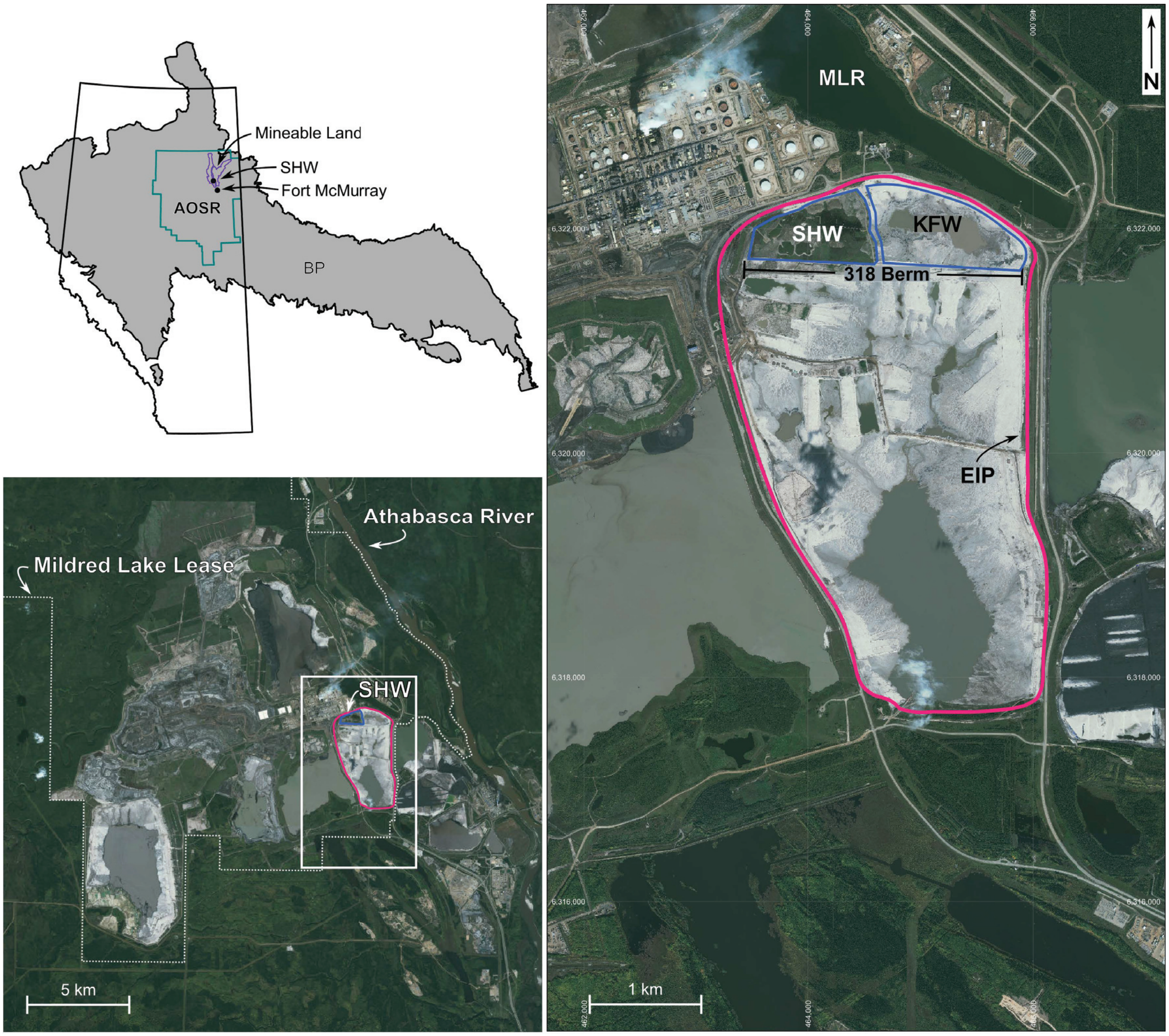

Figure 1: Sandhill Watershed (SHW) is located in the Athabasca Oil Sands Region (AOSR) in the Boreal Plains (BP) ecozone in Alberta. SHW is constructed on a composite tailings deposit (East In-Pit; EIP) on Syncrude's Mildred Lake Lease. SHW is separated from the southern portion of EIP by 318 Berm and will function in tandem with Kingfisher Watershed (KFW) in the final mine closure landscape. Mildred Lake Reservoir (MLR) is a fresh water reservoir that supplied water to SHW following construction.

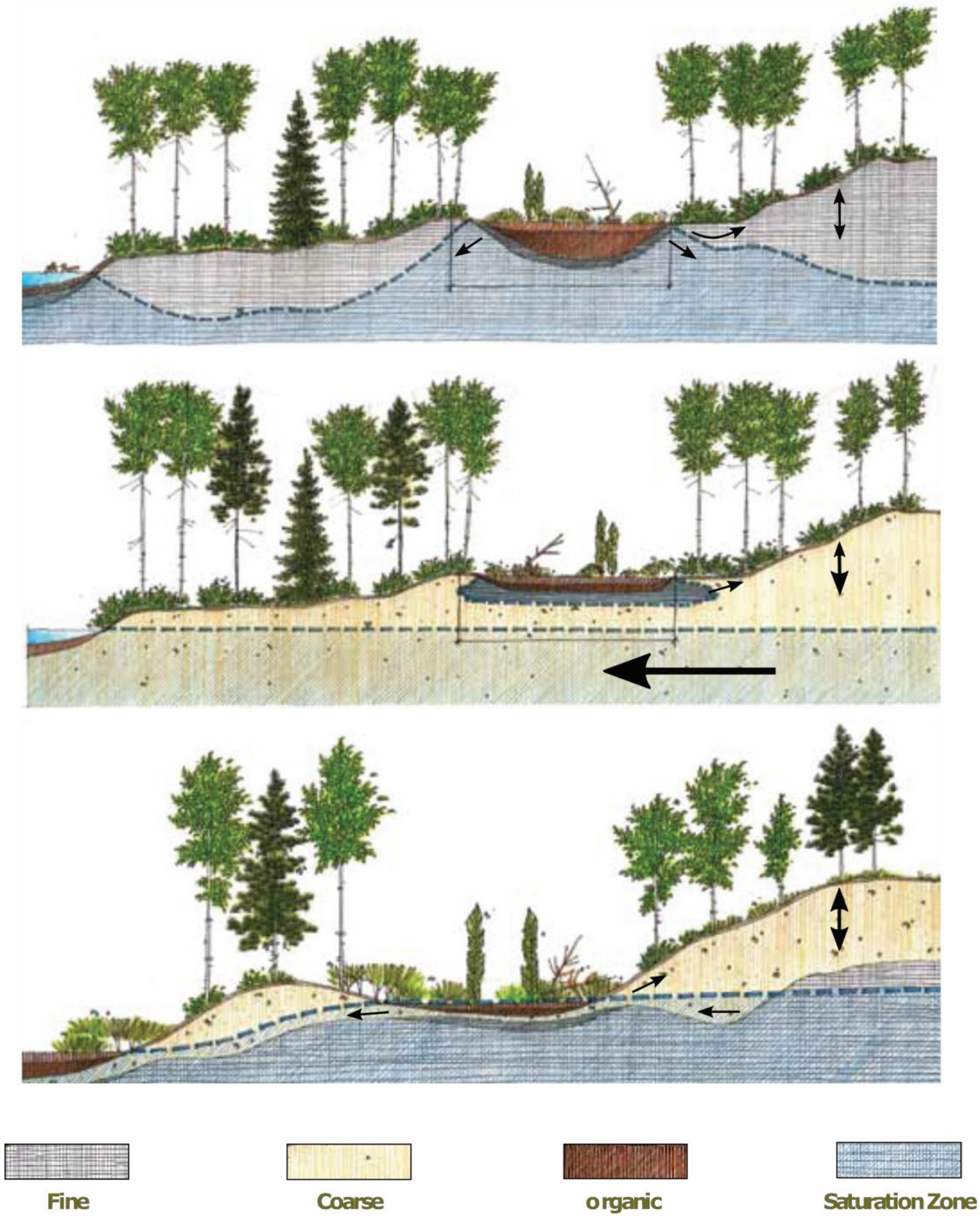

Figure 2: Hydrogeological conceptual model for hydrologic response areas (HRAs) in the Boreal Plain (descending): fine-textured, coarse-textured and veneer (coarse- over fine-texture). Forest and wetland hydrologic units (HUs) depicted. Dashed line represents the water table, arrows indicate flow direction and relative magnitude (adapted from Devito et al. 2012).

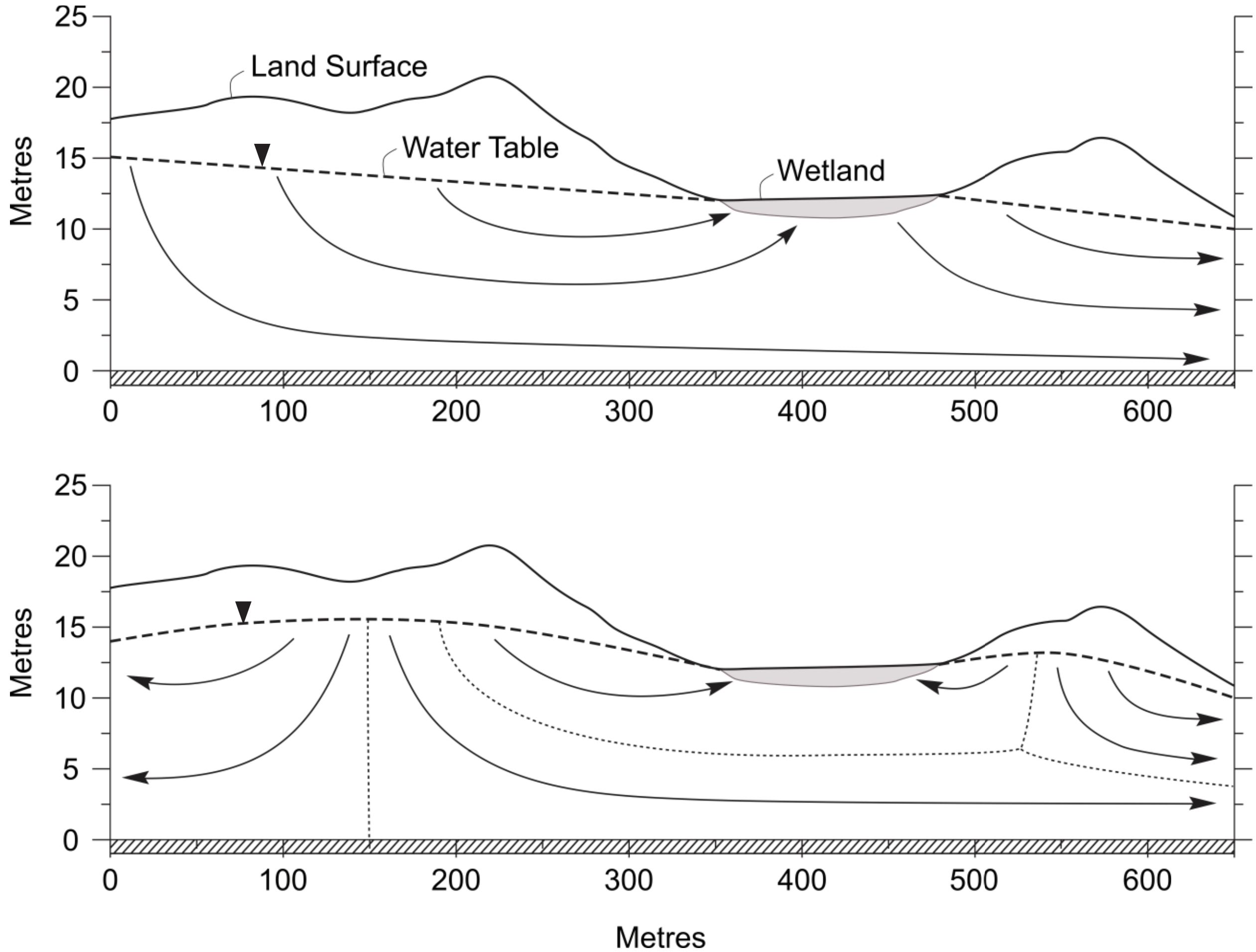

Figure 3: Hydrogeological conceptual models for two potential flow systems in a reconstructed watershed: an intermediate type of groundwater flow system (upper) with deeper groundwater flow paths that discharge in the wetland, and localized groundwater flow systems (lower) with shallow groundwater flow limited to the near surface and negligible groundwater discharge from deeper within the deposit. Lower boundary represents contact between composite tailings deposit and overlying tailings sand watershed. Groundwater movement in landscapes were adapted from Winter (2003).

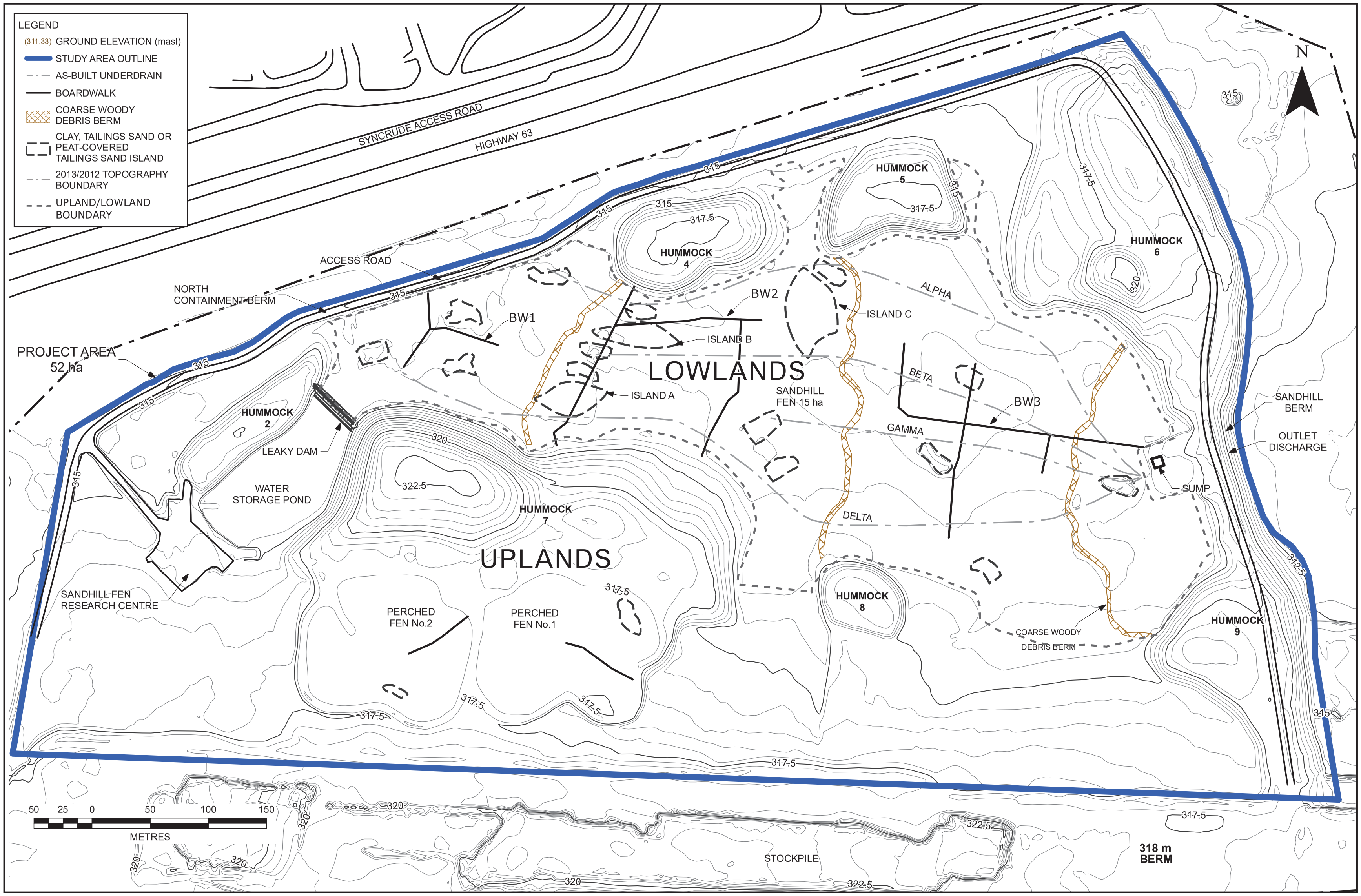

Figure 4: Topographic map of SHW with various infrastructure, topographic regions and design characteristics annotated (UTM Zone 12).

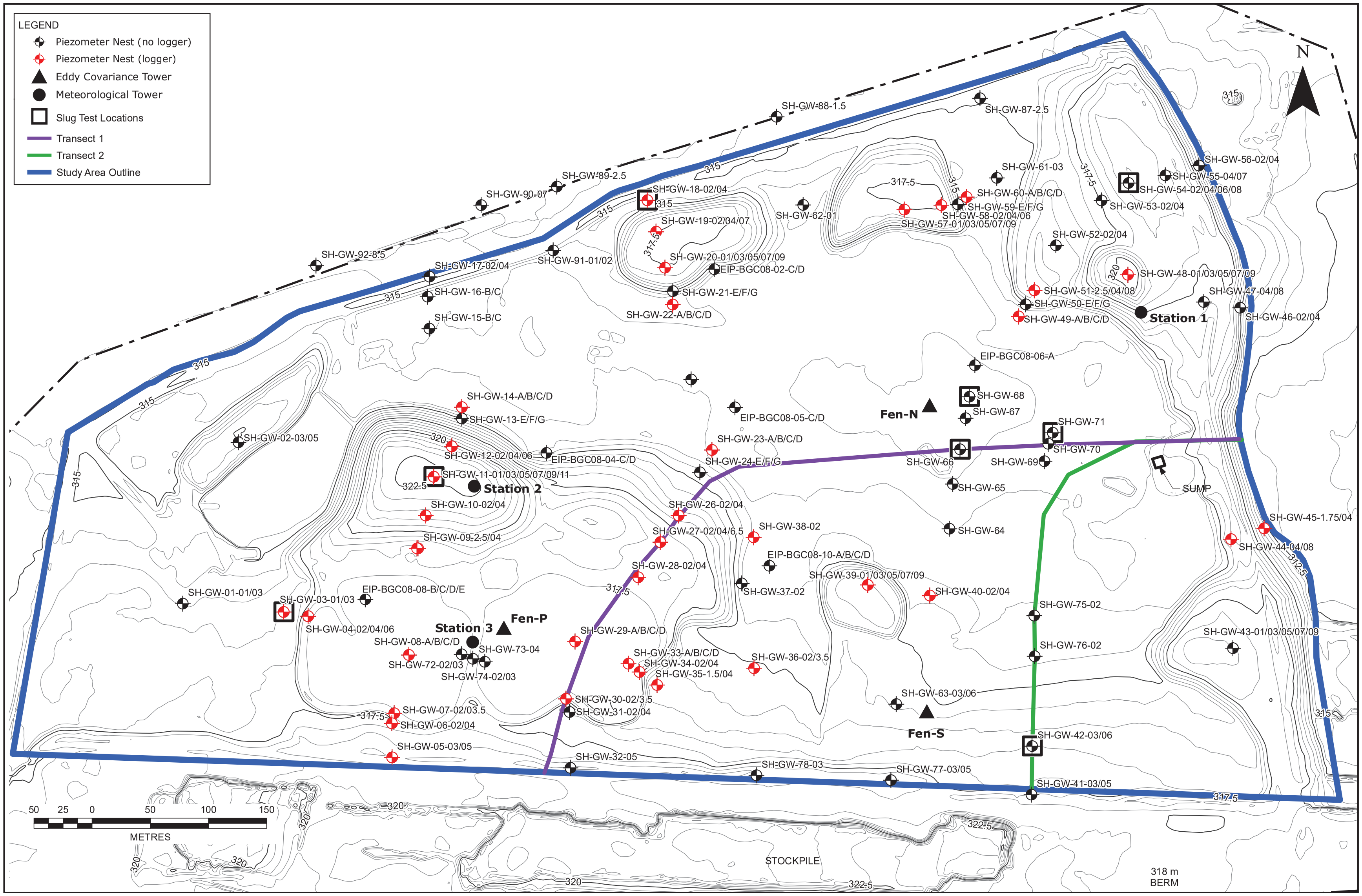

Figure 5: Site map of SHW (blue) with piezometer nests (with and without loggers), eddy covariance and meteorological tower locations. Transect 1 and Transect 2 correspond with different topographic configurations in the watershed, hummocks to wetlands, and slopes to wetlands, respectively. Boxes indicated locations where slug tests were performed.

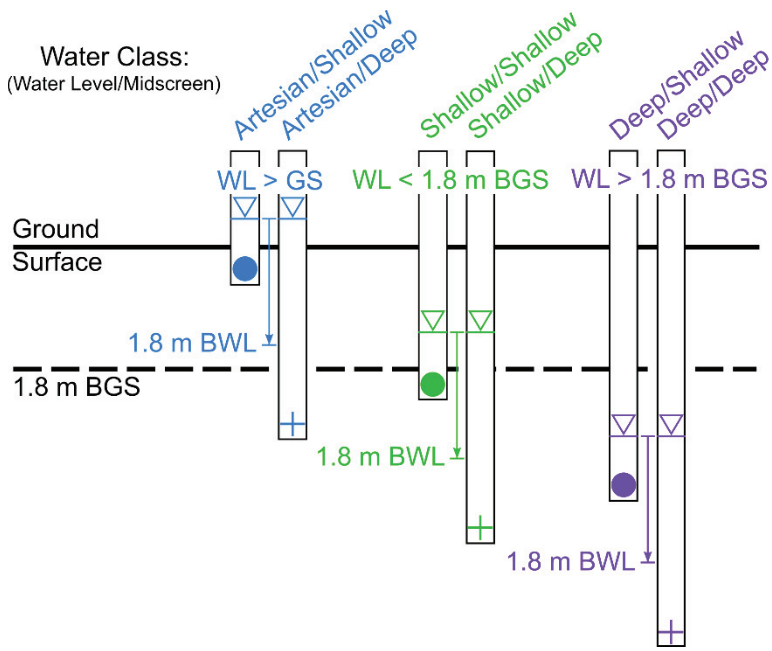

Figure 6: Conceptual diagram outlining 6 water classes defined by the depth to water level relative to ground surface (symbol color), and the depth of the midscreen relative to the water level (symbol shape). Specifically, symbol color indicates water level (WL) elevation in pipe below ground surface (BGS): blue (artesian = WL >GS); green (shallow = WL <1.8 m BGS); purple (deep = WL >1.8 m BGS). Symbol shape indicates midscreen (MS) elevation (i.e., sampling location) below water level (BWL): ● (shallow = MS <1.8 m BWL); + (deep = MS >1.8 m BWL). The symbology (color/shape) will remain consistent in subsequent figures to assist in water level, isotope and geochemical interpretation of groundwater collected from piezometers in the tailings sand (SH-GW piezometers).

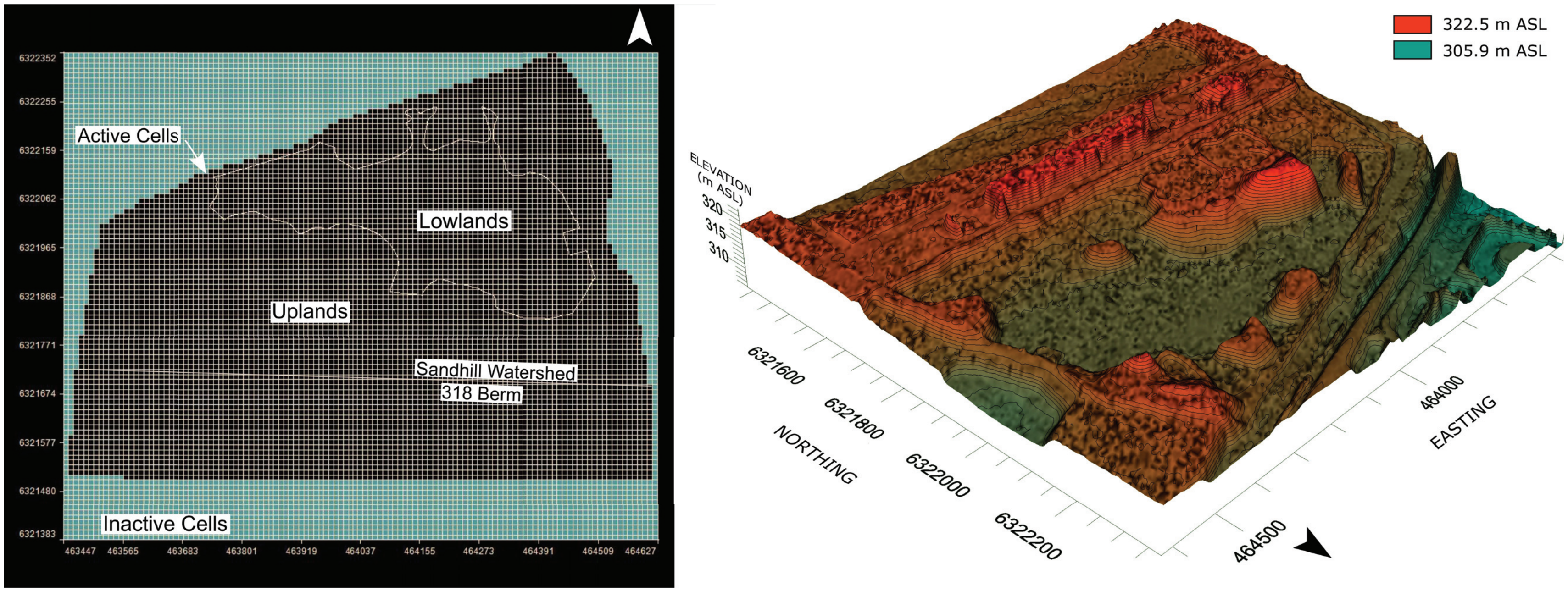

Figure 7: SHW numerical groundwater model domain and grid (left) with topography of the entire domain determined by LiDAR (right, UTM Zone 12, 10xVE; Syncrude Canada Ltd.). Uplands and lowlands are outlined, arrow indicates north. Model details are provided in Appendix H.

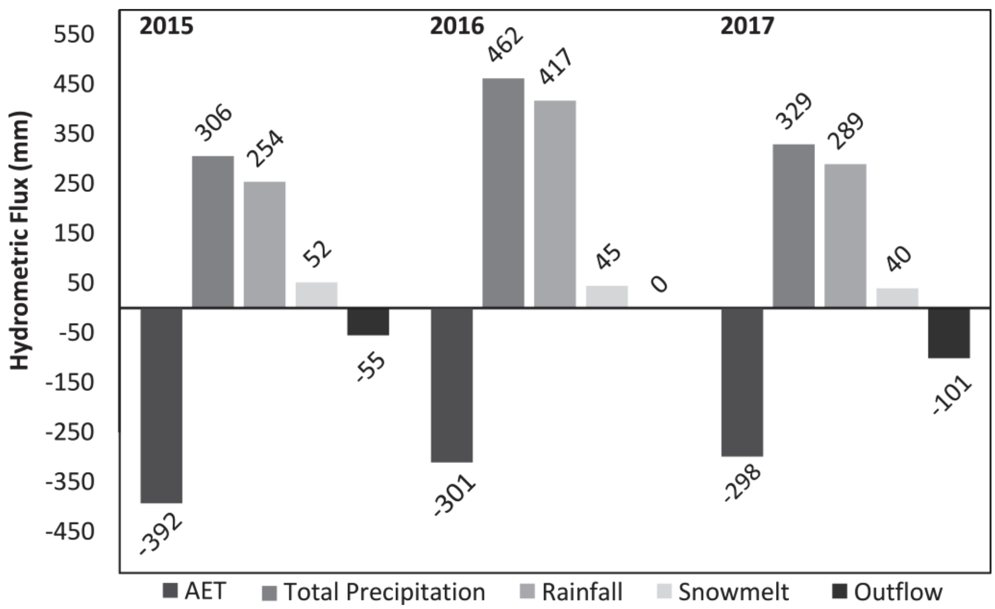

Figure 8: Annual hydrometric fluxes (mm) plotted for SHW for January 2015 to December 2017 (inclusive), with total actual evapotranspiration (AET; Lukenbach et al., 2019; S. Carey, unpublished data), total precipitation (rainfall and snowmelt, also shown separately), and managed outflows (via sump; Nicolls et al., 2016; K. Biagi, unpublished data) from watershed. Negative values indicate water removed from watershed.

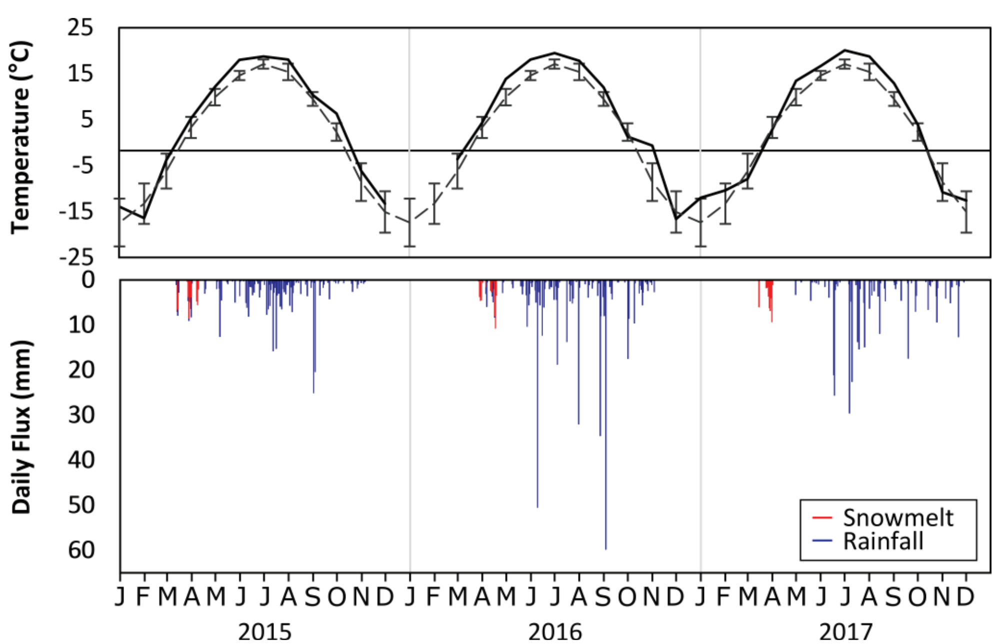

Figure 9: Monthly average temperatures (top) for SHW (solid black) and Fort McMurray Climate Normal data (dashed grey with standard deviations; Environment Canada, 2019), paired with a hyetograph (bottom) including snowmelt (red; M. Lukenbach, unpublished data) and rainfall (blue; O'Kane Consultants Inc.) from January 2015 to December 2017 (inclusive). Note data gap in winter 2015/2016 temperatures. Snowmelt and rainfall data are stacked where both occurred in a day. Only meteorological data from Station 1 are presented.

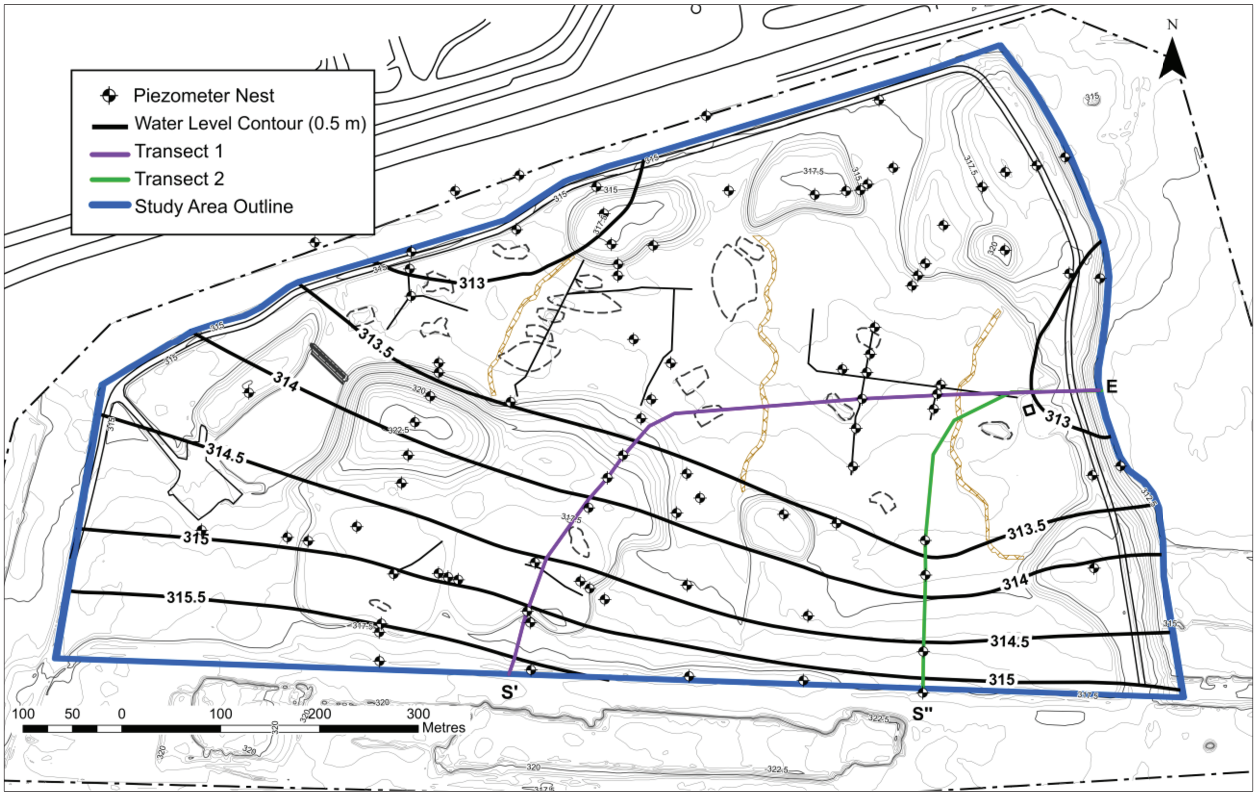

Figure 10: Topographic map of SHW (outlined in blue) with water table configuration (black contours in m ASL) for July 7, 2017. Water levels from shallowest piezometers with groundwater were used. Transects included for reference. Labelled infrastructure provided in Figure 4.

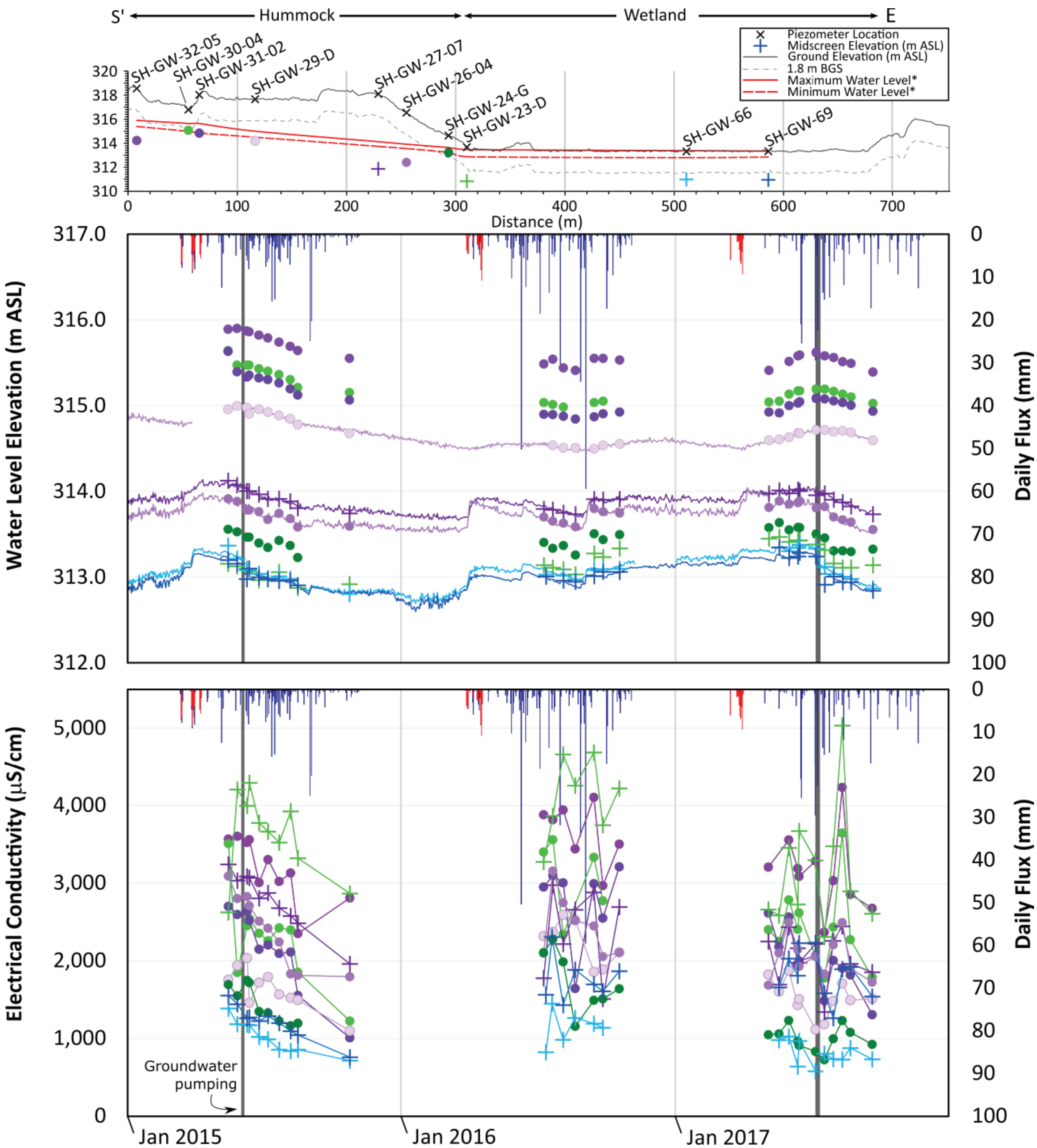

Figure 11a: Cross section paired with hydrographs (hydraulic head vs time), EC temporal plots (EC vs time) and daily flux data for Transect 1 from January 2015 to December 2017 (inclusive). Cross section demonstrates landscape position of piezometers with midscreen elevations, maximum and minimum manual water level measurements observed during the study period at each individual location. Point data in the hydrograph and temporal plot are manual measurement data; lines in hydrograph are continuous automated data (nest 66 and 69 provided by Carey, unpublished), and lines in EC temporal plots are to assist in interpretation (*i.e.,* not continuous data). Grey bar represents pumping event duration. Point data color and symbology are explained in Figure 6; line for 1.8 m below ground surface for reference only. Details for daily flux data are outlined in Figure 2.

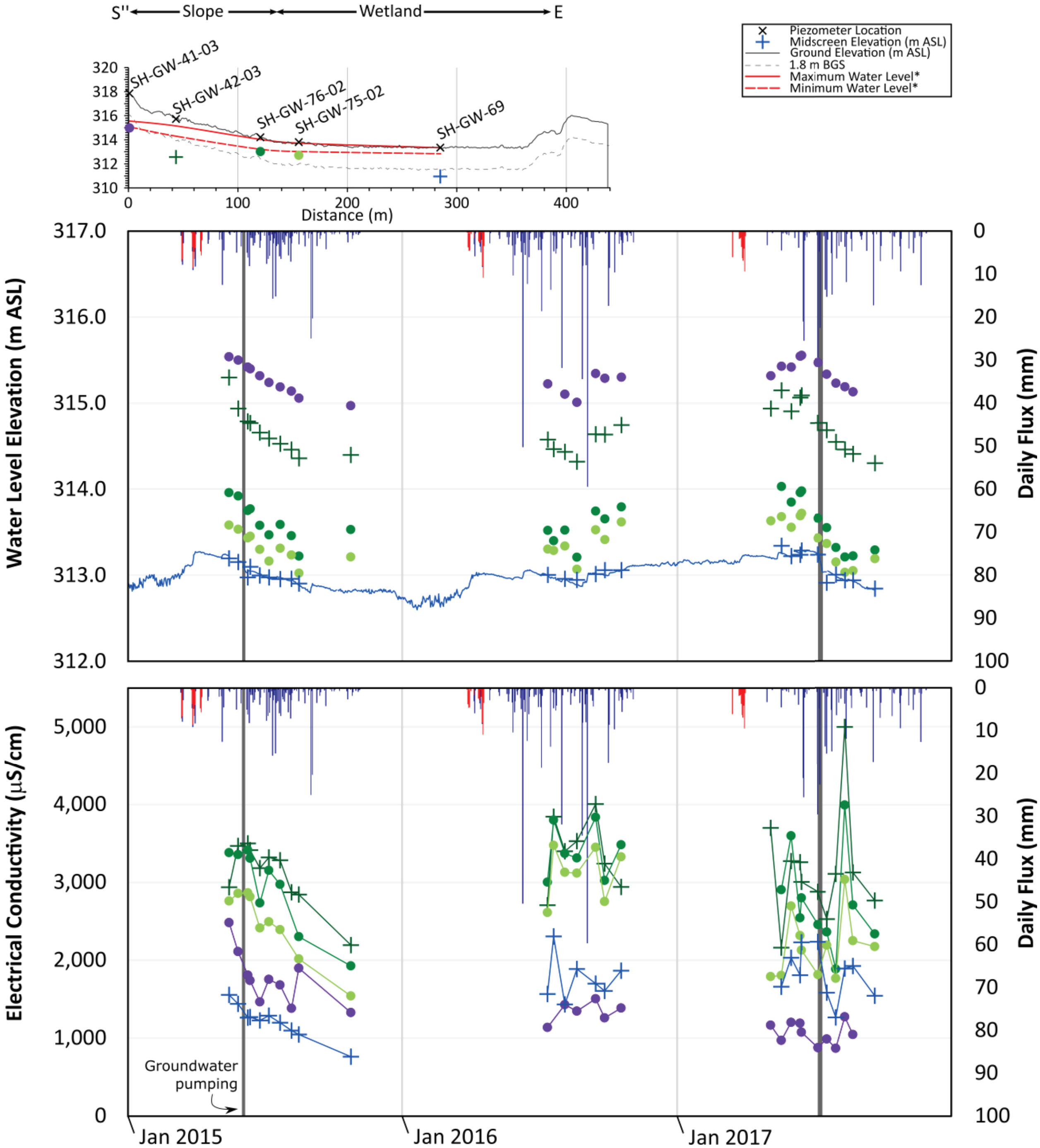

Figure 11b: Cross section paired with hydrographs (hydraulic head vs time) and EC temporal plots (EC vs time) and daily flux data for Transect 2 from January 2015 to December 2017 (inclusive). Details summarized in Figure 11a.

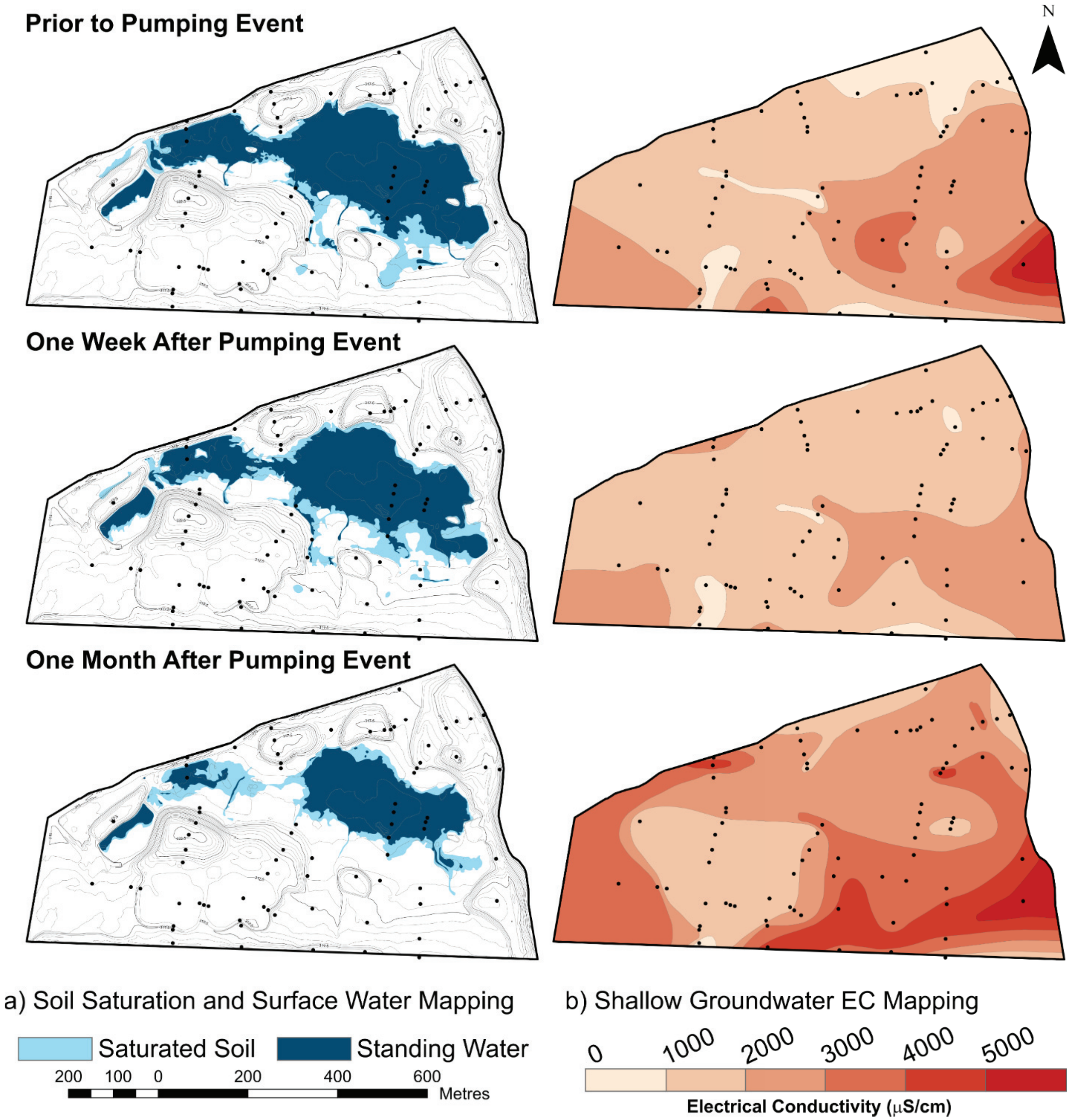

Figure 12: Soil wetness (a) and EC maps (b) from the summer of 2017 (in descending order): immediately before, one week and one month after the pumping event (-101 mm; Figure 11a/b). EC maps were plotted from the shallowest piezometers only where the midscreen fell within the uppermost 2 m of the water column to minimize deeper sampling effects.

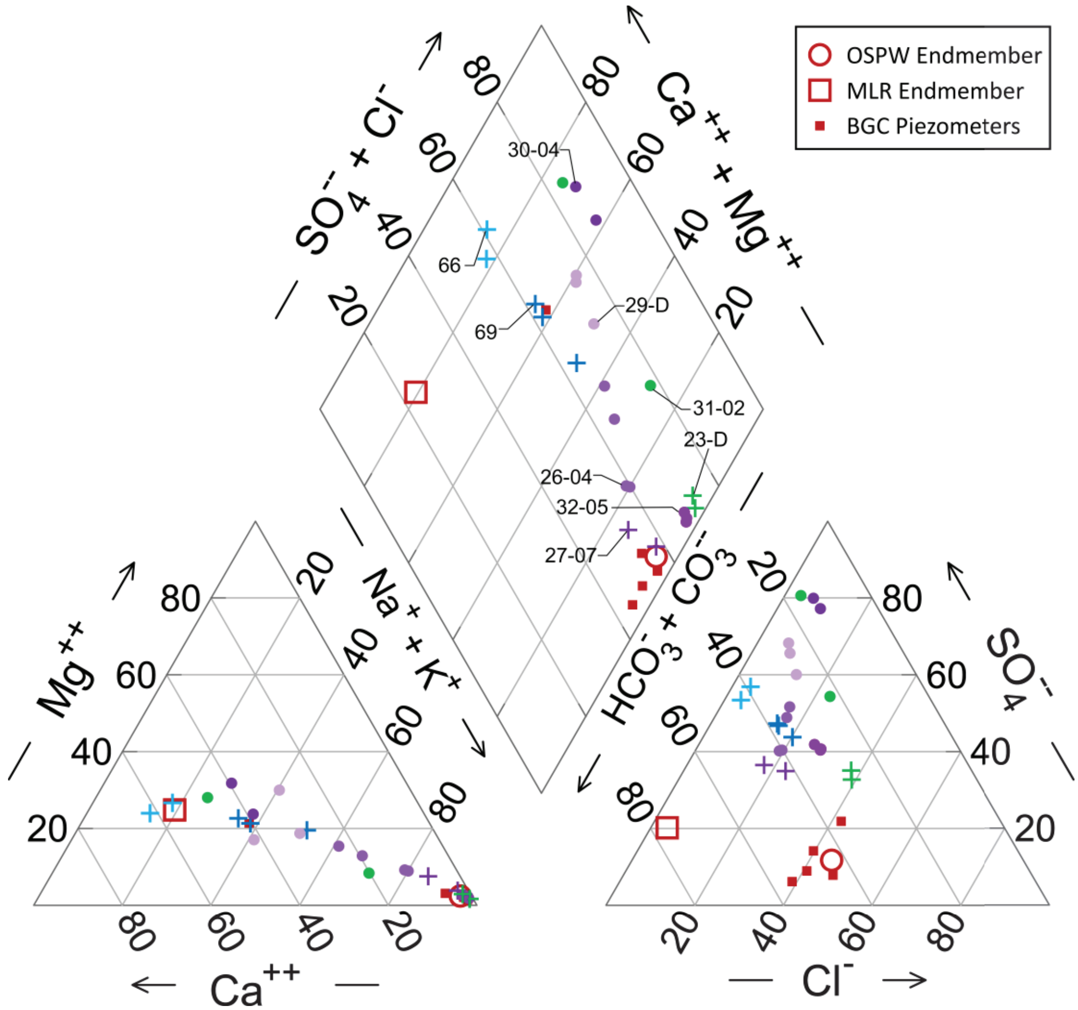

Figure 13a: Piper plot of major ions in groundwater collected annually from each SH-GW nest along Transect 1 late in late summer from 2015-2017. Only one representative piezometer is shown per nest, when groundwater was present. Representative and average endmember compositions (Mildred Lake Reservoir, MLR, and OSPW, respectively; Vessey et al., 2018; e-appendix) and deep GW samples (BGC-##-## piezometers) are plotted in red. All remaining data are GW samples from shallow piezometers in the tailings sand, symbology is consistent with water types in Figure 6 (SH-GW-##-##; shortened to ##-##). Deep GW samples (red ■) are only from 2017; no data were recorded for these piezometers in 2015 and 2016. Some piezometers are missing 2017 data due to analysis error; other piezometers have duplicates. Remaining point data color and symbology are explained in Figure 6 (SH-GW-##-##, shortened to ##-##).

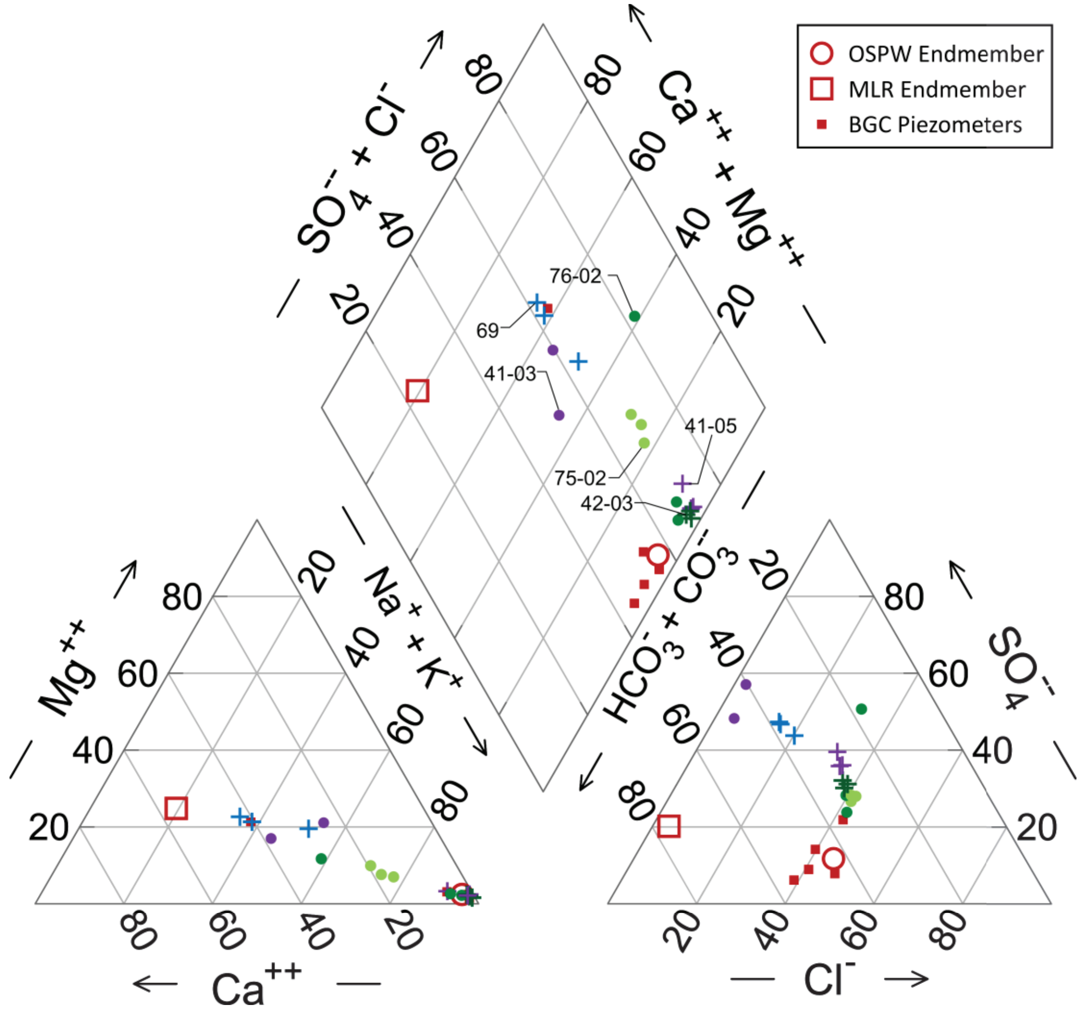

Figure 13b: Piper plot of major ions in groundwater collected annually from each SH-GW nest along Transect 2 in late summer from 2015-2017. Details summarized in Figure 13a.

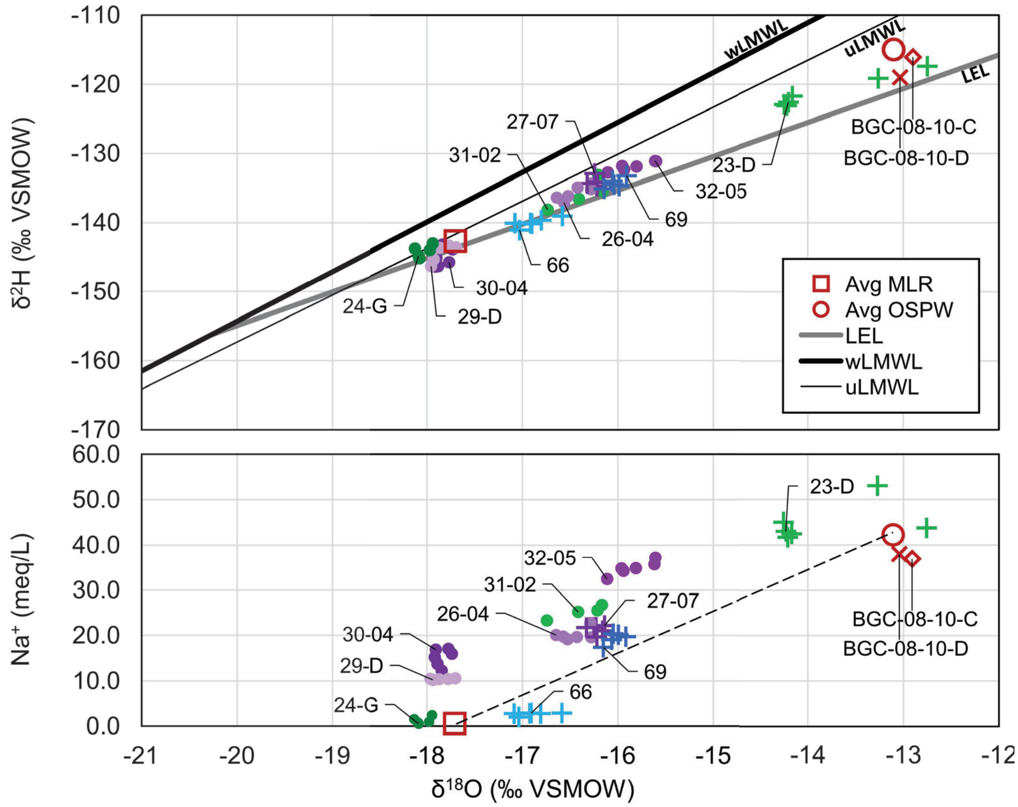

Figure 14a: Paired plots of δ^2H vs $\delta^{18}O$ (upper) and Na^+ vs $\delta^{18}O$ (lower) values collected inside representative piezometers from nests along Transect 1 during the summer field season of 2017. Representative and average endmember compositions (Mildred Lake Reservoir, MLR, and OSPW, respectively; Vessey et al., 2018; e-appendix) and deep GW samples (BGC-##-## piezometers) are plotted in red. All remaining data are GW samples from shallow piezometers in the tailings sand, symbology is consistent with water types in Figure 6 (SH-GW-##-##; shortened to ##-##). Full description of δ^2H vs $\delta^{18}O$ space in Appendix G (Figure G-3). Chemistry data were plotted with a theoretical mixing line between the Avg MLR and Avg OSPW endmember compositions to assist in interpretation. Weighted and unweighted Local Meteoric Water Lines (wLMWL and uLMWL) and Local Evaporation Line (LEL) were developed previously for SCL Mildred Lake Lease (Baer et al., 2016; Biagi et al., 2018).

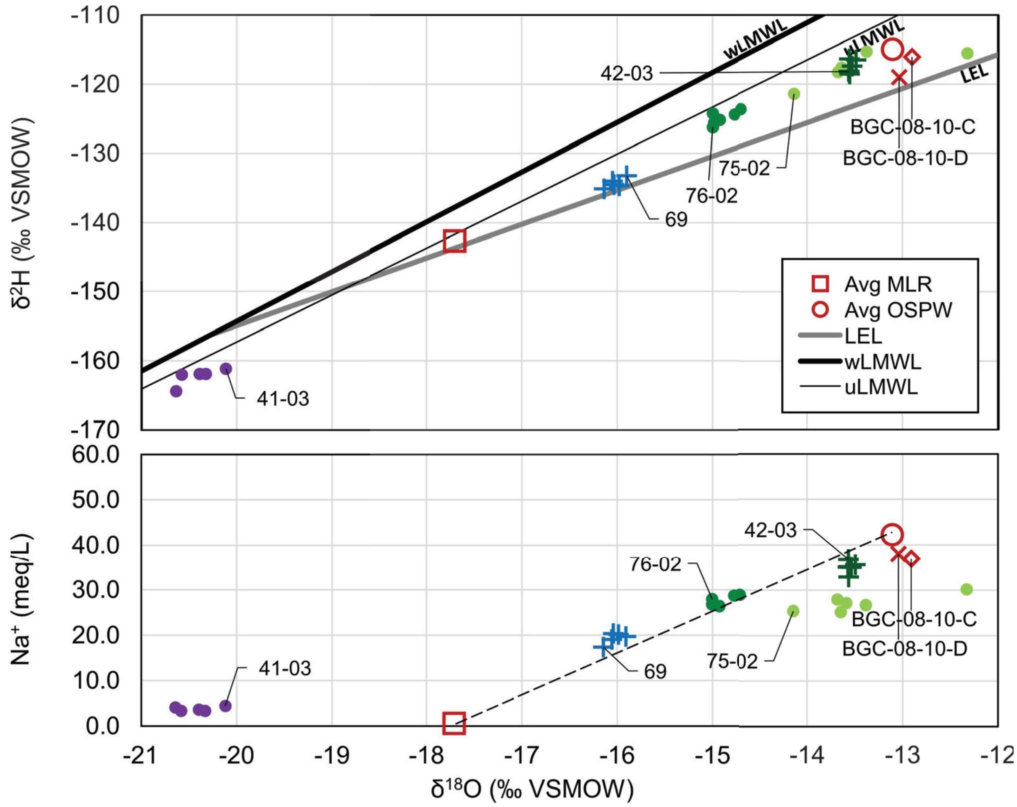

Figure 14b: Paired plots of δ^2H vs $\delta^{18}O$ (upper) and Na^+ vs $\delta^{18}O$ (lower) values collected inside the shallowest piezometer from nests along Transect 2 (slope to wetland) during the summer field season of 2017. Further details provided in Figure 14a.

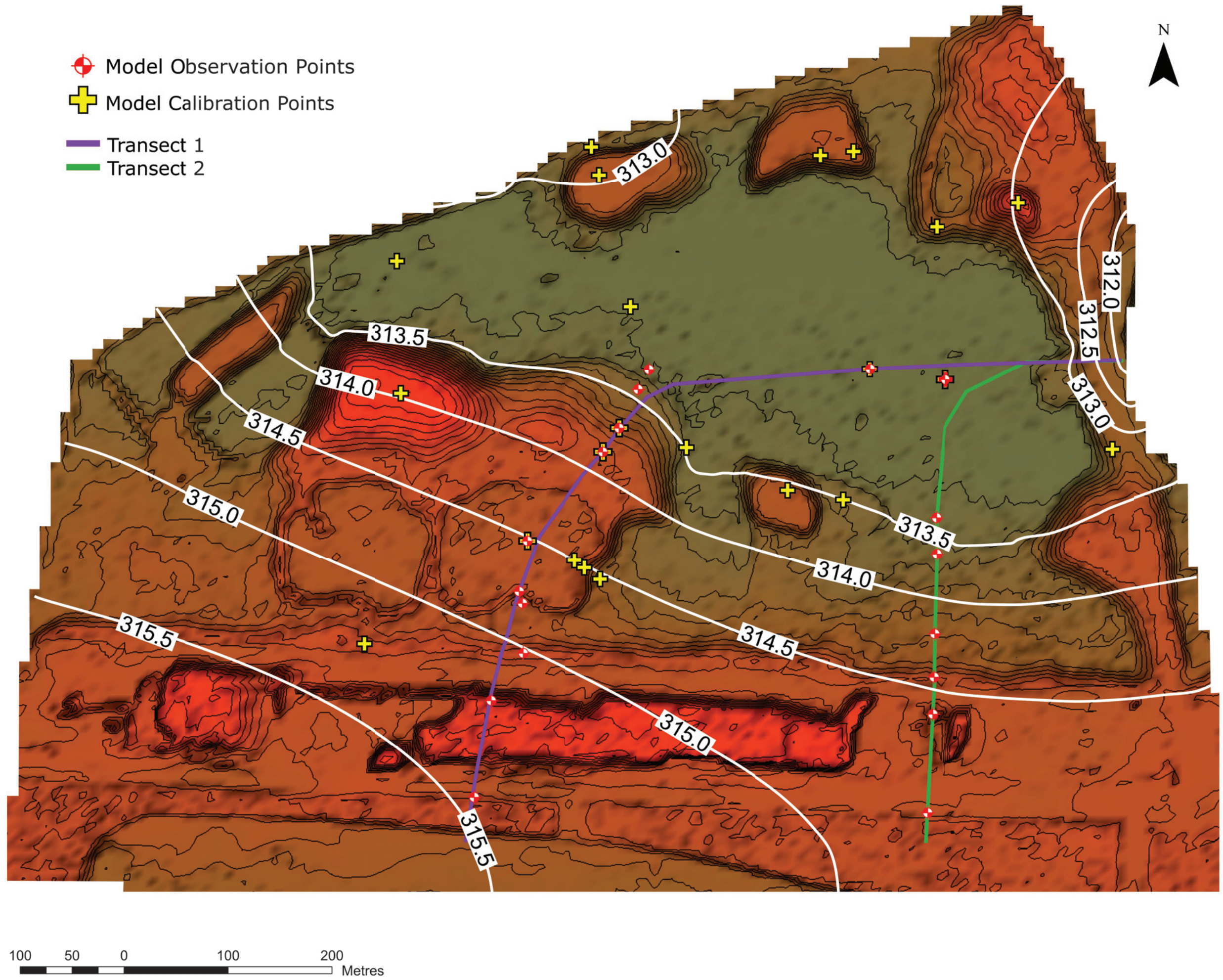

Figure 15: Water table map calculated from SHW steady state numerical groundwater model (hydraulic heads in white; m ASL). Calibration points correspond to piezometer locations where one year of continuous Levelogger data was available to calculate average water table elevations (October 2016-September 2017; e-appendix). Observation locations correspond to piezometers located along Transects 1 and 2. Details are summarized in Appendix H.

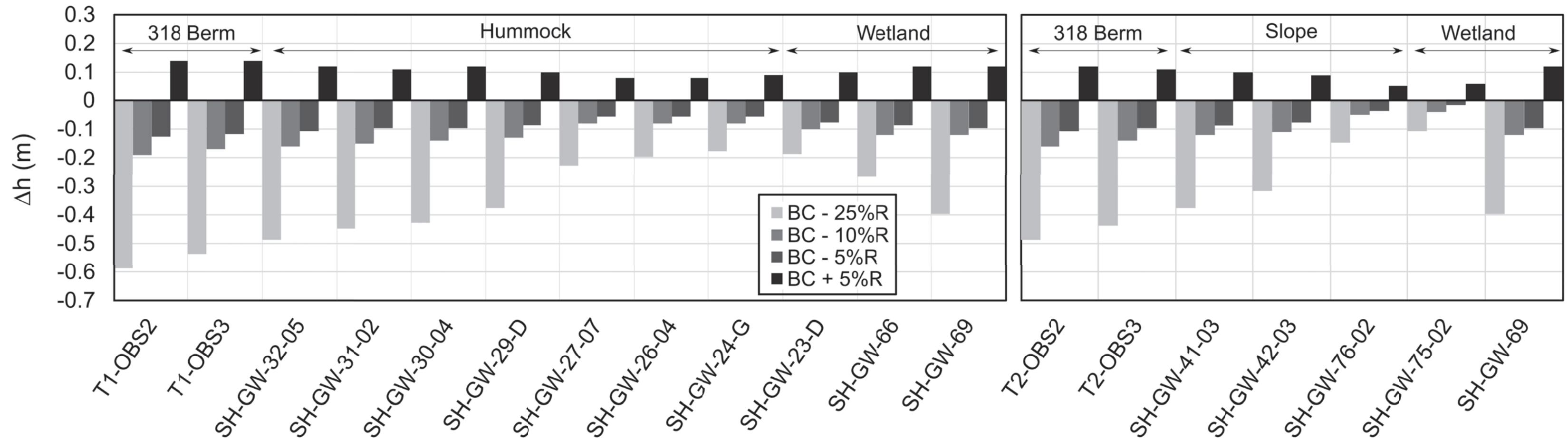

Figure 16: Differences between base case and observed hydraulic heads from four scenario tests at specified observation points along Transect 1 (left) and Transect 2 (right; Appendix H). For these scenarios, base case (BC) recharge (R) was reduced (-) by 25%, 10% and 5%, and increased (+) by 5%, respectively.

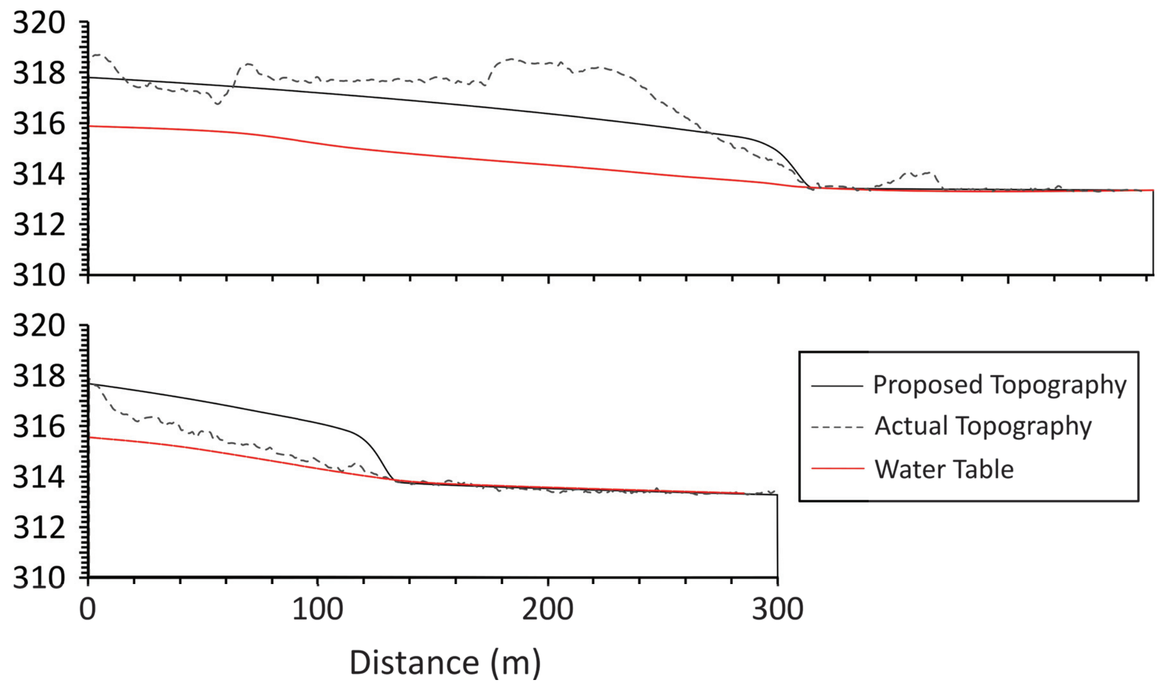

Figure 17: Proposed landform design based on the resulting groundwater system and solute distributions observed in SHW 5 years post-construction. Proposed topography overlies existing SHW topography to demonstrate moderately-tall hummocks with water tables approximately 2 m below ground surface, and a steep toe at the upland/lowland transition to minimize areal extent of seepage faces.

Work Cited

Andriashek, L. D., & Atkinson, N. (2007). *Buried channels and glacial-drift aquifers in the Fort McMurray region, northeast Alberta* (Report No. 2007-01). Alberta Energy and Utilities Board. Alberta Geological Survey, Earth Sciences, 170 p.

Atkinson, N., Utting, D. J., & Pawley, S. M. (2014). Landform signature of the Laurentide and Cordilleran ice sheets across Alberta during the last glaciation. *Canadian Journal of Earth Sciences*, 51(12), 1067-1083. DOI: 10.1139/cjes-2014-0112

Apostol, K. G., Zwiazek, J. J., & MacKinnon, M. D. (2004). Naphthenic acids affect plant water conductance but do not alter shoot Na^+ and Cl^- concentrations in jack pine (*Pinus banksiana*) seedlings. *Plant and Soil*, 263, 183-190. DOI: 10.1023/B:PLSO.0000047725.04930.bc

Alberta Environment and Parks (AEP). (2017). *Oil Sands Mine Reclamation and Disturbance Tracking by Year* [Data file]. Oil Sands Information Portal. Retrieved from https://data.environment.alberta.ca/Services/Land/LandRec.svc

Alberta Environment and Sustainable Resource Development (ESRD). (2015). Alberta Wetland Classification System. Water Policy Branch, Policy and Planning Division, Edmonton, AB.

BGC Engineering Inc. (BGC). (2014a). *Construction, Reclamation and Revegetation of Sandhill Fen - As built report, Final Report*, prepared for Syncrude Canada Ltd, September 4, 2014.

BGC Engineering Inc. (BGC). (2014b). *Sandhill Fen - As-Built Material Placement Maps, Final Report*, prepared for Syncrude Canada Ltd, February 3, 2014.

BGC Engineering Inc. (BGC). (2015). *Syncrude Canada Ltd. - Sandhill Fen Numerical Groundwater Modeling (Project No: 0534135), Final Report*, prepared for Syncrude Canada Ltd, June 12, 2015.

Baer, T. J. (2014). An evaluation of the use of natural stable isotopes of water to track water movement through oil sands mine closure landforms. MSc thesis, Civil Engineering, University of Saskatchewan, Saskatoon, SK. Retrieved from http://hdl.handle.net/10388/ETD-2014-03-1466

Baer, T., Barbour, S. L., & Gibson, J. J. (2016). The stable isotopes of site wide waters at an oil sands mine in northern Alberta, Canada. *Journal of Hydrology*, 541, 1155-1164. DOI: 10.1016/j.jhydrol.2016.08.017

Biagi, K. M., Oswald, C. J., Nicholls, E. M., & Carey, S. K. (2018). Increases in salinity following a shift in hydrologic regime in a constructed wetland watershed in a post-mining oil sands landscape. *Science of The Total Environment*, 653, 1445-1457. DOI: 10.1016/j.scitotenv.2018.10.341

Bothe, R. A., & Abraham, C. (1993). Evaporation and evapotranspiration in Alberta 1986 to 1992 addendum. Surface Water Assessment Branch, Technical Services & Monitoring Division, Water Resources Services, Alberta Environmental Protection.

Buttle, J. M., Creed, I. F., & Pomeroy, J. W. (2000). Advances in Canadian forest hydrology, 1995-1998. *Hydrological Processes*, 14(9), 1551-1578. DOI: 10.1002/1099-1085(20000630)14:9<1551::AID-HYP74>3.0.CO;2-J

Benyon, J. (2014). Characterization of Hydraulic Conductivity Profiles for Sandhill Fen Watershed Reclamation Materials. Undergraduate thesis, Earth and Atmospheric Sciences, University of Alberta, Edmonton, AB.

Canadian Association of Petroleum Producers, (CAPP). (2018). Canada's Oil Sands (No. 2018-0010). Document ID 316441. Retrieved from https://www.capp.ca/-/media/capp/customer-portal/publications/316441.pdf?modified=20180726144112 Accessed April 11, 2019

Daly, C., Price, J., Rezanezhad, F., Pouliot, R., Rochefort, L., & Graf, M. (2012). Initiatives in oil sand reclamation. In D. Vitt & J. Bhatti (Eds.), *Restoration and Reclamation of Boreal Ecosystems: Attaining Sustainable Development*. Cambridge: Cambridge University Press. DOI: 10.1017/CBO9781139059152.012

Devito, K. J., Creed, I. F., Rothwell, R. L., & Prepas, E. E. (2000). Landscape controls on phosphorus loading to boreal lakes: implications for the potential impacts of forest harvesting. *Canadian Journal of Fisheries and Aquatic Sciences*, 57(10), 1977–1984. DOI: 10.1139/cjfas-57-10-1977

Devito, K., Creed, I., Gan, T., Mendoza, C., Petrone, R., Silins, U., & Smerdon, B. (2005a). A framework for broad-scale classification of hydrologic response units on the Boreal

Plain: Is topography the last thing to consider? *Hydrological Processes*, 19(8), 1705−1714. DOI: 10.1002/hyp.5881

Devito, K. J., Creed, I. F., & Fraser, C. J. D. (2005b). Controls on runoff from a partially harvested aspen-forested headwater catchment, Boreal Plain, Canada. *Hydrological Processes,* 19, 3-25. DOI: 10.1002/hyp.5776

Devito, K., & Mendoza, C. (2006). Appendix C: Maintenance and dynamics of natural wetlands in western boreal forests: Synthesis of current understanding from the Utikuma Research Study Area. Appendices to the Guideline for Wetland Establishment on Reclaimed Oil Sands Leases Revised (2007) Edition.

Devito, K., Mendoza, C., & Qualizza, C. (2012). *Conceptualizing water movement in the Boreal Plains. Implications for watershed reconstruction*. Synthesis Report Prepared for the Canadian Oil Sands Network for Research and Development. Environmental and Reclamation Research Group. 165. DOI: 10.7939/R32J4H

Devito, K. J., Hokanson, K. J., Moore, P. A., Kettridge, N., Anderson, A. E., Chasmer, L., et al., (2017). Landscape controls on long-term runoff in subhumid heterogeneous Boreal Plains catchments. *Hydrological Processes*, 31(15), 2737-2751. DOI: 10.1002/hyp.11213

Environment Canada. (2017). Climate Data Online, Fort McMurray, AB. Retrieved from http://climate.weather.gc.ca/climate_normals/results_1981_2010_e.html?searchType=stnName&txtStationName=McM&searchMethod=contains&txtCentralLatMin=0&txtCentralLatSec=0&txtCentralLongMin=0&txtCentralLongSec=0&stnID=2519&dispBack=1

Ecological Stratification Working Group (ESWG). (1995). *A National Ecological Framework for Canada*. Agriculture and Agri-Food Canada, Research Branch, Centre for Land and Biological Resources Research and Environment Canada, State of the Environment Directorate and Ecozone Analysis Branch. Minister of Supply and Services Canada, Ottawa, ON.

Ferone, J. M., & Devito, K. J. (2004). Shallow groundwater-surface water interactions in pond-peatland complexes along a Boreal Plains topographic gradient. *Journal of Hydrology*, 292(1), 75−95. DOI: 10.1016/j.jhydrol.2003.12.032

Gillham, R. W. (1984). The capillary fringe and its effect on water-table response. *Journal of Hydrology*, 67(1), 307-324. DOI: 10.1016/0022-1694(84)90248-8

Government of Alberta. (2019). Oil Sands Facts and Statistics. Retrieved from https://www.alberta.ca/oil-sands-facts-and-statistics.aspx Accessed April 14, 2019

Gröning, M., Lutz, H. O., Roller-Lutz, Z., Kralik, M., Gourcy, L., & Pöltenstein, L. (2012). A simple rain collector preventing water re-evaporation dedicated for δ18O and δ2H analysis of cumulative precipitation samples. *Journal of Hydrology*, 448, 195-200. DOI: 10.1016/j.jhydrol.2012.04.041

Haitjema, H. M., & Mitchell-Bruker, S. (2005). Are water tables a subdued replica of the topography? *Groundwater*, 43(6), 781-786. DOI: 10.1111/j.1745-6584.2005.00090.x.

Hokanson, K. J., Mendoza, C. A., & Devito, K. J. (2019). Interactions between regional climate, surficial geology, and topography: Characterizing shallow groundwater systems in sub-humid, low-relief landscapes. *Water Resources Research*, 55, 284-297. DOI: 10.1029/2018WR023934

Howat, D. (2000). *Acceptable salinity, sodicity, and pH values for Boreal Forest Reclamation* (Report No. ESD/LM/00-2). Alberta Environment, Environmental Sciences Division, Edmonton Alberta. 201. Retrieved from https://open.alberta.ca/dataset/23ca14d3-f3fc-4be3-9e18-ccba6ca157d5/resource/20b5b1a4-e661-4e3b-92a9-19980d7215d7/download/salinitysodicityphborealreport-jun2000.pdf

Hvorslev, M. J. (1951). Time lag and soil permeability in ground-water observations, Bull. 36, U.S. Army Corps Eng. Waterways Experiment Station., Vicksburg, Miss.

Jacobs, D. F., & Timmer, V. R. (2005). Fertilizer-induced changes in rhizosphere electrical conductivity: relation to forest tree seedling root system growth and function. *New Forests*, 30, 147-166. DOI: 10.1007/s11056-005-6572-z

Johnson, E. A., & Miyanishi, K. (2008). Creating new landscapes at Alberta oil sands. *Annals of the New York Academy of Sciences*, 1134, 120-145. DOI: 10.1196/annals.1439.007

Keshta, N., Elshorbagy, A., & Carey, S. (2012). Impacts of climate change on soil moisture and evapotranspiration in reconstructed watersheds in northern Alberta, Canada. *Hydrological Processes*, 26(9), 1321-1331. DOI: 10.1002/hyp.8215

Ketcheson, S. J., Price, J. S., Carey, S. K., Petrone, R. M., Mendoza, C. A., & Devito, K. J. (2016). Constructing fen peatlands in post-mining oil sands landscapes: challenges and opportunities from a hydrological perspective. *Earth-Science Reviews*, 161, 130-139. DOI: 10.1016/j.earscirev.2016.08.007

Lukenbach, M. C., Spencer, C. J., Mendoza, C. A., Devito, K. J., & Landhäusser, S. M. (2019). Evaluating how landform design and soil covers influence groundwater recharge in a reclaimed soft tailings deposit. *Water Resources Research*, 55. DOI: 10.1029/2018WR024298

Longval, J., & Mendoza, C. (2014). *Initial Hydrogeological Instrumentation and Characterization of Sandhill Fen Watershed*, Final Report, prepared for Syncrude Canada Ltd, Department of Earth and Atmospheric Science, University of Alberta, Edmonton, Alberta.

MacKinnon, M. D., Matthews, J. G., Shaw, W. H., & Cuddy, R. G. (2001). Water quality issues associated with composite tailings (CT) technology for managing oil sands. *International Journal of Surface Mining, Reclamation and Environment*, 15(4), 235-256. DOI: 10.1076/ijsm.15.4.235.7416

Merlin, M. Leishman, F., Errington, R. C., Pinno, B.D., & Landhäusser, S. M. (2018). Exploring drivers and dynamics of early boreal forest recovery of heavily disturbed mine sites: a case study from a reconstructed landscape. *New Forests*, 50(2), 217-239. DOI: 10.1007/s11056-018-9649-1

McKenna, G. T. (2002). Sustainable Mine Reclamation and Landscape Engineering. PhD Thesis, Civil Engineering, University of Alberta, Edmonton, AB. DOI: 10.7939/R3H70882S

Mikula, R. J., Kasperski, K. L., Burns, R. D., & MacKinnon, M. D. (1996). *Nature and Fate of Oil Sands Fine Tailings.* In Suspensions: Fundamentals and Applications in the Petroleum Industry, edited by Laurier L. Schramm, 251:677-723. Washington, DC: American Chemical Society. DOI: 10.1021/ba-1996-0251.ch014

Natural Regions Committee (2006). Natural Regions and Subregions of Alberta. Compiled by D.J. Downing and W.W. Pettapiece. Government of Alberta. Pub. No. T/852.

Nicholls, E. M., Carey, S. K., Humphreys, E. R., Clark, M. G., & Drewitt, G. B. (2016). Multi-year water balance assessment of a newly constructed wetland, Fort McMurray, Alberta. *Hydrological Processes*, 30(16), 2739-2753. DOI: 10.1002/hyp.10881

O'Kane Consultants (2015). *Sandhill Fen Instrumented Watershed Program Performance Monitoring Report from January 2015 to December 2015*, Final Report, Prepared for Syncrude Canada Ltd, May 2015.

O'Kane Consultants (2016). *Sandhill Fen Instrumented Watershed Program Performance Monitoring Report from January 2016 to December 2016*, Final Report. Prepared for Syncrude Canada Ltd, January 26, 2017.

O'Kane Consultants (2017). *Sandhill Fen Instrumented Watershed Program Performance Monitoring Report from January 2017 to December 2017*, Final Report. Prepared for Syncrude Canada Ltd, December 11, 2017.

Pollard, J., McKenna, G. T., Fair, J., Daly, C. A., Wytrykush, C., & Clark, J. (2012). Design aspects of two fen wetlands constructed for reclamation research in the Athabasca oil sands. In *Proceedings of the Seventh International Conference on Mine Closure* (pp. 815-829). Australian Centre for Geomechanics.

Purdy, B. G., Ellen Macdonald, S., & Lieffers, V. J. (2005). Naturally saline boreal communities as models for reclamation of saline oil sand tailings. *Restoration Ecology*, 13(4), 667-677. https://doi-org.login.ezproxy.library.ualberta.ca/10.1111/j.1526-100X.2005.00085.x

Raine, M., Mackenzie, I., & Gilchrist, I. (2002). *CNRL Horizon Project environmental impact assessment. Vol 6 Appendix B* (Report No. 012-2220). Terrestrial Vegetation, Wetlands and Forest Resources Baseline (Golder Associates, Calgary, AB).

Redding, T. E., & Devito, K. J. (2008). Lateral flow thresholds for aspen forested hillslopes on the Western Boreal Plain, Alberta, Canada. *Hydrological Processes*, 22(21), 4287-4300. DOI: 10.1002/hyp.7038

Renault, S., Lait, C., Zwiazek, J. J., & MacKinnon, M. (1998). Effect of high salinity tailings waters produced from gypsum treatment of oil sands tailings on plants of the boreal forest. *Environmental Pollution*, 102, 177–184. DOI: 10.1016/S0269-7491(98)00099-2

Renault, S., Paton, E., Nilsson, G., Zwiazek, J. J., & MacKinnon, M. D. (1999). Responses of Boreal plants to high salinity oil sands tailings water. *Journal of Environment Quality*, 28(6), 1957–1962. DOI: 10.2134/jeq1999.00472425002800060035x

Riddell, J. T. F. (2008). Assessment of surface water – groundwater interaction at perched boreal wetlands, north-central Alberta. MSc thesis, Earth and Atmospheric Sciences, University of Alberta, Edmonton, AB. 160p.

Rooney, R. C., Bayley, S. E., & Schindler, D. W. (2012). Oil sands mining and reclamation cause massive loss of peatland and stored carbon. *Proceedings of the National Academy of Sciences*, 109(13), 4933-4937. DOI: 10.1073/pnas.1117693108

Scott, A. C., MacKinnon, M. D., & Fedorak, P. M. (2005). Naphthenic acids in Athabasca oil sands tailings waters are less biodegradable than commercial naphthenic acids. *Environmental Science and Technology*, 39(21), 8388-8394. http://doi.org/10.1021/es051003k

Schneider, R. R. (2013). Alberta's Natural Subregions Under a Changing Climate: Past, Present, and Future. Biodiversity Management and Climate Change Adaptation Project, Alberta Biodiversity Monitoring Institute.

Schoeneberger, P. J., & Wysocki, D. A. (2005). Hydrology of soils and deep regolith: A nexus between soil geography, ecosystems and land management. *Geoderma*, 126(1-2), 117-128. DOI: 10.1016/j.geoderma.2004.11.010

Simhayov, R. B., Price, J. S., Smeaton, C. M., Parsons, C., Rezanezhad, F., & Van Cappellen, P. (2017). Solute pools in Nikanotee Fen watershed in the Athabasca oil sands region. *Environmental Pollution*, 225, 150-162. DOI: 10.1016/j.envpol.2017.03.038

Smerdon, B. D., Devito, K. J., & Mendoza, C. A. (2005). Interaction of groundwater and shallow lakes on outwash sediments in the subhumid Boreal Plains of Canada. *Journal of Hydrology*, 314(1-4), 246-262. DOI: 10.1016/j.jhydrol.2005.04.001

Smerdon, B. D., Mendoza, C. A., & Devito, K. J. (2008). Influence of subhumid climate and water table depth on groundwater recharge in shallow outwash aquifers. *Water Resources Research*, 44, W08427. DOI: 10.1029/2007WR005950

Spennato, H. M., Ketcheson, S. J., Mendoza, C. A., & Carey, S. K. (2018). Water table dynamics in a constructed wetland, Fort McMurray, Alberta. *Hydrological Processes*, 32(26), 3824-3836. DOI: 10.1002/hyp.13308

Thompson, R. L., Mooder, R. B., Conlan, M. J. W., & Cheema, T. J. (2011). Groundwater flow and solute transport modelling of an oil sands mine to aid in the assessment of the performance of the planned closure landscape. In Fourie A. Tibbett, M., & Beersing A. (Eds.), Mine Closure 2011: Proceedings of the Sixth International Conference on Mine Closure. September 18-21, 2011 Lake Louise, Alberta. Australian Centre for Geomechanics. Nedlands, Western Australia. Volume 2: Post-Closure Monitoring and Responsibilities. 389–398.

Thompson, C., Mendoza, C. A., Devito, K. J., & Petrone, R. M. (2015). Climatic controls on groundwater-surface water interactions within the Boreal Plains of Alberta: Field observations and numerical simulations. *Journal of Hydrology*, 527, 734-746. DOI: 10.1016/j.jhydrol.2015.05.027

Timmer, V. R., & Teng, Y. (2004). Pretransplant fertilization of containerized *Picea mariana* seedlings: calibration and bioassay growth response. Canadian Journal of Forest Research, 34(10), 2089–2098. DOI: 10.1139/x04-088

Tóth, J. (1963). A theoretical analysis of groundwater flow in small drainage basins. *Journal of Geophysical Research*, 68(16), 4795-4812. DOI: 10.1029/JZ068i016p04795

Tóth, J. (1978). Gravity-induced cross-formational flow of formation fluids, Red Earth region, Alberta, Canada: Analysis, patterns, and evolution. *Water Resources Research*, 14(5), 805-843. DOI: 10.1029/WR014i005p00805

Vessey, C. J., Lindsay, M. B. J., & Barbour, S. L. (2019). Sodium transport and attenuation in soil cover materials for oil sands mine reclamation. *Applied Geochemistry*, 100, 42-54. DOI: 10.1016/j.apgeochem.2018.10.023

Vitt, D. H., & Chee, W. L. (1990). The relationships of vegetation to surface water chemistry and peat chemistry in fens of Alberta, Canada. *Vegetatio*, 89(2), 87–106. DOI: 10.1007/BF00032163

Vitt, D. H., House, M., & Hartsock, J. (2016). Sandhill Fen, An initial trial for wetland species assembly on in-pit substrates: Lessons after three years. *Botany*, 94, 1015–1025. DOI: 10.1139/cjb-2015-0262

Wells, C. M., & Price, J. S. (2015). A hydrologic assessment of a saline-spring fen in the Athabasca oil sands region, Alberta, Canada-a potential analogue for oil sands reclamation. *Hydrological Processes*, 29(20), 4533–4548. DOI: 10.1002/hyp.10518.

Waddington, J. M., Morris, P. J., Kettridge, N., Granath, G., Thompson, D. K., & Moore, P. A. (2015). Hydrological feedbacks in northern peatlands: Hydrological feedbacks in northern peatlands. *Ecohydrology*, 8(1), 113-127. DOI: 10.1002/eco.1493

Winter, T. C. (2001). The concept of hydrologic landscapes. *Journal of the American Water Resources Association*, 37(2), 335-349. DOI: 10.1111/j.1752-1688.2001.tb00973.x

Winter, T. C., Rosenberry, D. O., & LaBaugh, J. W. (2003). Where does the ground water in small watersheds come from? *Groundwater*, 41(7), 989-1000. DOI: 10.1111/j.1745-6584.2003.tb02440.x

Wylynko, D., & Hrynyshyn, J. (2014). *Guidelines for Wetlands Establishment on Reclaimed Oil Sands Leases* (Third Edition). Cumulative Environmental Management Association. Fort McMurray, Alberta.

Wytrykush, C., Vitt, D., Mckenna, G., & Vassov, R. (2012). Designing landscapes to support peatland development on soft tailings deposits. In D. Vitt & J. Bhatti (Eds.), *Restoration and Reclamation of Boreal Ecosystems: Attaining Sustainable Development*. Cambridge: Cambridge University Press. DOI: 10.1017/CBO9781139059152.011

Appendices

Appendix A - Sandhill Watershed Site Description

Appendix A - Sandhill Watershed Site Description

I. Scope of Work

This appendix provides maps and photos to assist in site description and reclamation methods. Within the maps, the infrastructure, installations, and soil placements are outlined for Sandhill Watershed (SHW). These maps have been updated from existing maps (Figure A-1 and A-3; BGC, 2012) or have been included simply to assist with interpretations (Figure A-4 to Figure A-8; BGC, 2014b).

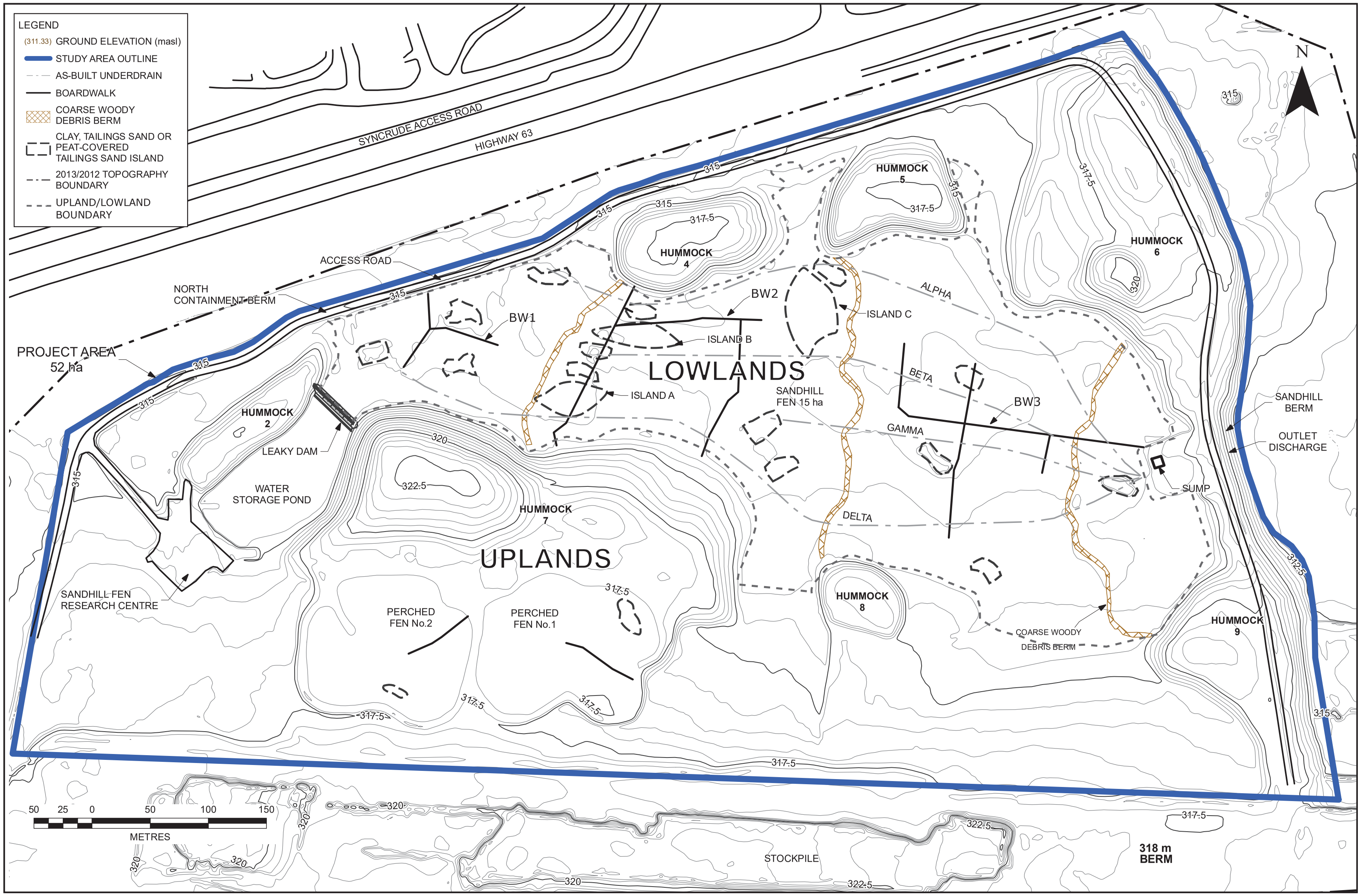

Figure A-1: Topographic map of SHW with infrastructure, topographic regions and design characteristics annotated.

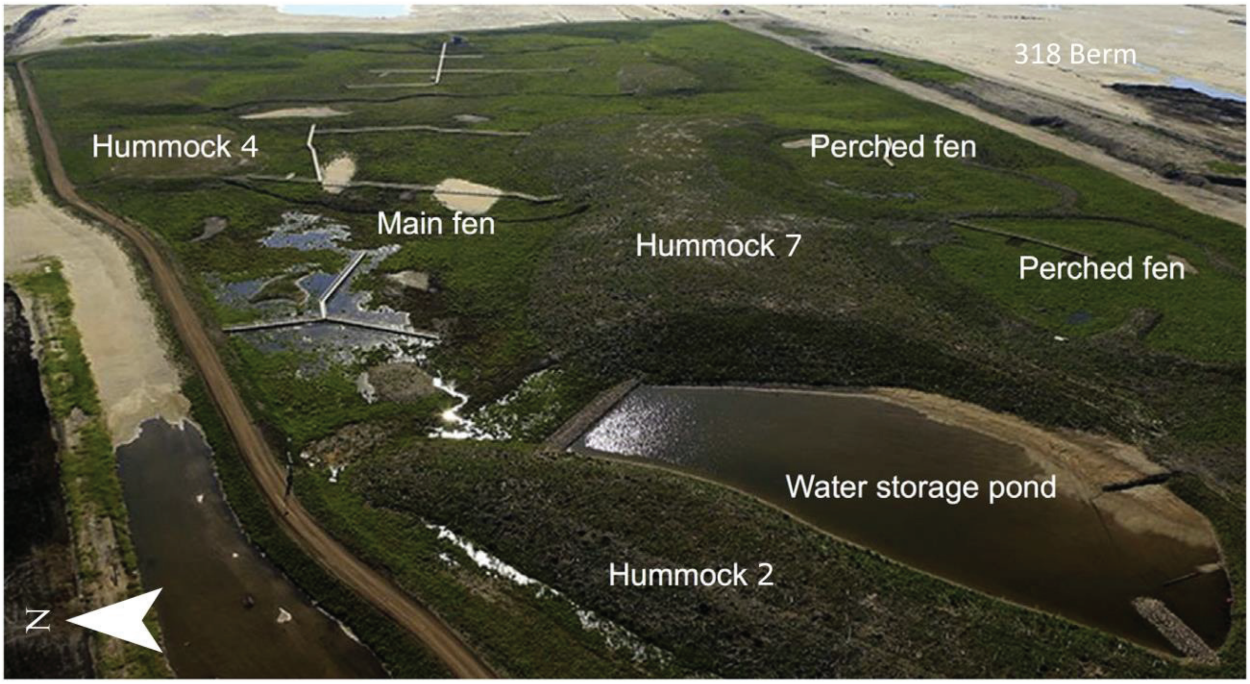

Figure A-2: Aerial photo of SHW from the northwest corner of the watershed. Photo taken by Syncrude Canada Ltd, modified from Ketcheson et al., (2016).

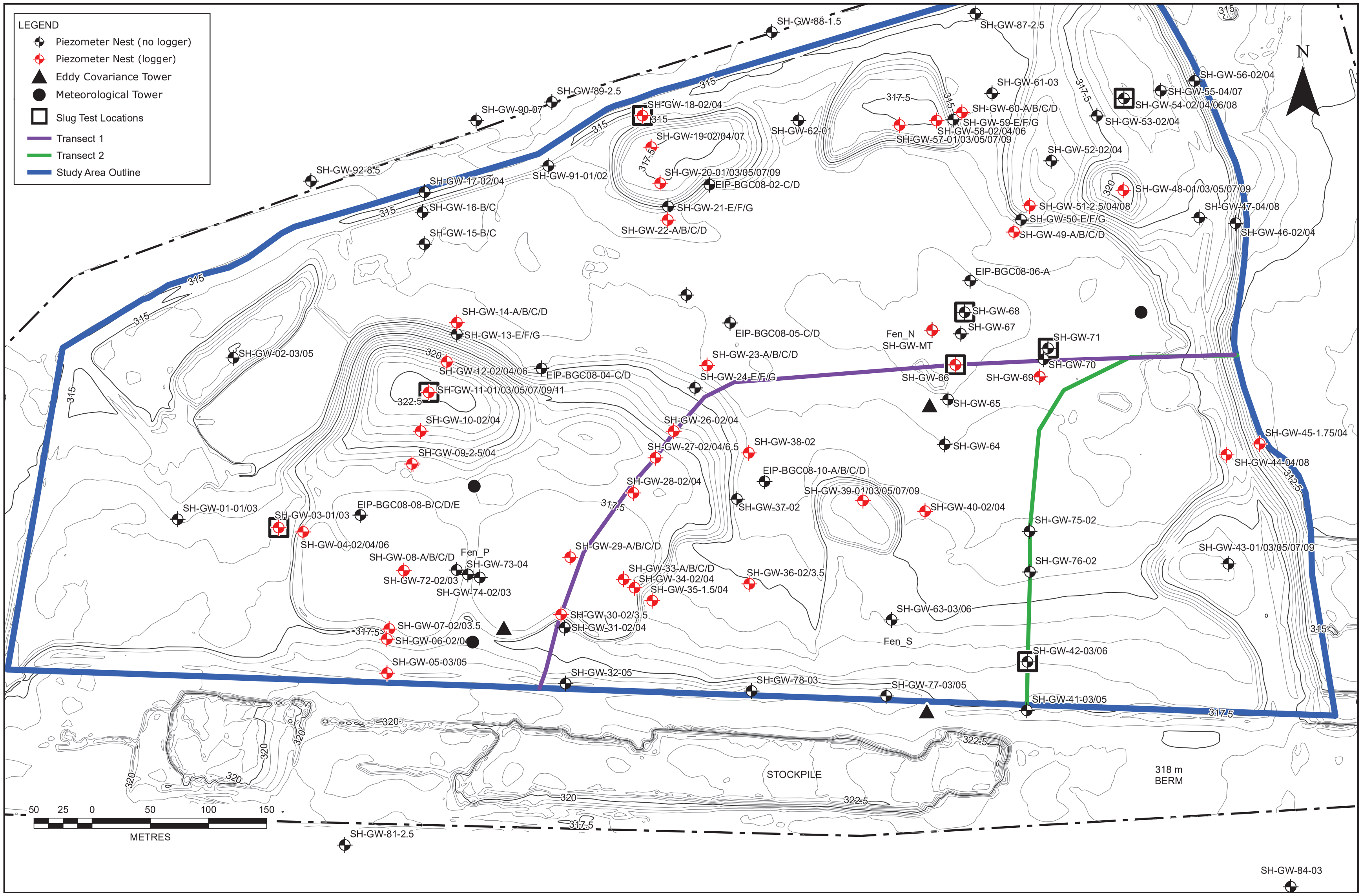

Figure A-3: Site Map of SHW (blue) with piezometer nests (with and without loggers), eddy covariance and meteorological tower locations. Transect 1 and Transect 2 correspond to different topographic configurations in the watershed, hummocks-to-wetlands, and slopes-to-wetlands, respectively. Boxes indicate locations where slug tests were performed.

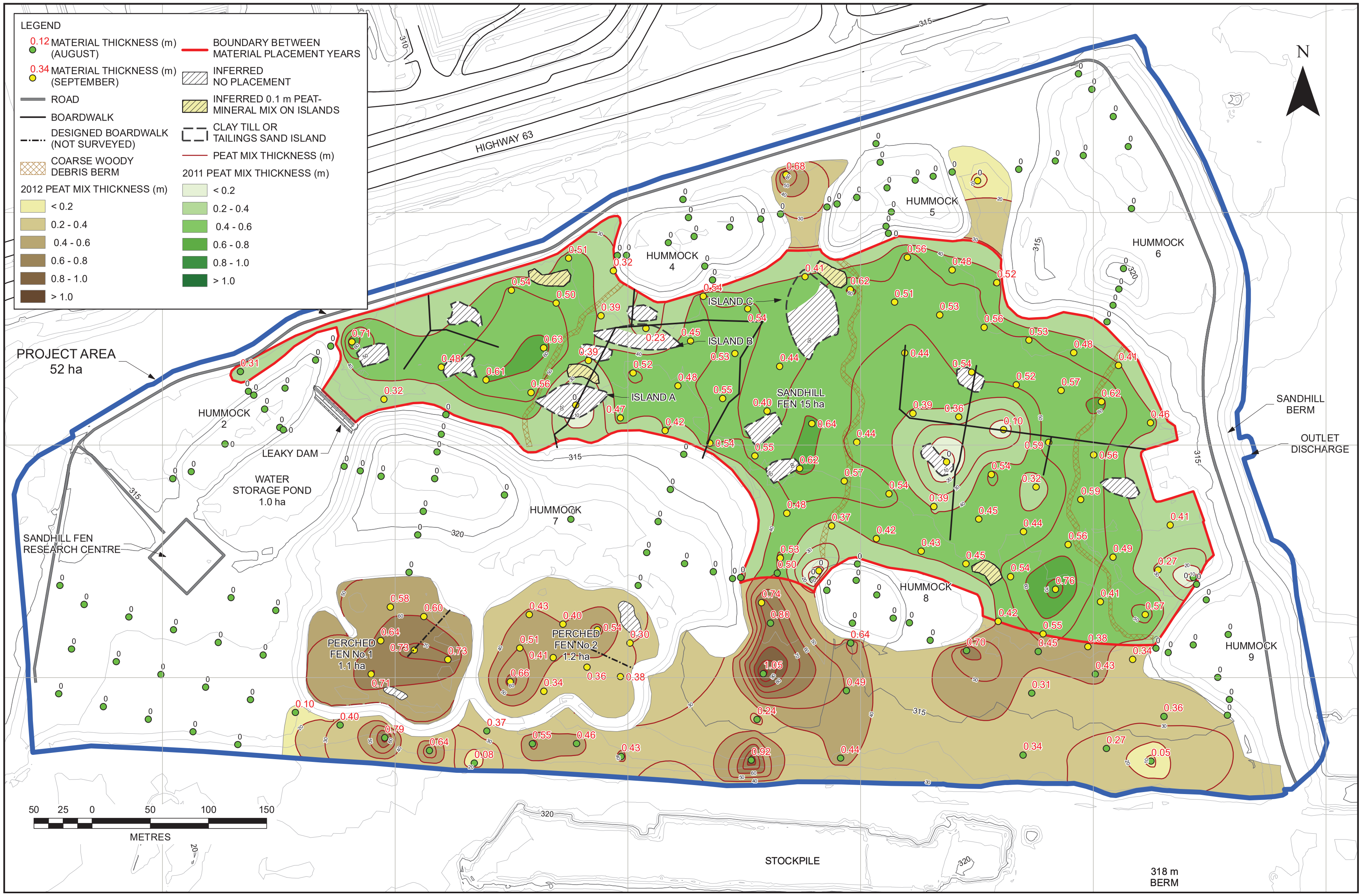

Figure A-4: Isopach map of peat-mineral-mix (PMM) topsoil prescribed in the uplands and lowlands.

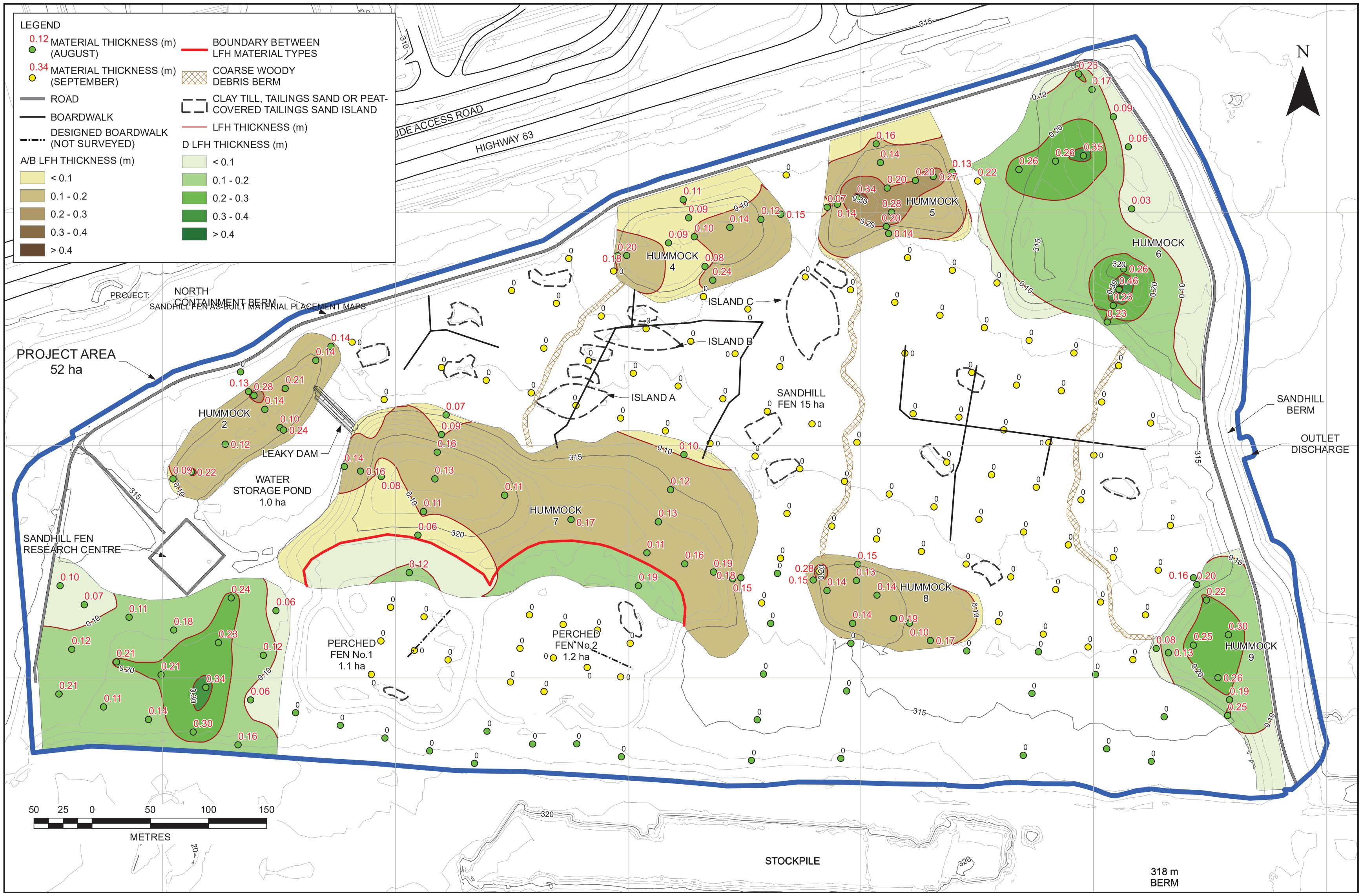

Figure A-5: Isopach map of topsoil prescriptions applied to hummocks, including LFH-A/B ecosite (brown) and LFH-D ecosite (green).

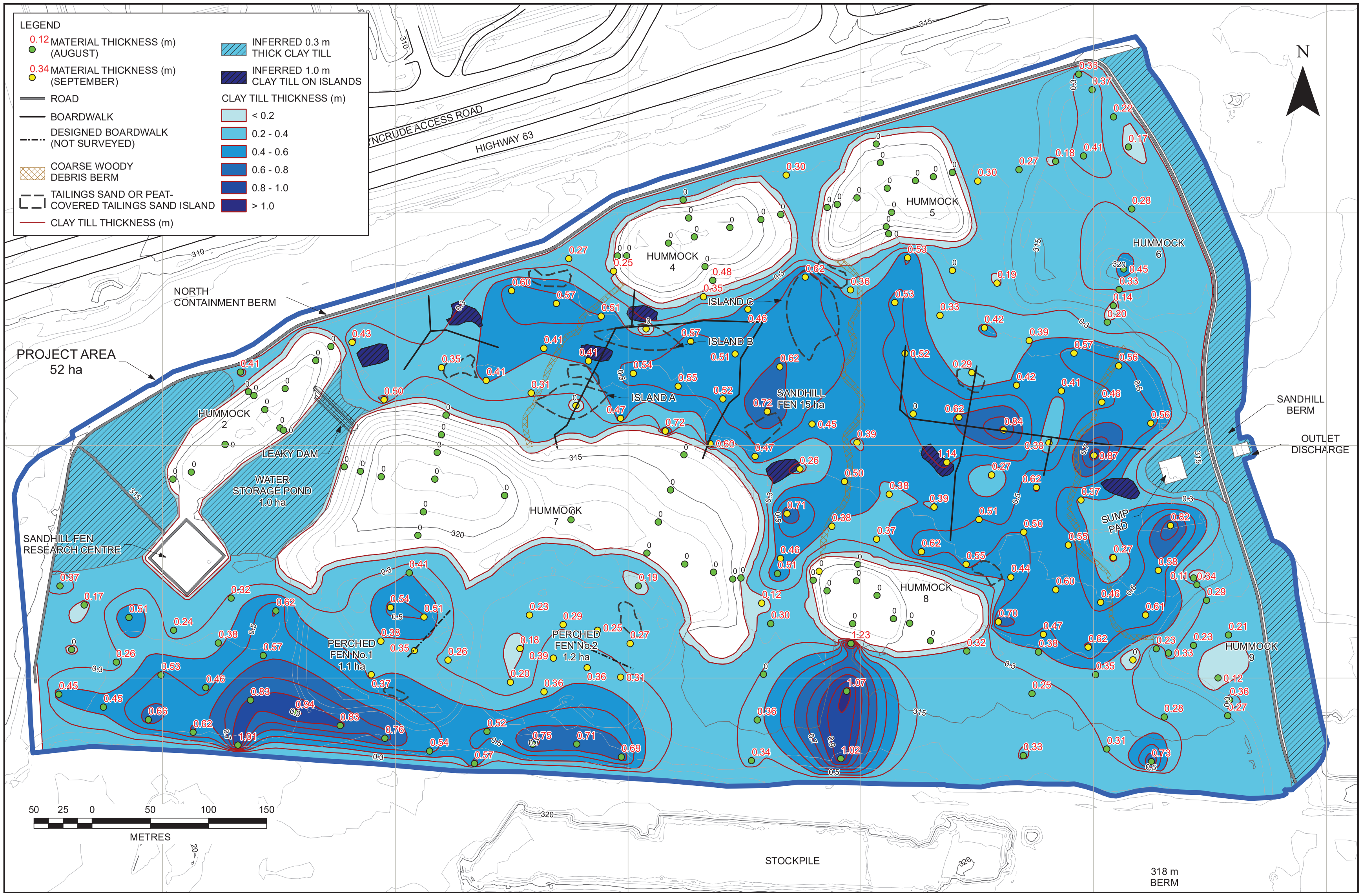

Figure A-6: Isopach map of clay till subsoil applied to the uplands and lowlands.

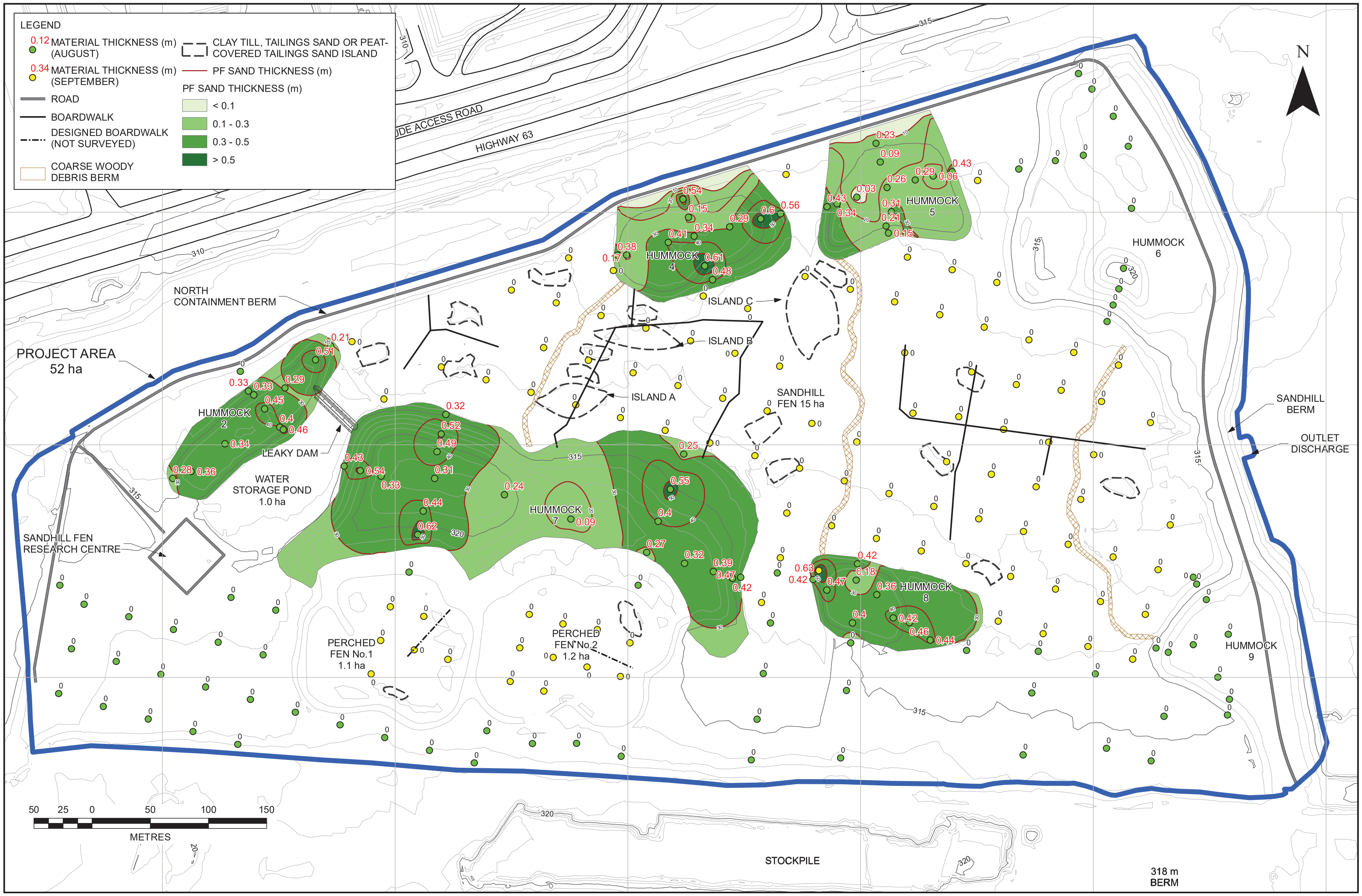

Figure A-7: Isopach map of PF sand subsoil prescribed to hummocks 2, 4, 5, 7, and 8.

Figure A-8: Surface of sculpted tailing sand immediately below the subsoils.

Appendix B - Water Level Data

Appendix B - Water Level Data

I. Scope of Work

This appendix contains various water level data presented in the form of hydrographs, vertical hydraulic gradients, and water table maps. Hydrographs have been developed for two primary transects, Transect 1 and Transect 2 (previously described in thesis), and three sub-transects (Transects 3, 4 and 5) located on Hummock 4, 6 and 7, respectively (Figure 5). The plotted data were from the shallowest piezometers in the nest that also had the longest data record. Automated data was included when available. Vertical hydraulic gradients are provided in a time series to demonstrate the range in values and to show they are temporary and intermittent. Finally, water table maps were developed at various points through the study period, from the hydraulic heads obtained from the shallowest piezometers in a given nest. While the water levels in the piezometers often rise above the screen (providing a potentiometric water level) the vertical hydraulic gradients were considered negligible; therefore, the water levels in the shallowest piezometers are considered an accurate representation of the water table.

II. Methods

Manual groundwater measurements were collected from shallow piezometers bi-weekly to monthly during the field season (May-October) from 2013 to 2017 with a temperature, level, and conductivity meter (TLC; Solinst, Canada; Figure 5). When standing water was present adjacent to a piezometer, surface water elevations relative to the top of the piezometer were collected.

Automated water level measurements were recorded hourly, ranging from intermittently to year-round, from 44 pressure transducers located in representative piezometer locations over 5 years (2013-2017; Figure 5). Data were logged by a pressure transducer (Solinst Levelogger-Edge or Solinst-Levelogger) and were compensated with barometric data collected on-site

(Solinst Barologger-Edge). Representative daily water level data were obtained by averaging three hourly measurements: before, at, and after noon (*i.e.*, 11:00, 12:00, 13:00). Water level data and EC data are discussed further in Appendices B and C, respectively.

III. Results

Results are presented in the following order: hydrographs (Transects 1 to 5), vertical hydraulic gradients (uplands, lowlands and transition areas), and water table maps (2015-2017). Water table maps are organized chronologically, as indicated by the map header. Only data from 2015 to 2017 are presented here.

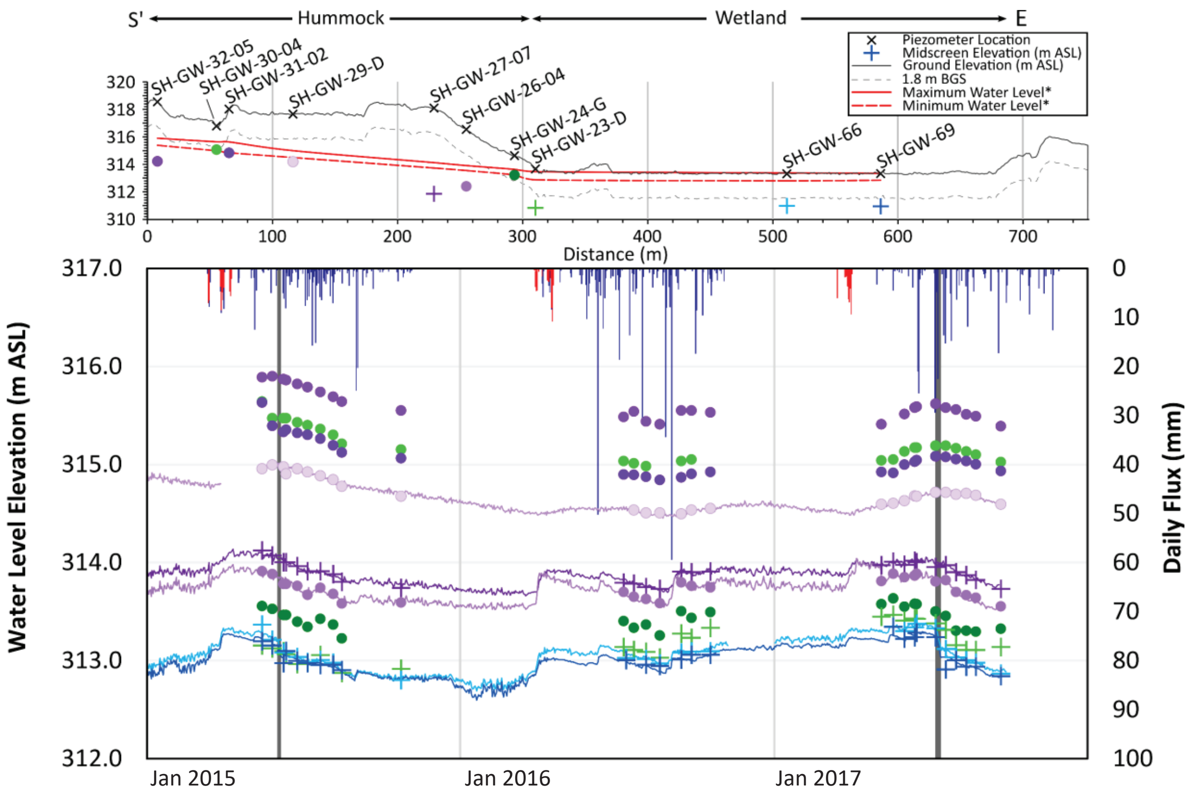

Figure B-1a: Cross section of Transect 1 paired with hydrograph (hydraulic head vs time) and daily flux data from January 2015 to December 2017 (inclusive). Cross section demonstrates landscape position of piezometers with midscreen elevations, maximum and minimum manual water level measurements observed during the study period at each individual location. Point data in the hydrograph and temporal plot are manual measurement data; lines in hydrograph are continuous automated data (nest 66 and 69 provided by Carey, unpublished). Grey bar represents pumping event duration. Point data color and symbology are explained in Figure 6; line for 1.8 m below ground surface for reference only. Details for daily flux data are outlined in Figure 2.

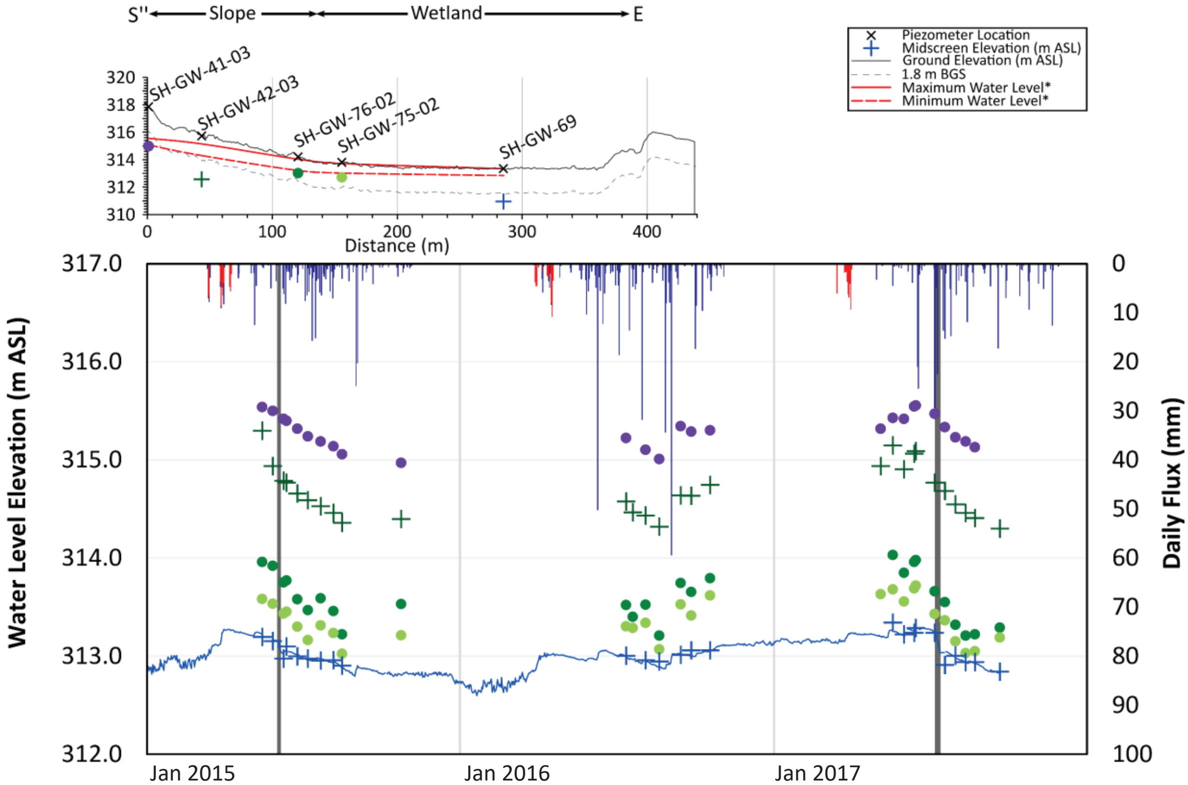

Figure B-1b: Cross section paired with hydrographs and daily flux data for Transect 2 from January 2015 to December 2017 (inclusive). Details summarized in Figure B-1a.

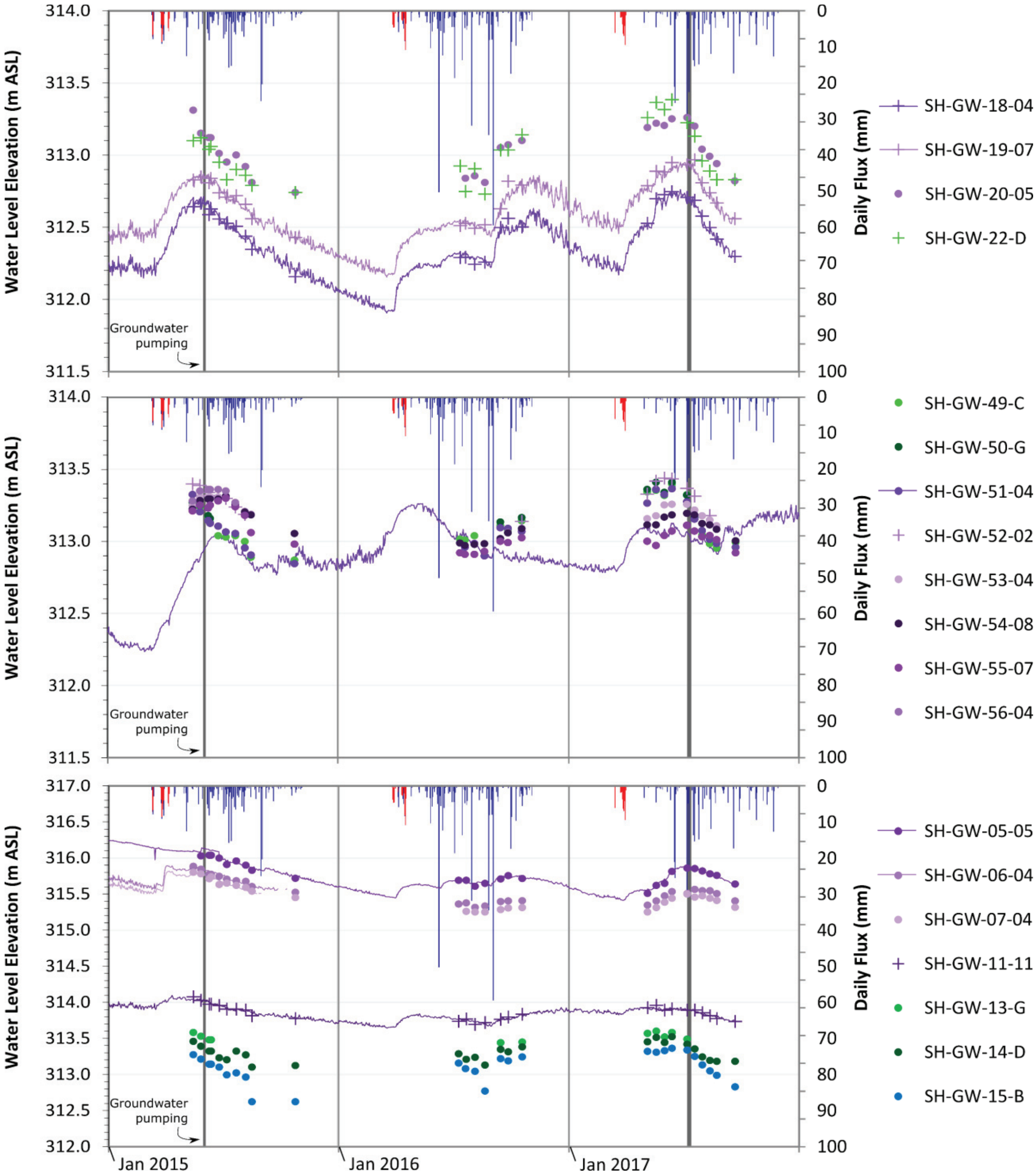

Figure B-2: Hydrographs developed for piezometers located along sub-transects 3, 4 and 5 (top down) located on Hummock 4, Hummock 6 and Hummock 7, respectively, from 2015 to 2017. Details summarized in Figure B-1a.

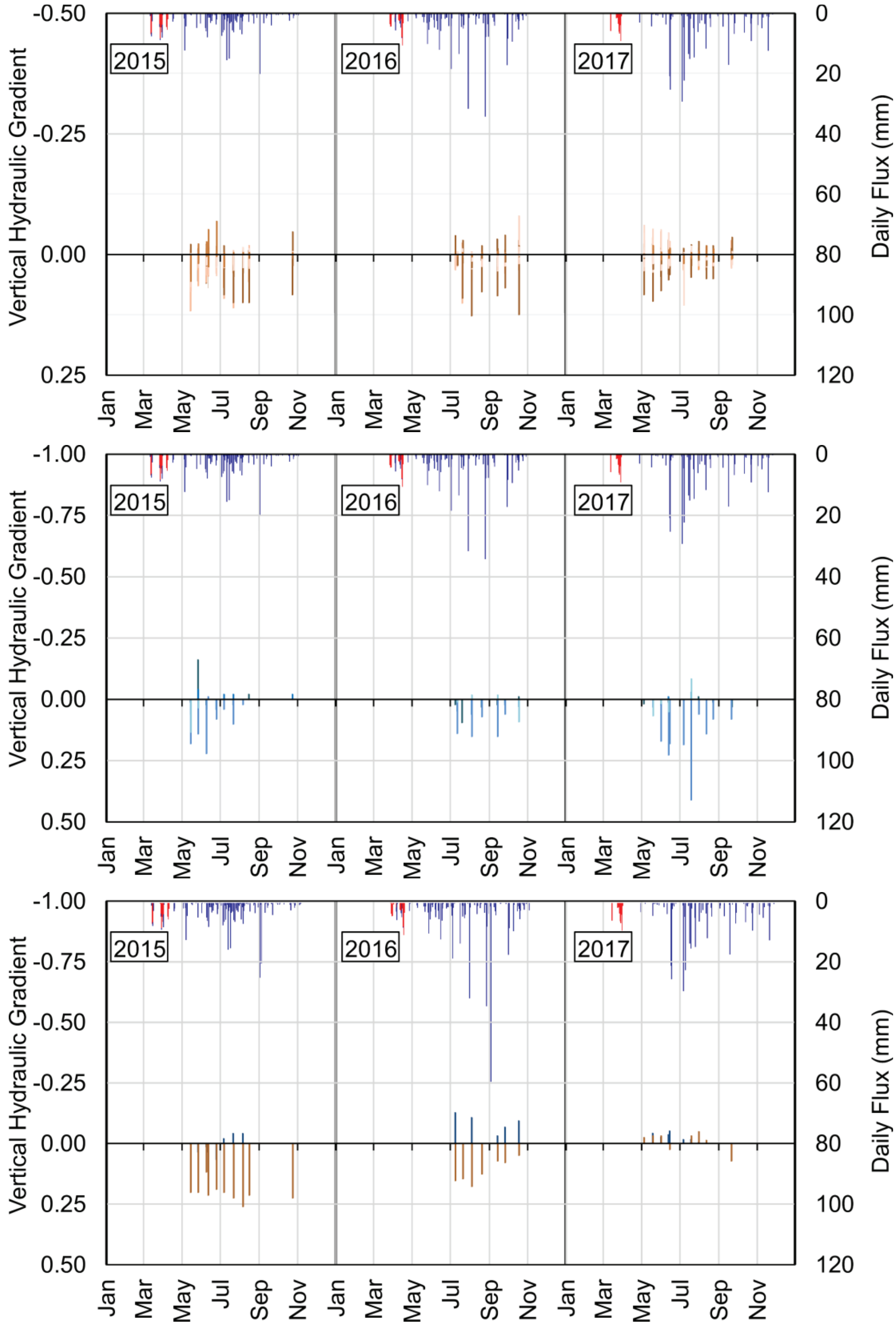

Figure B-3: Vertical hydraulic gradients calculated from each nest, where data were available, measured in (top down) the uplands, wetlands and at nest 23 (toe of the slope) during the study period. Nest 23 shows vertical gradients across the clay (blue; between 23-A and 23-C) and the tailings sand (orange; between 23-C and 23-D). Positive values indicate downward flow, negative values indicate upward flow.

SHFW - Water Table Map - 2015-MAY-27

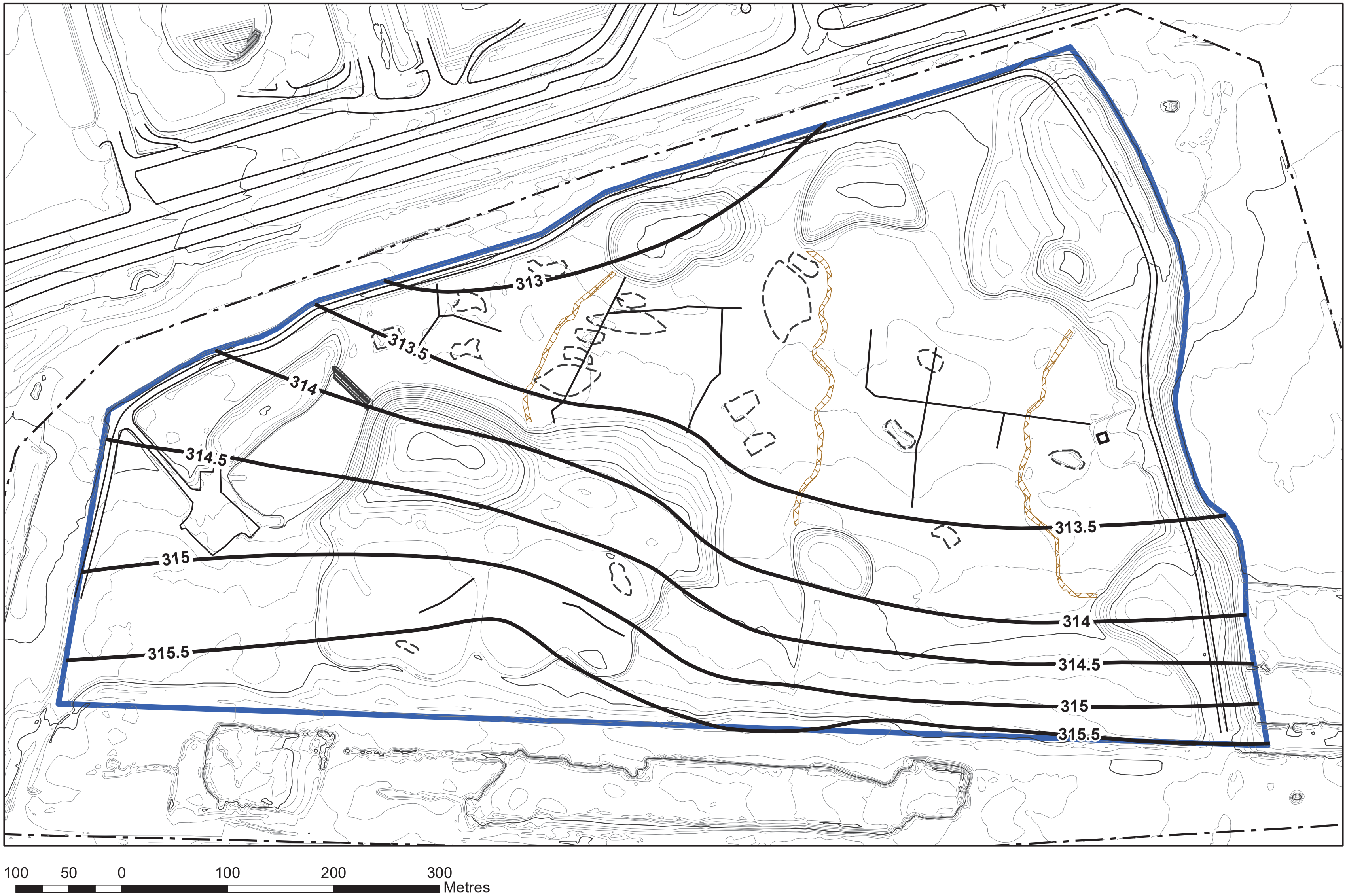

WTMap-2015-05-27

SHFW - Water Table Map - 2015-AUG-06

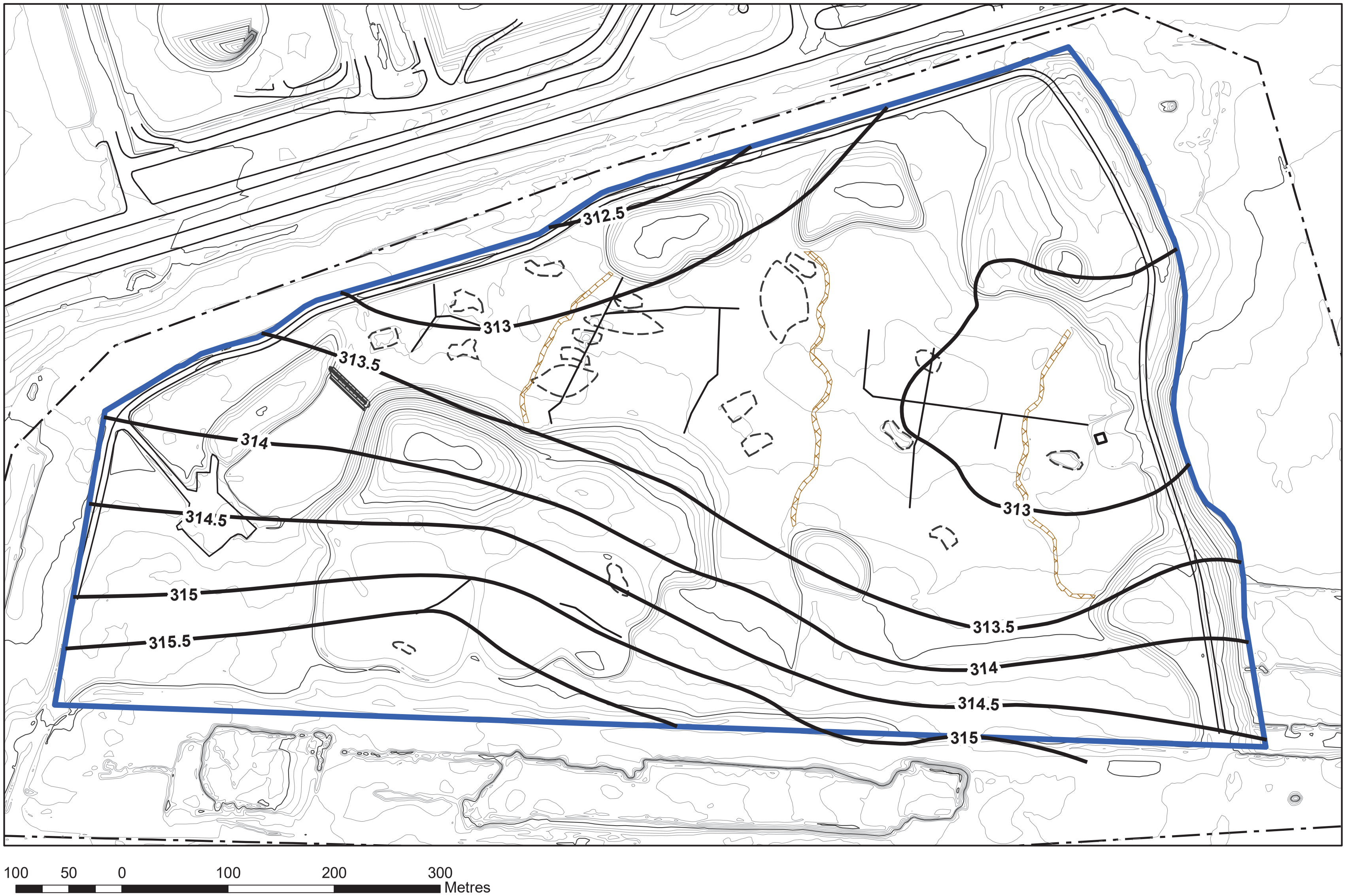

WTMap-2015-08-06

SHFW - Water Table Map - 2015-OCT-24

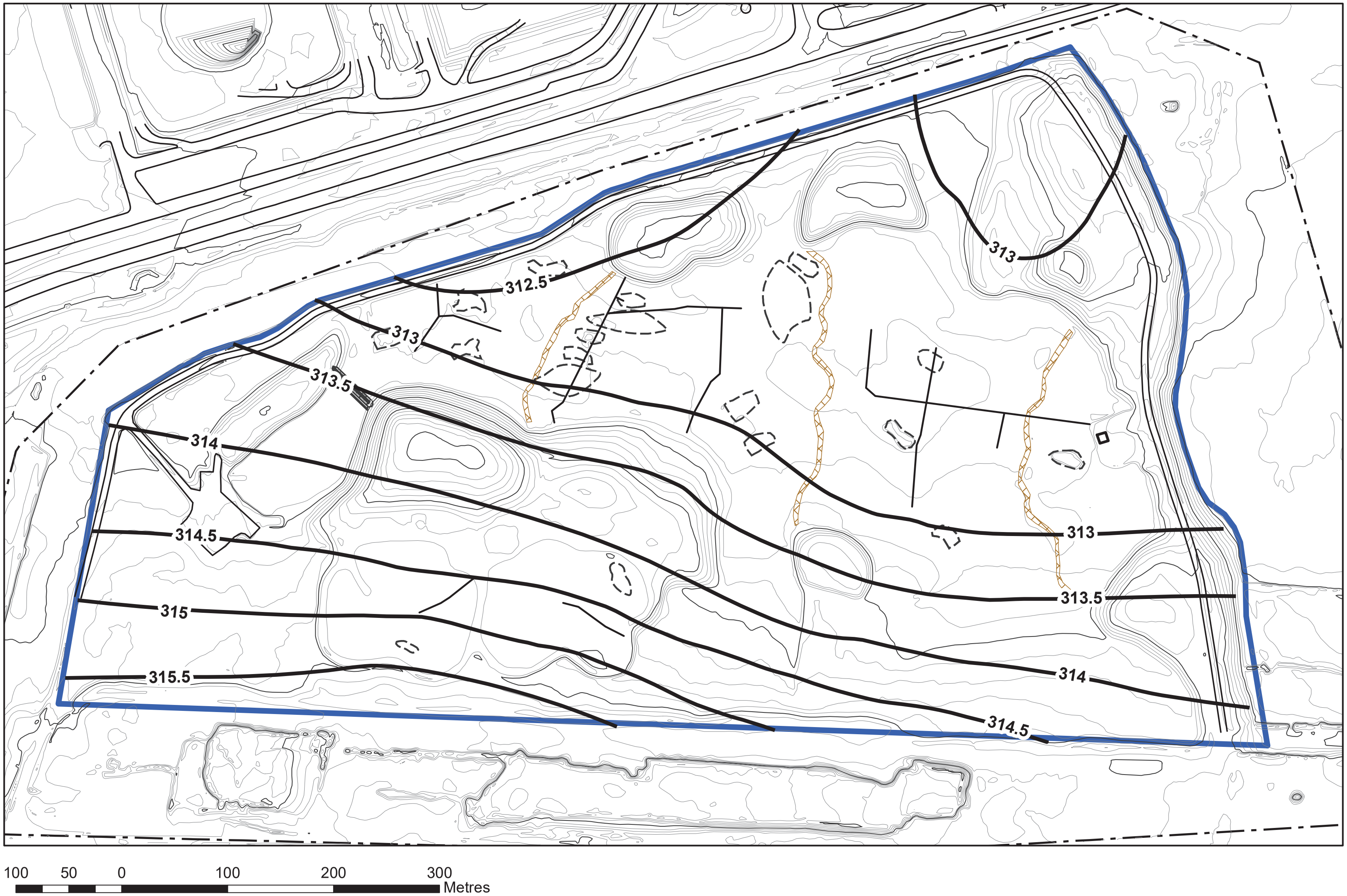

WTMap-2015-10-24

SHFW - Water Table Map - 2016-JUL-09

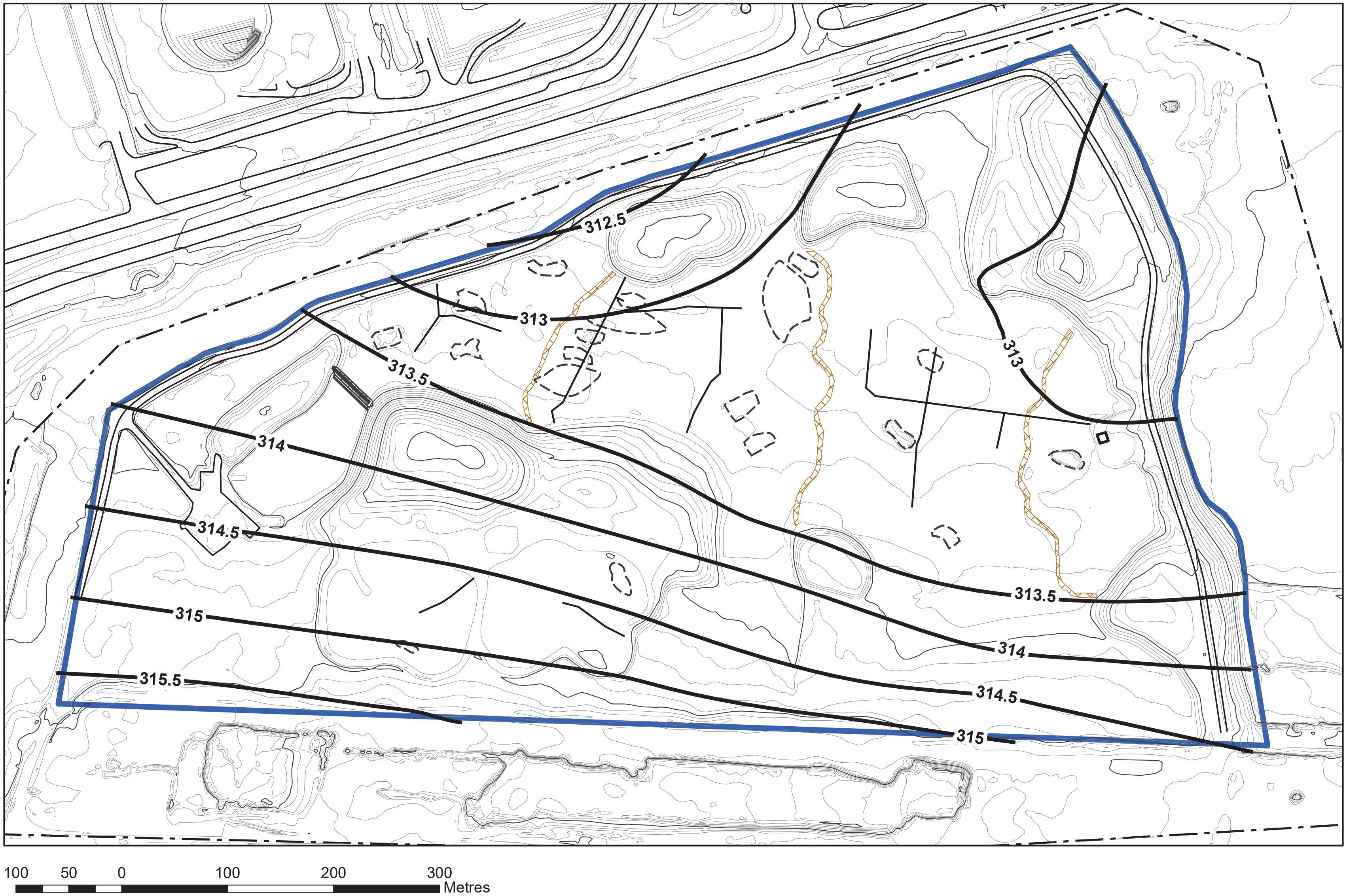

WTMap-2016-07-09

SHFW - Water Table Map - 2016-OCT-18

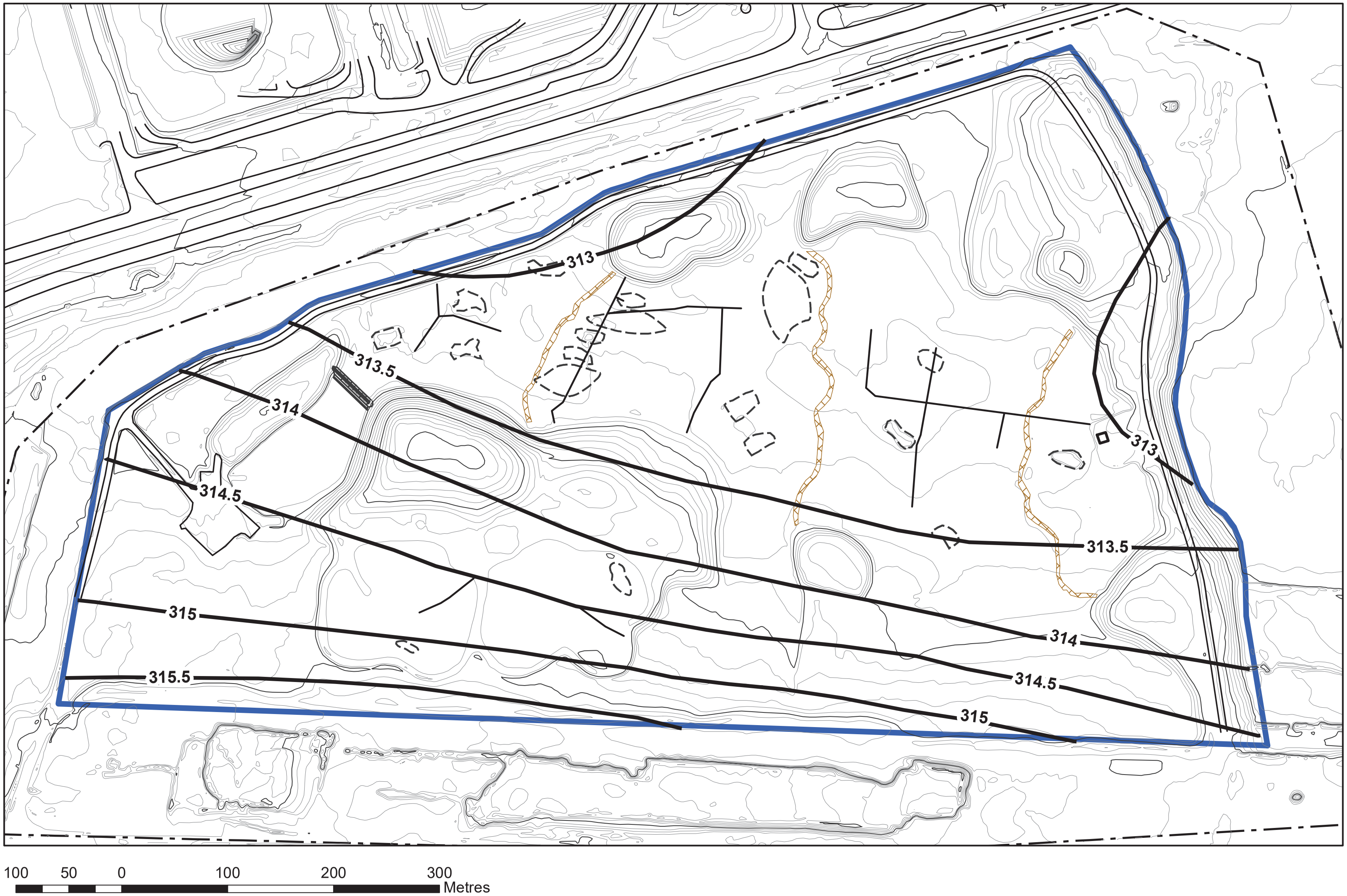

WTMap-2016-10-18

SHFW - Water Table Map - 2017-MAY-05

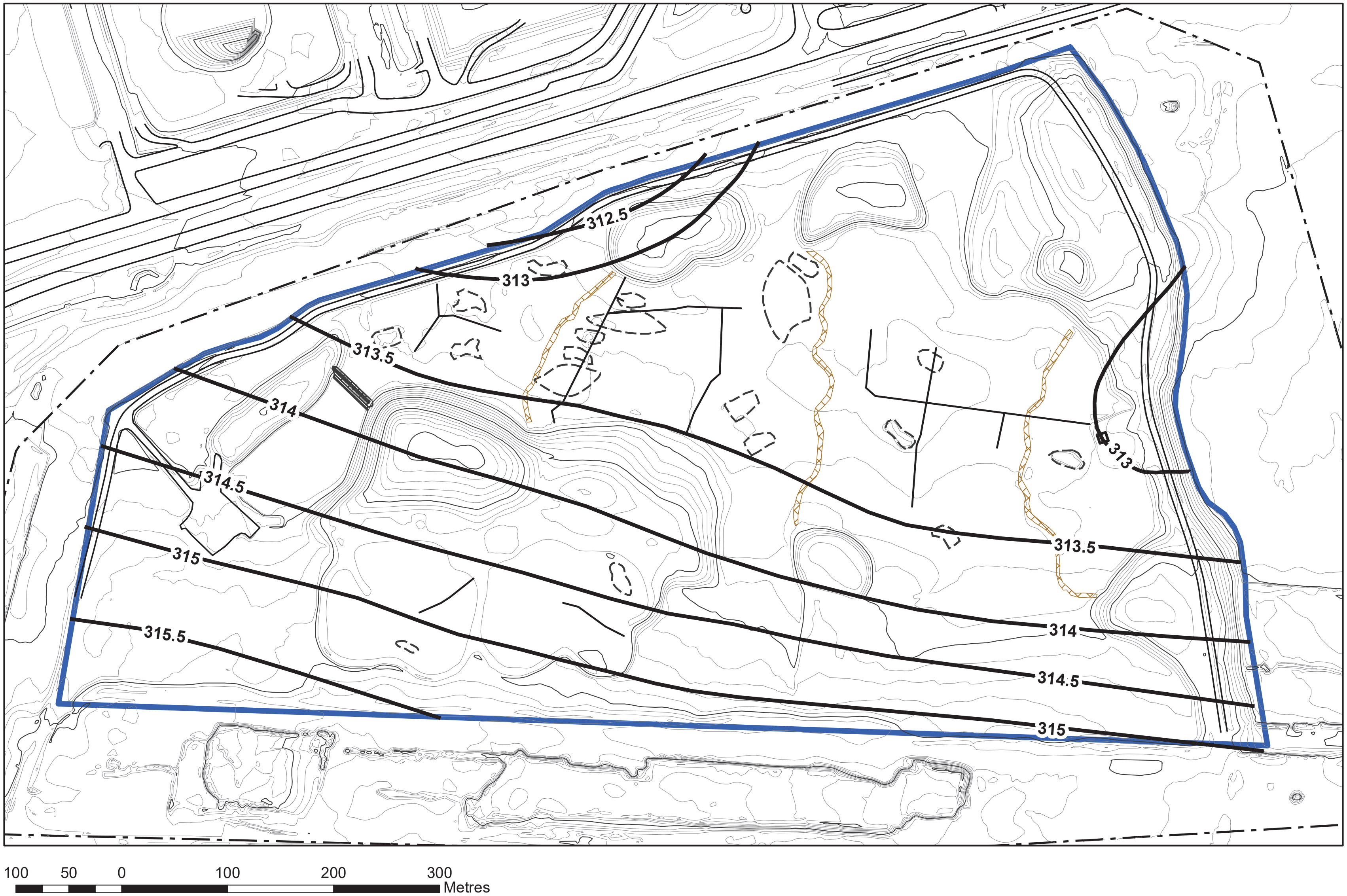

WTMap-2017-05-05

SHFW - Water Table Map - 2017-JUN-01

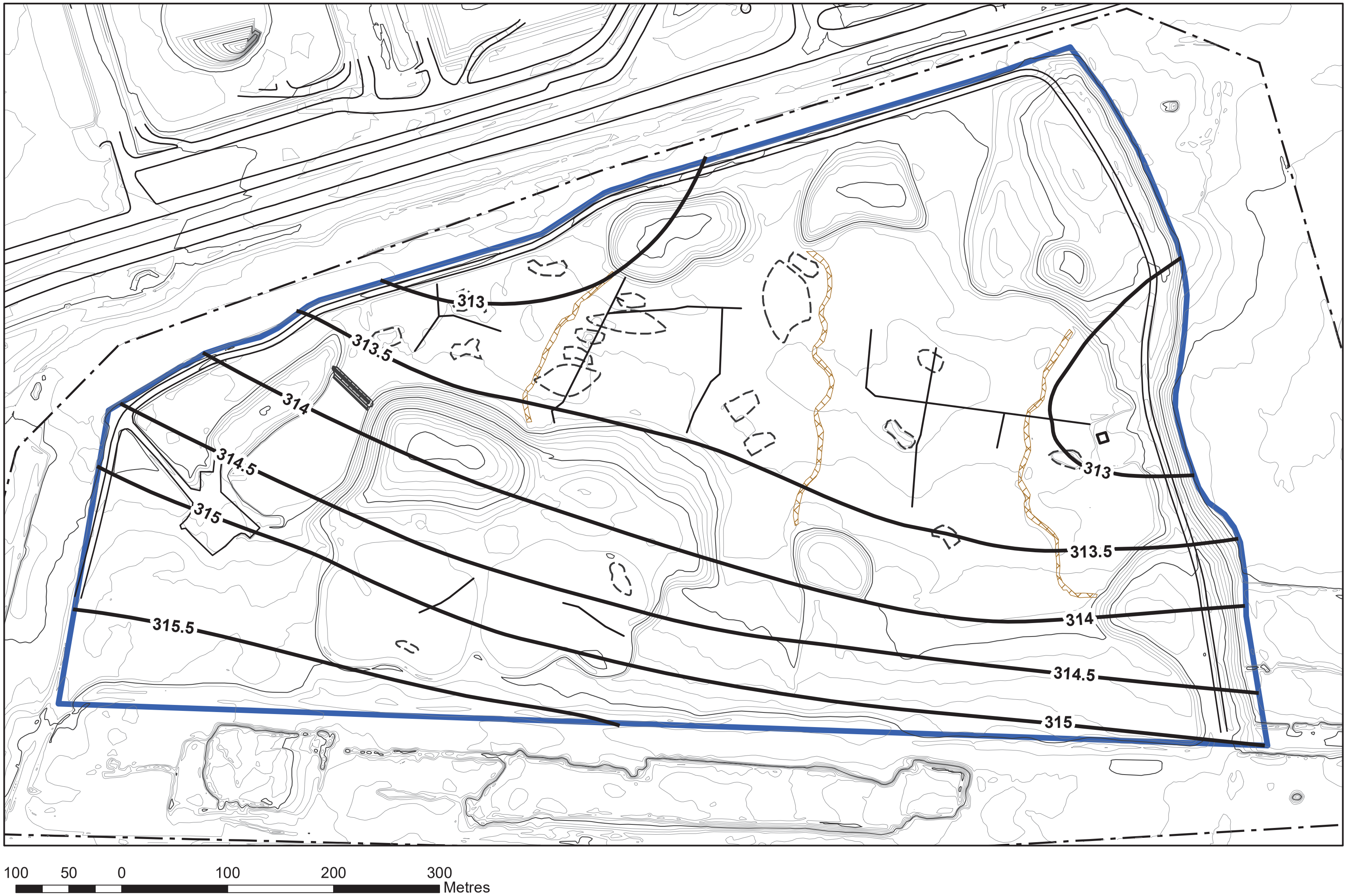

WTMap-2017-06-01

SHFW - Water Table Map - 2017-JUL-07

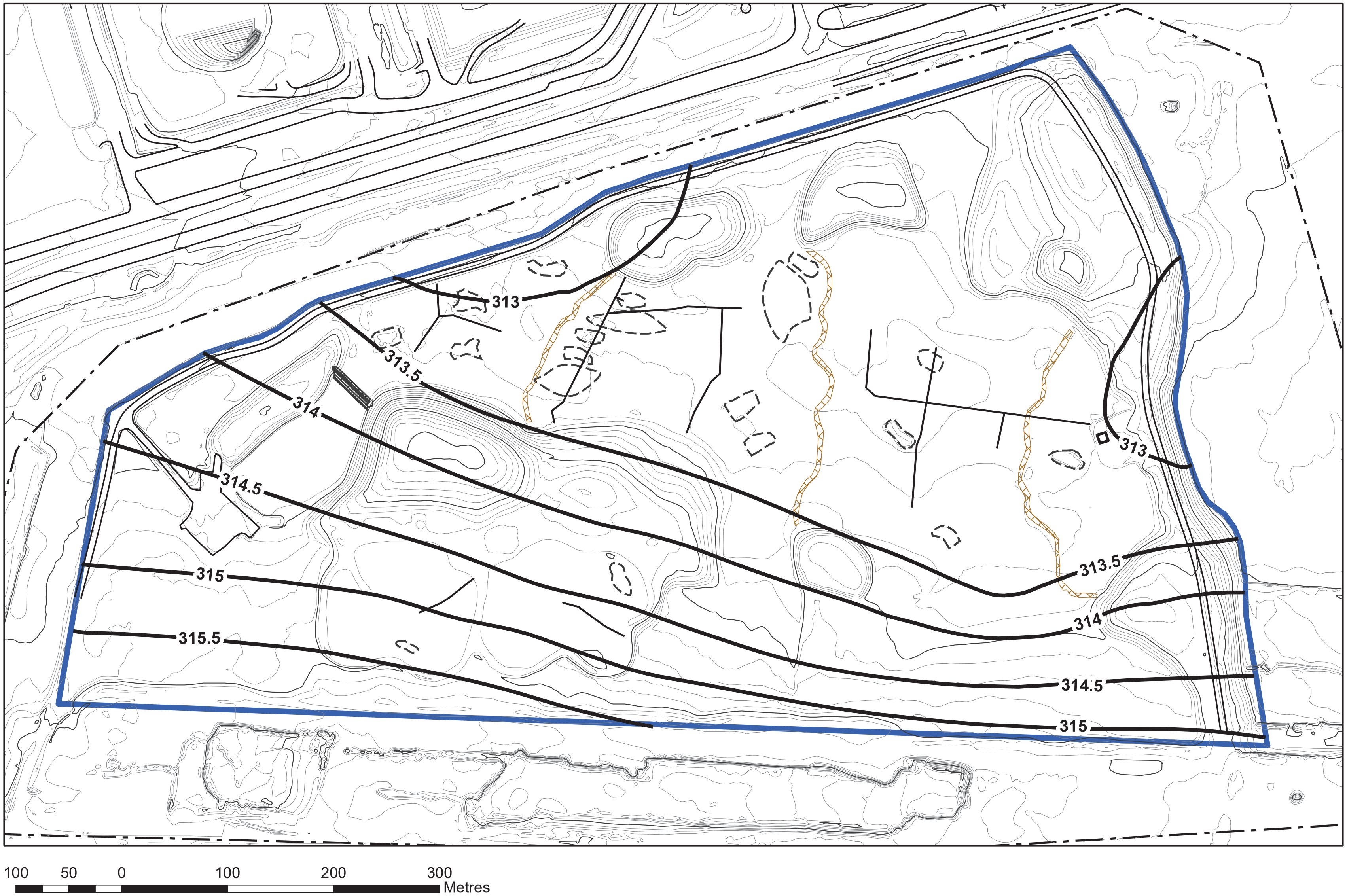

WTMap-2017-07-07

SHFW - Water Table Map - 2017-AUG-12

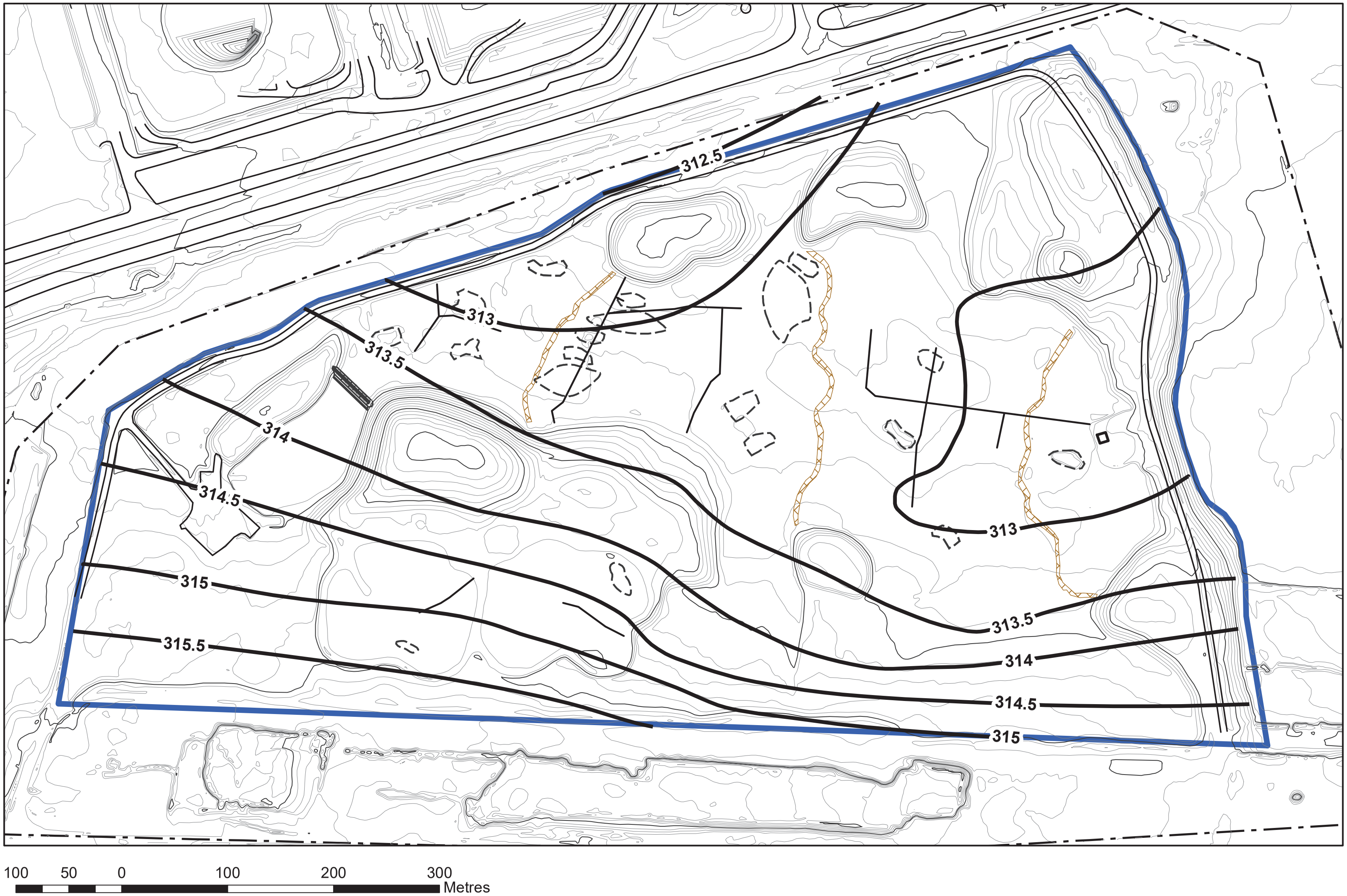

WTMap-2017-08-12

SHFW - Water Table Map - 2017-SEP-21

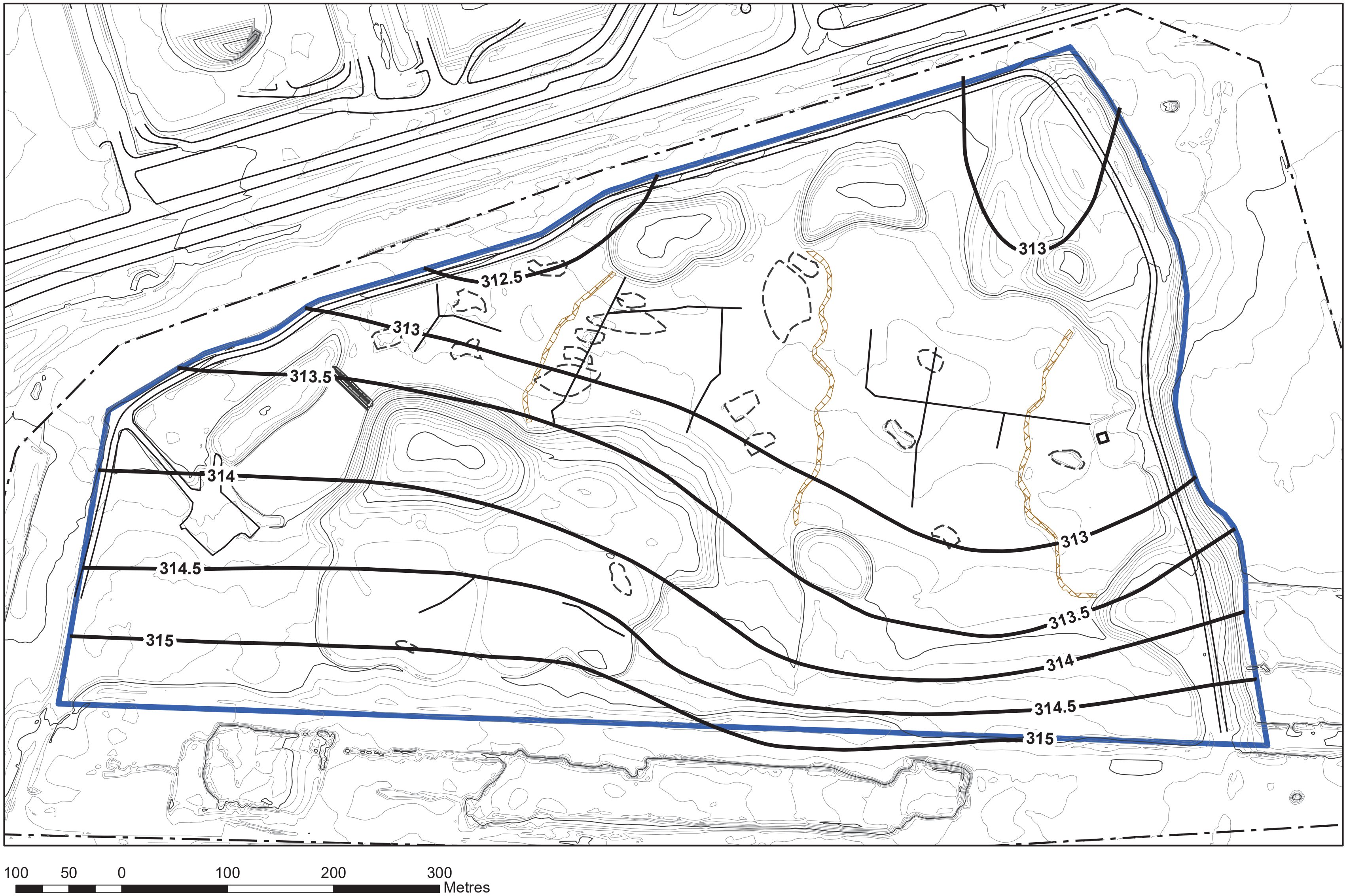

WTMap-2017-09-21

Appendix C - Electrical Conductivity Data

Appendix C - Electrical Conductivity Data

I. Scope of Work

This appendix contains electrical conductivity (EC) data presented in the form of EC temporal graphs, and groundwater EC maps. The temporal graphs have been developed for Transect 1 and Transect 2, previously described in the thesis (Figure 5), and three sub-transects (Transects 3, 4 and 5) located on Hummock 4, 6 and 7, respectively. The plotted data were from the shallowest piezometers in the nest that also had the longest data record. Electrical conductivity maps were developed at various points through the study period, from the electrical conductivity obtained only from piezometers screened within 2 metres of the water table. This was to reduce biases that deeper groundwater, with elevated electrical conductivity, may introduce. The EC maps are representative of groundwater EC distributions; therefore, they do not include surface water measurements.

II. Methods

Manual groundwater measurements were collected from shallow piezometers bi-weekly to monthly during the field season (May-October) from 2013 to 2017 with a temperature, level, and conductivity meter (TLC; Solinst, Canada; Figure 5). When standing water was present adjacent to a piezometer, surface water measurements were also taken; however, the data presented here are only groundwater values.

III. Results

Results are presented in the following order: EC temporal graphs (Transects 1 to 5) and EC maps (2015-2017). EC maps are organized chronologically, as indicated by the map header. Only data from 2015 to 2017 are presented here.

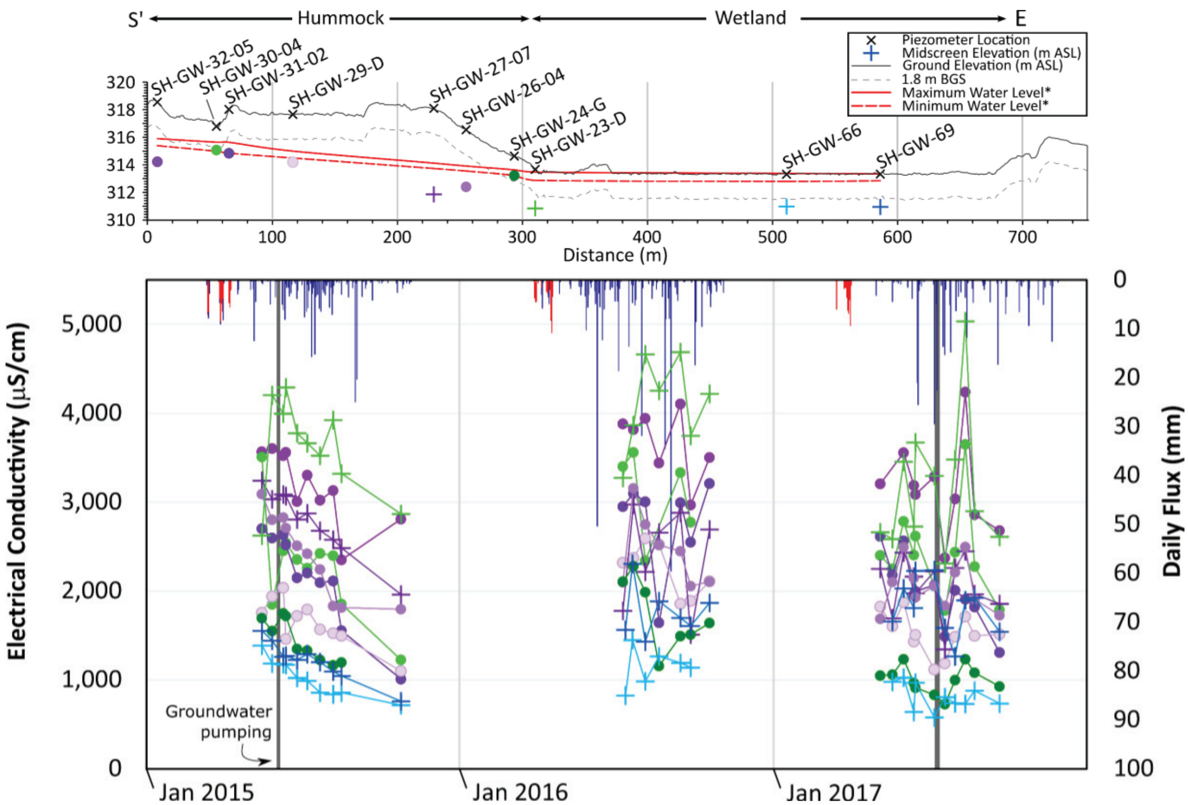

Figure C-1a: Cross section of Transect 1 paired with EC temporal graph and daily flux data from January 2015 to December 2017 (inclusive). Cross section demonstrates landscape position of piezometers with midscreen elevations, maximum and minimum manual water level measurements observed during the study period at each individual location. Point data in the temporal plot are manual measurement data; lines in hydrograph are continuous automated data (nest 66 and 69 provided by Carey, unpublished). Grey bar represents pumping event duration. Point data color and symbology are explained in Figure 6; line for 1.8 m below ground surface for reference only. Details for daily flux data are outlined in Figure 2.

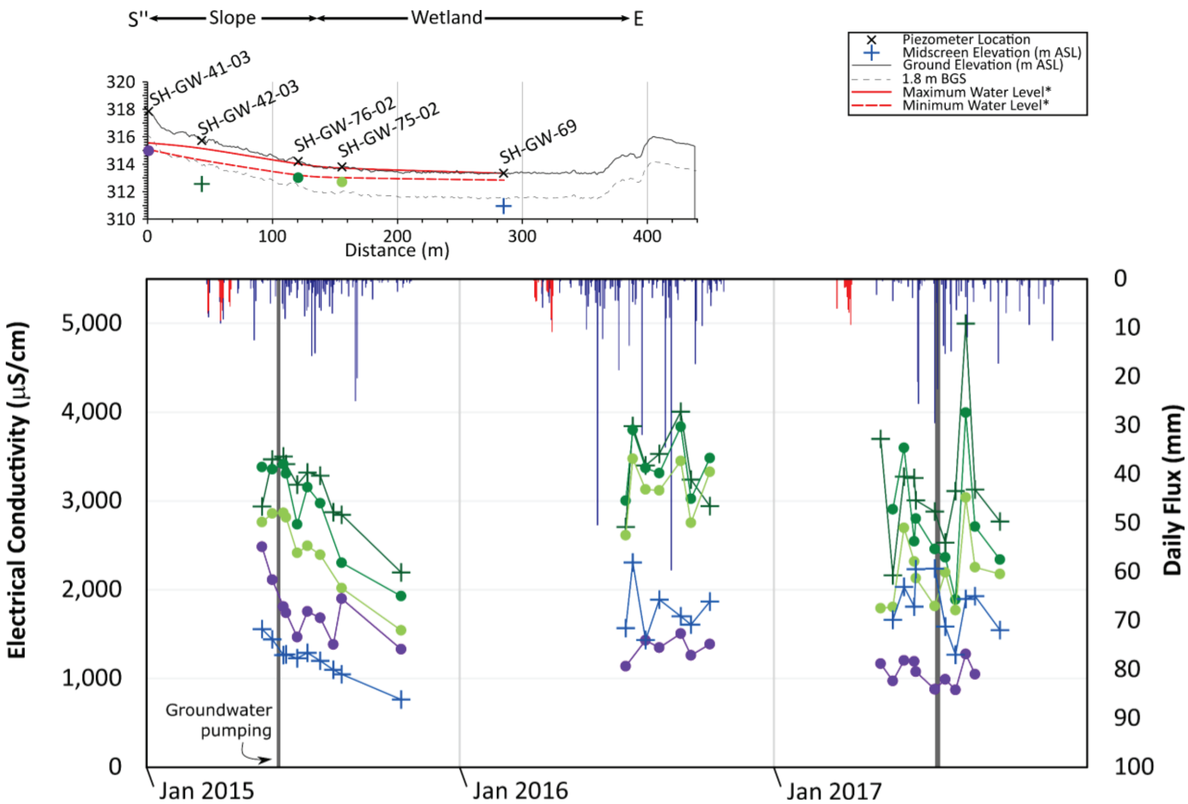

Figure C-1b: Cross section paired with EC temporal graph and daily flux data for Transect 2 from January 2015 to December 2017 (inclusive). Details summarized in Figure C-1a.

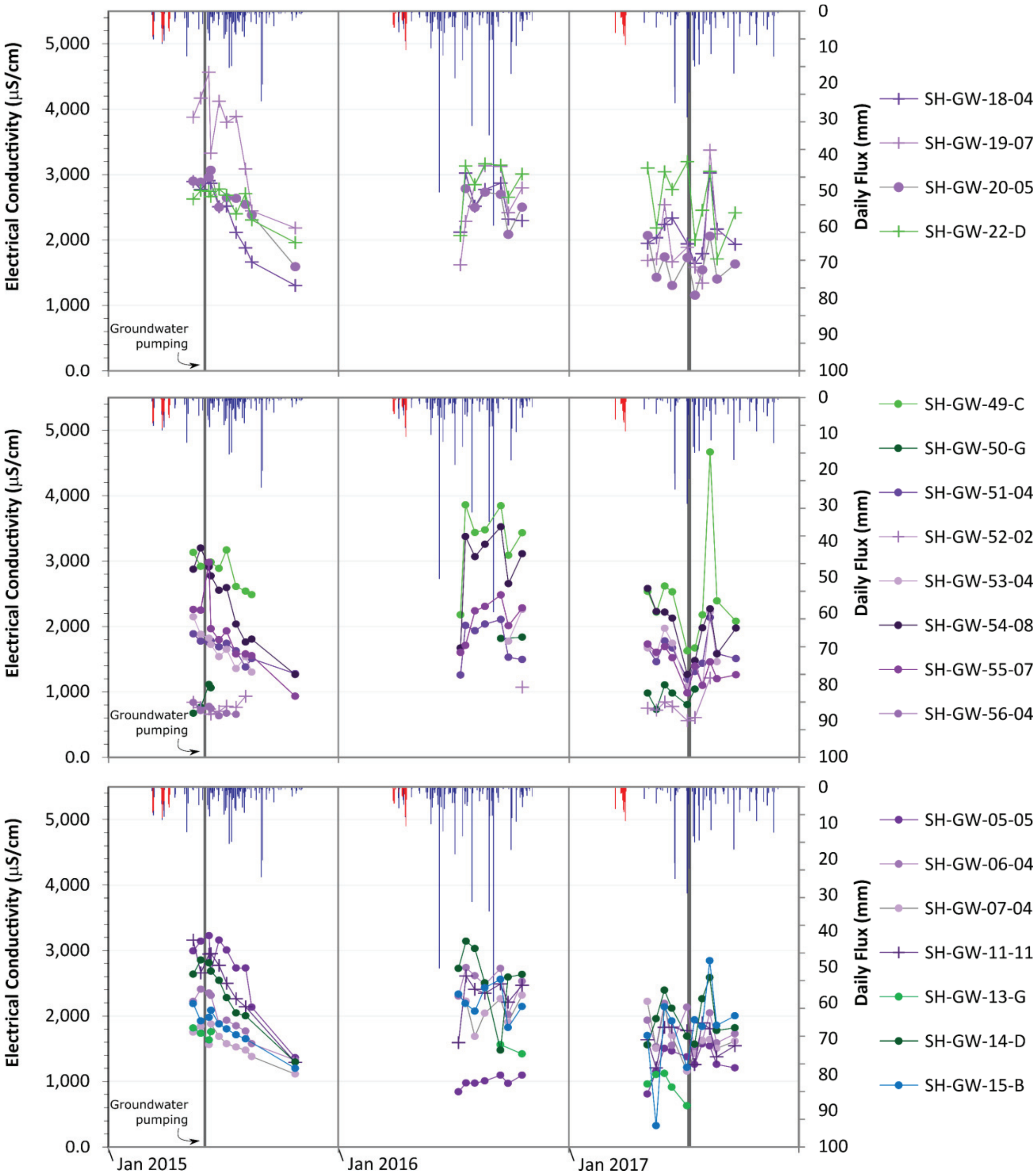

Figure C-2: Hydrographs developed for piezometers located along sub-transects 3, 4 and 5 (top down) located on Hummock 4, Hummock 6 and Hummock 7, respectively, from 2015 to 2017. Details summarized in Figure C-1a.

SHW - GW EC Map - 20160721 - Shallow MS Only (<2 m BWL)

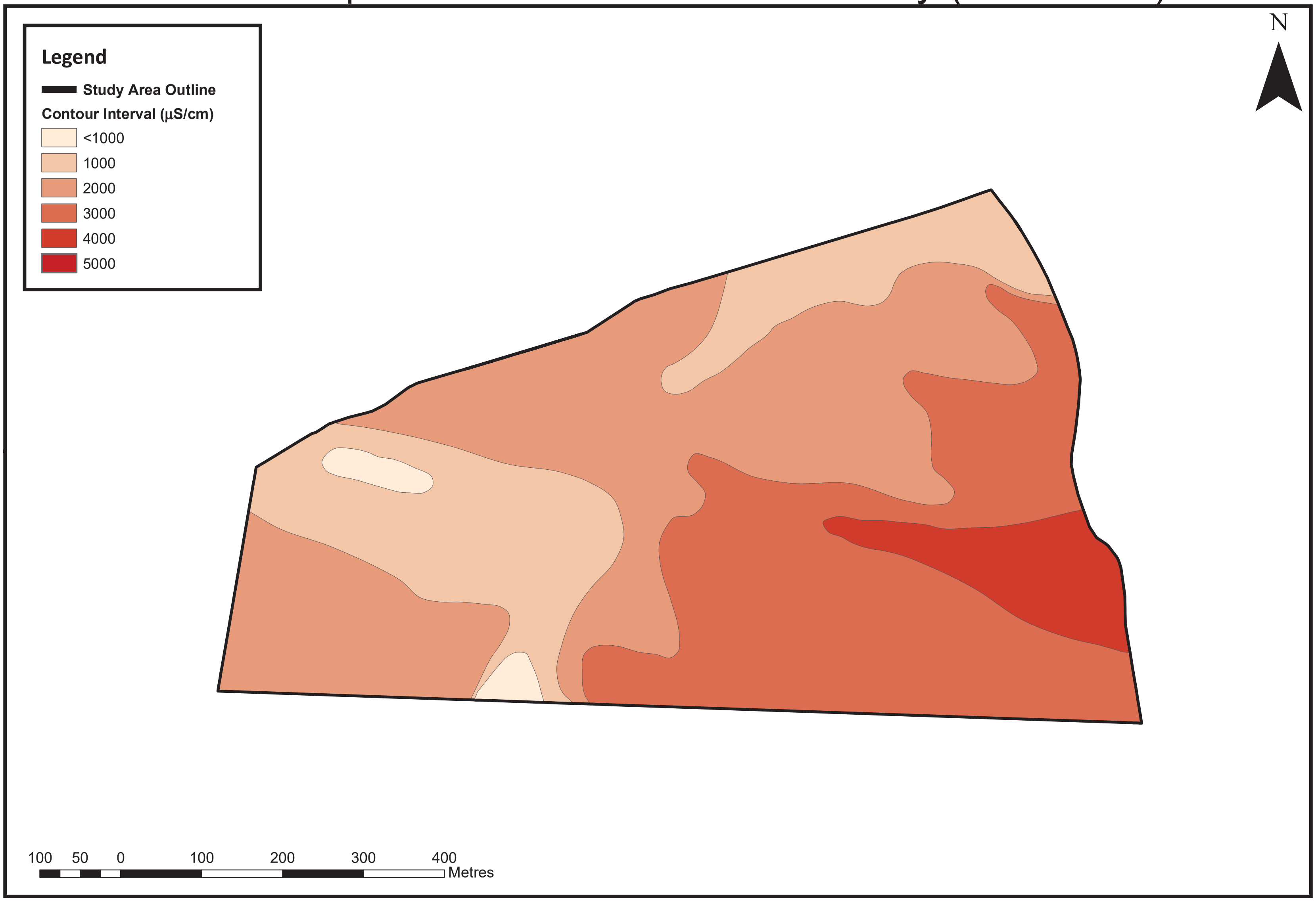

Map created by P. Twerdy 20190121

SHW - GW EC Map - 20160804 - Shallow MS Only (<2 m BWL)

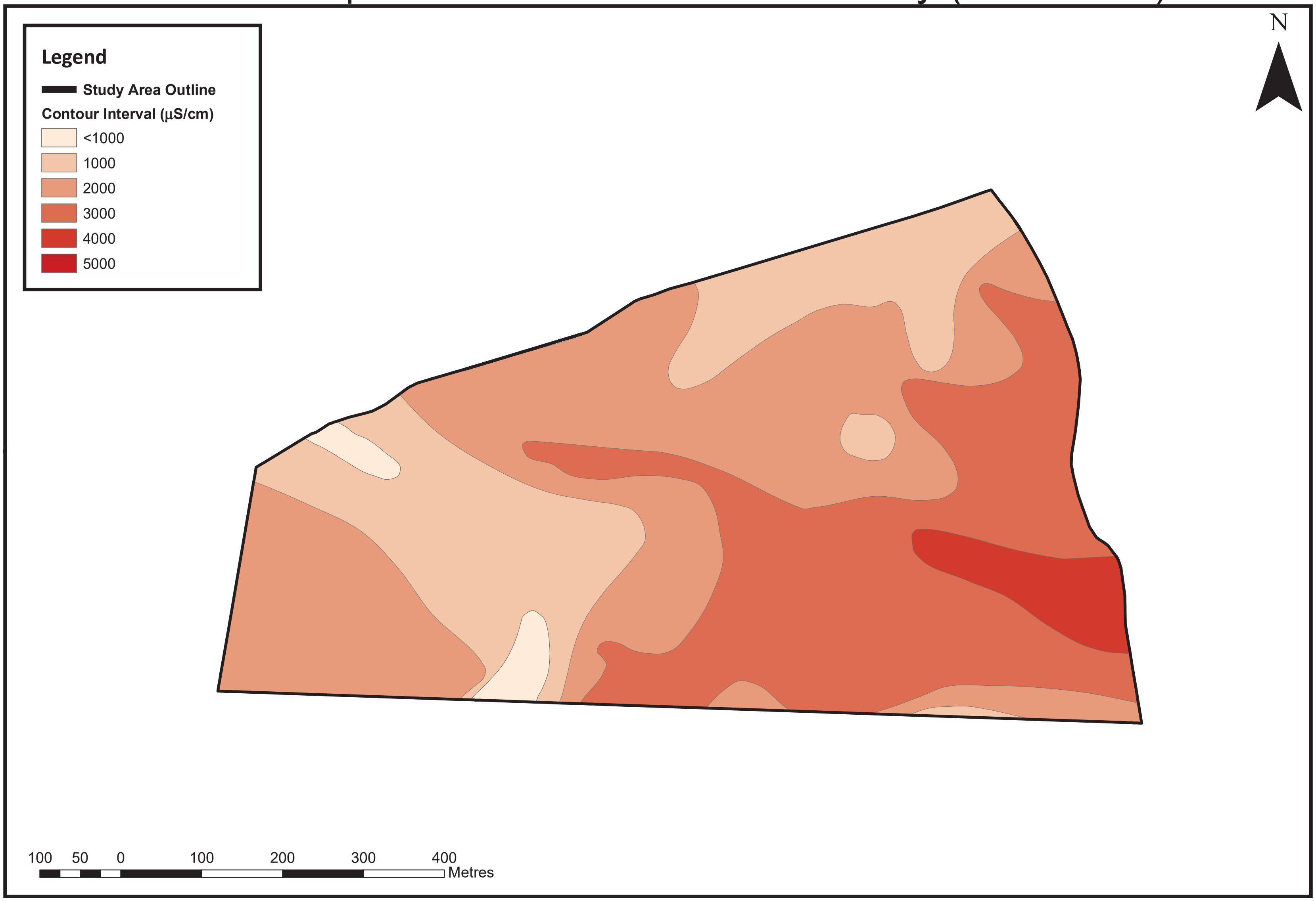

Map created by P. Twerdy 20190121

SHW - GW EC Map - 20160820 - Shallow MS Only (<2 m BWL)

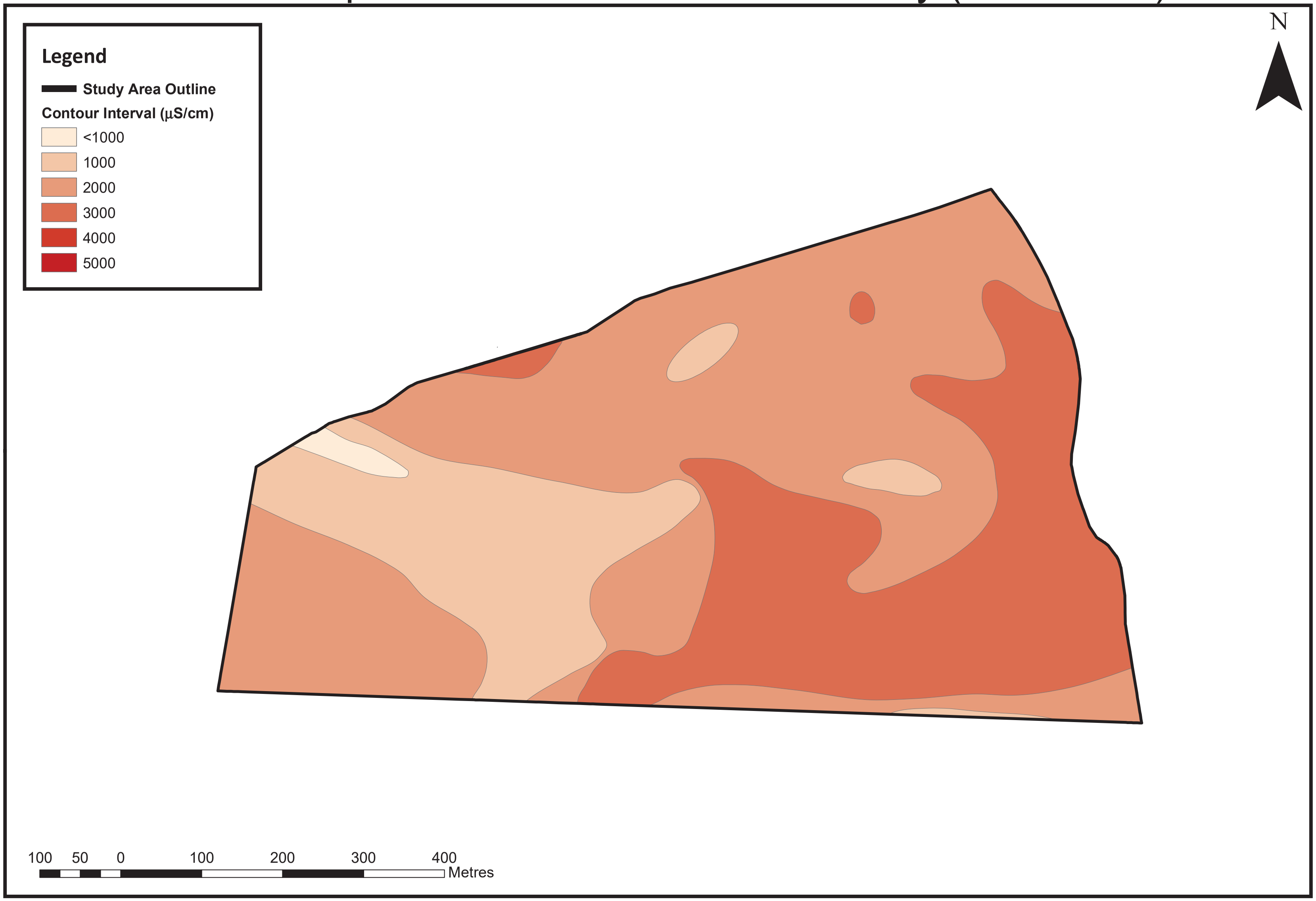

Map created by P. Twerdy 20190121

SHW - GW EC Map - 20160914 - Shallow MS Only (<2 m BWL)

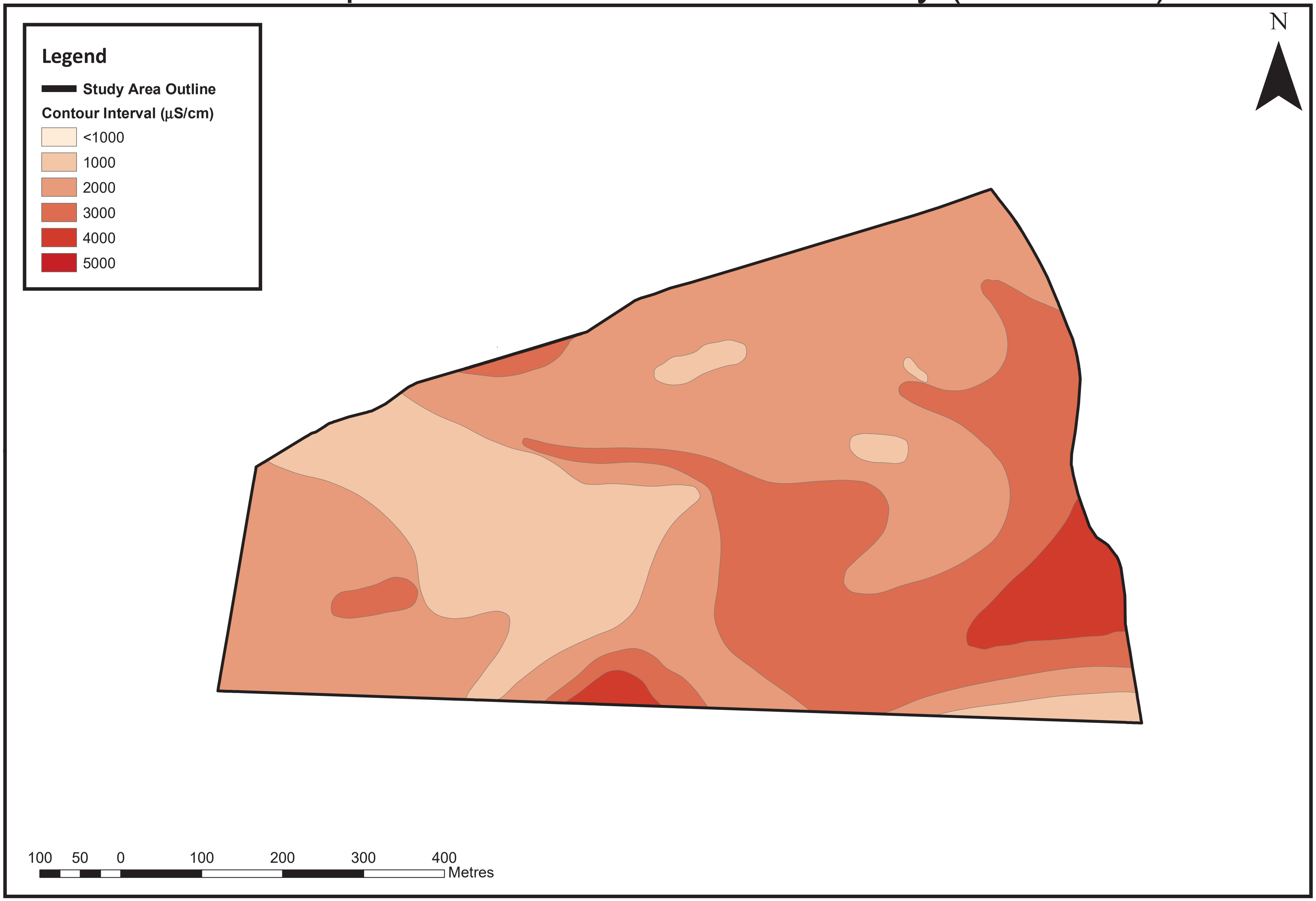

Map created by P. Twerdy 20190121

SHW - GW EC Map - 20170707 - Shallow MS Only (<2 m BWL)

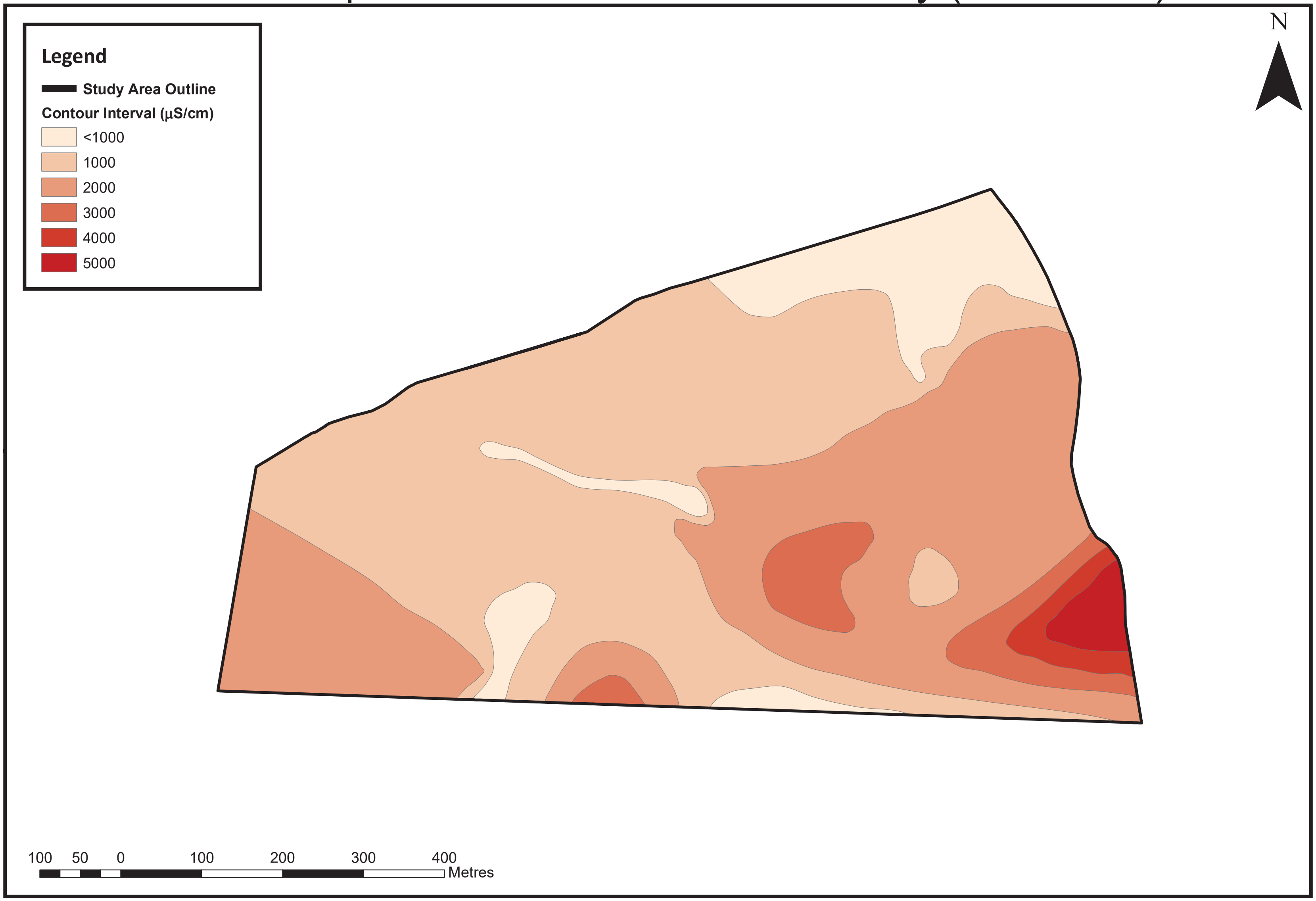

Map created by P. Twerdy 20190121

SHW - GW EC Map - 20170719 - Shallow MS Only (<2 m BWL)

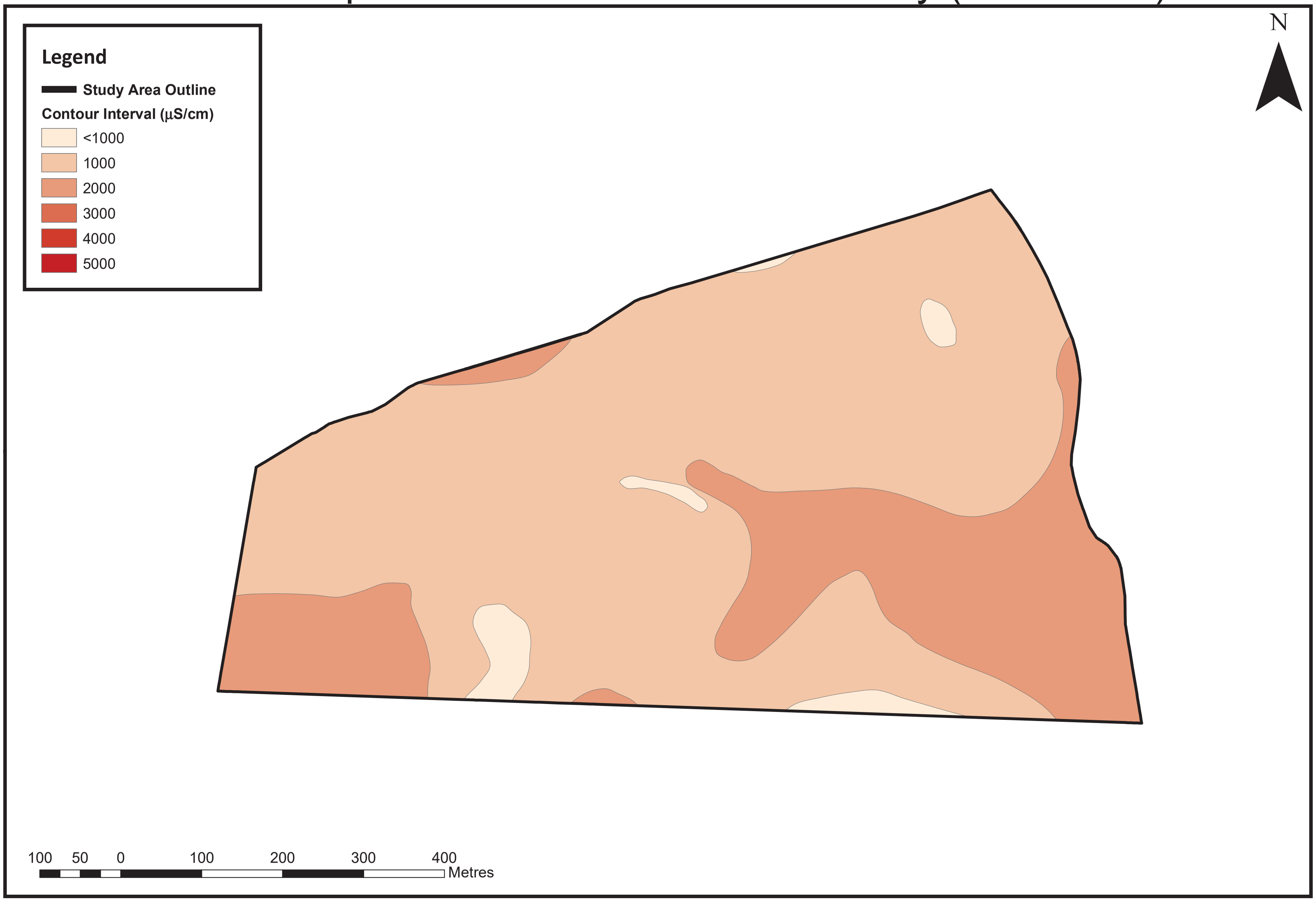

Map created by P. Twerdy 20190121

SHW - GW EC Map - 20170812 - Shallow MS Only (<2 m BWL)

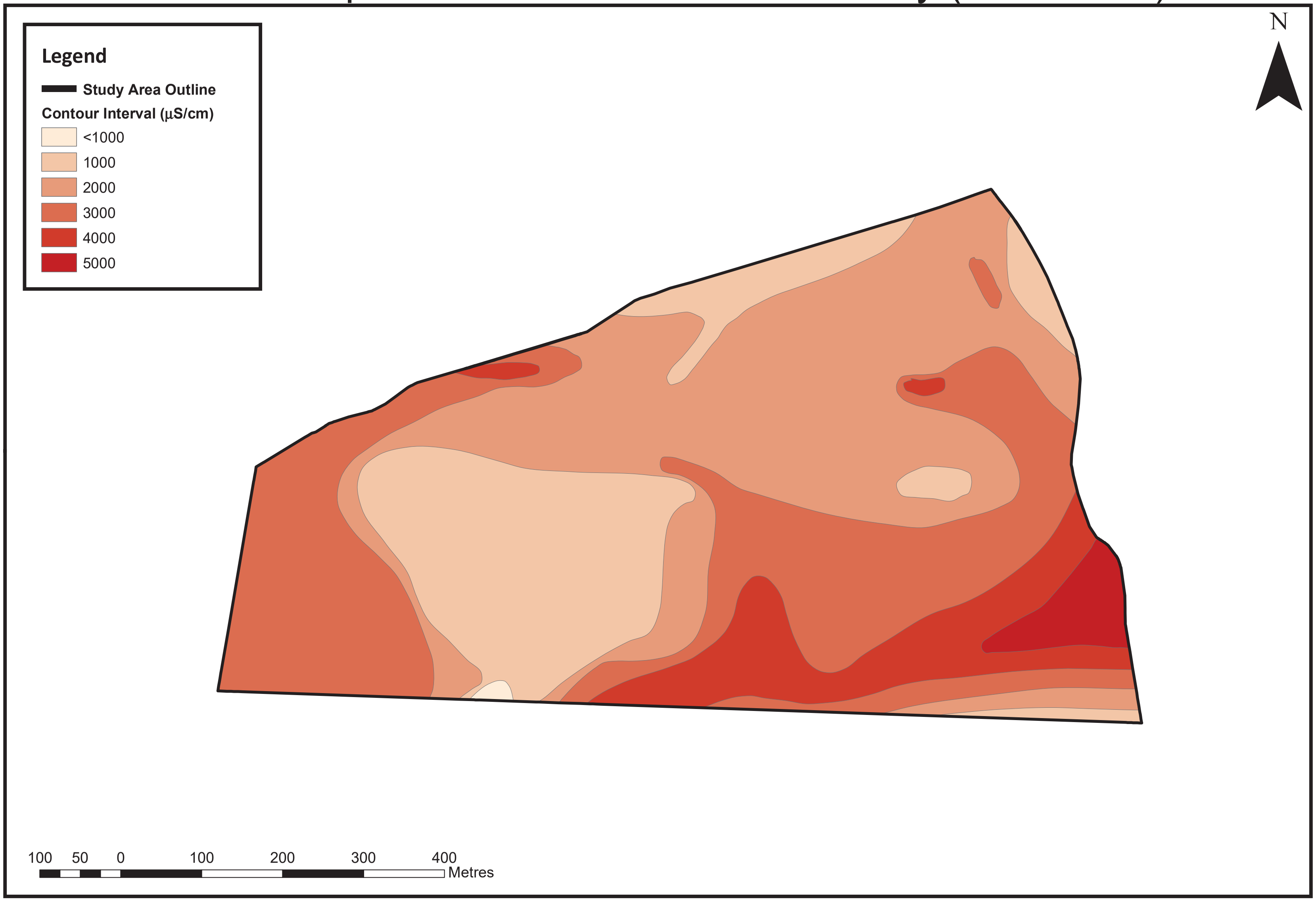

Map created by P. Twerdy 20190121

Appendix D - Soil Saturation & Wetness Maps

Appendix D - Soil Saturation & Wetness Maps

I. Scope of Work

This appendix contains all soil saturation and wetness maps collected during the study period. They were mapped to evaluate the areal extent of saturated and standing water areas in the watershed, as each field season progressed.

II. Methods

Soil saturation and wetness mapping required delineating the extent of standing water, saturated soil and unsaturated soil intermittently throughout the field seasons (May-October) utilizing the squishy-boot method (Devito et al., 2005b). Mapping was done manually, with a map and a GPS receiver in 2013-2015, and digitally, on an Apple iPad with Bluetooth-enabled GPS (BadElf) and mapping software (ArcGIS) in 2016 and 2017. Maps from 2013 to 2015 were subsequently digitized using the same software.

III. Results

Soil wetness maps are organized chronologically, as indicated by the map header. Only data from 2015 to 2017 are presented here.

SHFW - Soil Saturation and Wetness Mapping - 2015-MAY-16

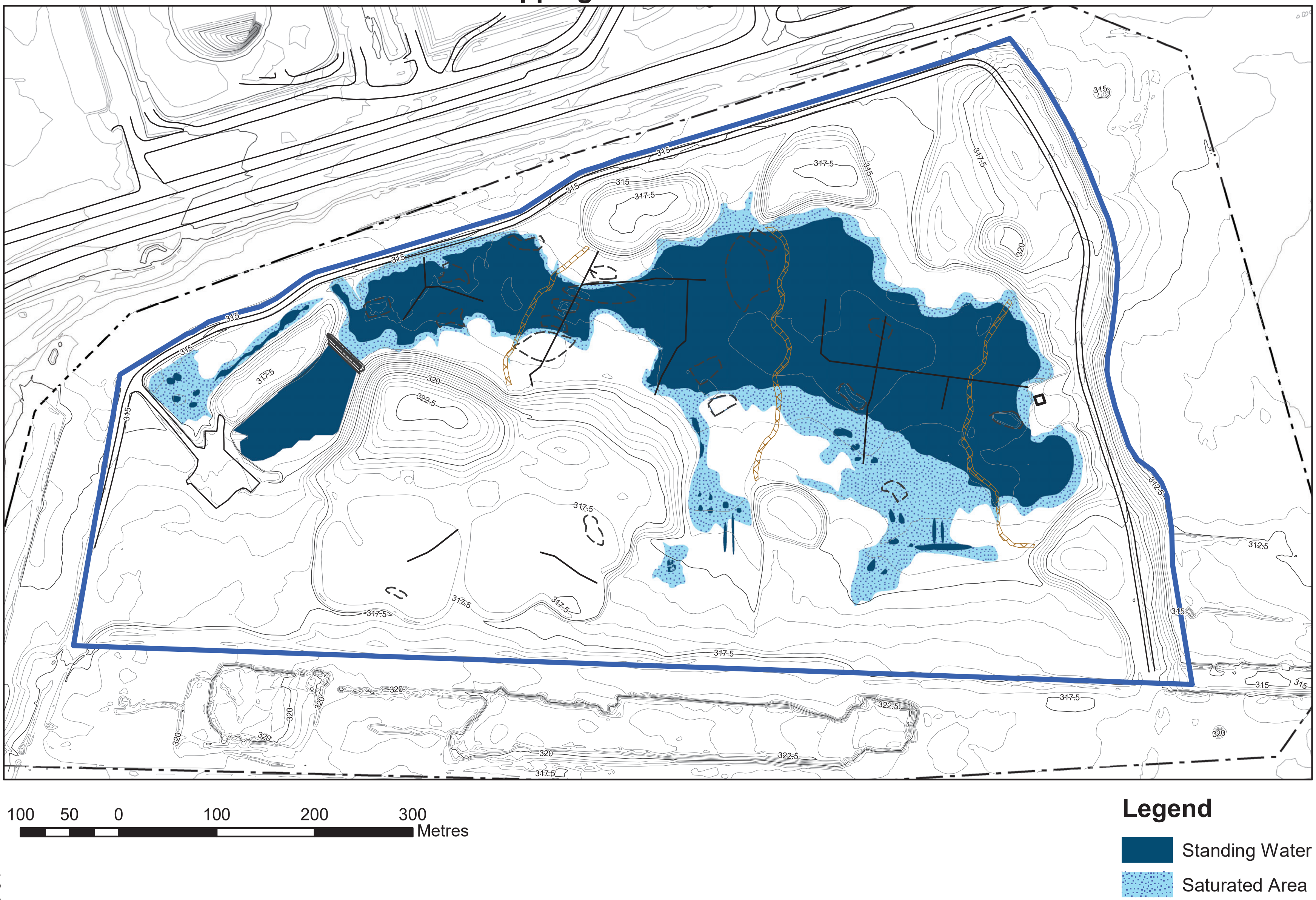

SHFW - Soil Saturation and Wetness Mapping - 2015-MAY-31

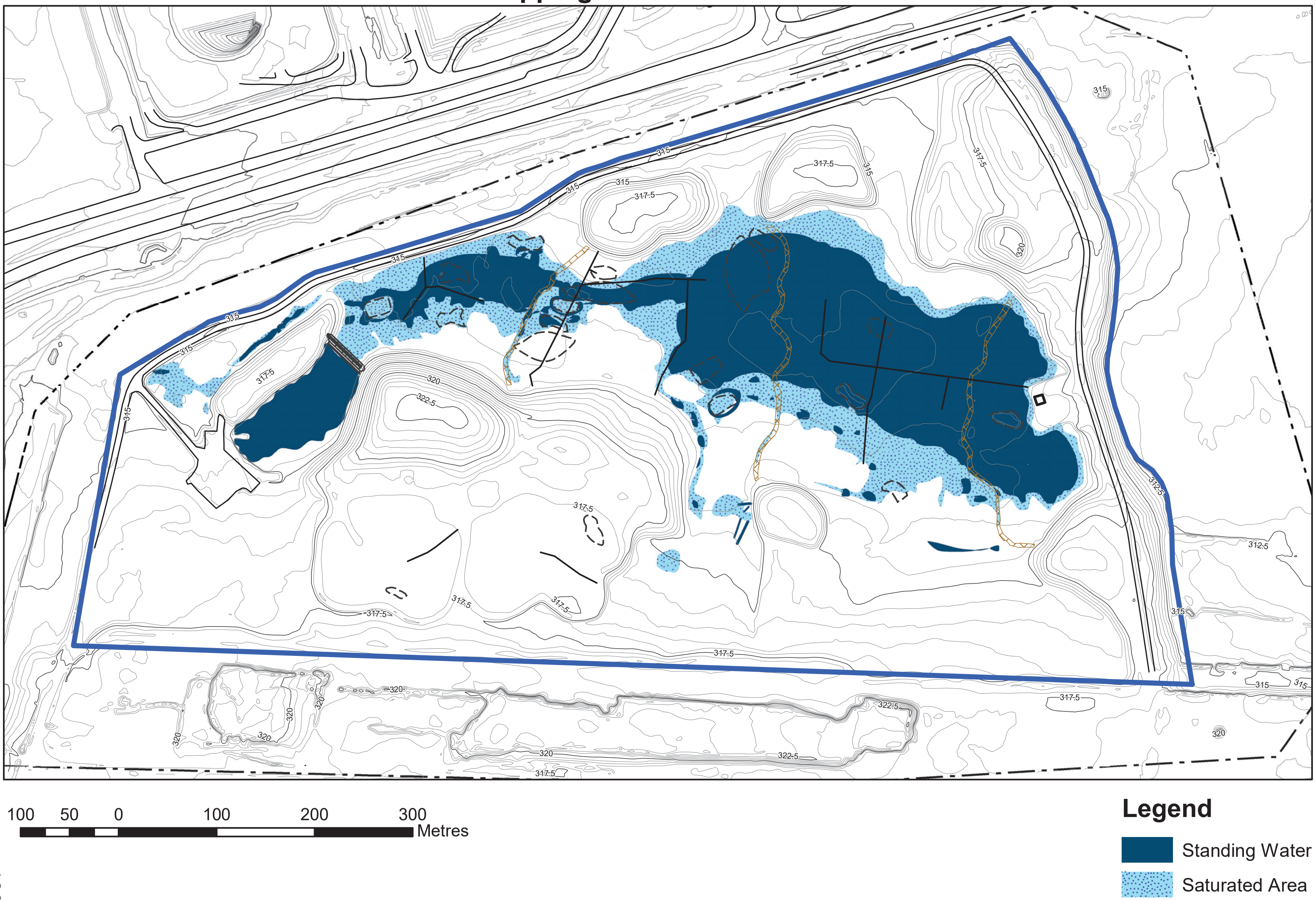

SHFW - Soil Saturation and Wetness Mapping - 2015-JUN-10

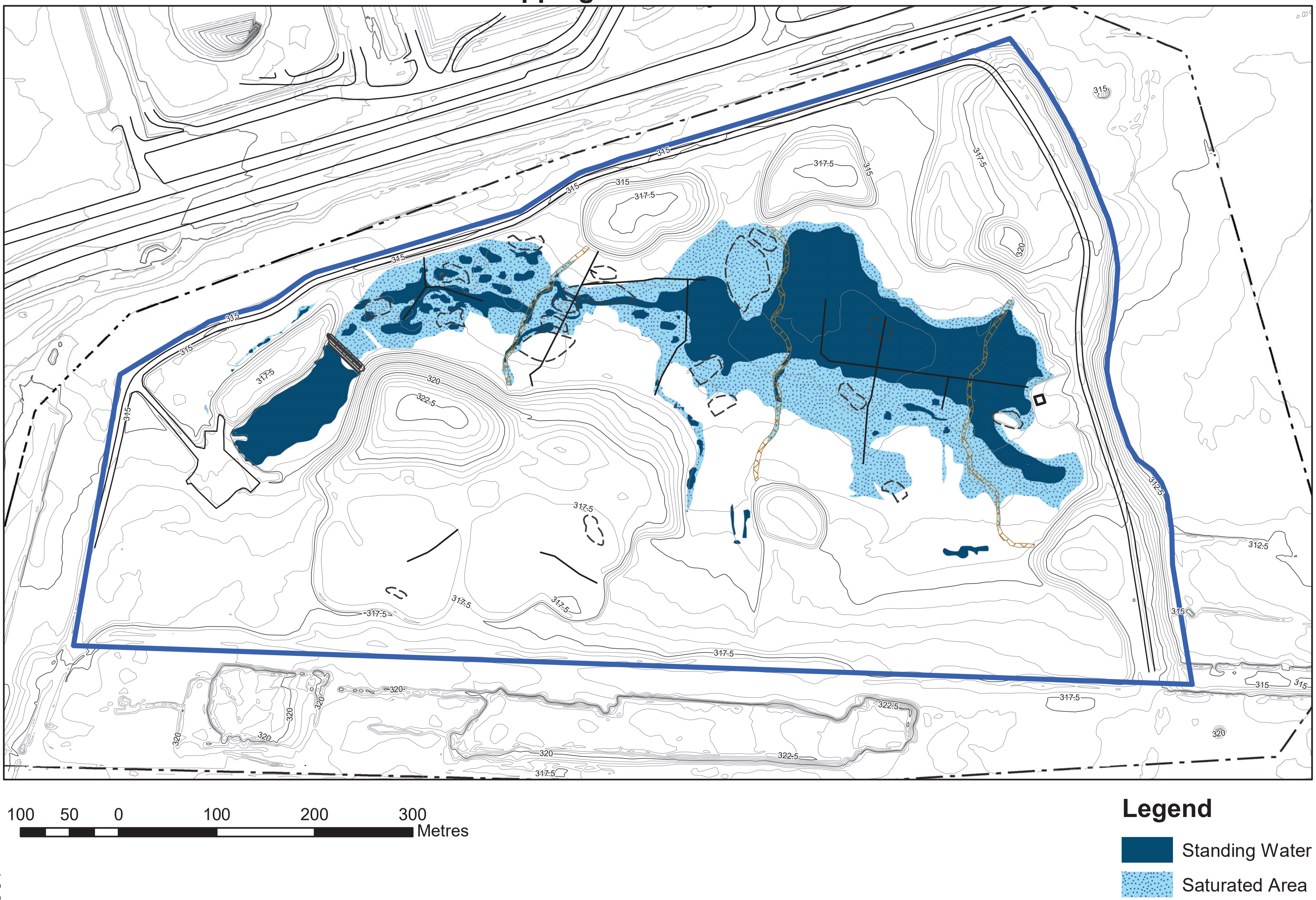

SHFW - Soil Saturation and Wetness Mapping - 2015-JUN-26

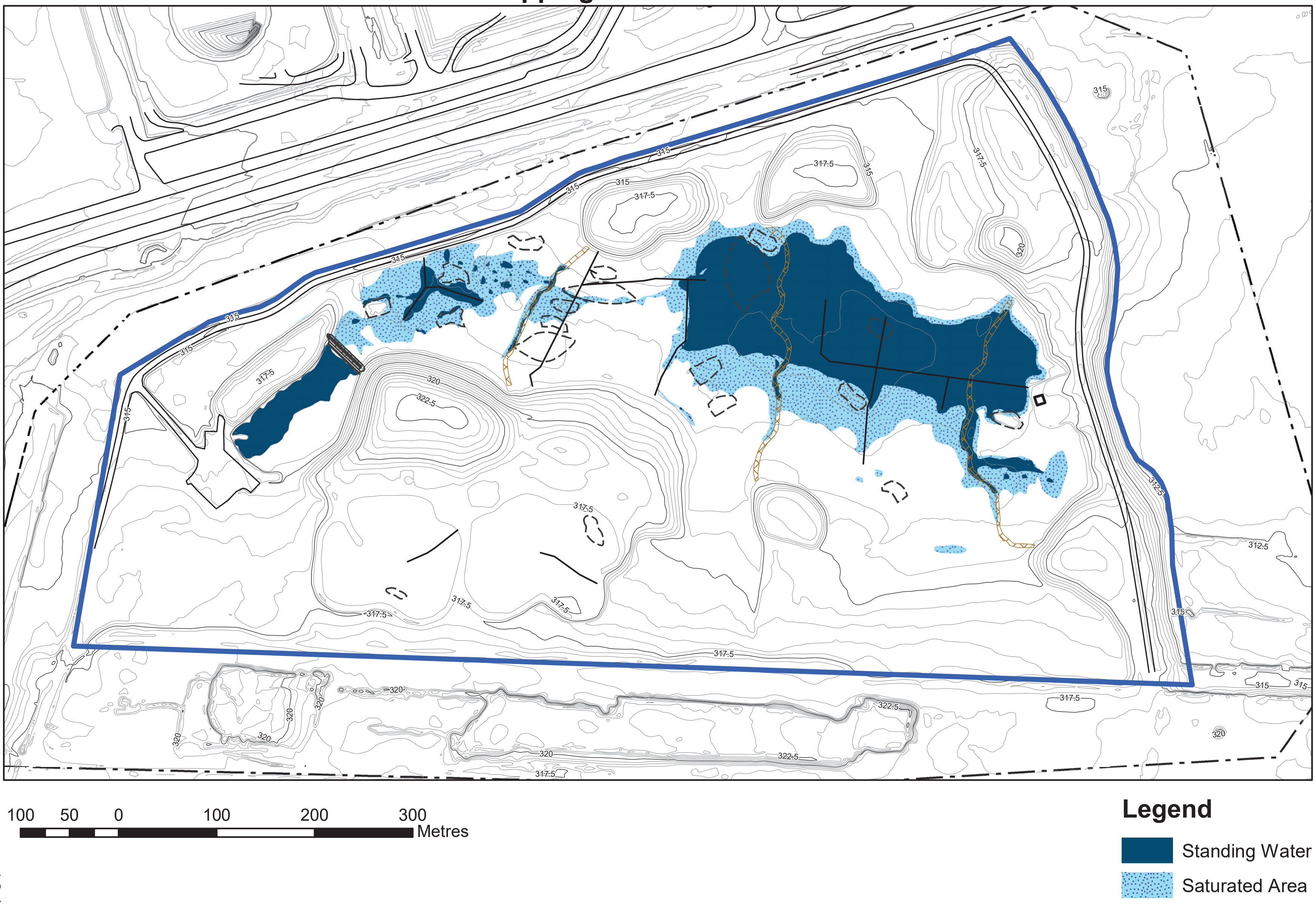

SHFW - Soil Saturation and Wetness Mapping - 2015-JUL-10

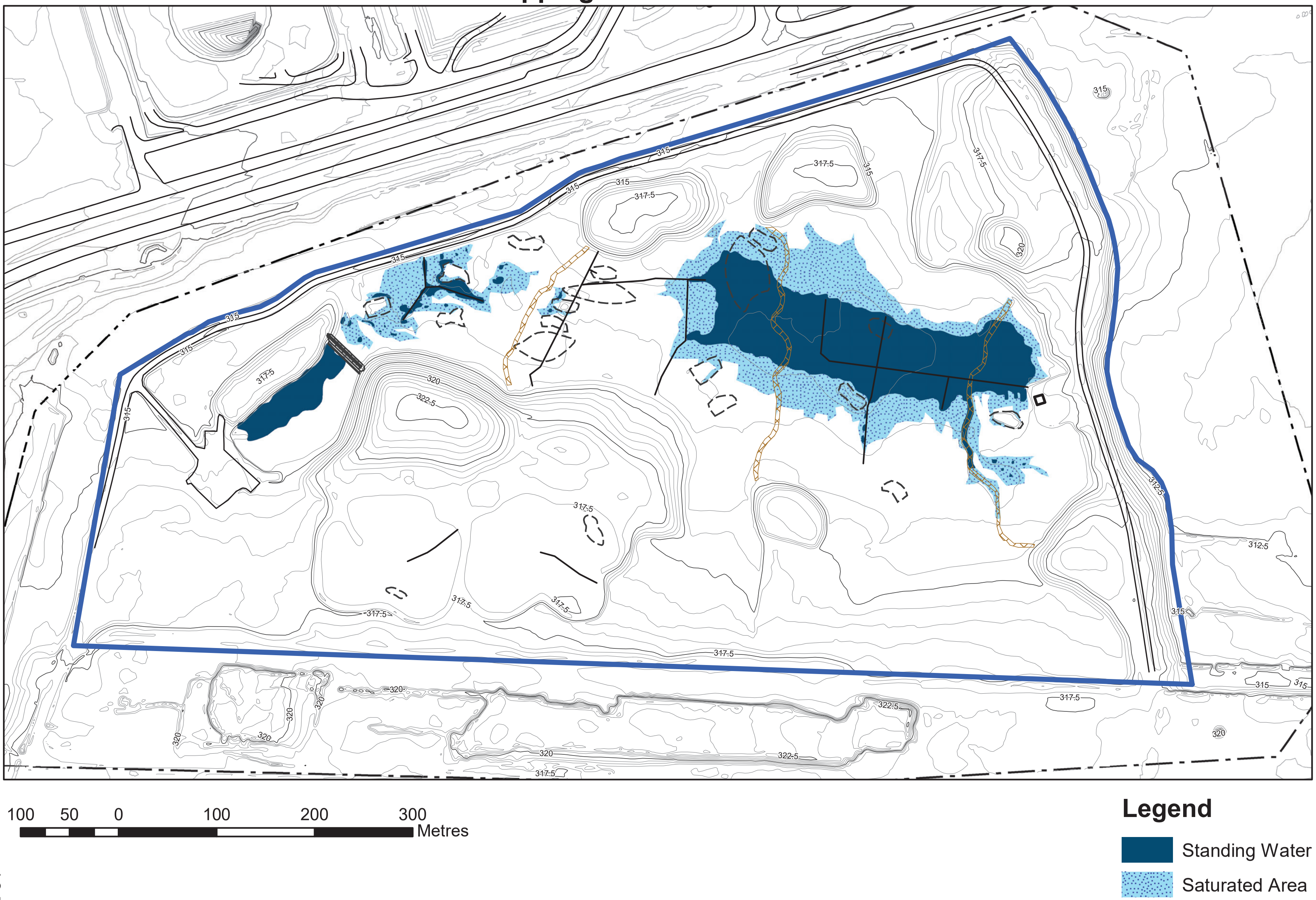

SHFW - Soil Saturation and Wetness Mapping - 2015-JUL-23

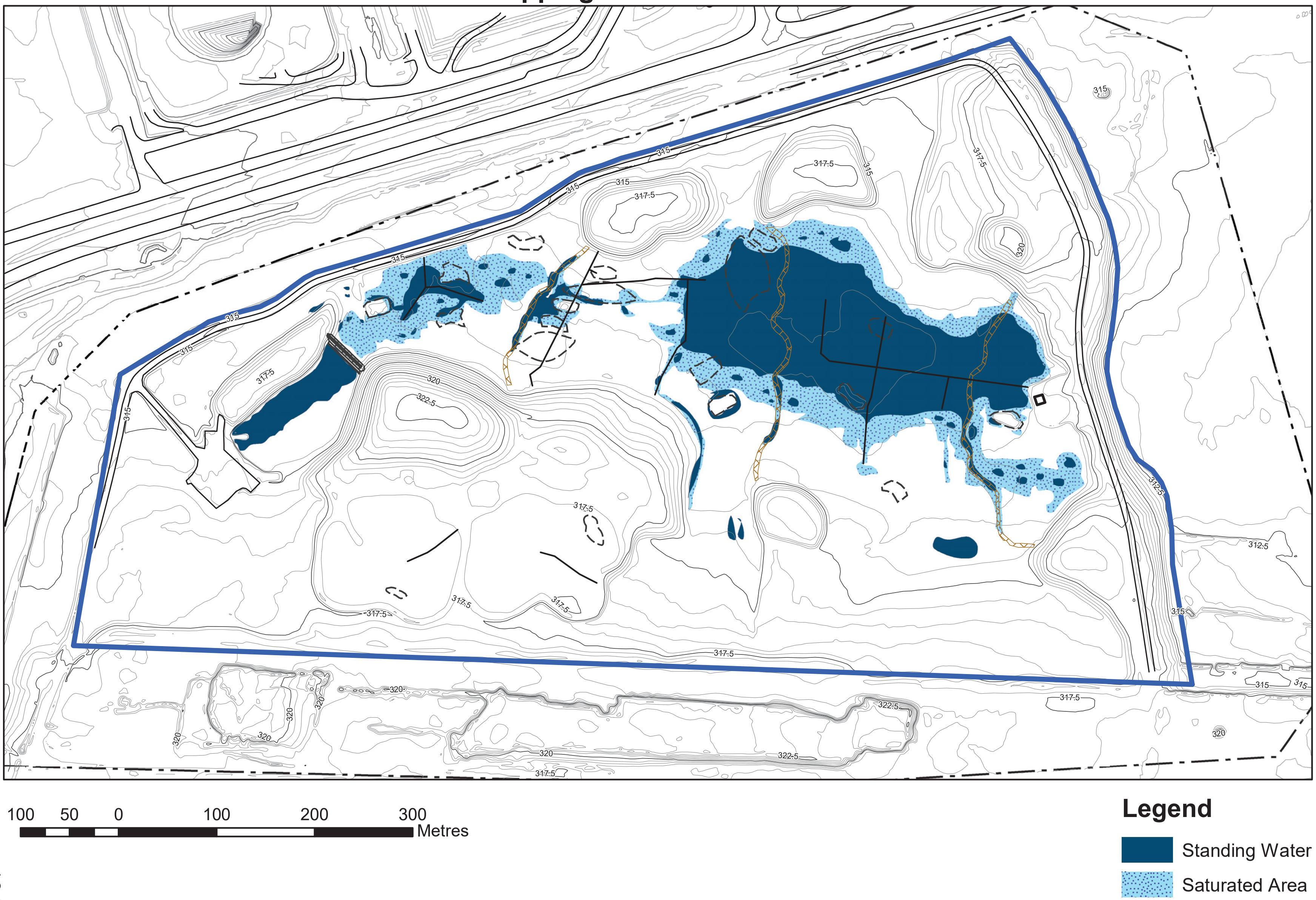

SHFW - Soil Saturation and Wetness Mapping - 2015-AUG-07

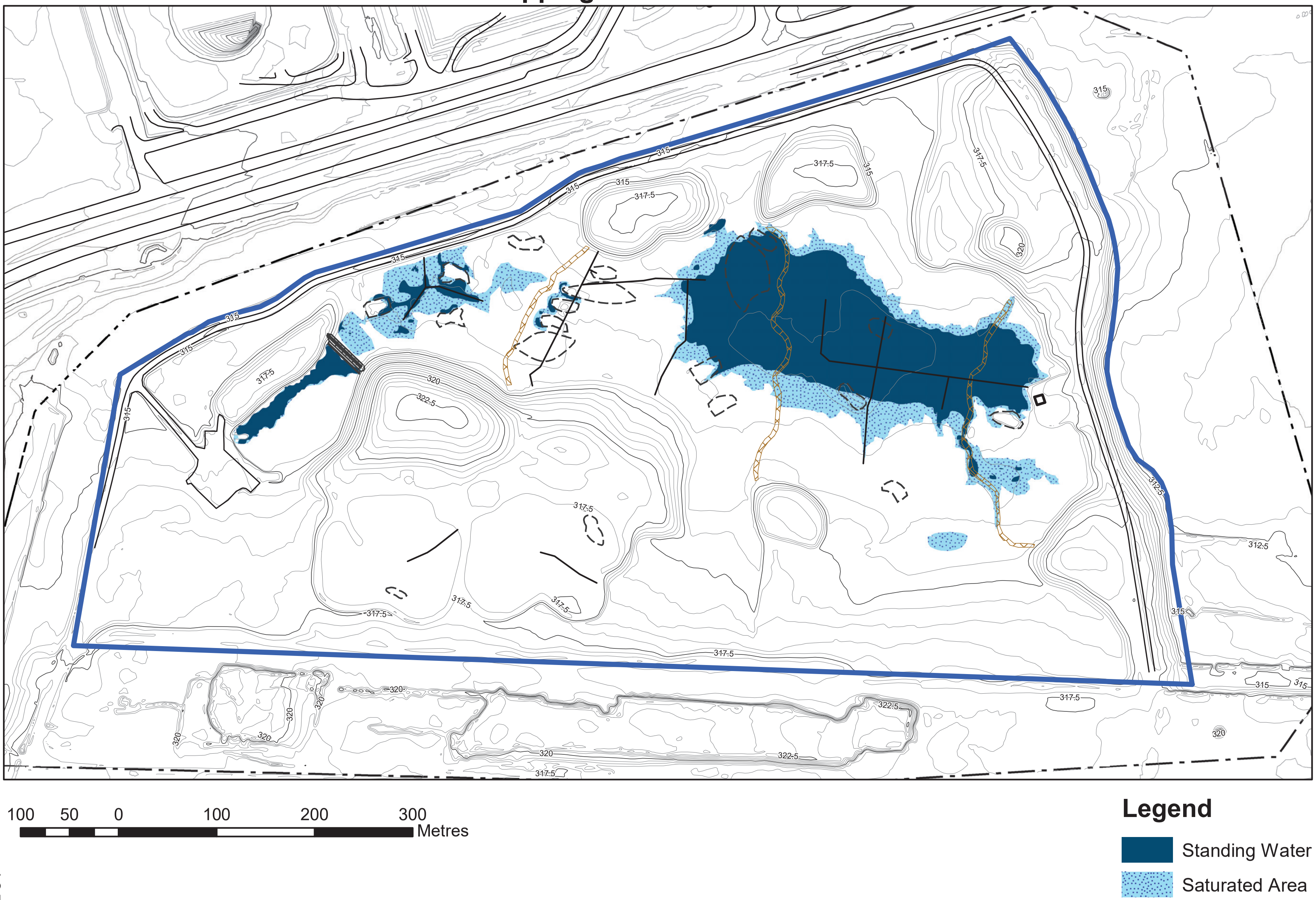

SHFW - Soil Saturation and Wetness Mapping - 2015-AUG-17

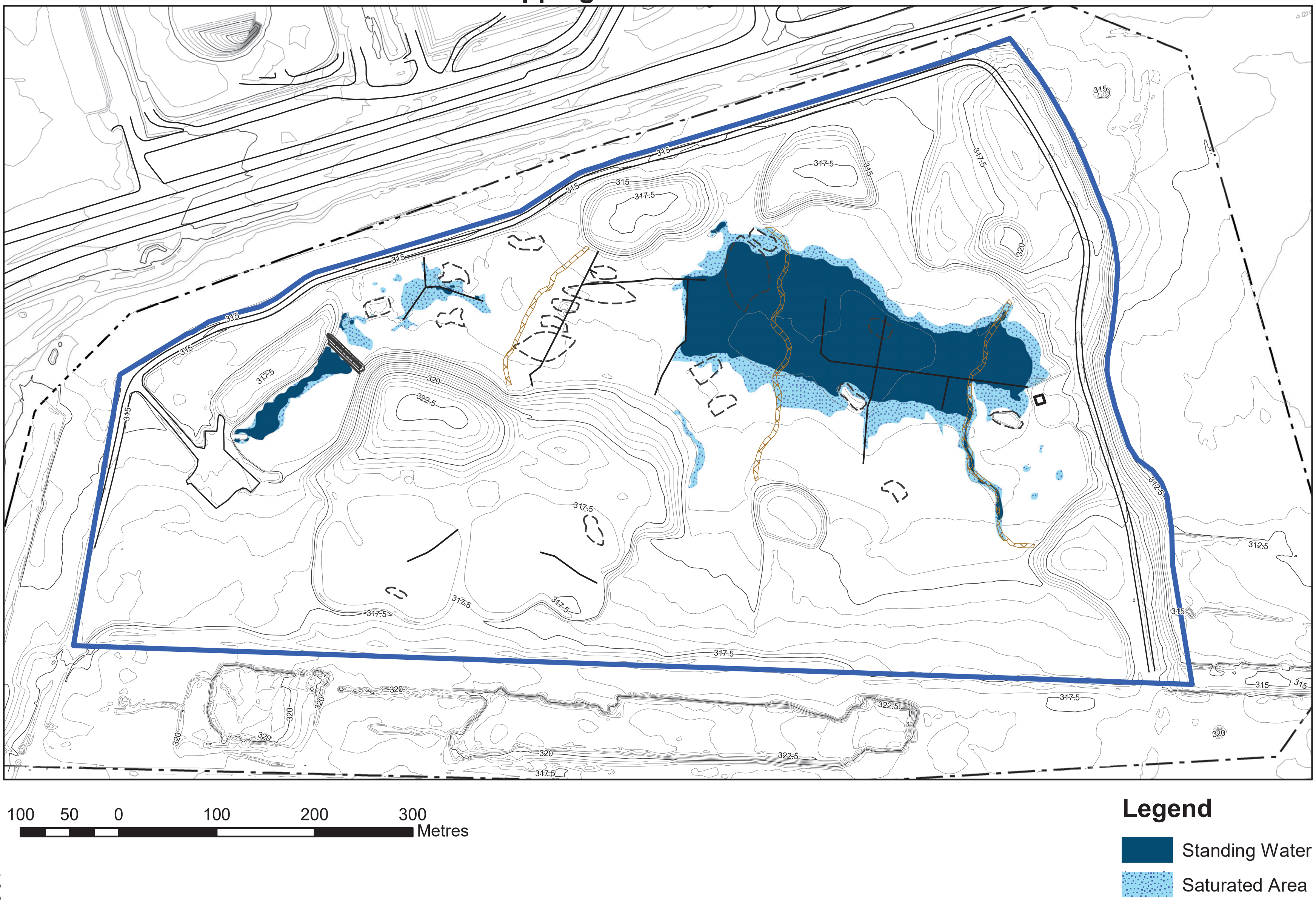

SHFW - Soil Saturation and Wetness Mapping - 2015-OCT-25

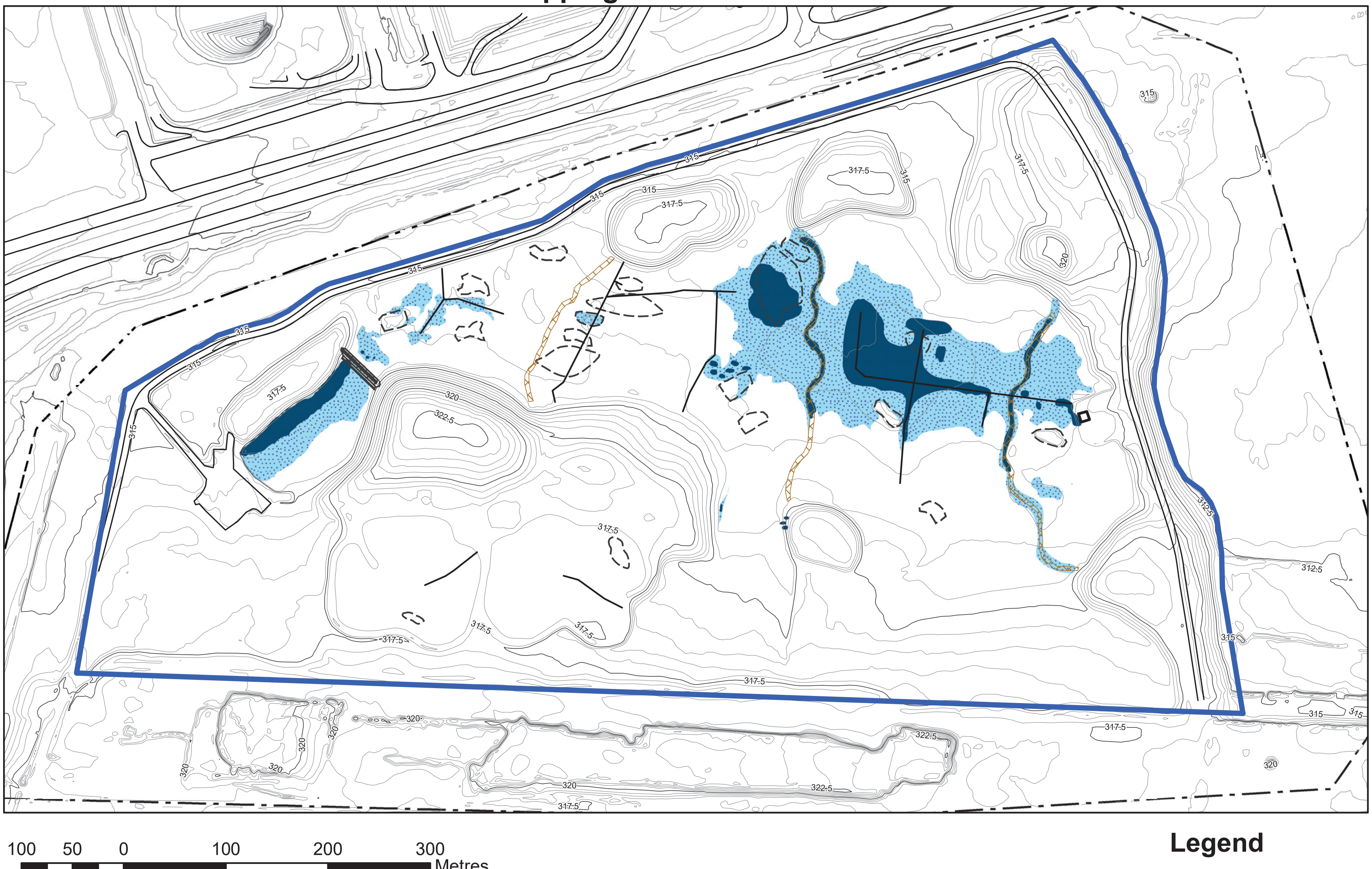

SHFW - Soil Saturation and Wetness Mapping - 2016-JUL-12

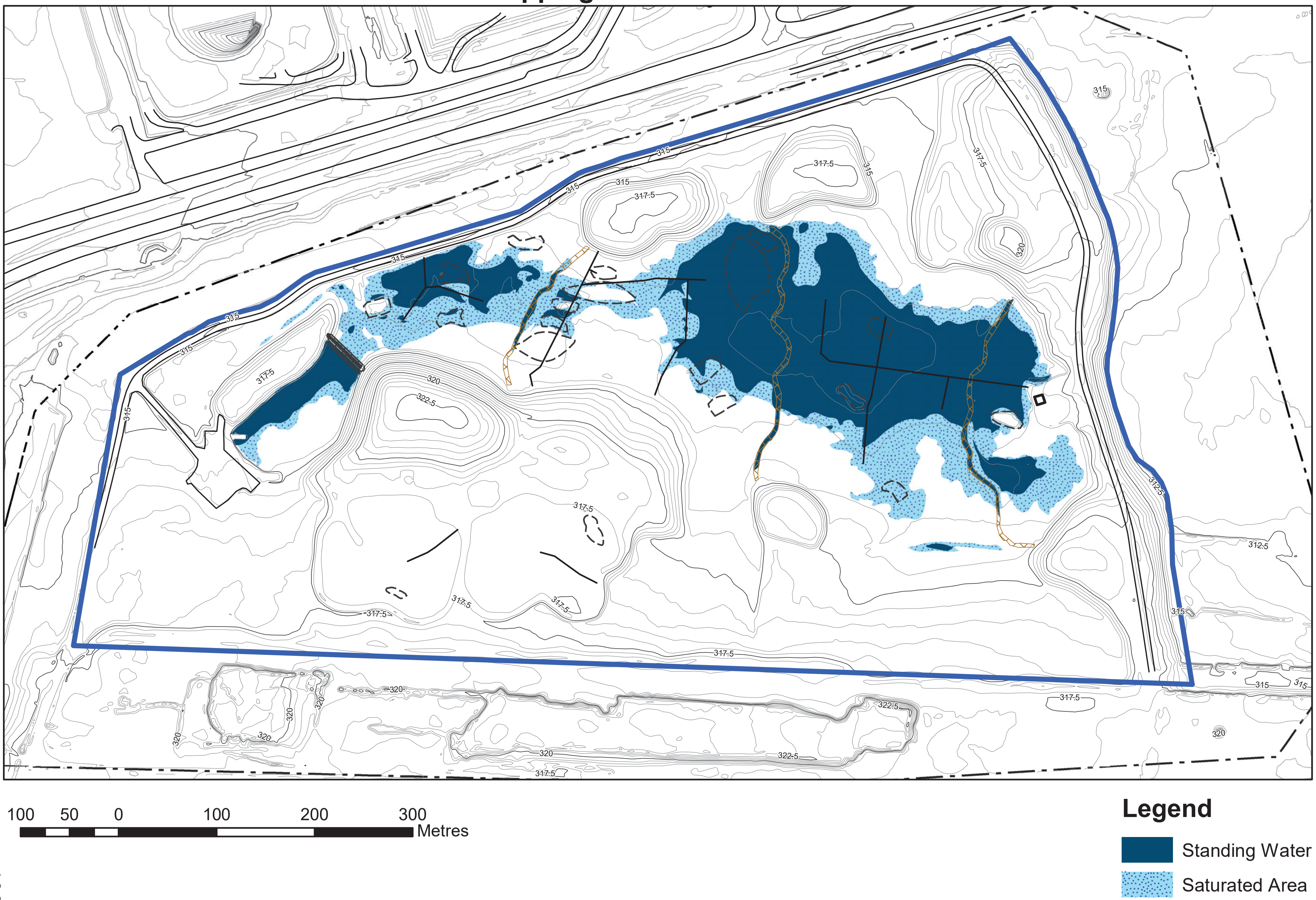

SHFW - Soil Saturation and Wetness Mapping - 2016-JUL-22

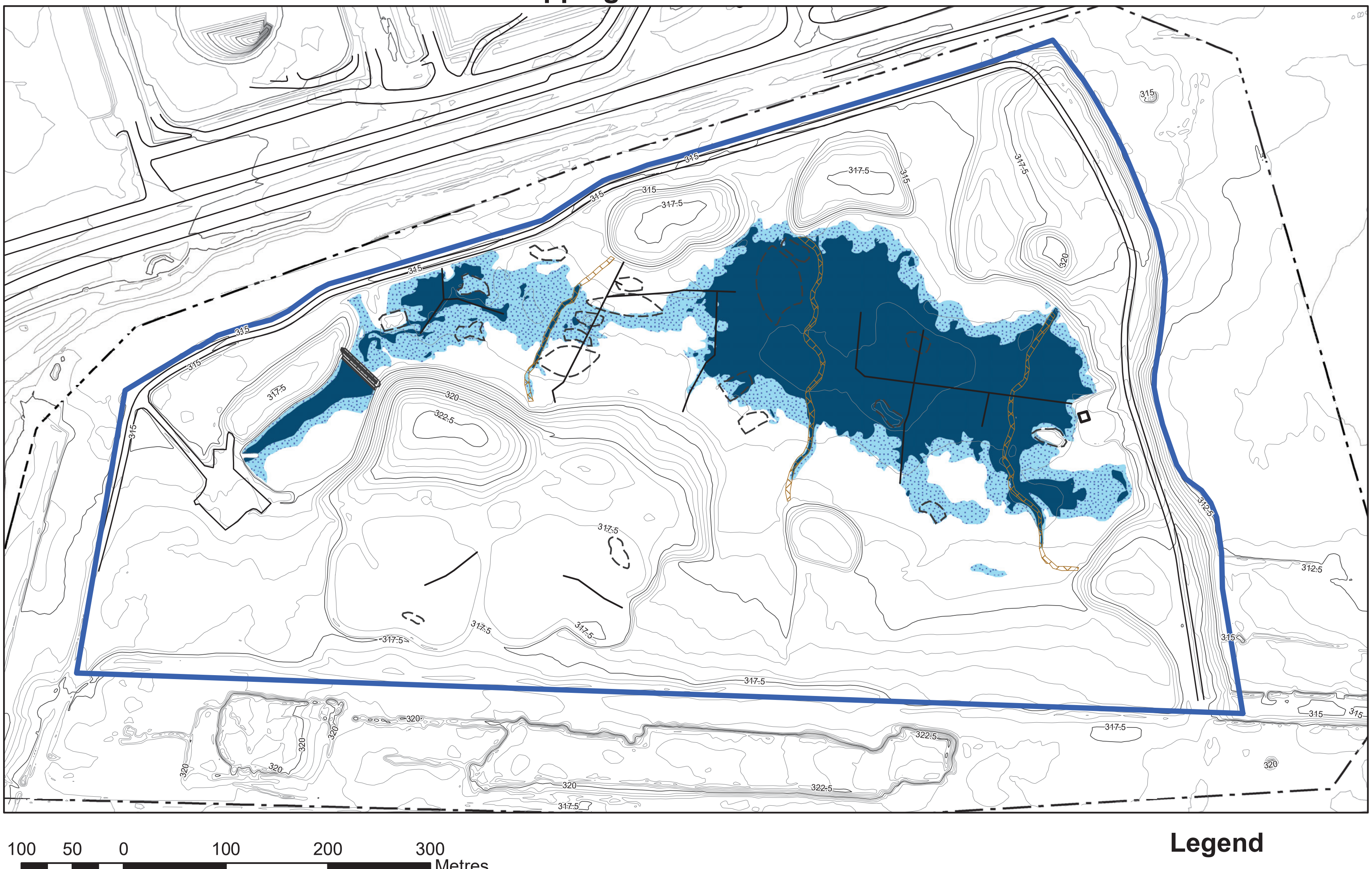

SHFW - Soil Saturation and Wetness Mapping - 2016-AUG-03

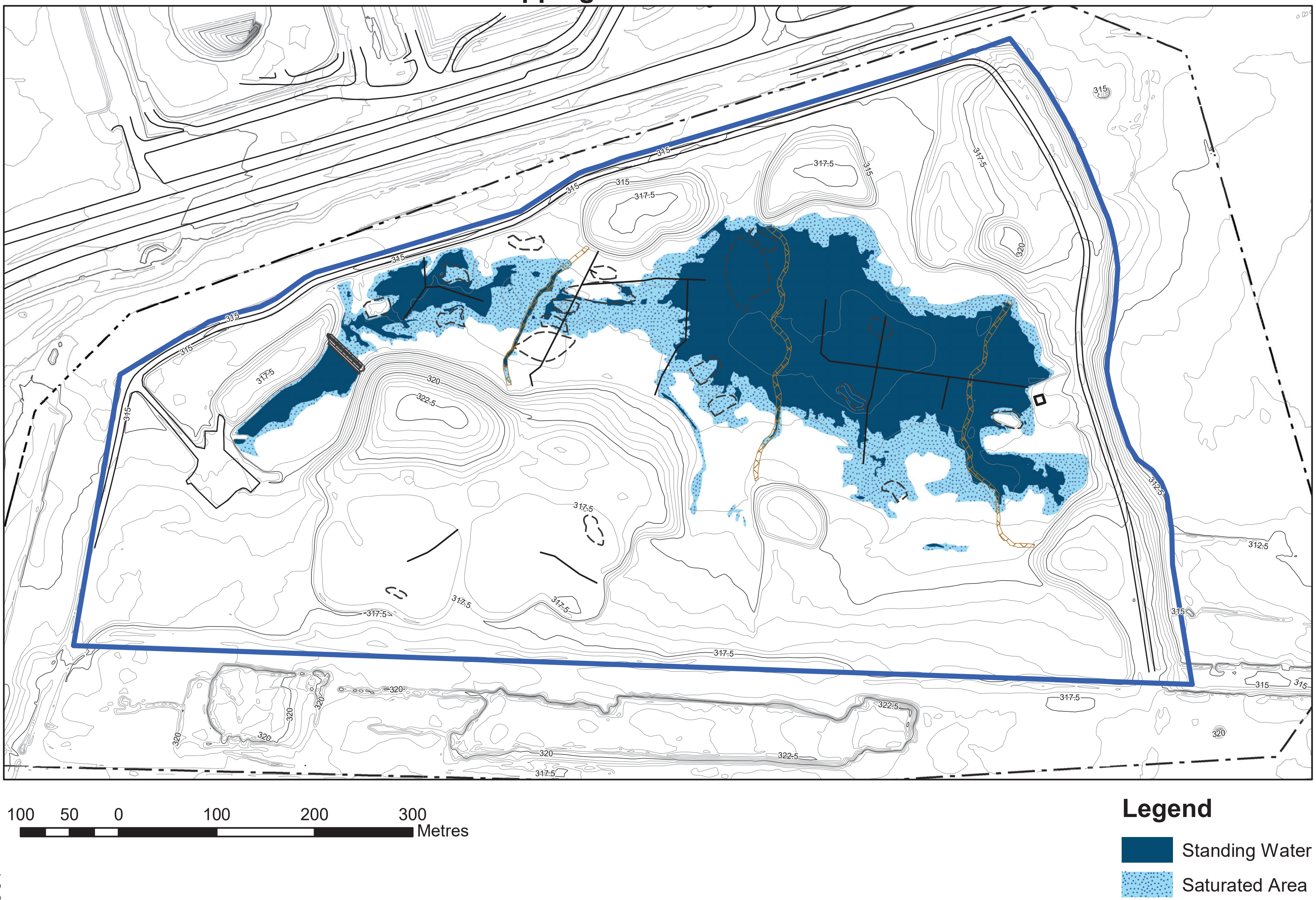

SHFW - Soil Saturation and Wetness Mapping - 2016-AUG-21

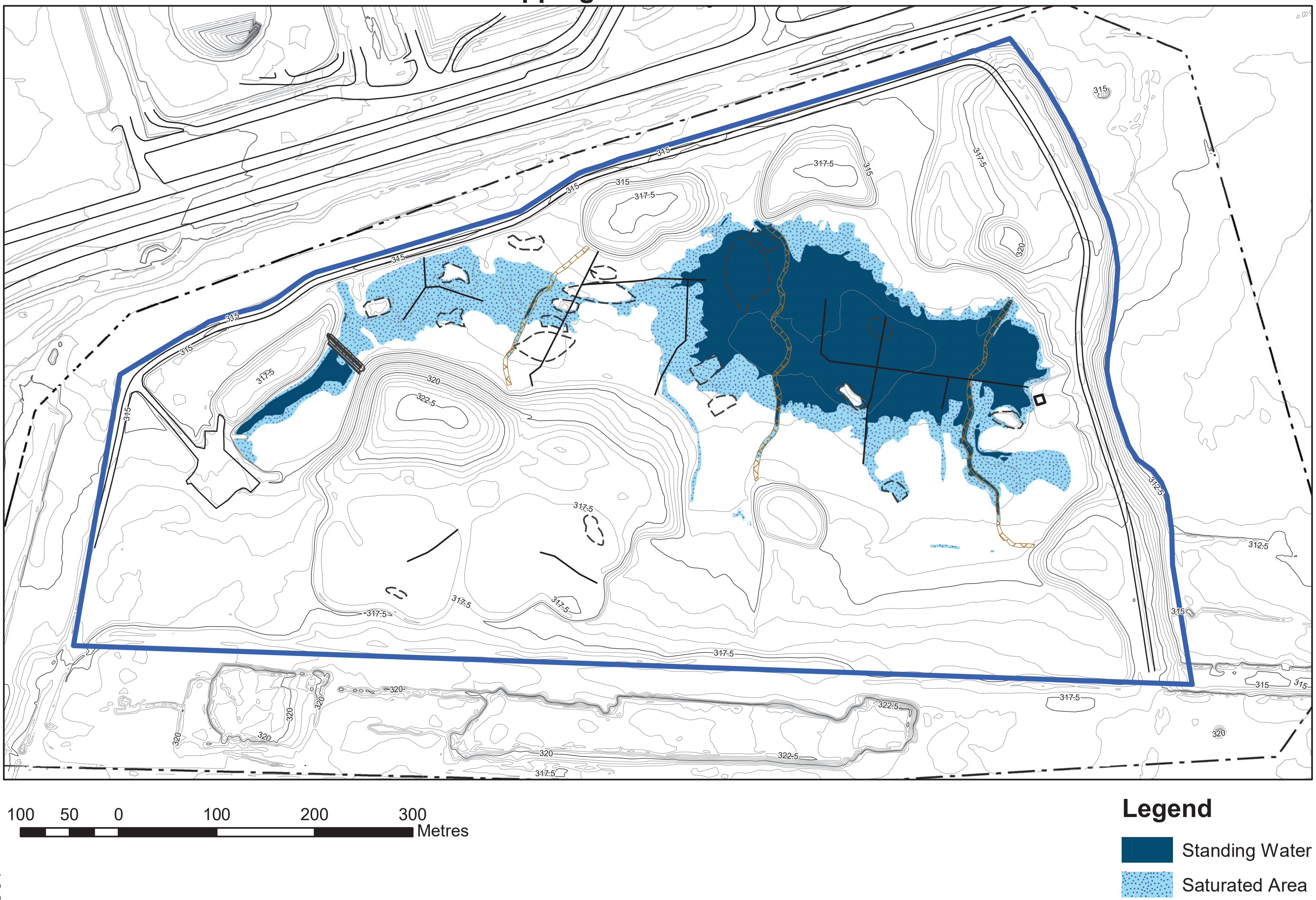

SHFW - Soil Saturation and Wetness Mapping - 2016-SEP-15

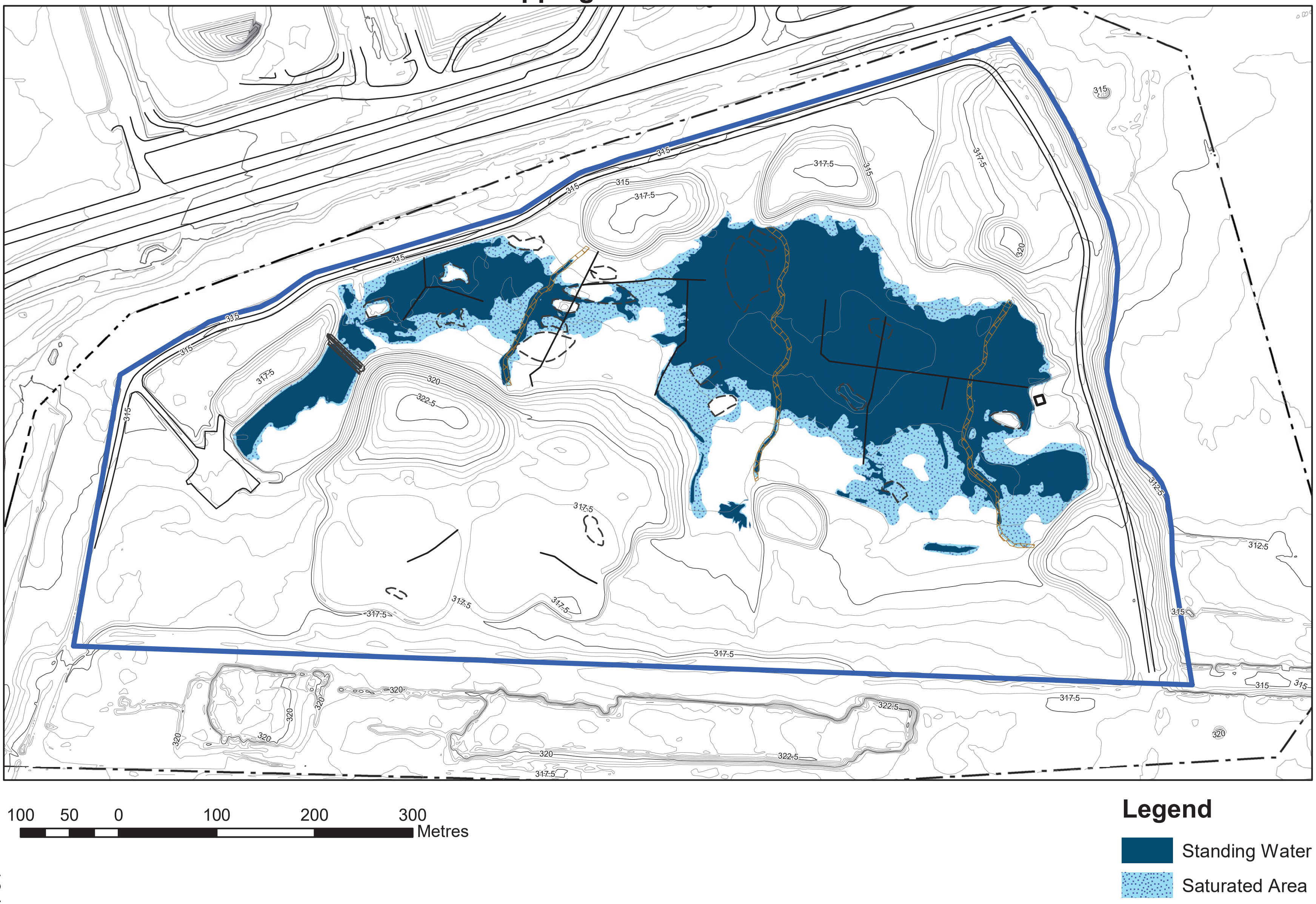

SHFW - Soil Saturation and Wetness Mapping - 2016-SEP-28

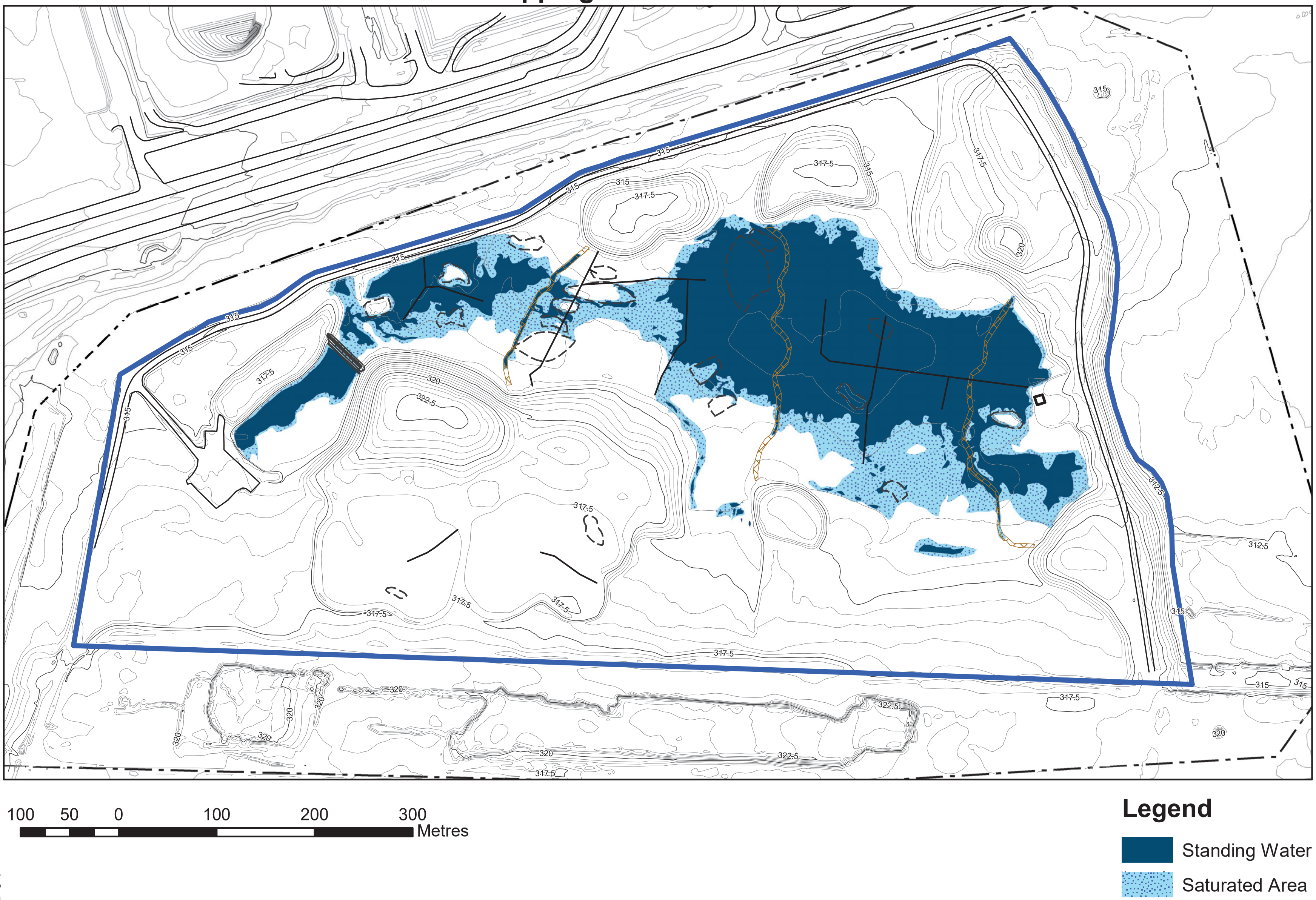

SHFW - Soil Saturation and Wetness Mapping - 2017-MAY-21

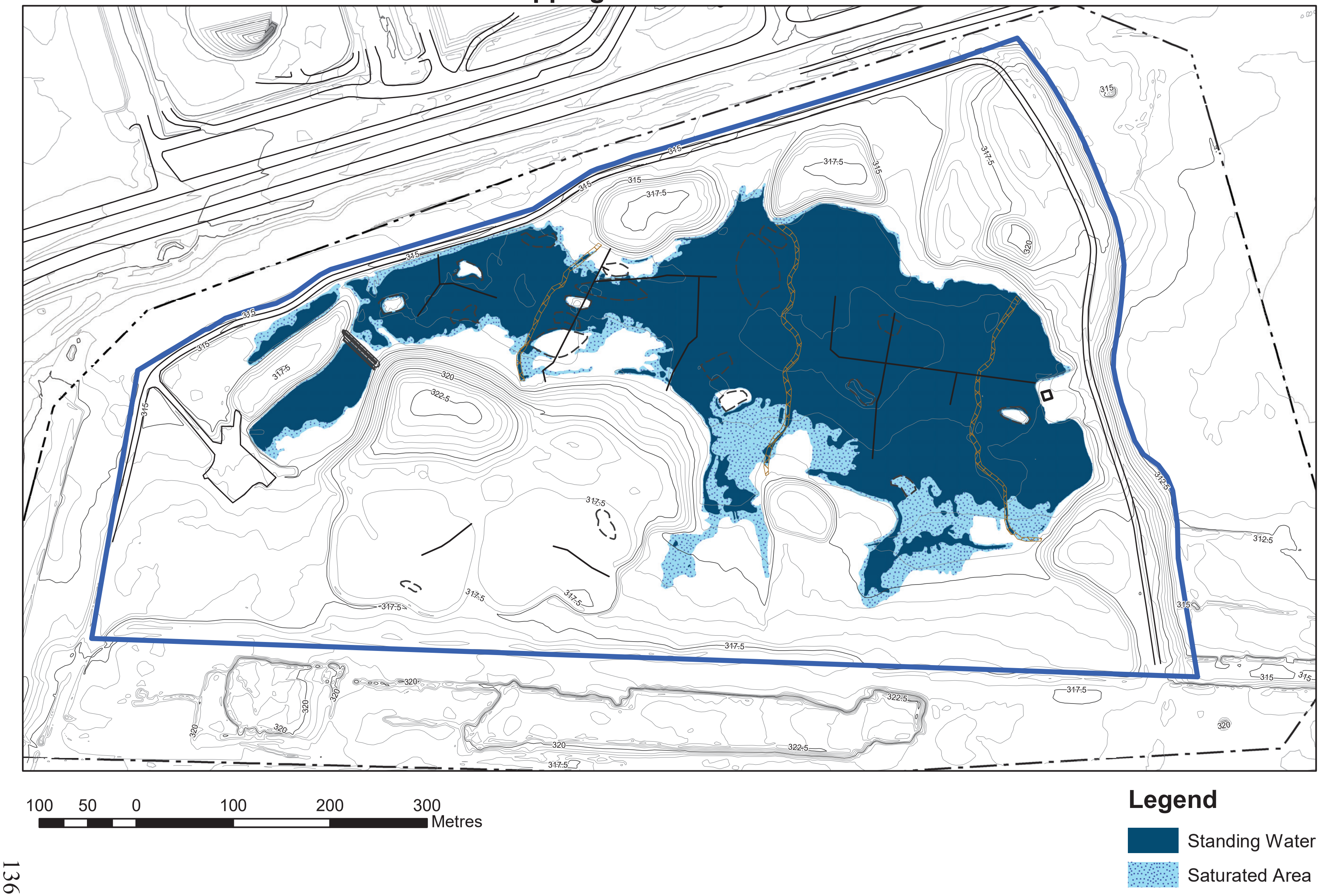

SHFW - Soil Saturation and Wetness Mapping - 2017-JUN-03

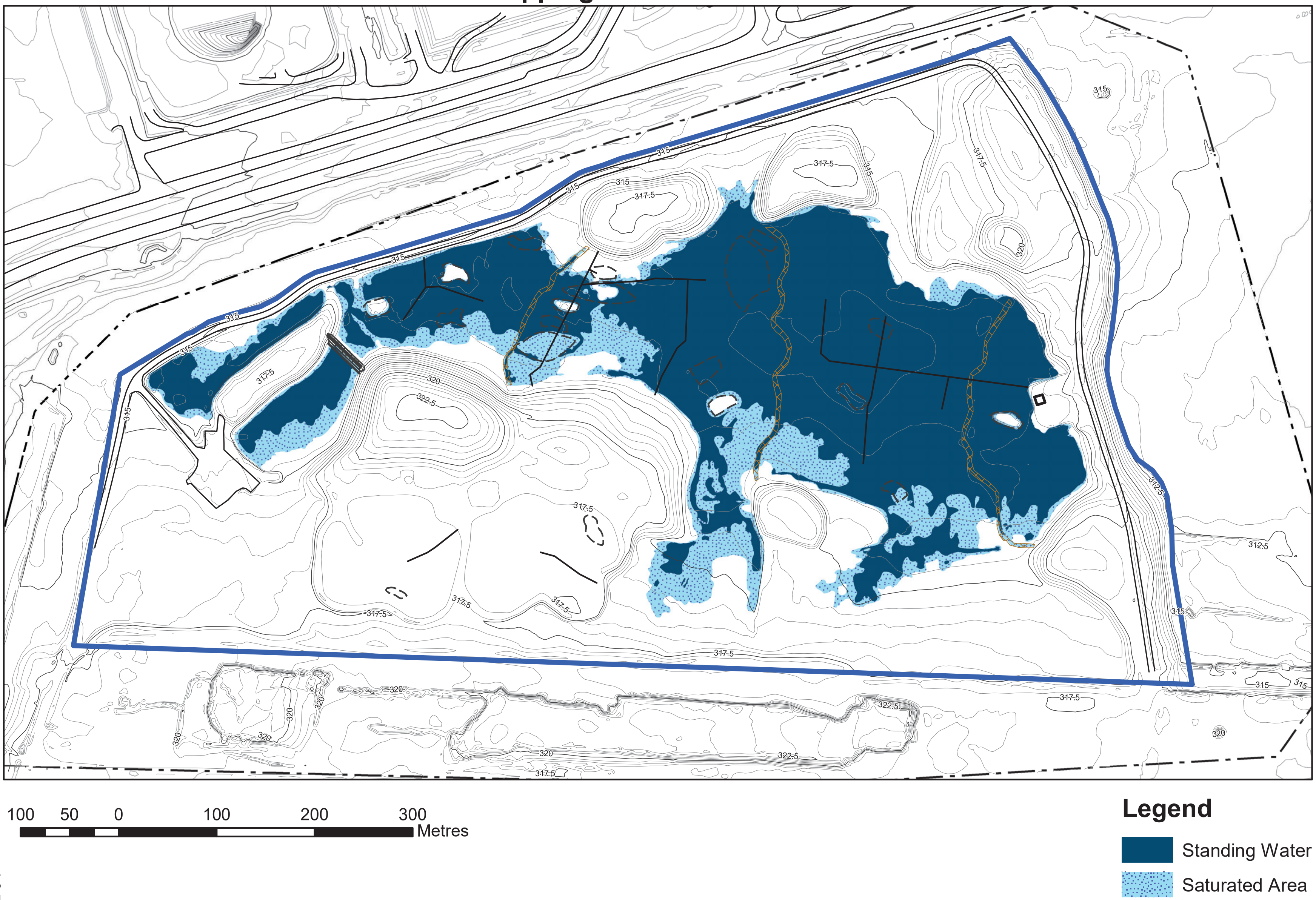

SHFW - Soil Saturation and Wetness Mapping - 2017-JUL-05

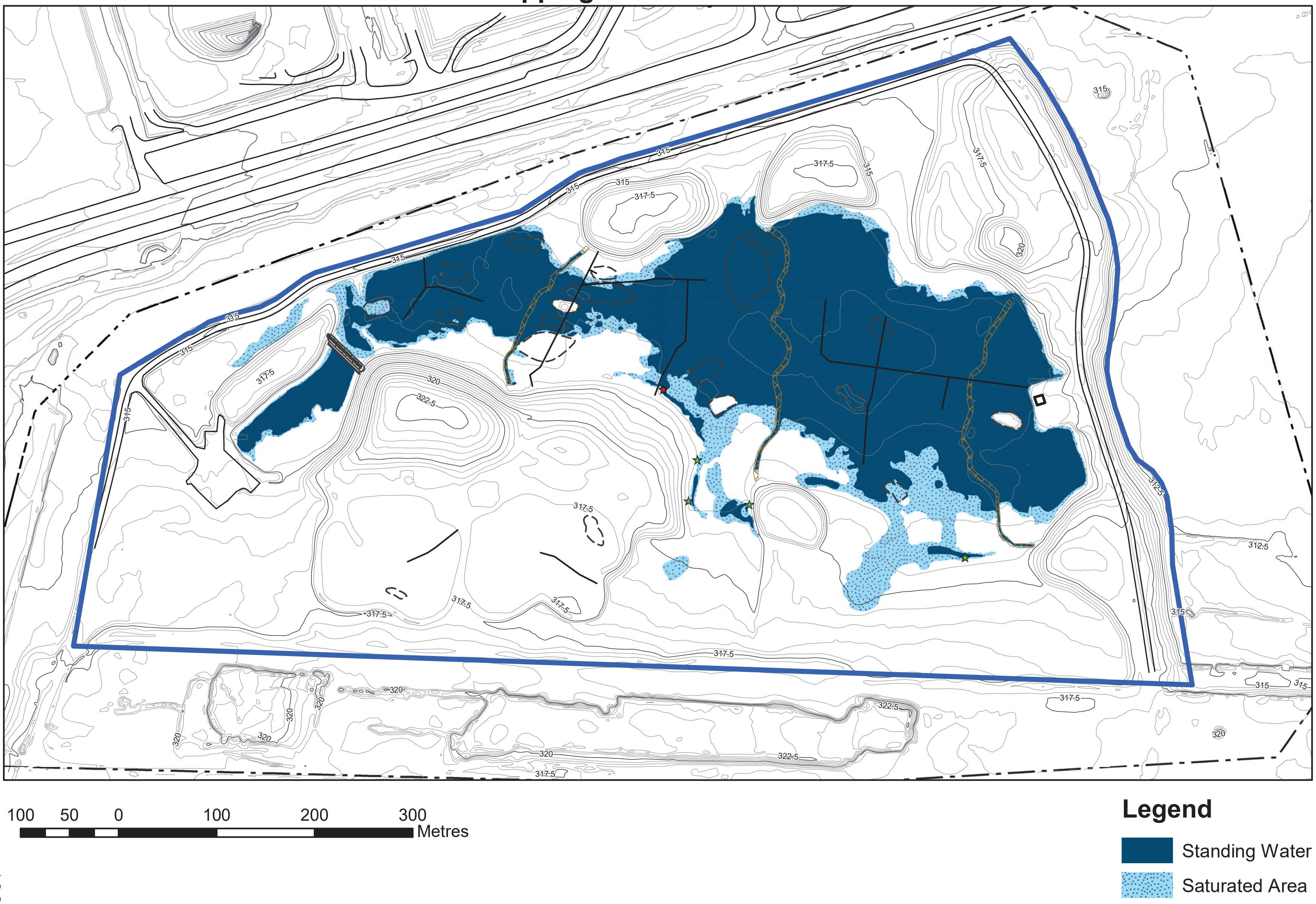

SHFW - Soil Saturation and Wetness Mapping - 2017-JUL-17

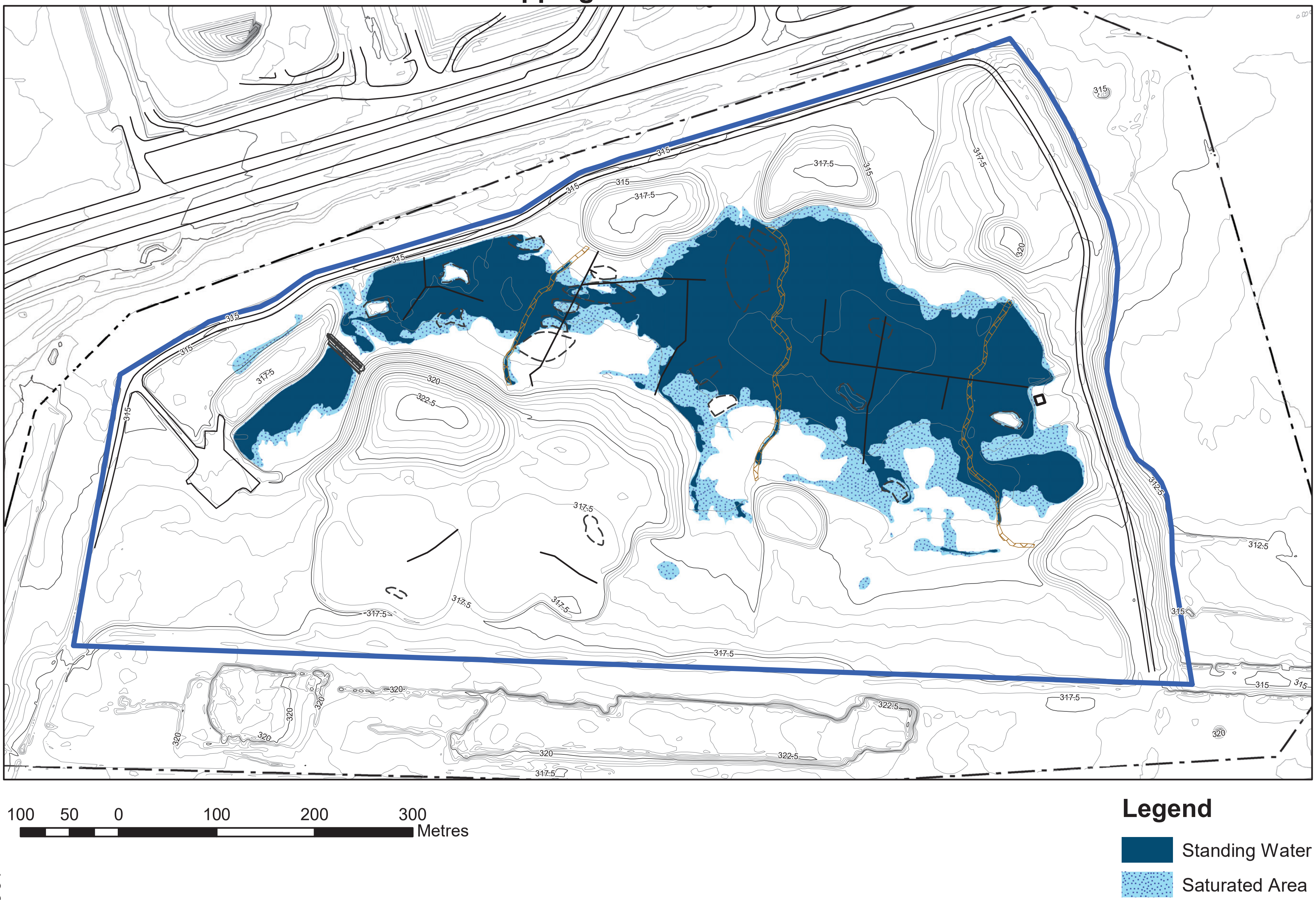

SHFW - Soil Saturation and Wetness Mapping - 2017-JUL-29

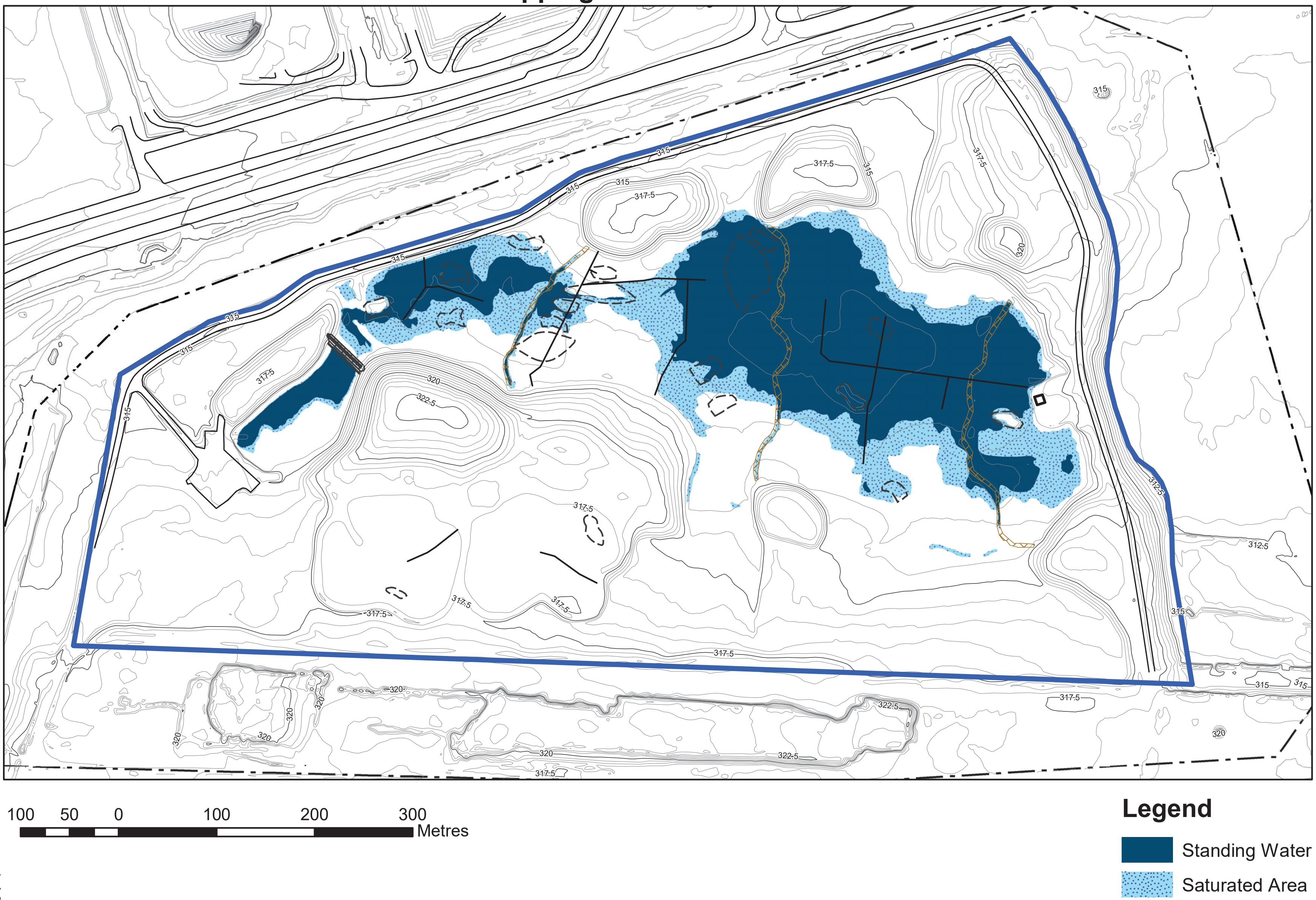

SHFW - Soil Saturation and Wetness Mapping - 2017-AUG-13

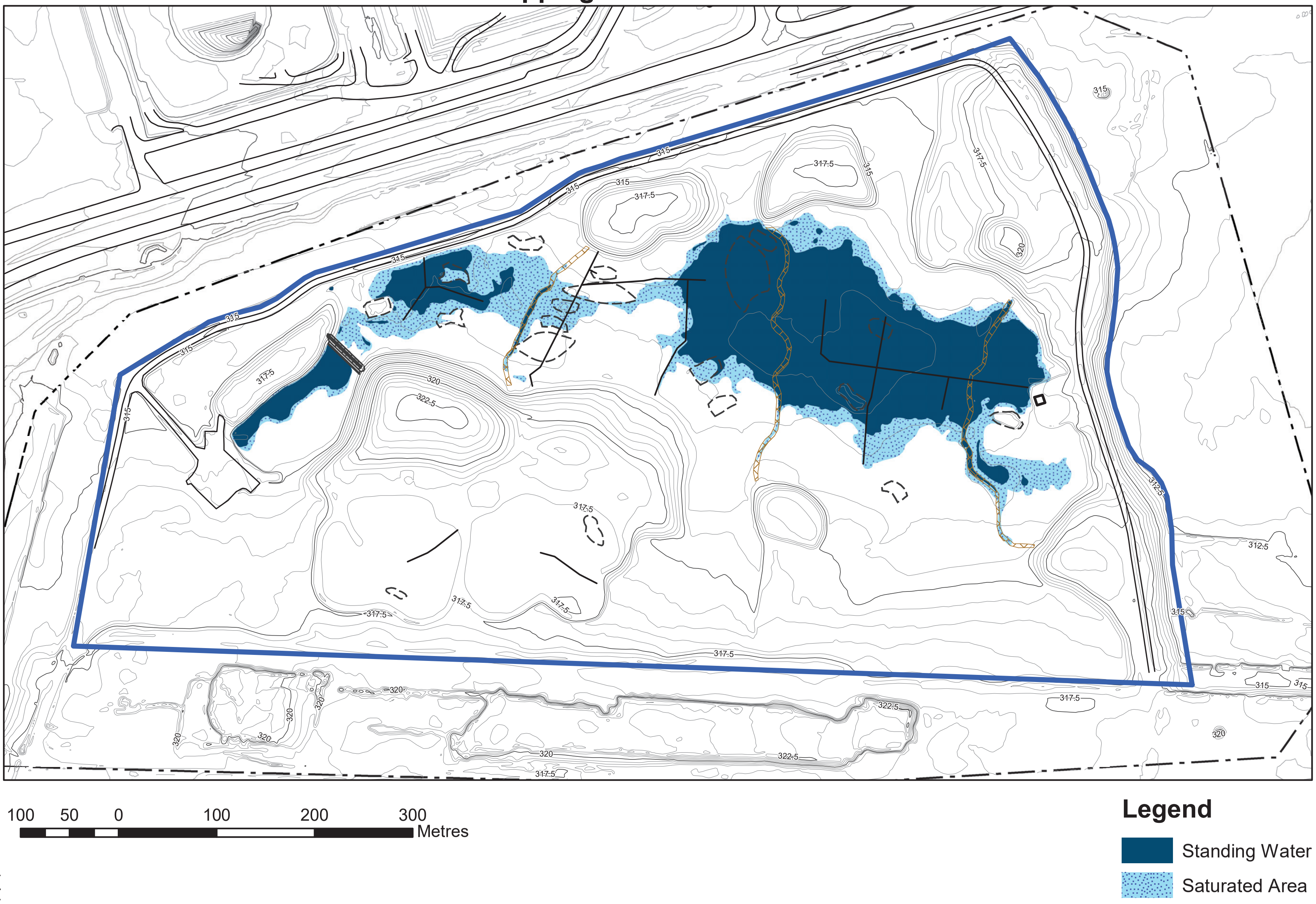

SHFW - Soil Saturation and Wetness Mapping - 2017-AUG-22

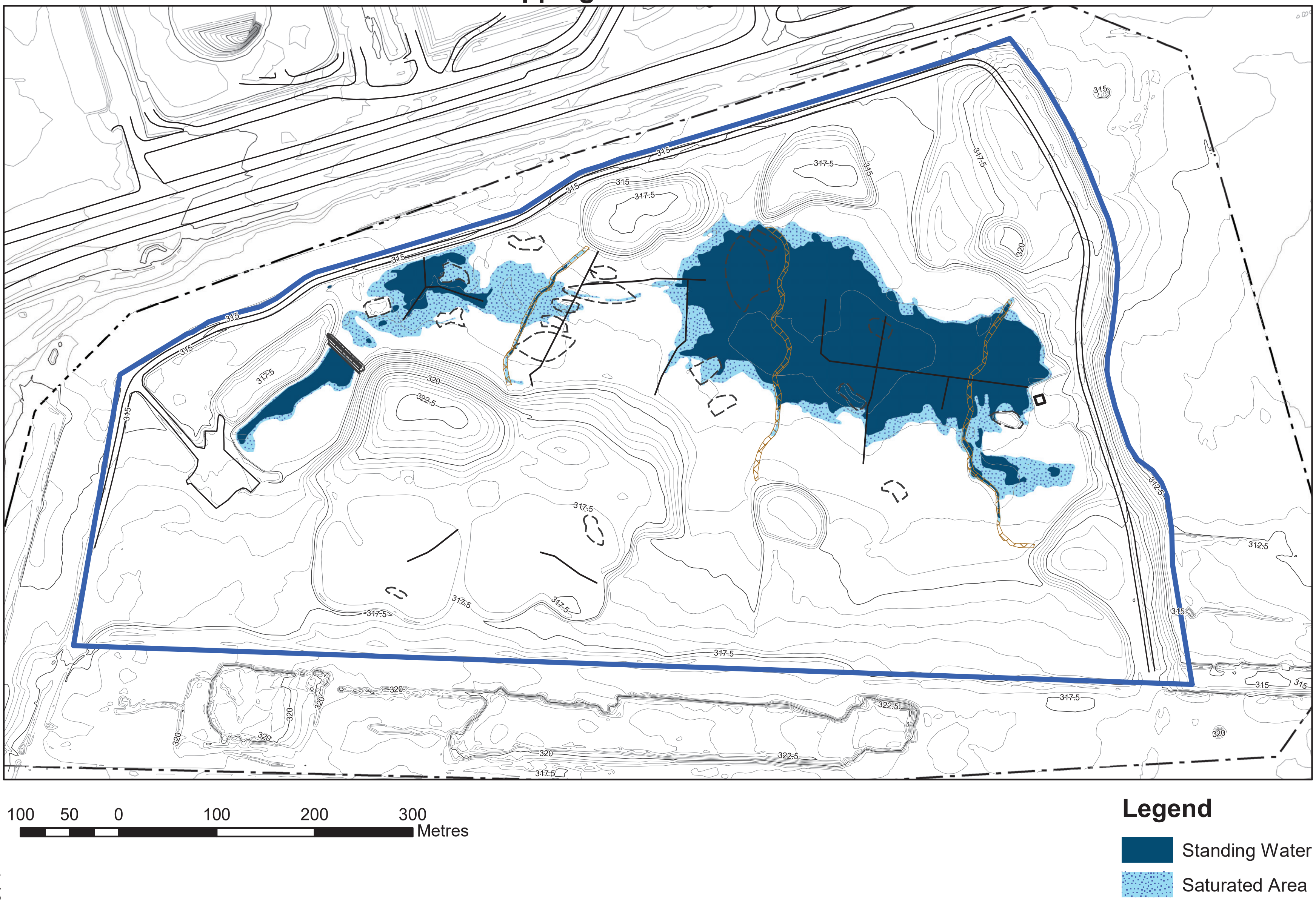

SHFW - Soil Saturation and Wetness Mapping - 2017-SEP-22

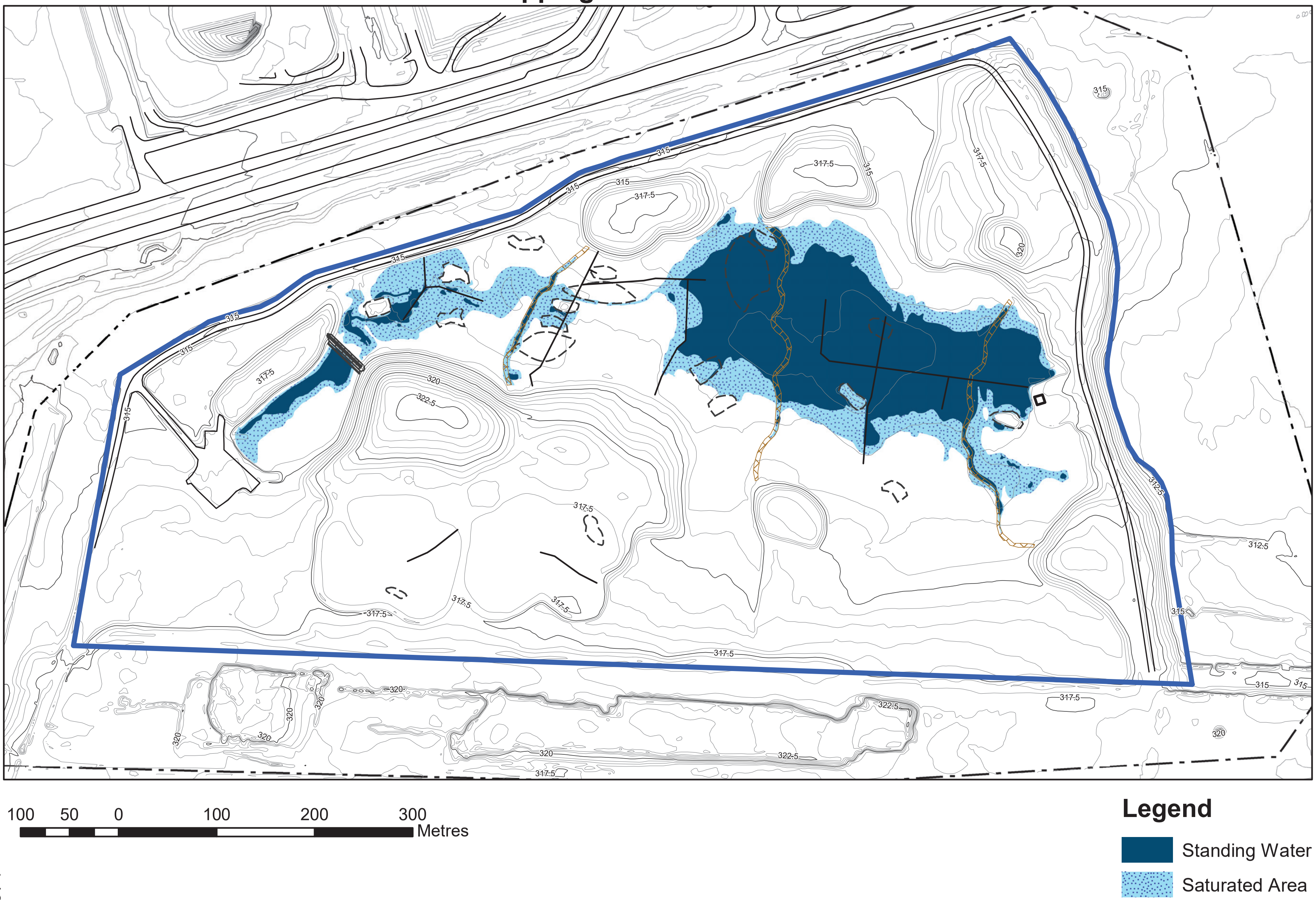

Appendix E - Annual Geochemical Sampling

Appendix E - Annual Geochemical Sampling

I. Scope of Work

This appendix contains geochemical data for the surface, groundwater and deep tailings presented in the form of Piper plots. Given that samples were only collected once per year, and tended to be similar year-to-year, a temporal analysis proved difficult. Therefore, piezometers were assigned to one of six groundwater classes to assist in evaluating the spatial distribution of major ions, and to simplify interpretations. The water class assigned to a piezometer was determined by the average depth of the water level relative to ground surface, and the average depth of the midscreen relative to the water level observed in the piezometer. This classification is outlined in the thesis (Figure 6) and explained in detail in Appendix F.

II. Methods

Geochemical sampling for major and minor ions, EC, and pH occurred midsummer, once per year, from 2013 to 2017, from all SH-GW piezometers when enough water was available. Samples of surface water were obtained adjacent to any pipe when standing water was observed (except for 2016). Samples from BGC piezometers were only collected in 2013, 2014 and 2017. All piezometers and wells were purged approximately two weeks prior to sampling. Samples were obtained using a one-inch rolling ball bailer attached to a string; the lowermost portion of the bailer was used to acclimate the sample bottle and the remainder was collected as the sample. The bailer was rinsed between samples. Water samples were collected in 250 mL poly sample bottles, filled to zero headspace, and filtered upon returning to the lab (via vacuum filtration with a 0.45 μm filter). Samples were refrigerated until analyses were performed by Syncrude Canada Ltd, in Edmonton, AB. A charge balance error (CBE) was calculated to assess sample analysis quality; samples exceeding 10% CBE were excluded from the results. Analyses and instrumentation are summarized in Table E-1.

For endmember geochemistry, eighteen groundwater samples were collected from BGC piezometers in SHW during 2013 and 2014 and were averaged to define the major ions of oil sands process-affected water (OSPW) geochemical endmember composition. Only one geochemical sample was collected and analyzed from MLR during the study period, in 2015 (Vessey et al., 2018).

III. Results

Results are presented by water classes first (surface water and artesian piezometers, then shallow/shallow, shallow/deep, deep/shallow, deep/deep water classes), then samples from the primary transects (Transect 1 and Transect 2; Figure 5) were plotted for comparison. Only data from 2015 to 2017 are presented here.

Table E-1 – Annual General Chemistry Analyses, conducted by Syncrude Research and Development

Type of Analysis	Years	Chemistry Sampled	Units	Instrumentation
ALK[1]	2013-2017	pH, CO_3, HCO_3, Total Alkalinity $CaCO_3$	mg/L or (-)	Metrohm Alkalinity 855 Robotic Titrator
ANI[1]	2014	F, Cl, NO_2, NO_3, PO_4, SO_4, Br, Citrate	mg/L	IC performed on ion chromatography (DX-600, Dionex).
	2015-2017	F, Cl, NO_2, NO_3, PO_4, SO_4, Br, Citrate	mg/L	IC performed on ion chromatography (ICS-5000, Dionex).
EAW[2]	2013-2015	Al, B, Ba, Ca, Cd, Co, Cr, Cu, Fe, K, Li, Mg, Mn, Mo, Na, Ni, P, Pb, S, Sb, Se, Si, Sn, Sr, Ti, V, Zn, Zr,	PPM	ICP-AES performed on Inductively-Coupled Plasma Atomic Emission Spectrometer, Agilent Technologies, Varian, VISTA, RL model with radial mounted torch.
EMA[2]	2016-2017	Ag, Al, As, B, Ba, Be, Ca, Cd, Co, Cr, Cu, Dy, Fe, Hg, K, Li, Mg, Mn, Mo, Na, Ni, P, Pb, Rb, Sb, Se, Si, Sn, Sr, Th, Ti, Tl, U, V, W, Y, Zn, Zr,	mg/L	ICP-MS performed on Inductively-Coupled Plasma Mass Spectrometer (ICP-MS), PerkinElmer NexION 300D
pH and Cond[1]	2013-2017	pH and EC	µS/cm or (-)	Jenway 4330 (pH electrode (Glass Body Single-Junction Ag/AgCl Combination Electrode - Accumet 13-620-285 / and / Conductivity cell (ATC ~k=1.00) Jenway 027 013)

All samples were vacuum filtered using 0.7 µm filter paper in the lab prior to analyses.
Electrical conductivity was not temperature corrected in the lab.

[1] Filtered through 0.45 µm filter before subsampling.

[2] Filtered through 0.1 µm filter before subsampling.

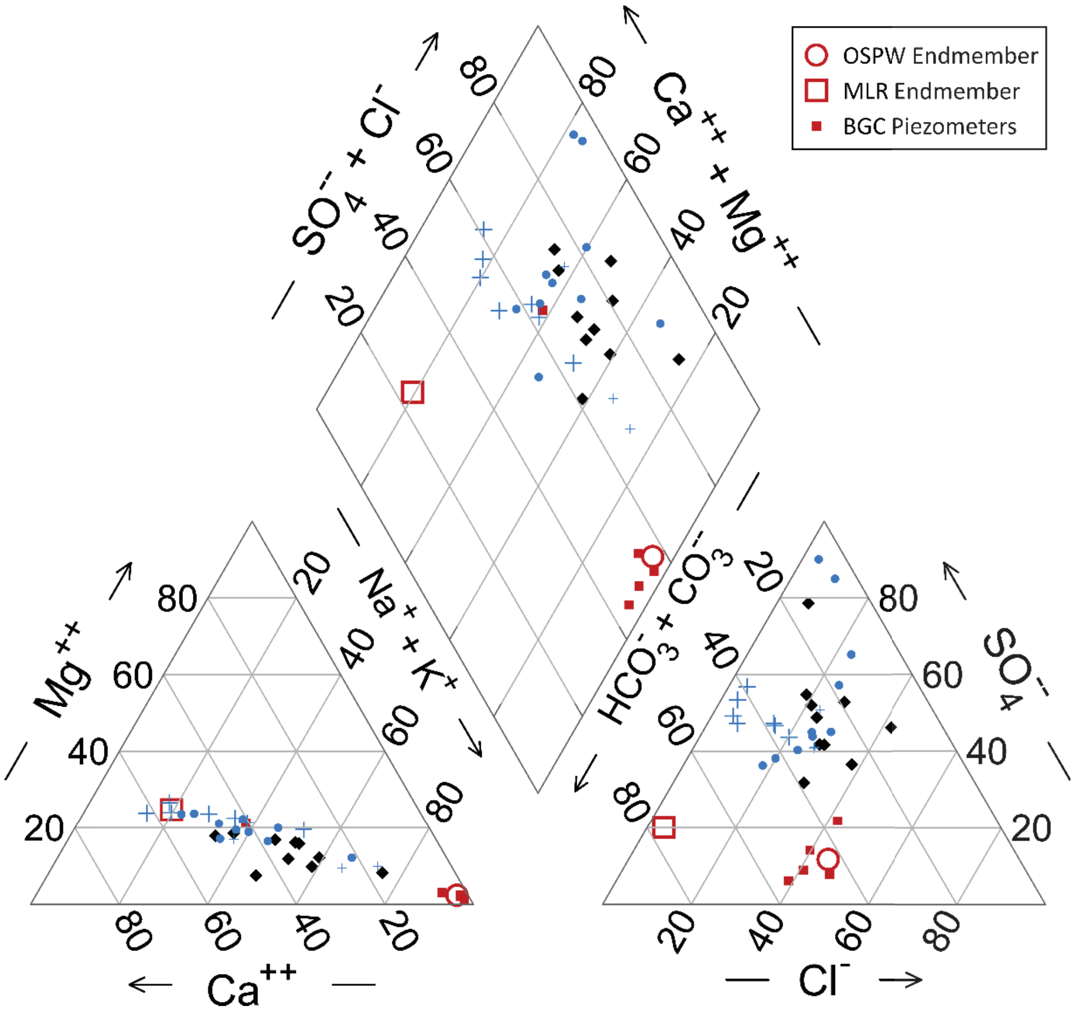

Figure E-1: Piper plot of surface and groundwater major ions (black and blue, respectively) from annual groundwater sampling in SHW (2015-2017). End member compositions (MLR and OSPW) and deep groundwater (BGC-##-## piezometers) are plotted in red; all other groundwater samples are from piezometers completed in the tailing sand (SH-GW-##-##). Specifically, values are from piezometers with artesian conditions (WL >0 m AGS), subdivided based on the relative depth of the midscreen below the water level in the piezometer (shallow, "o", MS <1.8 m BWL and deep, "+", MS >1.8 m BWL, respectively). Groundwater symbology explained in Figure 6.

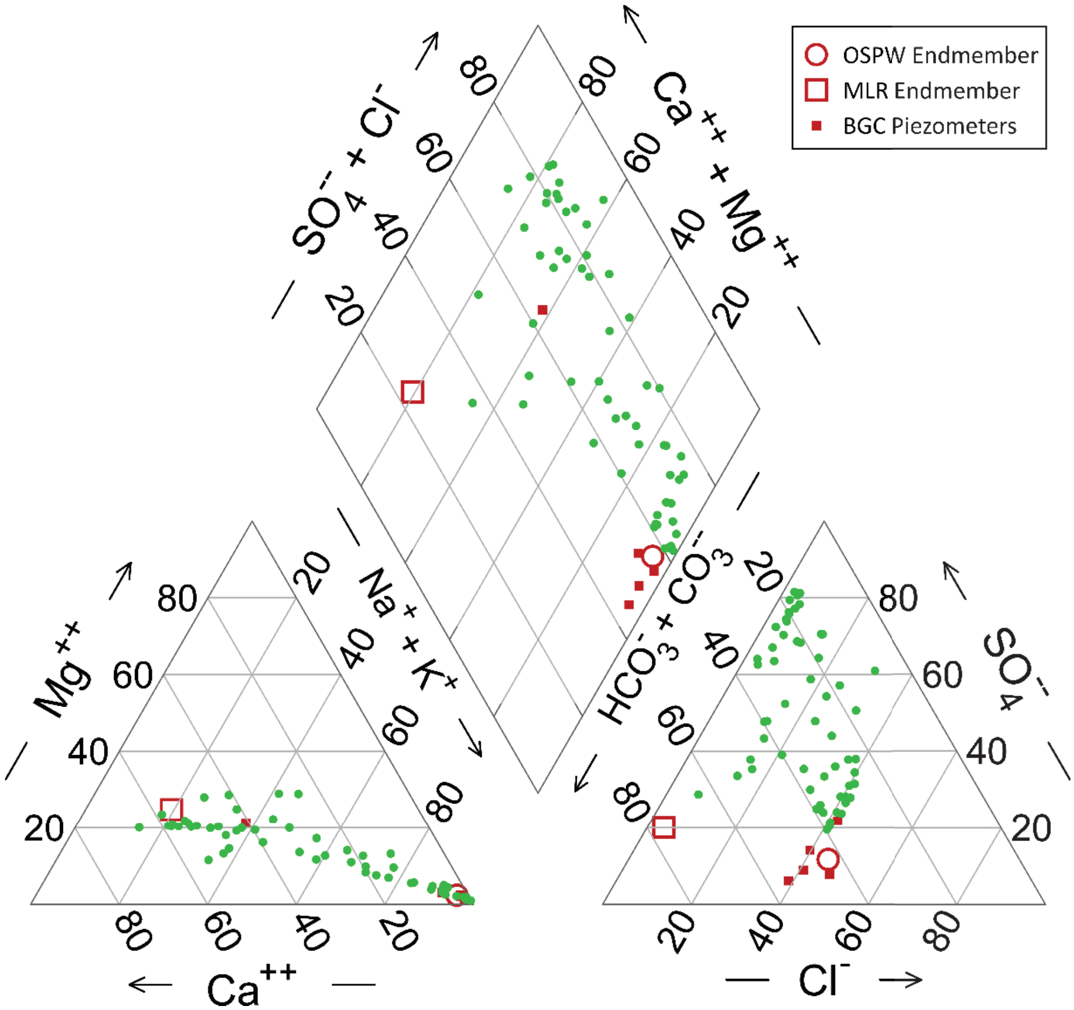

Figure E-2: Piper plot of groundwater major ions from annual groundwater sampling in SHW (2015-2017). Specifically, values are from piezometers with shallow water tables (WL < 1.8 m BGS) and shallow midscreens relative to the water level in the piezometer (shallow, "o", MS < 1.8 m BWL). Details are summarized in Figure E-1. Groundwater symbology further explained in Figure 6.

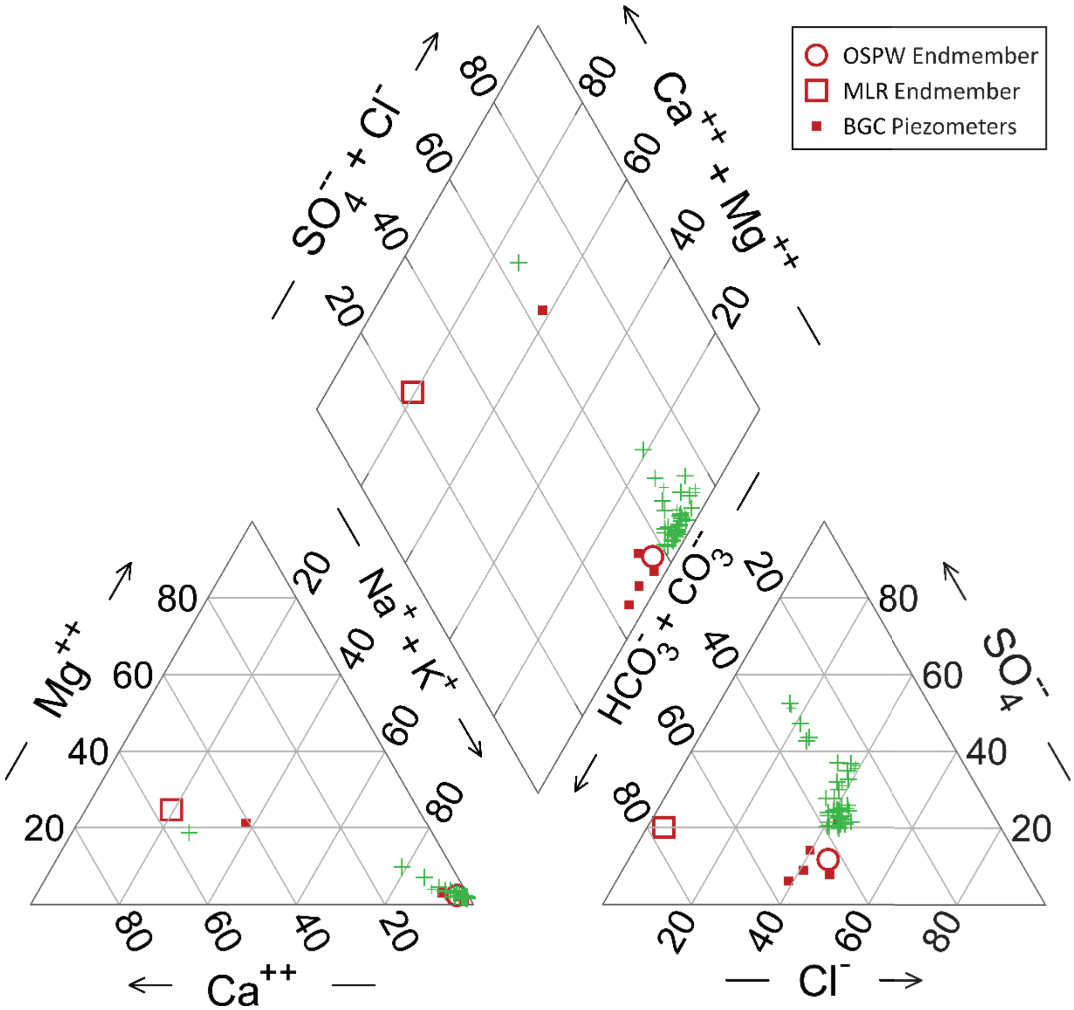

Figure E-3: Piper plot of groundwater major ions from annual groundwater sampling in SHW (2015-2017). Specifically, values are from piezometers with shallow water tables (WL <1.8 m BGS) and deep midscreens relative to the water level in the piezometer (deep, "+", MS >1.8 m BWL). Details are summarized in Figure E-1. Groundwater symbology further explained in Figure 6.

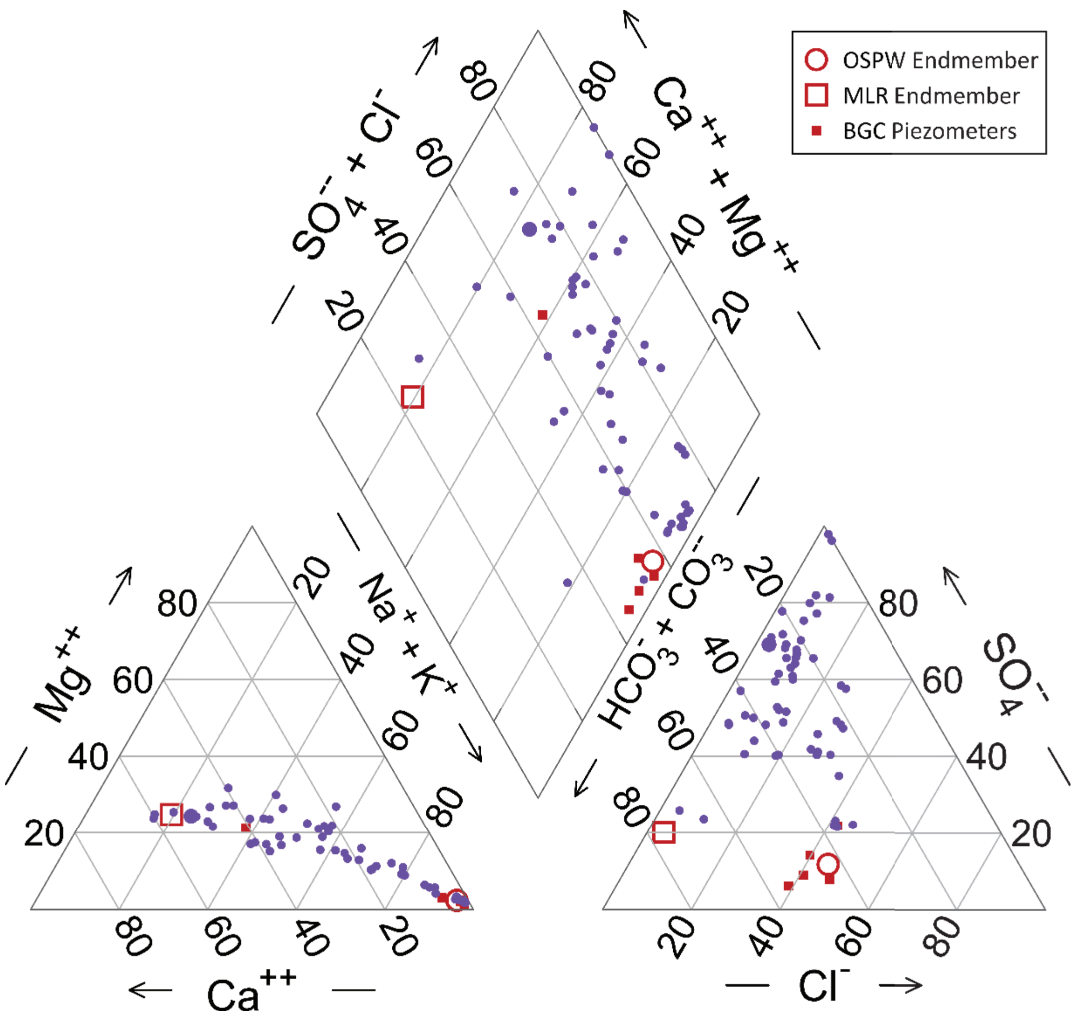

Figure E-4: Piper plot of groundwater major ions from annual groundwater sampling in SHW (2015-2017). Specifically, values are from piezometers with deep water tables (WL >1.8 m BGS) and shallow midscreens relative to the water level in the piezometer (shallow, "o", MS <1.8 m BWL). Details are summarized in Figure E-1. Groundwater symbology further explained in Figure 6.

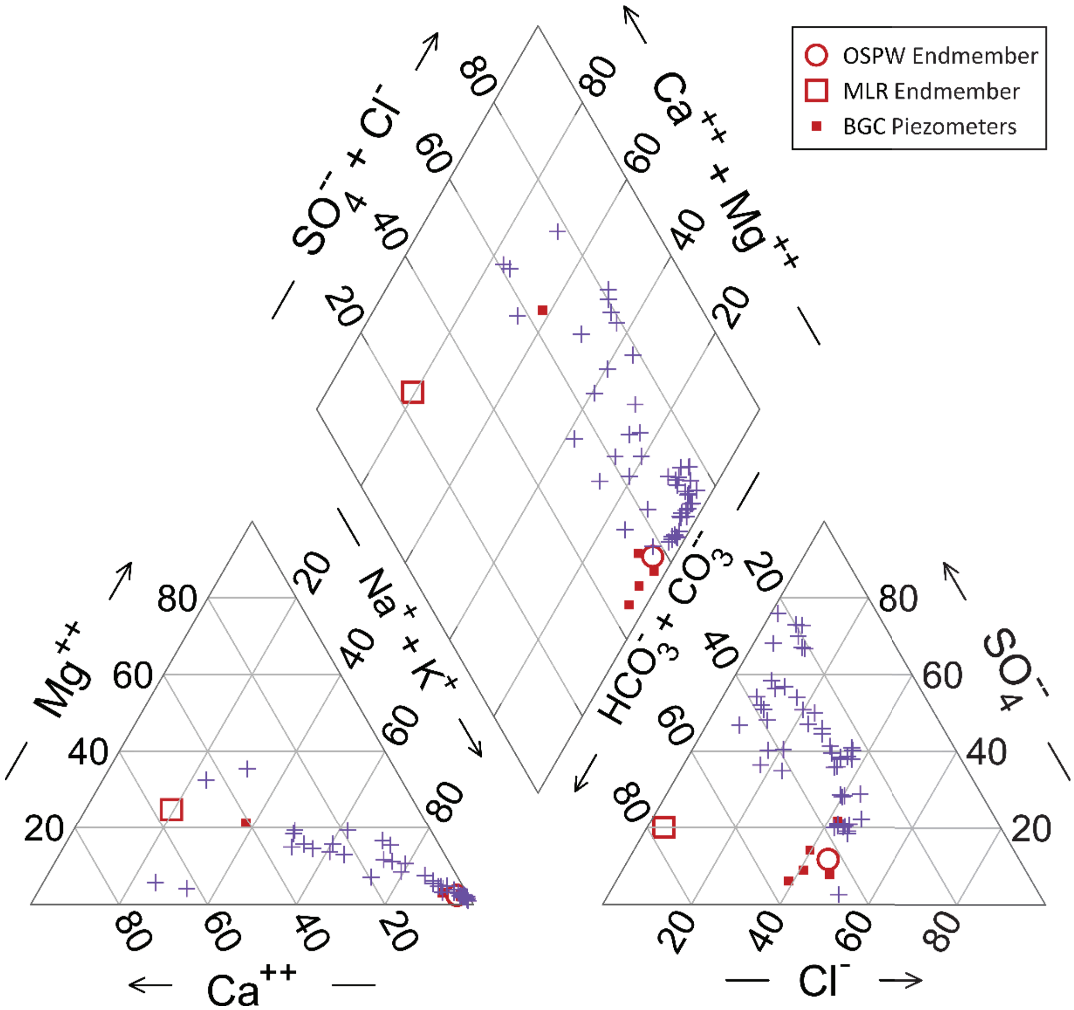

Figure E-5: Piper plot of groundwater major ions from annual groundwater sampling in SHW (2015-2017). Specifically, values are from piezometers with deep water tables (WL >1.8 m BGS) and deep midscreens relative to the water level in the piezometer (deep, "+", MS >1.8 m BWL). Details are summarized in Figure E-1. Groundwater symbology further explained in Figure 6.

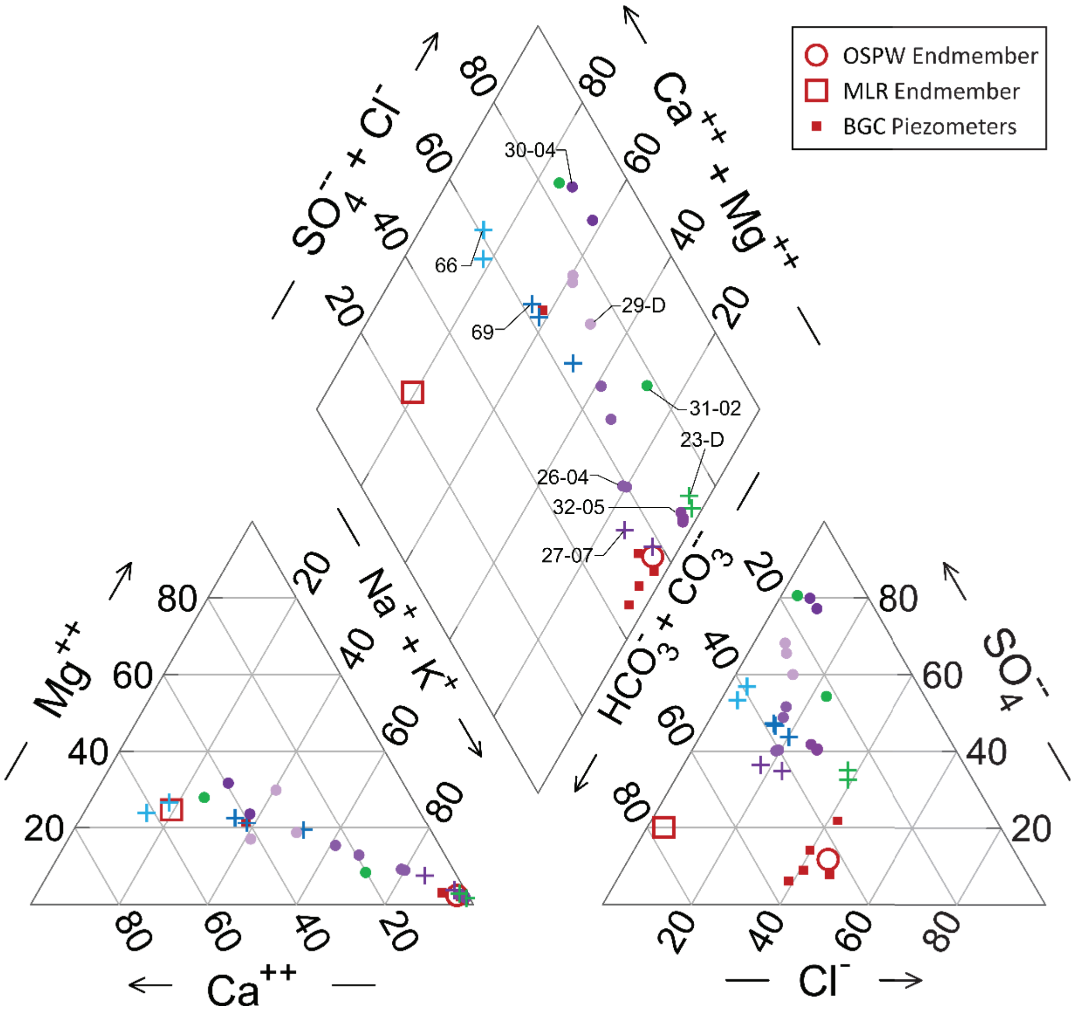

Figure E-6a: Piper plot of major ions in groundwater collected annually from each SH-GW nest along Transect 1 late in the summer from 2015-2017. Only one representative piezometer is shown per nest, when groundwater was present. Representative and average end-member compositions (Mildred Lake Reservoir, MLR, and OSPW, respectively; Vessey et al., 2018; e-appendix) and deep GW samples (BGC-##-## piezometers) are plotted in red. All remaining data are GW samples from shallow piezometers in the tailing sand, symbology is consistent with water types in Figure 6 (SH-GW-##-##; shortened to ##-##). Deep GW samples (red ■) are only from 2017; no data were recorded for these piezometers in 2015 and 2016. Some piezometers are missing 2017 data due to analysis error; other piezometers have duplicates.

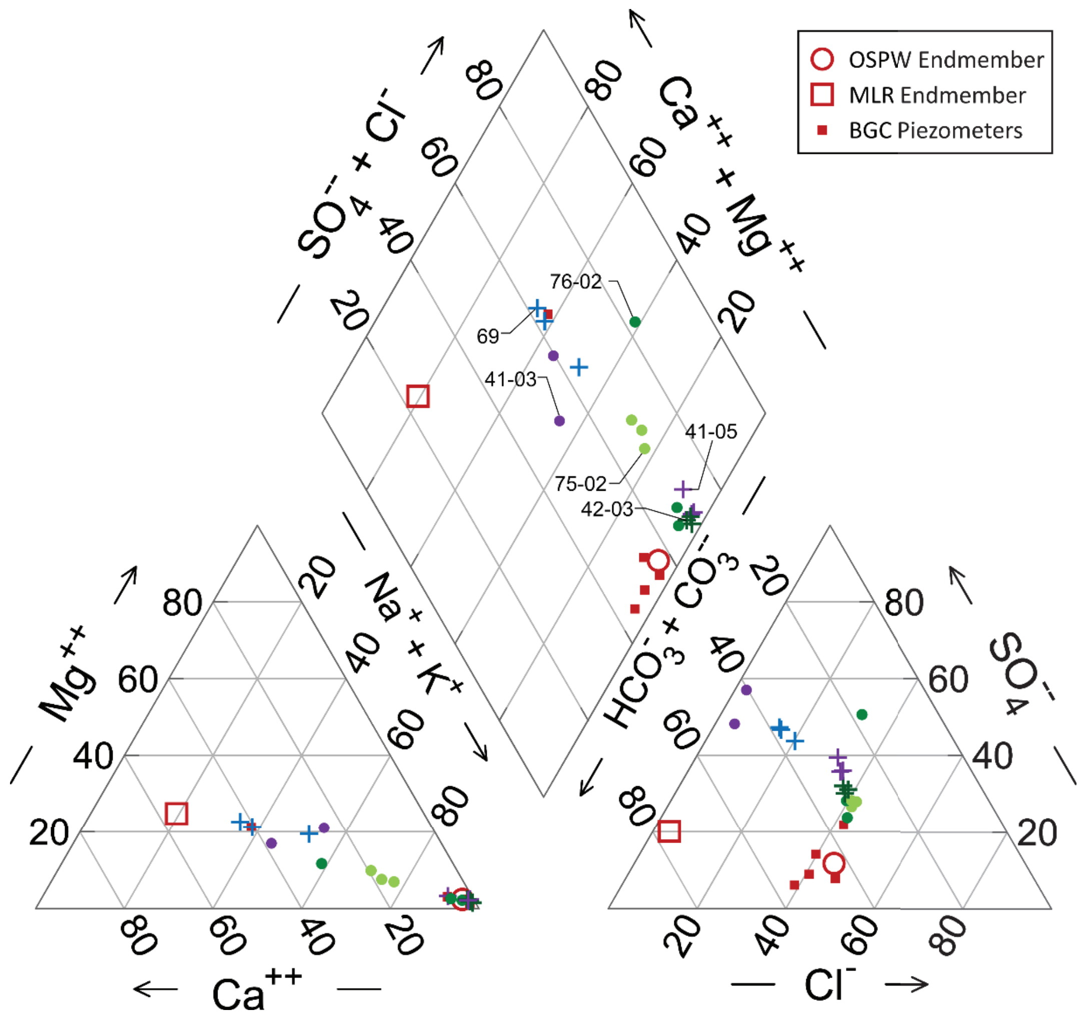

Figure E-6b: Piper plot of major ions in groundwater collected annually from each SH-GW nest along Transect 2 late in the summer from 2015-2017. Details are summarized in Figure 6a.

Appendix F - Stable Water Isotopes, Geochemistry & EC

Appendix F - Stable Water Isotopes, Geochemistry & EC

I. Scope of Work

The objective of this work was to perform a spatio-temporal analysis of stable water isotopes and sodium concentrations to elucidate the mechanisms behind solute movement and their distribution in the shallow groundwater of Sandhill Watershed. Understanding how hotspots, or localized areas of elevated Na^+ (associated with oil sands process-affected water, OSPW), develop in SHW have important implications for ensuring near surface water quality remains within a tolerable range for vegetation in reclaimed landscapes. Previously, geochemical data from surface water and water table wells indicated these hotspots developed in areas where the water table fluctuates near ground surface (Biagi et al., 2018). This study uses groundwater data (water levels, EC, Na^+, $\delta^{18}O$ and δ^2H isotopes) from piezometers along two transects oriented parallel to the primary (S-E) flow path to investigate the sources of elevated electrical conductivity/Na^+ in hot spots. More specifically, manual water level and electrical conductivity measurements are paired with stable water isotope ($\delta^{18}O$ and δ^2H) and geochemical (Na^+) data to explain groundwater solute distribution and movement through two different landscape configurations, a) hummock-to-wetland, and b) slope-to-wetland). It should be noted these data were presented, in part, for a poster presentation for credit in a course at the University of Saskatchewan.

II. Background

Groundwater Endmember Compositions

The conceptual groundwater mixing model for this study site anticipates three endmember compositions: OSPW, Mildred Lake Reservoir water (MLR) and precipitation. OSPW is present in the pore spaces of the hydraulically-placed composite tailings and tailings sand cap, as well as the residual, antecedent moisture in the variably saturated pore spaces of mechanically-placed tailings used to sculpt the topography in SHW (discussed elsewhere in thesis). Consequently, OSPW was originally distributed throughout the watershed prior to reclamation. OSPW has elevated concentrations of NaOH, $CaSO_4$ and NaCl due to bitumen processing, gypsum additions, and recycling of formation waters (Mikula et al., 1996); therefore, as discussed elsewhere in the thesis, limiting discharge of groundwater with elevated EC to the root zone is fundamental for ensuring reclaimed vegetation could thrive (Renault et al., 1998, 1999).

Mildred Lake Reservoir (MLR) is a fresh water reservoir on Syncrude's Mildred Lake Lease with inputs from both Athabasca River and precipitation (Baer et al., 2016). Water from MLR was pumped into Sandhill Watershed's water storage pond during the summers of 2012, 2013 and 2014 to freshen the watershed's surficial groundwater immediately following construction (Nicholls et al., 2016, Wytrykush et al., 2012). The water storage pond was engineered to release fresh water to the down-gradient wetland. Water was also discharged to the "perched fens", south of hummock 7 in 2012 and 2013 (Wytrykush et al., 2012).

Finally, groundwater recharge via precipitation and infiltration varies throughout the watershed. Since SHW has a sub-humid climate, annual precipitation inputs can be either greater than or less than evapotranspiration losses, which readily affects groundwater recharge and water table configurations in shallow, unconfined aquifers (Shoeneberger & Wysocki, 2005). Recharge rates within the reconstructed watershed are also influenced by depth to water table, antecedent moisture conditions, soil type, depth of rooting zone and overall vegetation growth (Lukenbach et al., 2019), which means various topographic configurations (*e.g.*, hummocks, swales and slopes) and reclamation prescriptions can affect recharge distributions and groundwater flow system.

Transects

The two transects chosen for this study exist along the primary (S-E) flow path and have different topographic configurations (Transect 1 and Transect 2; Figure F-1). Transect 1 intersects a hummock that extends from the southern boundary of the watershed (318.5 m ASL) for approximately 320 m before transitioning into the lowlands (*i.e.,* wetland, 313.3 m ASL). Transect 2 intersects a slope that extends from the southern topographic high (318.2 m ASL) for 140 m as it transitions into the lowlands (313.3 m ASL). Average depths to water table in Transect 1 and Transect 2 is 2.96 ± 1.02 m BGS and 1.67 ± 0.87 m BGS, respectively (Appendix B).

Hydrologic Conceptual Model

Published work from the early years following watershed construction (2013-2015) suggested evapoconcentration was likely the primary mechanism for solute movement/distribution in the shallow subsurface of the watershed (Biagi et al., 2018). Essentially, rising water tables fill the previously shallow unsaturated pore spaces above the water table following an influx of water (precipitation). As water tables gradually return to pre-event levels, the pore water evaporates (evapotranspiration) leaving solutes concentrated in the vadose available for dissolution on the next rewetting event (Simhayov et al., 2017). Upwelling and vertical discharge of OSPW were also hypothesized to be the sources of elevated sodium (Biagi et al., 2018; Vessey et al., 2018; Vitt et al., 2016); however, negligible vertical hydraulic gradients were observed at various locations throughout the uplands and lowlands over the study period (Appendix B). Therefore, groundwater ridging, lateral seepage faces, and evapoconcentration are likely the best hypotheses to explain the mechanisms behind the development of these hotspots.

III. Methods

Groundwater Sampling & Analyses

A subset of groundwater samples was collected six times over the 2017 summer field season, every 2-4 weeks, from piezometers located along two transects in SHW (Figure F-1). These samples were used specifically for a short, spatio-temporal analysis of sodium concentrations, ECs and stable water isotopes.

All piezometers were purged once, two weeks prior to the first sample collection. Samples were collected at the mid-screen following manual water measurements (Appendix B). Most of the groundwater samples collected were from the shallowest piezometers in nests installed in the tailing sand that consistently had groundwater present throughout the summer (Figure F-1). Exceptions were for three nests that each had deeper samples submitted to develop a vertical profile (*i.e.,* nests 31, 39 and 41) and one nest that had two groundwater samples collected from the deeper piezometers installed in the underlying, deeper composite tailings (BGC-08-10-C and BGC-08-10-D).

Groundwater samples were collected and stored using a 1" rolling ball bailer to acclimate and fill a 15 mL polystryene conical tube filled to zero head space. Samples were stored at room temperature at the University of Alberta until they were filtered and analyzed for stable water isotopes (Isobrine Solutions Inc.) followed by common metals (Alessi Research Group). Oxygen and hydrogen stable isotope compositions were determined from mechanically and chemically cleaned samples using IRMS; standard deviations (σ) for $\delta^{18}O$ and $\delta^{2}H$ were equal to or better than 0.2 ‰ and 2.0 ‰, respectively ($\pm 1\sigma$). The elemental composition of groundwater samples

(B, Na, Mg, Al, Si, K, S, Ca, Mn, Fe, Ni, Cu, Zn, Br, Sr, Ba) was determined by inductively coupled plasma mass spectrometry (ICP-MS) using an Agilent 8800 ICP-MS/MS (Agilent Technologies, Mississauga, ON). Raw and diluted (10x) samples were analyzed to reduce risk of errors from common metal interference. Data below sample-specific detection limits (BDL), or above an acceptable relative standard deviation (RSD >10% = AAS) were not used.

Precipitation Sampling & Analyses

Rain water isotope samples were collected intermittently during the 2017 field season. Precipitation was collected using the method of Gröning et al., (2011). Single rain events were collected when possible; however, multiple small rain events were often captured within one sample and total event volumes were not available. Consequently, precipitation samples could not be volume weighted by event. Samples were analyzed for stable water isotopes (Isobrine Solutions Inc), where oxygen and hydrogen stable isotope compositions were determined from mechanically and chemically cleaned samples using IRMS, in the same manner as the groundwater samples (described above). The standard deviations for $\delta^{18}O$ and $\delta^{2}H$ were equal to or better than 0.2 ‰ and 2.0 ‰, respectively ($\pm$ 1σ).

Data Analyses

- Piezometer Water Classes

While the purpose of this analysis was to evaluate groundwater isotopes at/near the water table, using the existing piezometers/infrastructure/apparatus in SHW made it difficult to directly sample at the water table. Within one nest, the midscreens of piezometers could be separated vertically by approximately 2-4 metres. This meant that, in some cases, if the shallowest piezometer in a nest "missed" the water table, the next shallowest piezometer could potentially sample water from just under 4 metres below the water table. In a watershed where a shallow groundwater system was expected to develop, chemistry and isotopes could vary spatially and vertically; the chemistry within a column of water could vary considerably over small distances, with depth. Natural breaks in the installation and water level data allowed for "water classes" to be developed based on a) the water level (WL) elevation in the piezometer relative to ground surface (GS; "artesian" = WL > GS, "shallow" = WL <1.8 m BGS, and "deep" = WL >1.8 m BGS), and b) midscreen (MS) elevation (*i.e.* water sampling elevation) relative to water level ("shallow" = MS <1.8 m BWL, or "deep" = MS >1.8 m BWL). Classes are consistently referred to by the relative water level elevations first, and relative midscreen elevations second. For example, shallow/deep indicates groundwater is less than 1.8 metres below ground surface, but the midscreen is more than 1.8 m below water level, thereby sampling deeper into the column of water. A conceptual diagram for these water classes is outlined in Figure F-2 using symbology color and shape to assist in subsequent isotope and geochemical interpretations; special attention should be paid the water level elevation relative to ground surface and the midscreen elevation relative to the water level (read: sampling elevation) when interpreting all geochemical and isotope data.

- Groundwater Mixing Model

A groundwater mixing model was developed for SHW by defining endmember compositions (OSPW and Mildred Lake Reservoir, MLR) and using EC, chemistry and stable water isotopes to characterize the surface water, and shallow and deep groundwater in piezometers across SHW. These endmembers were used to determine the sources of groundwater at various locations in the watershed and elucidate mechanisms of solute movement along two transects in the watershed with different topographic configurations. Endmember compositions were obtained from the literature where the data record is incomplete. Eighteen groundwater samples collected from

BGC piezometers in SHW during 2013 and 2014 were averaged to define the major ions of OSPW geochemistry and were paired with the average OSPW isotope composition from Baer et al., (2016) to collectively represent the OSPW endmember composition in SHW. Only one geochemical sample was collected and analyzed from MLR during the study period, in 2015 (Vessey et al., 2018); this data point was paired with the average isotope endmember composition for MLR presented in Baer (2014), both of which are considered to adequately represent the 2013 and 2014 MLR water added to SHW.

Table F-1: Average isotope and geochemical endmember compositions

Isotope Endmember	**$\delta^{18}O$ (‰ VSMOW) ± 1σ**	**$\delta^{2}H$ (‰ VSMOW) ± 1σ**	**n**	**Source**
Avg OSPW	-13.1 ± 1.2	-115 ± 6.1	145	Baer et al., 2016
Avg MLR	-17.7 ± 0.5	-142.7 ± 1.6	8	Baer, 2014

Geochemical Endmember	**Na^{+} (meq/L) ± 1σ**	**EC (µS/cm) ± 1σ**	**n**	**Source**
Avg OSPW	42.2 ± 2.1	4060 ± 174	18	electronic appendix
MLR	0.5 ± (-)	281 ± (-)	1	Vessey et al., 2018

- Stable Water Isotopes & Aqueous Geochemistry Data

The isotope conceptual model for SHW will be developed in $\delta^{2}H$ and $\delta^{18}O$ space by plotting endmember isotope compositions (OSPW, MLR and 2017 unweighted precipitation) against the Local Evaporation Line (LEL; Biagi et al., 2018) and weighted and unweighted Local Meteoric Water Lines (wLMWL and uLMWL, respectively; Baer et al., 2016) developed on Mildred Lake Lease (Table F-2). Baer (2014) compiled precipitation data (snow and rain from 2009 and 2012; n=83) and developed the wLMWL (utilizing the least squares regression method), which is consistent with other LMWL in the province (Baer et al., 2016). The uLMWL was developed similarly, with non-volume-weighted data. Biagi et al., (2018) compiled surface water data from

SHW during the summer of 2014 (n=49) and subsequently developed the LEL by performing a regression on the data.

Precipitation data were plotted against the uLMWL, given the samples were not volume-weighted; however, all other samples should be interpreted using the wLMWL (Baer et al., 2016). Groundwater isotope data were analyzed in dual isotope space (δ^2H vs $\delta^{18}O$) and were paired with chemistry (Na^+ vs $\delta^{18}O$) space to examine relationships between groundwater and endmember's isotope and geochemical compositions in Transect 1 and Transect 2. A theoretical mixing line was included in the Na^+ vs $\delta^{18}O$ plot (dashed line) to assist with interpretation.

Table F-2: Site Specific LMWLs and LEL from the literature

Line	**Equation of the Line**	**Source**
Local Evaporation Line (LEL)	$\delta^2H = 4.9\ (\delta^{18}O) - 56.8‰$	Biagi et al., 2018
Unweighted Local Meteoric Water Line (uLMWL)	$\delta^2H = 6.8\ (\delta^{18}O) - 21.3‰$	Baer et al., 2016
Weighted Local Meteoric Water Line (wLMWL)	$\delta^2H = 7.2\ (\delta^{18}O) - 10.3‰$	Baer et al., 2016

- Spatial/Temporal Isotope & Electrical Conductivity Data

Groundwater isotope and electrical conductivity data were plotted as isoscapes and chemoscapes (respectively) to demonstrate their spatial and temporal trends in each transect. The chemoscapes and isoscapes were paired with temporal precipitation data, as well as cross sections that provide topography, water level, and installation information. Na^+ data could not be plotted as a chemoscape due to the large variability in values.

- Vertical Isotope, EC & Na^+ Data

Groundwater isotopes, EC's, and Na^+ gradients were compared from 3 piezometer nests in the watershed (nests 31, 39, 41) to evaluate changes in the vertical water column with depth, where data were available. A theoretical mixing line was included in the Na^+ vs $\delta^{18}O$ plot (dashed line) to assist with interpretation. Note piezometer nest 39 data were all collected on the same day, nest 31 were one week apart, and nest 41 were one month apart (electronic appendix).

- Relationship between EC & Na^+

All EC and Na^+ data were plotted together to evaluate proportions of sodium in the shallow groundwater at various points along different topographic configurations to help discern patterns.

IV. Results & Discussion

Stable Water Isotopes & Geochemistry (Na+)

Of the three endmembers that exist within SHW, OSPW was the most isotopically enriched endmember, plotting above the LEL, and had the highest concentration of sodium (Figure F-3). MLR is more isotopically depleted than OSPW, plotting closer to the LEL/wLMWL intersection, and has very low sodium concentrations. This is due, in part, to MLR regularly being topped up with fresh Athabasca River water, which is also isotopically similar to precipitation in the area (Baer et al., 2016). Precipitation values collected during the summer of 2017 were plotted along the uLMWL developed by Baer et al., (2016) because samples were not volume-weighted (Figure F-3). Precipitation samples exceeding ± 0.2‰ $\delta^{18}O$ and ± 2.0‰ $\delta^{2}H$ of the uLMWL were removed from the analysis, as they likely experienced evaporation within the collecting chamber during longer intervals between sample collection. Of the nine rain samples that were collected, five were removed for this reason.

Groundwater (GW) samples that were collected from piezometers completed in the tailing sand (SH-GW-##-## piezometers) predominantly plot between average OSPW and MLR $\delta^{2}H/\delta^{18}O$ signatures, and between the wLMWL and LEL for both Transect 1 and Transect 2 (Figure F-4a and F-4b, respectively). GW samples that have deviated from the wLMWL and are enriched isotopically (higher $\delta^{2}H/\delta^{18}O$ values) could either indicate evaporation has occurred, increasing the proportion of heavy isotope in the remaining water (samples plot near/along the LEL), or that mixing has occurred between endmembers (samples plot between MLR and OSPW endmembers). Na^+ concentrations (meq/L) were plotted with $\delta^{18}O$ to help resolve these processes; however, GW samples that plot along an isotope mixing line do not always plot along the chemical mixing line, indicating other factors may be influencing ion distributions than simply mixing between endmembers.

Generally, samples with depleted $\delta^2H/\delta^{18}O$ values that fall near the wLMWL/LEL intersection indicate higher proportions of P and/or MLR in the groundwater, and tend to have the lowest sodium concentrations, whereas GW samples that are more isotopically enriched also have the highest concentrations of sodium, consistent for GW with higher proportions of OSPW. The most isotopically depleted GW samples plot well below the LEL, likely indicating GW primarily sourced from cold water recharge (*i.e.* snowmelt; Figure F-4b).

In Transect 1, where groundwater is deeper underground (WL >1.8 m BGS), isotopes either show slight to moderate mixing from MLR to OSPW, or have fresh water compositions near precipitation signatures, regardless of the position of the midscreen in the water column (deep/shallow and deep/deep). All deep/shallow and deep/deep samples plot above the theoretical mixing line for sodium (dashed line Figure F-4a). Water in the shallow/shallow class (WL <1.8 m BGS, MS <1.8 m BWL) follow this pattern for isotopes and geochemistry too. However, shallow/deep groundwater indicates samples from piezometers with shallow water levels relative to ground surface and deeper midscreens relative to water level are much more prone to variation and have the highest proportion of OSPW of all groundwater samples in Transect 1. While the data collected in the wetland are both classified as artesian/deep, SH-GW-66 demonstrates isotope and geochemical signatures consistent with evaporated precipitation and SH-GW-69 indicates isotope and geochemical mixing has occurred between the two endmembers (Figure F-4a).

Compared to Transect 1, Transect 2 has a much greater presence of OSPW. Samples with enriched isotopes and sodium values indicates groundwater is much more heavily mixed with OSPW for both shallow/shallow and shallow/deep water classes. Shallow/deep groundwater is more stable, with less variability compared to shallow/shallow groundwater. The groundwater furthest from ground surface (*i.e.* SH-GW-41-03) plots below the LEL, near the wLMWL, and is likely indicating cold recharge from snowmelt, with no indication of mixing with the underlying OSPW endmember.

Spatial/Temporal Observations using Chemoscapes & Isoscapes

Water levels were consistent throughout the summer below the uplands/hummock in Transect 1 but fluctuated up to 30 cm in the uplands of Transect 2 and lowlands (most notably after the 100 mm pumping event mid-July; Appendix B). The largest precipitation events occurred in June and July (>20 mm/d), while the remainder of the summer had smaller events allowing the watershed to dry through the growing season.

GW $\delta^{18}O$ and EC values remained consistent throughout the field season particularly in areas where the water level was further below ground surface in the uplands (WL >1.8 m BGS, below hummocks) and in the wetlands, where water was sometimes above ground surface (Figure F-5a and F-5b). The largest fluctuations in $\delta^{18}O$ and EC values are associated with upland locations with shallow water tables relative to ground surface in both Transect 1 and Transect 2 (WL <1.8 m BGS). In the uplands of Transect 1, below hummocks, piezometers that sample GW closer to the water level (shallow in the water column; MS <1.8 m BWL) tend to be more stable with fresher, depleted $\delta^{18}O$ signatures and lower EC values (*e.g.,* SH-GW-30 and SH-GW-29) compared to deeper groundwater samples (MS >1.8 m BWL). This differs from the piezometers that sample near the water level in the slope of the uplands of Transect 2 (MS <1/8 m BWL), which show more enriched $\delta^{18}O$ and EC values (*i.e.,* SH-GW-75 and -76; shallow/shallow), consistent with deeper groundwater samples obtained upslope (MS >1.8m BWL). GW sampled deeper relative to the shallow water level at the toe of hummock in Transect 1 (*i.e.,* SH-GW-23; shallow/deep) tended to fall around enriched isotope and geochemical values observed in a deeper piezometer upslope in Transect 2 (*i.e.,* SH-GW-42-03; shallow/deep).

Interestingly, the piezometers SH-GW-23-D, -66 and -69 analyzed from Transect 1 have nearly the same water level relative to ground surface, have MS installed at nearly the same depth (*i.e*., elevation), and yet they are vastly different in their geochemical and isotopic compositions (Figure F-5a). Since calculated vertical hydraulic gradients are negligible over long periods (Appendix B), the position along the flow path and topography preceding the nest likely influence the depth of the fresh water lens in each area.

Vertical Profile of δ18O, EC & Na+

To ensure the values observed from different sampling depths across each transect were not an artifact of location in the watershed, vertical profiles were developed for three nests where data were available. Consistently, the shallowest samples from each nest (obtained from MS <1.8 m BWL, shallow/shallow and deep/shallow) were more depleted isotopically and geochemically compared to the samples collected from the same location, deeper within the water column (MS >1.8 m BWL, shallow/deep and deep/deep; Figure F-6). The groundwater sampled from deeper within the water column became isotopically enriched and plotted nearly perfectly along the MLR/OSPW mixing line, with some of the highest proportions of OSPW observed in all samples.

Given that nested piezometers here are separated vertically by approximately 2 metres at each location, the vertical isotope and geochemical gradient between fresh water (P or MLR) and

OSPW can range from both extremes (SH-GW-41-03/05) to moderately mixed (SH-GW-31-02/04) to almost entirely mixed with OSPW (SH-GW-39-05/07/09)

Relationship between EC & Na+

All groundwater samples from Transects 1 and 2 were plotted in EC vs Na^+ space using the water classes defined in Figure F-2 (Figure F-7). General patterns emerged when comparing samples based on water classes: shallow/shallow samples tended to be moderately mixed toward the OSPW endmember, shallow/deep samples were heavily mixed with OSPW, and the deep/shallow and deep/deep water tended to fall on the fresher end of moderately mixed groundwater.

The samples collected in the wetland (artesian/deep) did not plot together. SH-GW-66 is located along Transect 1 flow path which is sourced from water that is more isotopically depleted. SH-GW-69 is located at the end of both flow paths, one of which is more isotopically enriched with OSPW water (Transect 2) than the other (Transect 1), creating a more mixed signature (Figure F-1 and Figure F-7).

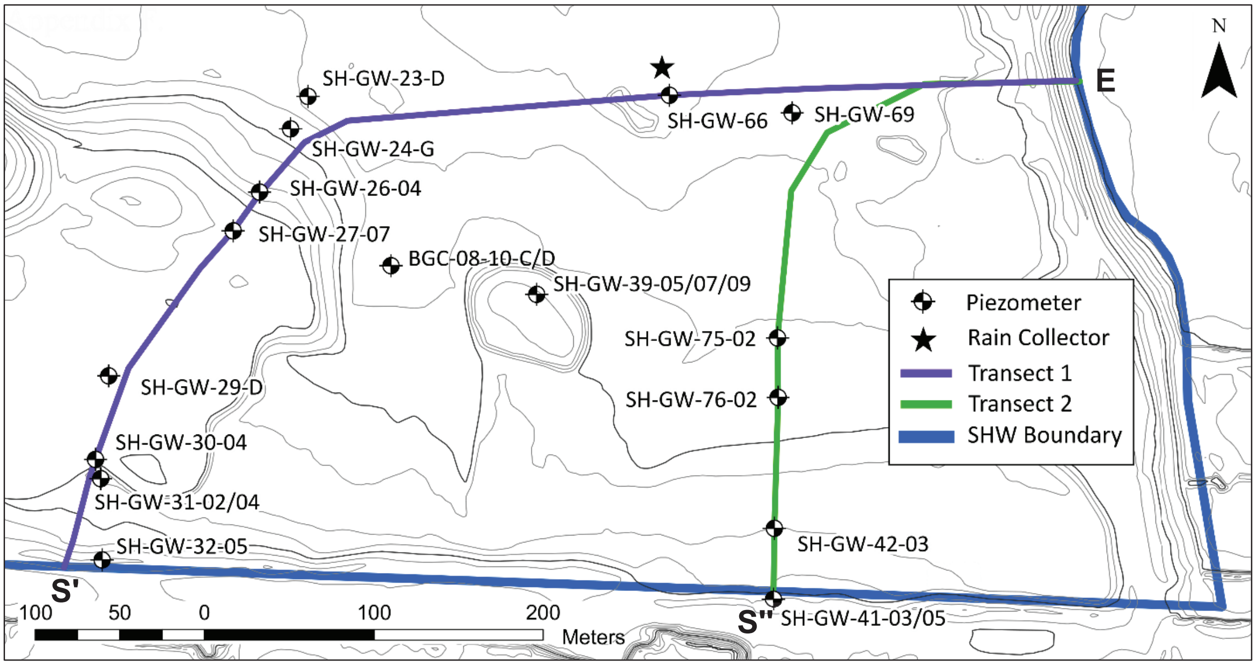

Figure F-1: Southeast corner of Sandhill Watershed (SHW) showing all piezometer nests used to sample groundwater isotopes and geochemistry, most falling along Transect 1 (hummock-to-wetland) and Transect 2 (slope-to-wetland). One piezometer was analyzed per nest (e.g. SH-GW-##-##), unless otherwise indicated (e.g. SH-GW-##-##/##). Sampling location of the rainwater collector is provided.

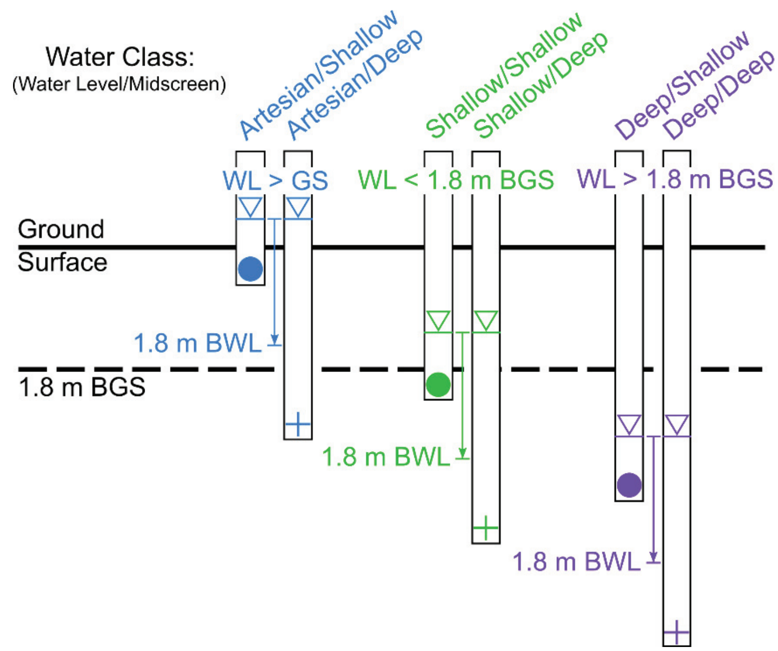

Figure F-2: Conceptual diagram outlining 6 water classes defined by the water level depth relative to ground surface (symbol color), and the depth of the midscreen relative to the water level (symbol shape). The symbology (color, shape) will remain consistent in subsequent figures to assist in isotope and geochemical interpretation of groundwater collected from piezometers in the tailings sand (SH-GW-##-##). Specifically, GW symbology color indicates water level elevation in pipe relative to ground surface (Artesian, blue = WL >GS; Shallow, green = WL <1.8 m BGS; Deep, purple = WL >1.8 m BGS), and symbol shape indicates midscreen elevation of pipe (read: water sampling elevation) relative to water level (Shallow, ● = MS <1.8 m BWL; Deep, + = MS >1.8 m BWL).

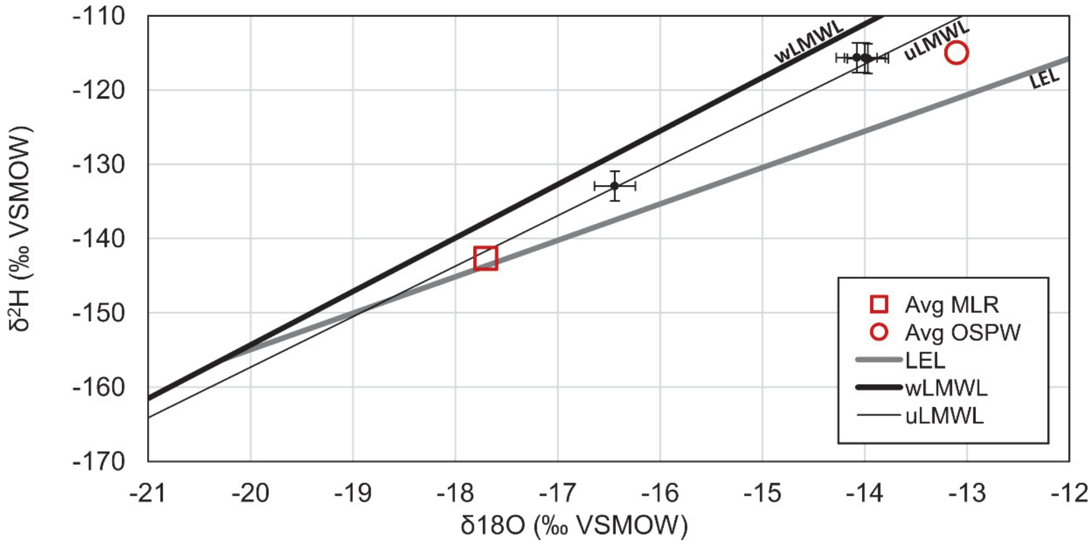

Figure F-3: Average δ^2H and $\delta^{18}O$ endmember compositions for Mildred Lake Reservoir (Avg MLR) and Average Oil Sands Process-affected Water (Avg OSPW) plotted with precipitation data collected during the summer of 2017 (black). Weighted and unweighted Local Meteoric Water Lines (wLMWL and uLMWL) and Local Evaporation Line (LEL) were developed previously for SCL Mildred Lake Lease and will all be included in subsequent δ^2H and $\delta^{18}O$ figures (Baer et al., 2016; Biagi et al., 2018). Precipitation were plotted against the site-specific unweighted Local Meteoric Water Line (uLMWL); data exceeding ± 0.2 ‰ and ± 2.0 ‰ for $\delta^{18}O$ and δ^2H were not included (error bars shown).

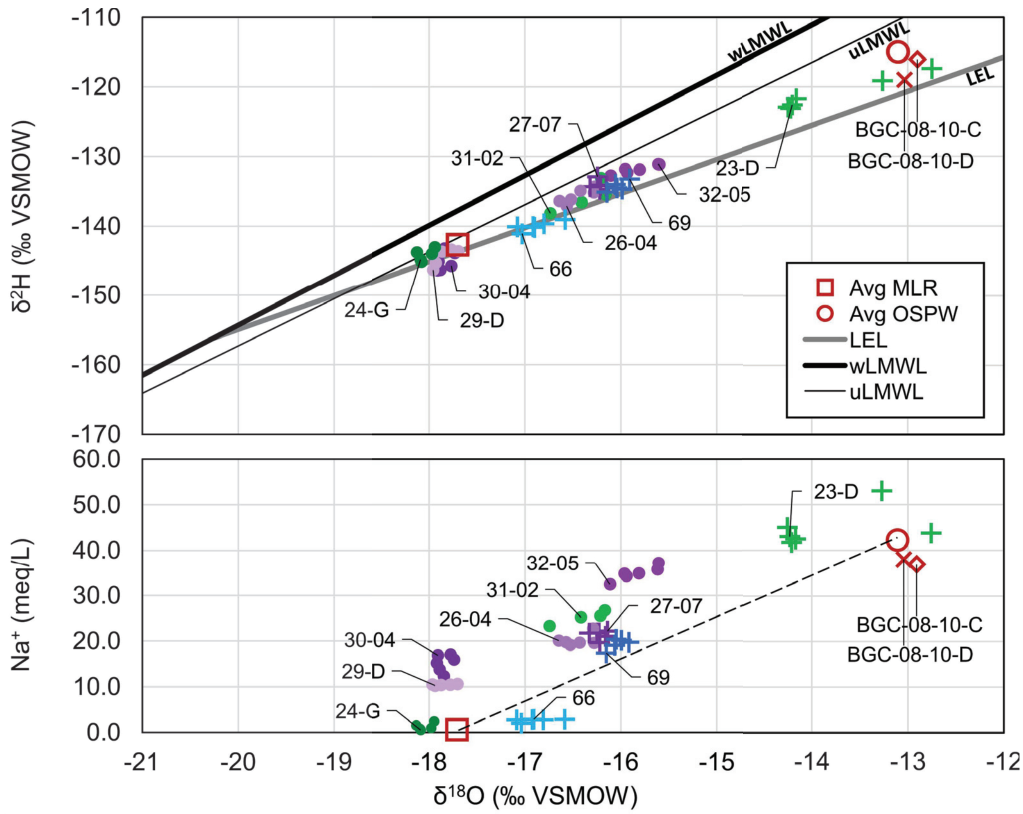

Figure F-4a: Paired plots of δ^2H vs $\delta^{18}O$ (upper) and Na^+ vs $\delta^{18}O$ (lower) values collected inside the shallowest piezometer from nests along Transect 1 (hummock-to-wetland) during the summer field season of 2017. Average endmember compositions and deep GW samples (BGC-##-## piezometers) are plotted in red. All remaining data are GW samples from shallow piezometers in the tailings sand, symbology is consistent with water classes in Figure F-2 (SH-GW-##-##; shortened to ##-##). Full description of δ^2H vs $\delta^{18}O$ space in Figure F-3. Chemistry data were plotted with a theoretical mixing line between the Avg MLR and Avg OSPW endmember compositions.

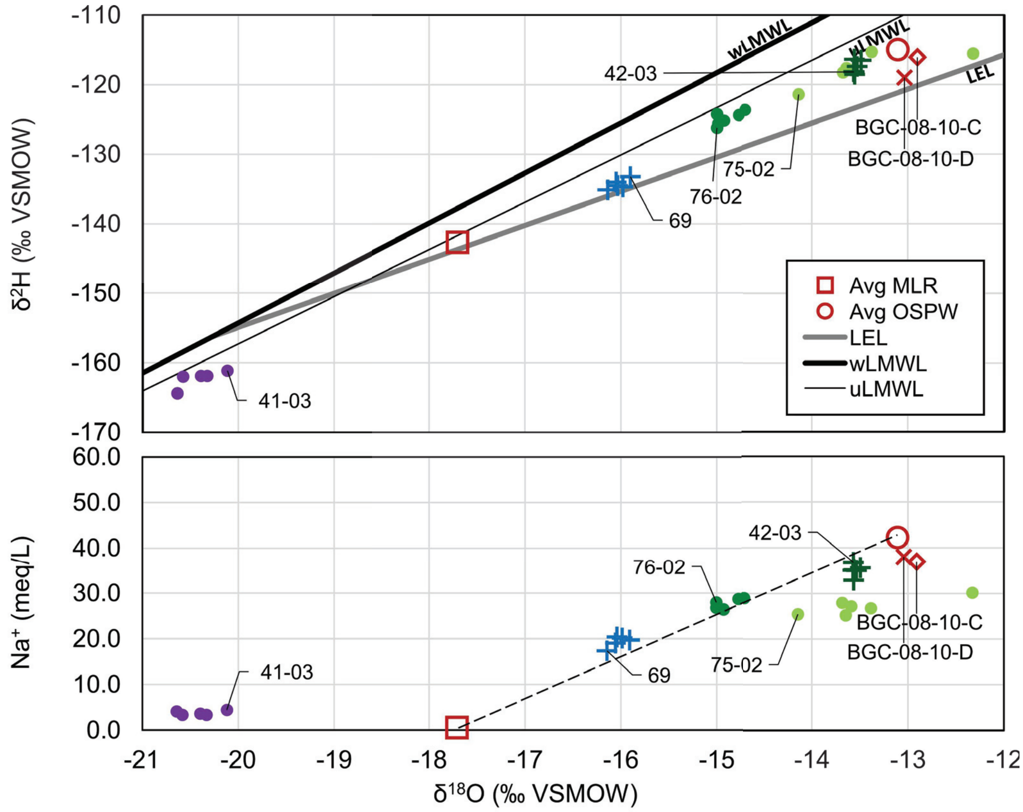

Figure F-4b: Paired plots of δ^2H vs $\delta^{18}O$ (upper) and Na^+ vs $\delta^{18}O$ (lower) values collected inside the shallowest piezometer from nests along Transect 2 (slope-to-wetland) during the summer field season of 2017. Further details provided in Figure F-4a.

5a

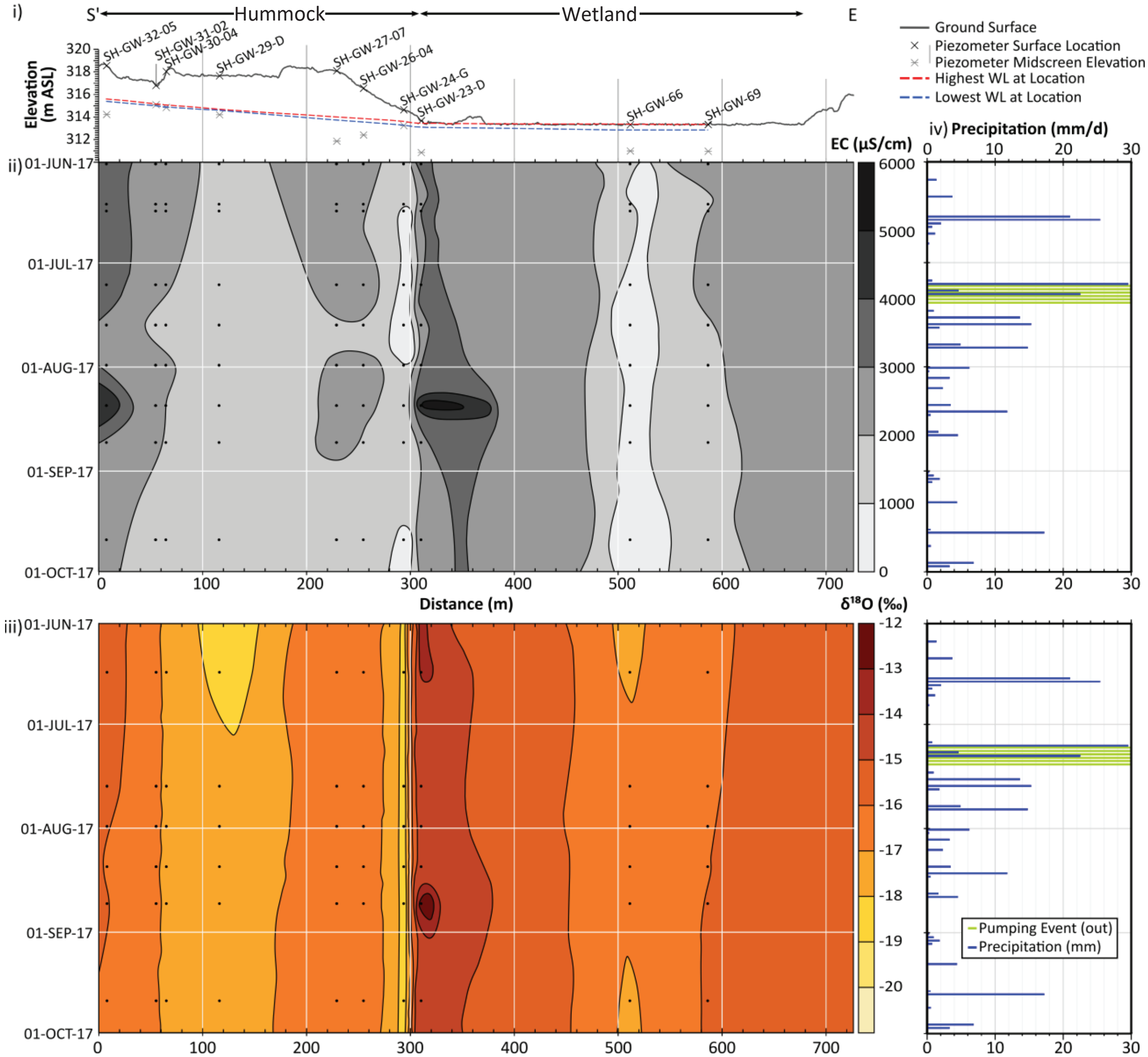

Figure F-5a: Transect 1 (hummock-to-wetland) i) cross sections simultaneously plotted with spatio-temporal contour maps of ii) EC (chemoscape) and iii) $\delta^{18}O$ values (isoscape) that are both paired with iv) precipitation and pumping data for the duration of the 2017 field season. Black dots in isoscapes and chemoscapes indicate sampling dates and locations; darkest contours indicate highest values. Map view of transect outlined in Figure F-1.

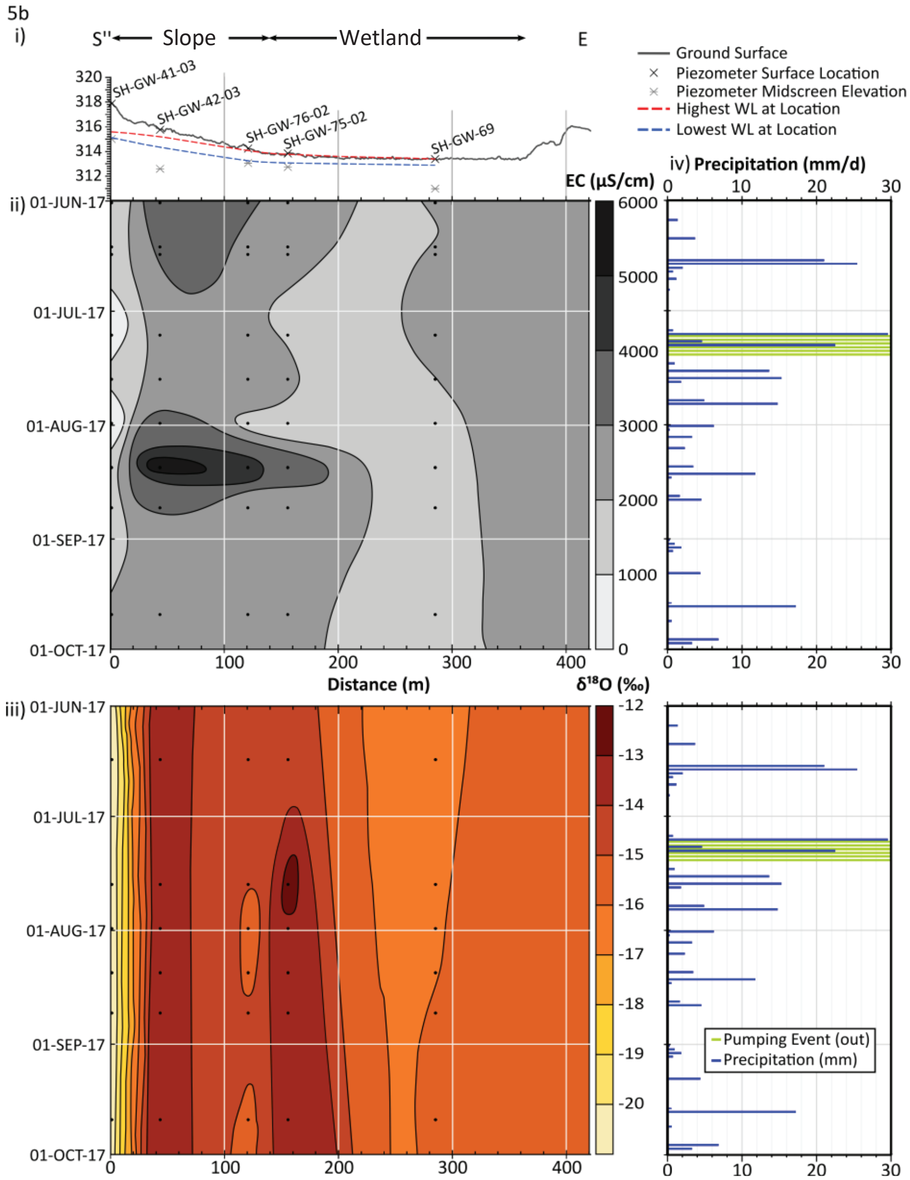

Figure F-5b: Transect 2 (slope-to-wetland) i) cross sections simultaneously plotted with spatio-temporal contour maps of ii) EC (chemoscape) and iii) $\delta^{18}O$ values (isoscape) that are both paired with iv) precipitation and pumping data for the duration of the 2017 field season. Further details provided in Figure F-5a.

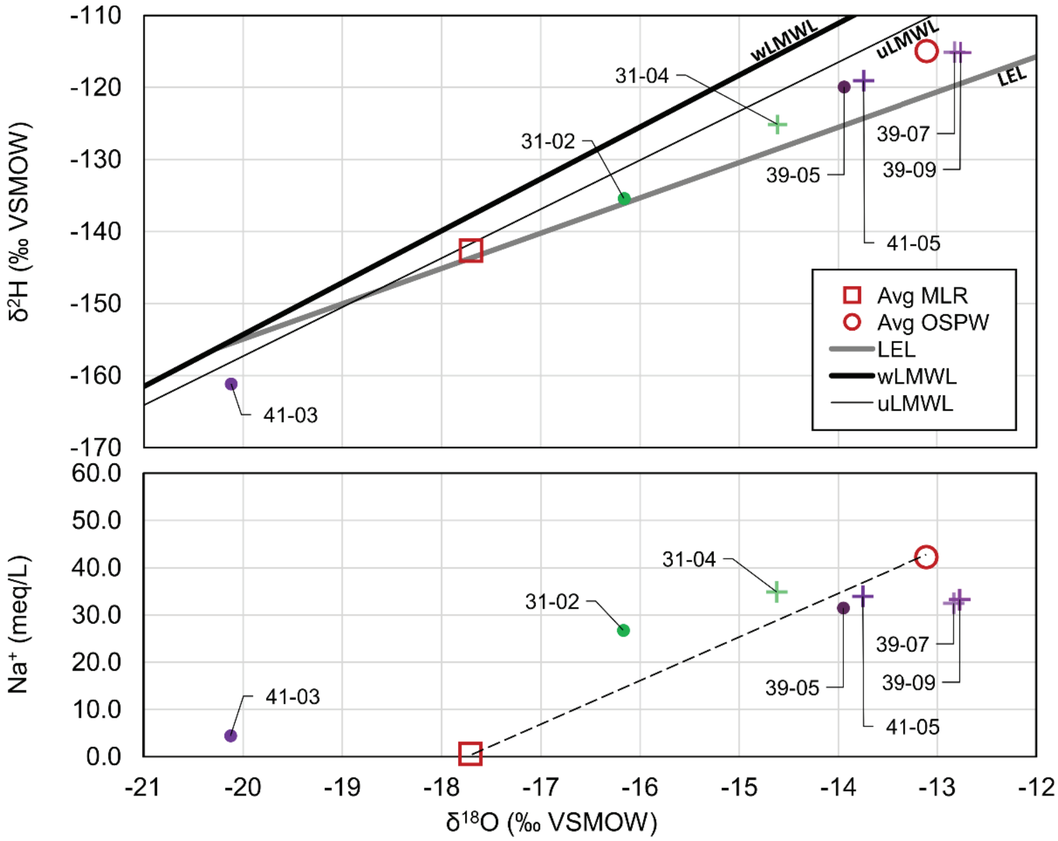

Figure F-6: Paired plots of $\delta^{H}2$ vs $\delta^{18}O$ (upper) and Na^{+} vs $\delta^{18}O$ (lower) values collected inside the shallowest and deepest piezometers from three nests during the summer of 2017. Futher details provided in Figure F-4a.

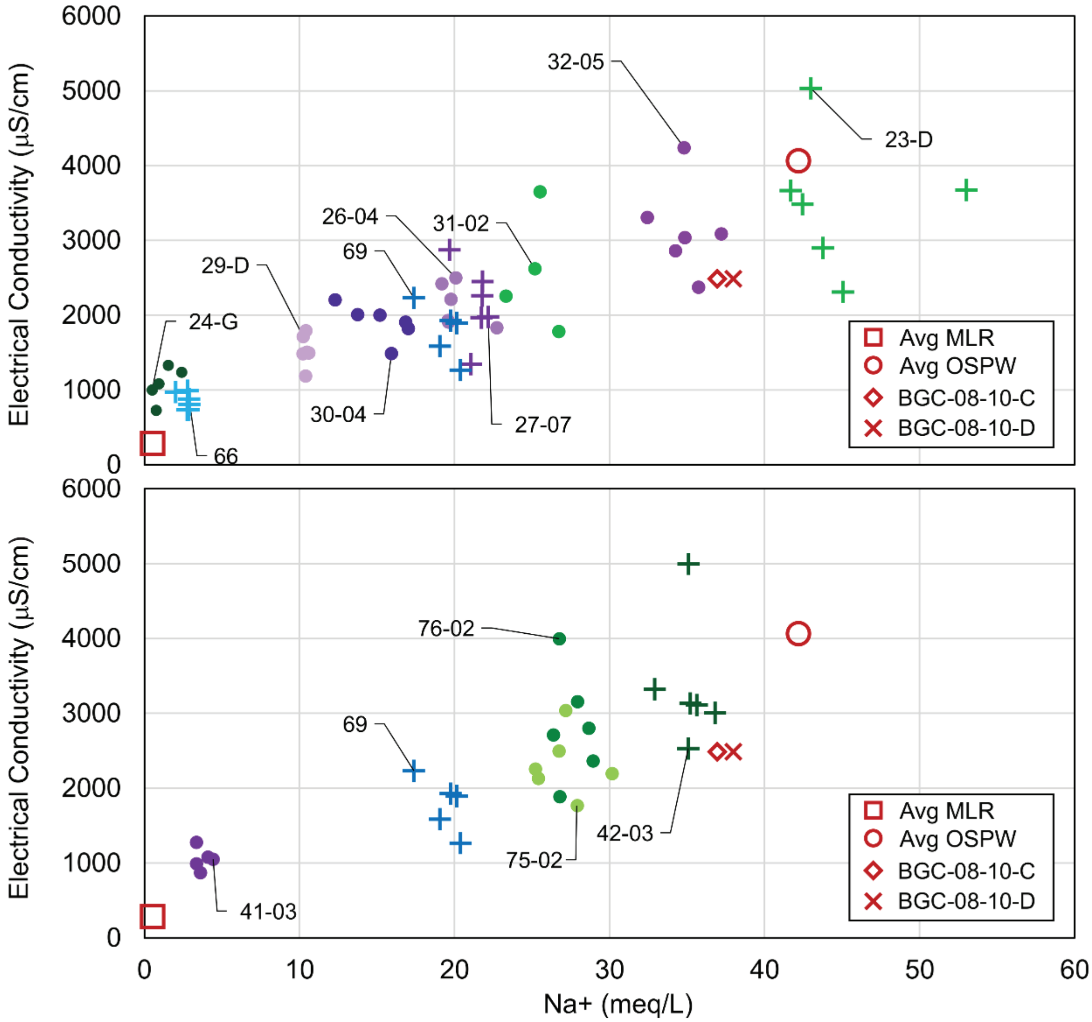

Figure F-7: EC vs Na^+ plotted for all groundwater (GW) samples analyzed from Transect 1 (hummock-to-wetland; upper) and Transect 2 (slope-to-wetland; lower) during the summer of 2017. Average endmember compositions and samples from BGC-##-## piezometers are plotted in red; all remaining symbols are GW samples from shallow piezometers in the tailings sand, symbology is consistent with water classes in Figure F-2 (SH-GW-##-##; shortened to ##-##).

Appendix G - Piezometer Slug Tests

Appendix G - Piezometer Slug Tests

I. Scope of Work

Hydraulic conductivities were evaluated in the summer of 2017 to supplement historical tailings sand slug test data, determine the hydraulic conductivity of peat-mineral-mix (PMM), and evaluate changes in hydraulic conductivity over time. Hydraulic conductivities were evaluated in the tailings sand, and in the PMM, utilizing Hvorslev (1951) slug test methods. Sites were chosen based on historical tailings sand tests, and access for PMM.

II. Methods

Slug tests were performed once at five different locations in the tailings sand in 2017 to supplement historical tailings sand hydraulic conductivity values. Multiple tests were performed at three locations to assess the hydraulic conductivity of the PMM in the wetland (Figure 5; Hvorslev, 1951). A 0.5 to 1 L freshwater slug was added to upland piezometers. A Solinst Levelogger-Edge was used to capture the initial rise in water level and subsequent recovery; the transducer was set to record at 1 second intervals. For PMM slug tests, a piezometer was pushed into the peat and surface water immediately adjacent to the piezometer was used as the slug. Analysis involved using the methods of Hvorslev (1951), which complement historical hydraulic conductivity analyses of the tailings sand, including bail tests (Longval & Mendoza, 2014) and Guelph Permeameter tests to asses in situ saturated hydraulic conductivity (Benyon, 2014).

III. Results

Tables summarizing the tailings sand and PMM hydraulic conductivities (K) are provided (Table G-1 and Table G-2 respectively), followed by Hvorslev analysis graphs provided, in order: 03-03, 11-11, 18-04, 42-06, 54-08, 66, 68, 71. Inner diameter of the piezometers are

0.0254 m with a 0.31 m screen. Lower K is from the radius of the borehole (2 ¾” diameter borehole = 6.985 cm), upper K is from the radius of the inner diameter of the piezometer.

Table G-1: Tailings sand hydraulic conductivity values compared with historical data

Well ID	Values from Longval and Mendoza (2014)			Values from 2017 Slug Tests		
	T_0 (s)	Lower K (m/s)	Upper K (m/s)	T_0 (s)	Lower K (m/s)	Upper K (m/s)
03-03	126	4.5E-6	6.6E-6	62	9.2E-6	1.3E-5
11-11	213	2.7E-6	3.9E-6	200	2.8E-6	4.2E-6
18-04	57	1.0E-5	1.5E-5	62	9.2E-6	1.3E-5
42-06	118	4.8E-6	7.0E-6	58	9.8E-6	1.4E-5
54-08	63	9.0E-6	1.3E-5	132	4.3E-6	6.3E-6

Table G-2: Peat-mineral-mix hydraulic conductivity values

Well ID	T_0 (s)		Upper K (m/s)
66-Test 1	2.0		4.2E-04
66-Test 2	3.0		2.8E-04
66-Test 3	2.0		4.2E-04
66-Test 4	3.5		2.4E-04
66-Test 5	3.0		2.8E-04
66-Test 6	3.0		2.8E-04
66-Test 7	2.0		4.2E-04
66-Test 8	2.0		4.2E-04
68-Test 1	3.0		2.8E-04
68-Test 2	2.0		4.2E-04
68-Test 3	2.5		3.3E-04
71-Test1	5.0		1.7E-04
71-Test2	5.5		1.5E-04
71-Test 3	6.3		1.3E-04
		Max	4.2E-04
		Min	1.3E-04
		Mean	3.0E-04
		σ	1.0E-04

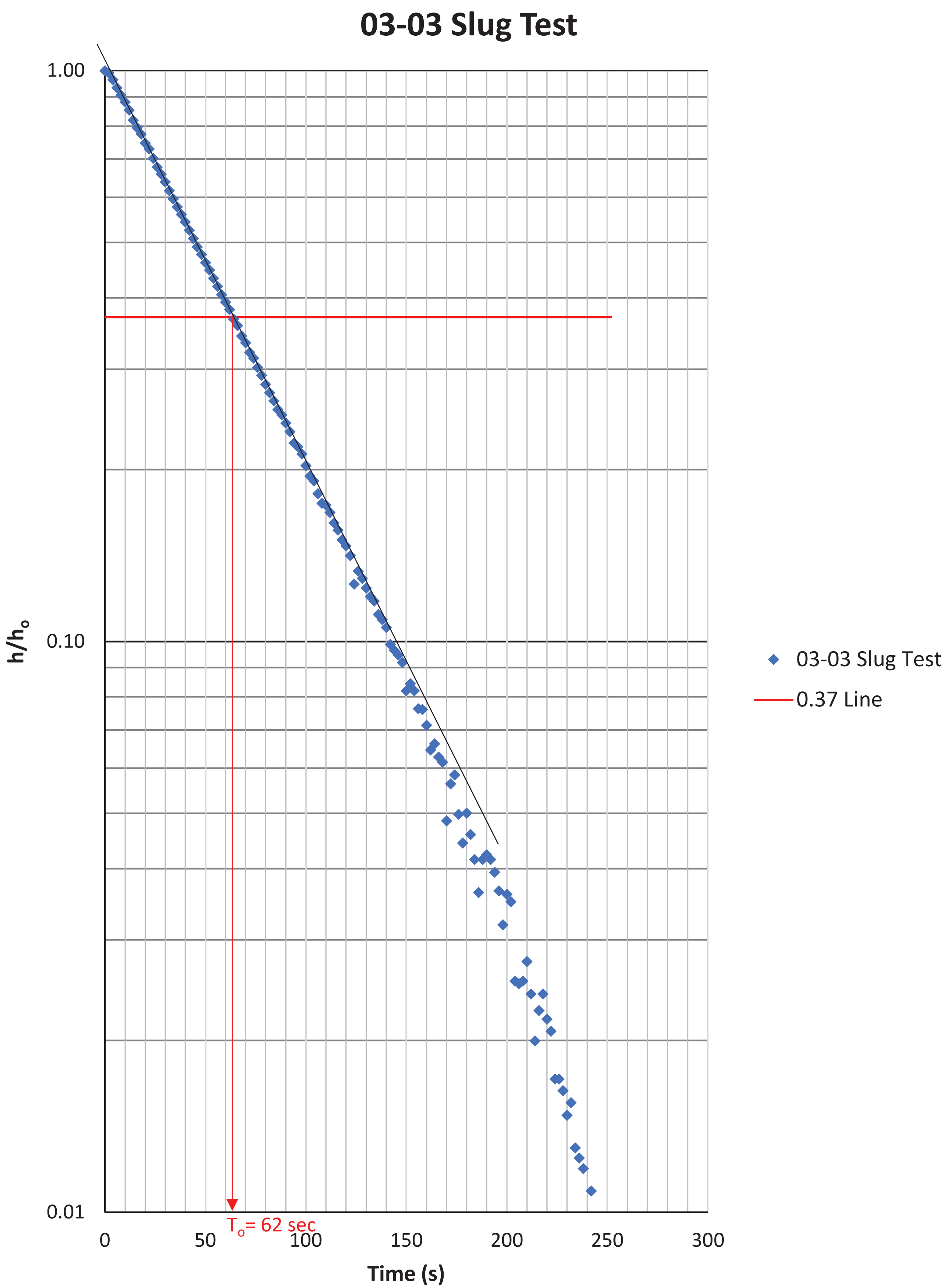
03-03 Slug Test
1.00
0.10
0.01
h/h$_o$
T_o= 62 sec
0
50
100
150
200
250
300
Time (s)
03-03 Slug Test
0.37 Line

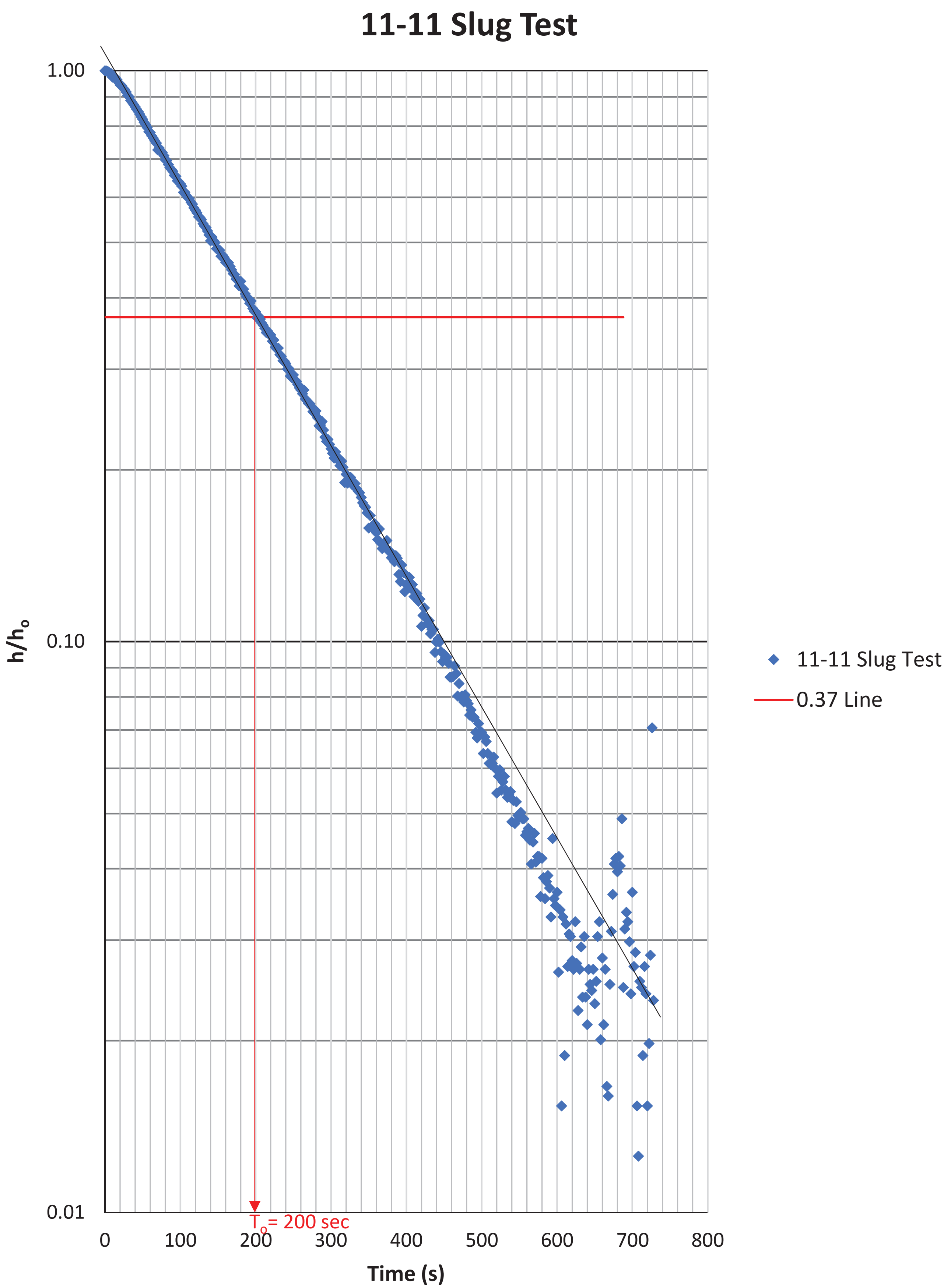
11-11 Slug Test
1.00
0.10
0.01
h/h$_o$
0
100
200
300
400
500
600
700
800
Time (s)
T$_o$= 200 sec
11-11 Slug Test
0.37 Line

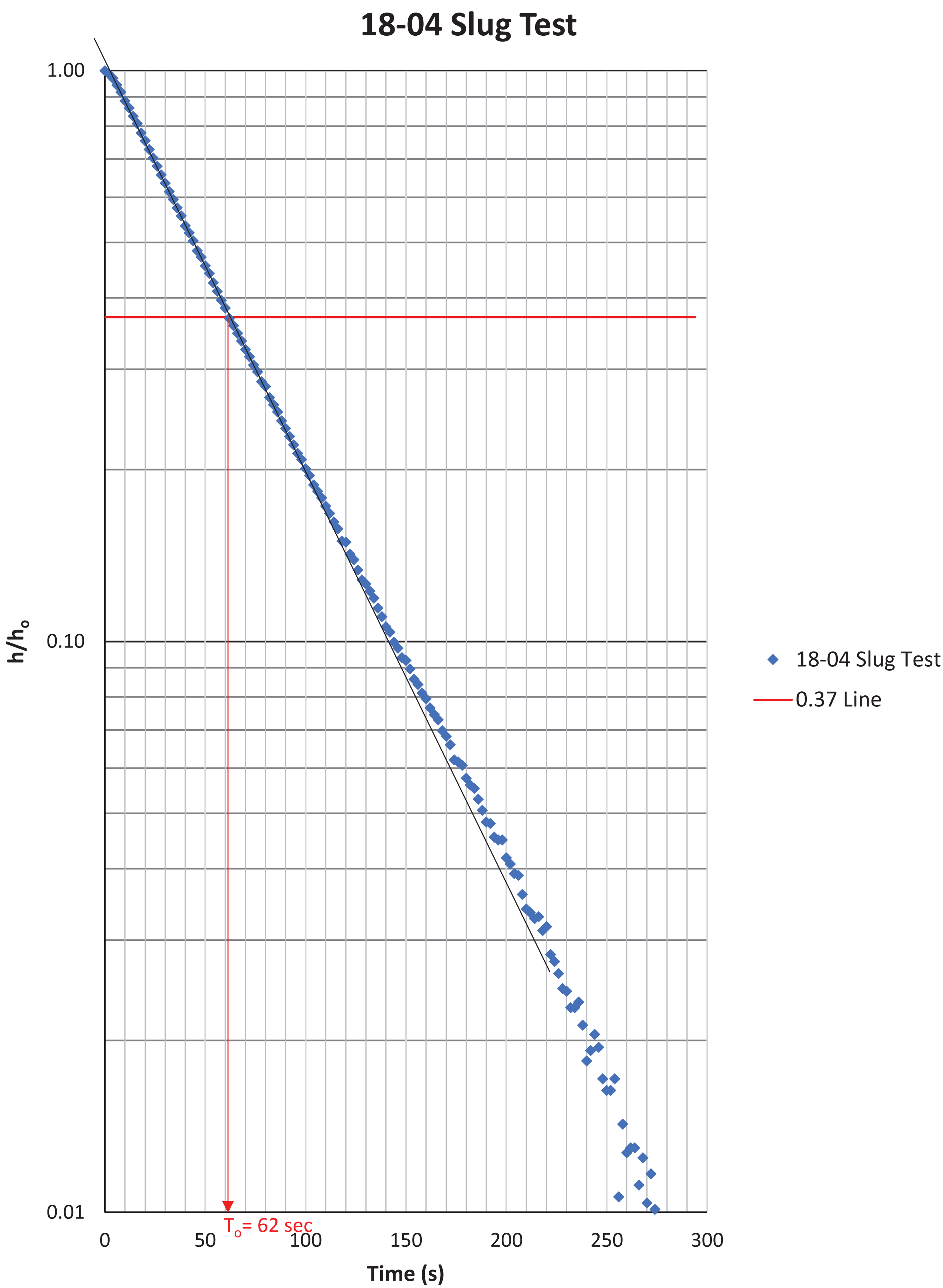
18-04 Slug Test
1.00
0.10
0.01
h/h_o
T_o= 62 sec
0
50
100
150
200
250
300
Time (s)
18-04 Slug Test
0.37 Line

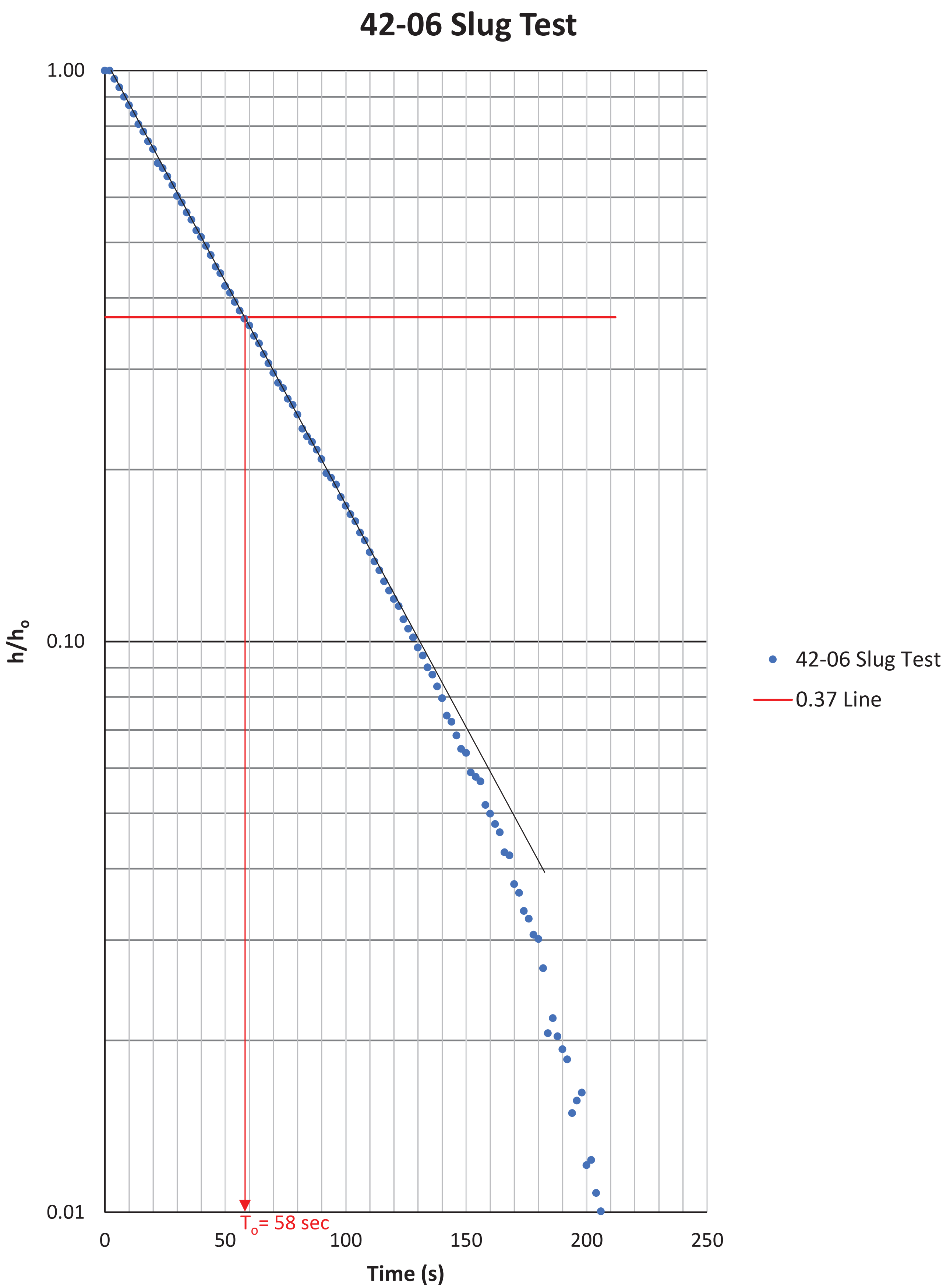
42-06 Slug Test
1.00
0.10
0.01
h/h_o
0
50
100
150
200
250
Time (s)
T_o= 58 sec
42-06 Slug Test
0.37 Line

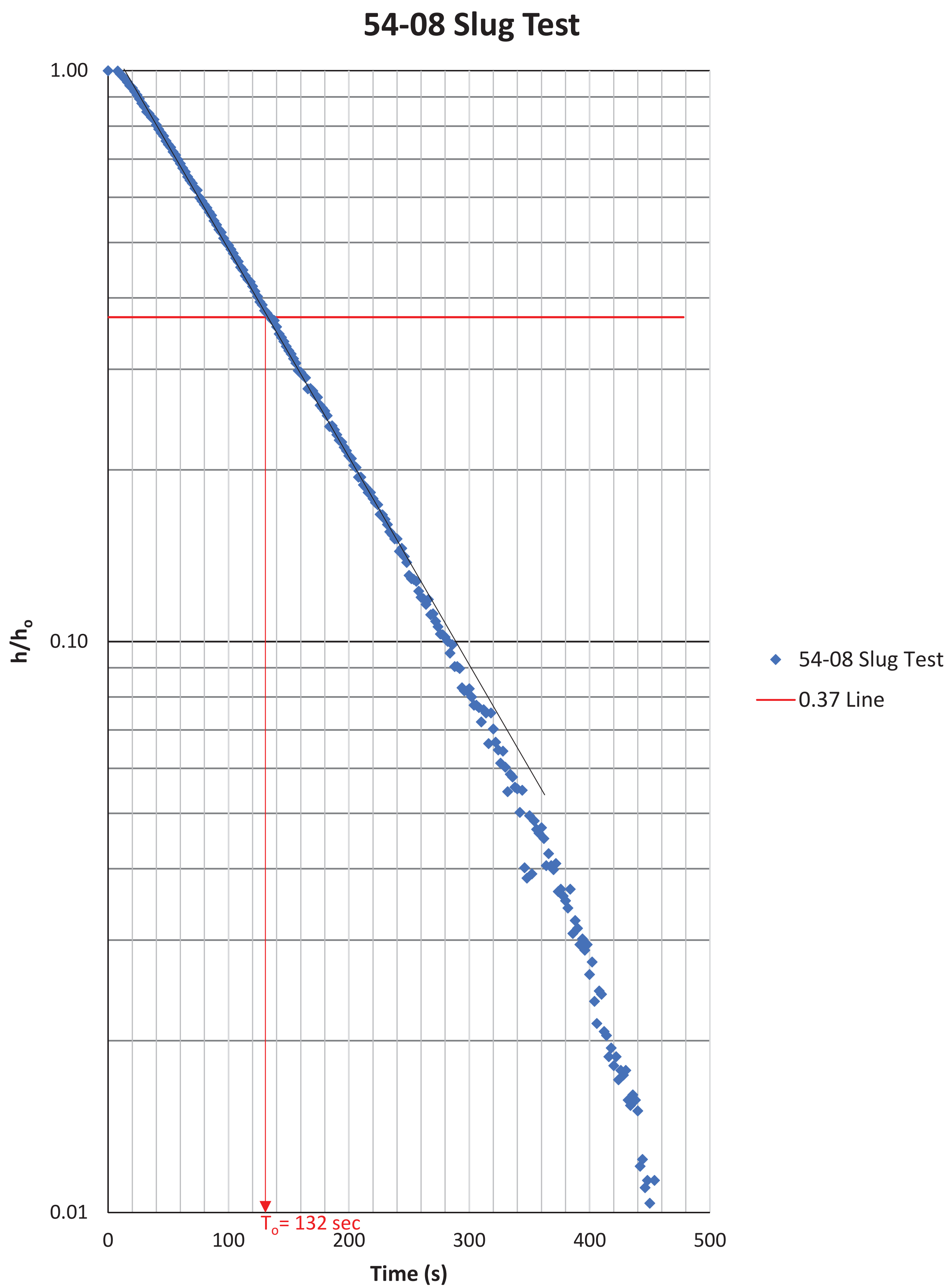
54-08 Slug Test
1.00
0.10
0.01
h/h$_o$
0
100
200
300
400
500
Time (s)
T_o= 132 sec
54-08 Slug Test
0.37 Line

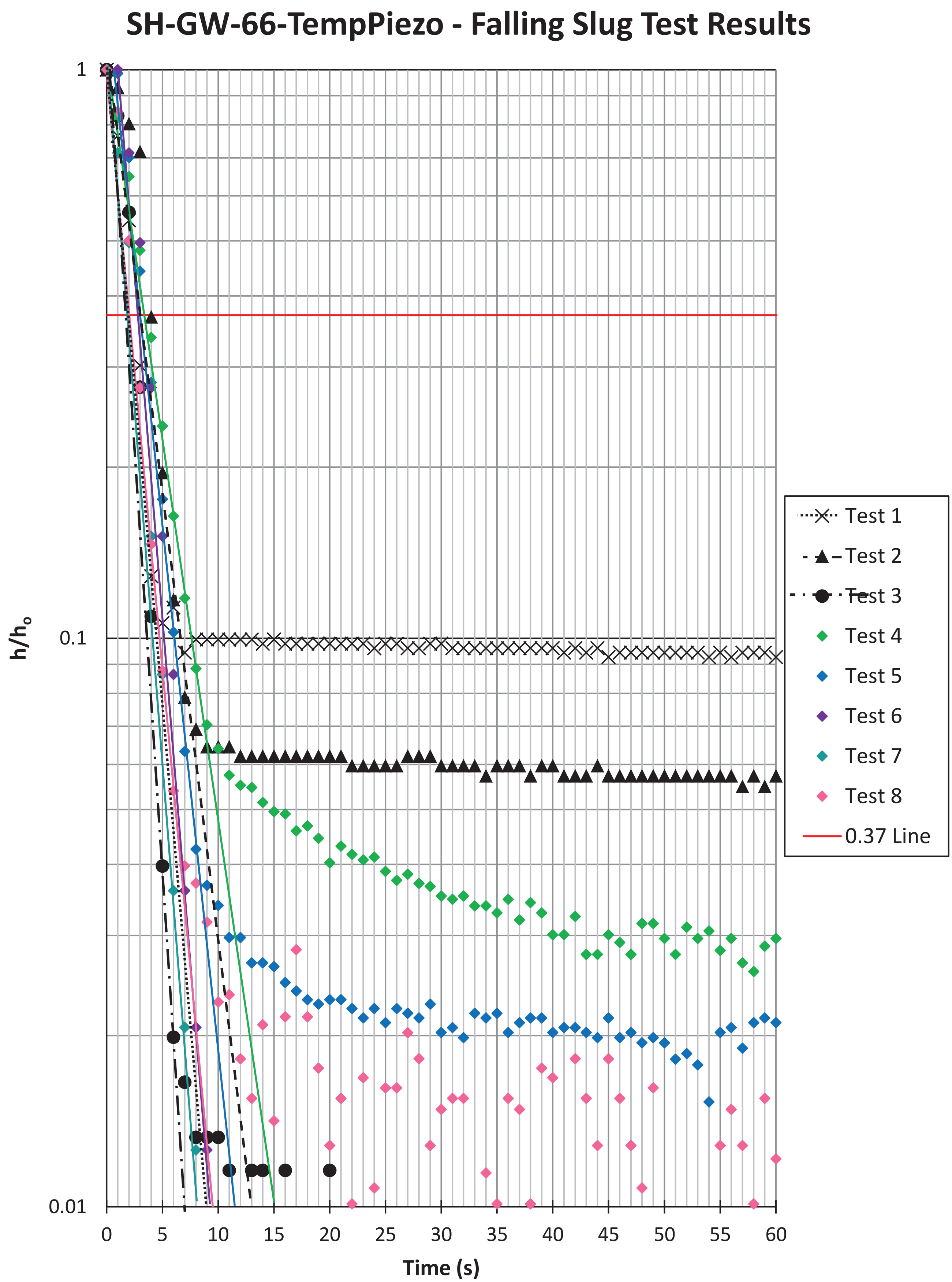

SH-GW-66-TempPiezo - Falling Slug Test Results
h/h$_o$
1
0.1
0.01
0
5
10
15
20
25
30
35
40
45
50
55
60
Time (s)
Test 1
Test 2
Test 3
Test 4
Test 5
Test 6
Test 7
Test 8
0.37 Line

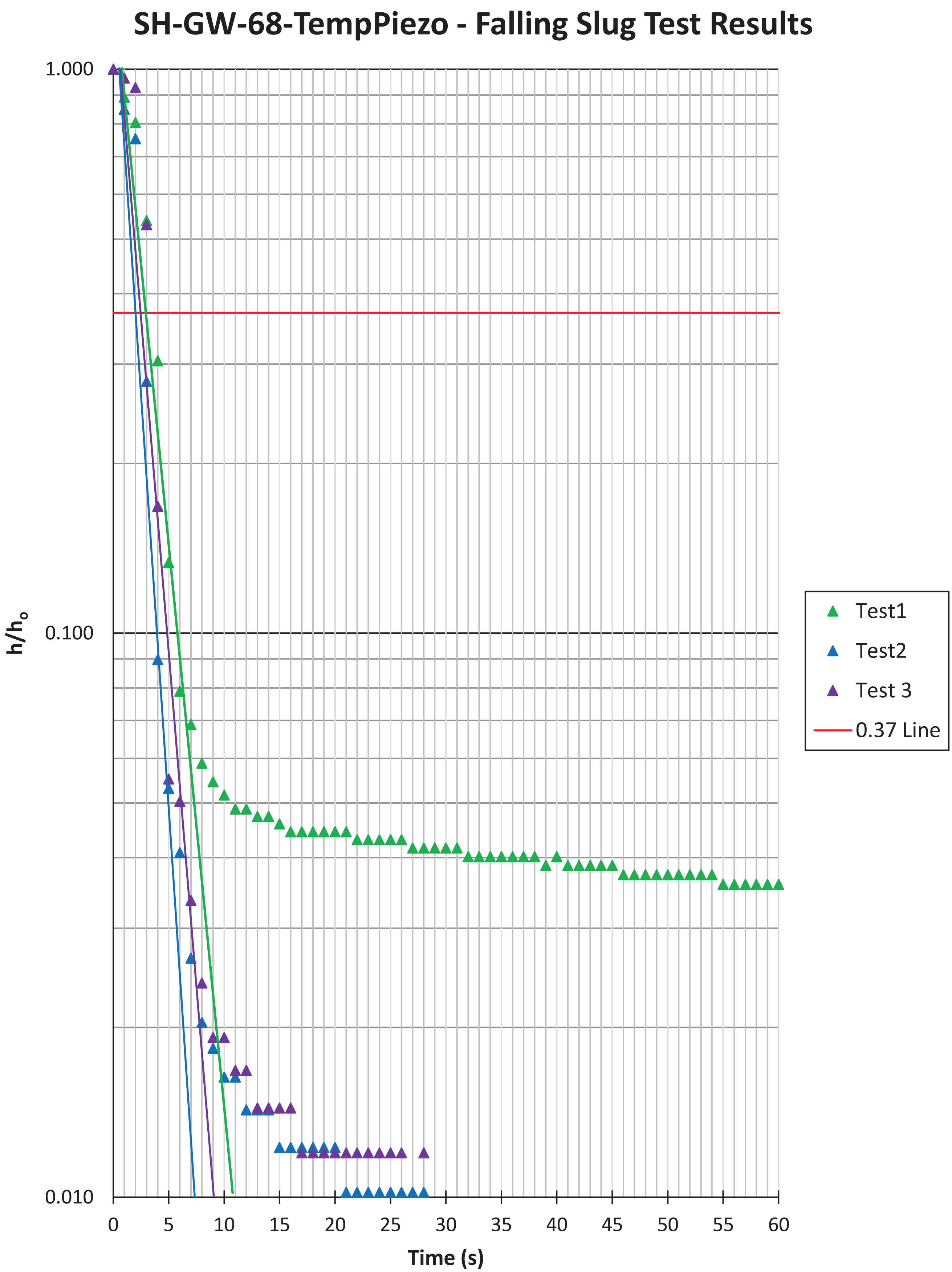
SH-GW-68-TempPiezo - Falling Slug Test Results
1.000
0.100
0.010
h/ho
0
5
10
15
20
25
30
35
40
45
50
55
60
Time (s)
Test1
Test2
Test 3
0.37 Line

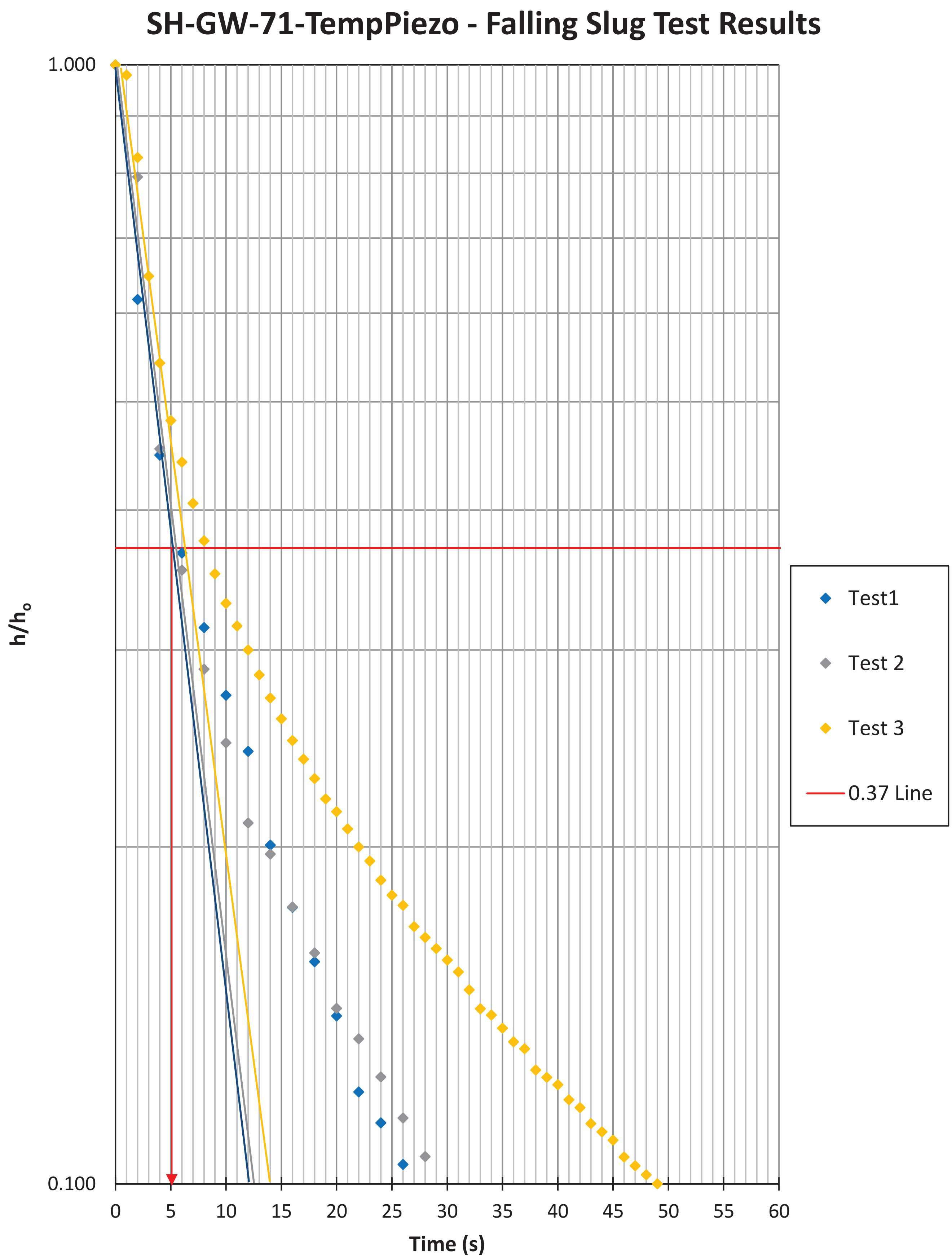

SH-GW-71-TempPiezo - Falling Slug Test Results
1.000
0.100
h/h$_o$
0
5
10
15
20
25
30
35
40
45
50
55
60
Time (s)
Test1
Test 2
Test 3
0.37 Line

Appendix H - Numerical Groundwater Modelling

Appendix H - Numerical Groundwater Modelling

I. Scope of Work

To assist in conceptualizing groundwater movement through the reconstructed watershed, a three-dimensional groundwater flow model was developed utilizing a digital elevation model (DEM; D. Heisler, SCL, pers. com.) and hydrostratigraphy of the watershed, as well as recent climatic fluxes, to simulate steady-state conditions. The goal of the model was to reproduce the average water table configuration observed in SHW, quantify the volumetric flows through the watershed and evaluate the sensitivity of the calibration parameters (*i.e.*, hydraulic conductivity and recharge) on the flow system. The calibrated model was also used to explore potential scenarios with changes in climate or evapotranspiration.

II. Model Design

The three-dimensional, finite-difference groundwater model was developed using Visual MODFLOW (Waterloo Hydrogeologic, 2018). The steady-state model was calibrated to 22 monitoring points in the watershed, using automated water level data from 20 piezometers that had annual continuous data (time gaps were less than one month) from mid-September 2016 to mid-September 2017, and interpolated data at the remaining 2 locations (nest 15 and 25; Figure H-1). Data from automated measurements, rather than manual measurements, were used as calibration points to minimize the bias toward summer water levels that would be introduced by relying on summer field season manual measurements. Water table maps (Appendix B) and soil saturation and wetness maps (Appendix D) were referenced for the general water table configuration within the watershed. These field observations were compared to the simulated hydraulic heads, water table elevation and configuration, and volumetric flows during model calibration.

Recharge rates used in this model were taken from values derived from Lukenbach et al., (2019). Lukenbach et al., (2019) estimated recharge rates by using HYDRUS modelling software to simulate flow through the unsaturated hummocks at SHW. The simulations were calibrated to three years of data collected from 126 soil moisture access tubes, 9 soil pits, and three meteorological and eddy covariance towers in SHW (discussed previously; Figure 5). The hydrostratigraphic properties used by Lukenbach et al., (2019) were based on field measurements and observations when available (Appendix G; Benyon, 2014), or were approximated from engineering designs (BGC, 2014a; BGC, 2015). Simulated hydraulic conductivities from Lukenbach et al., (2019) were referenced as needed when developing the groundwater model. Unsaturated flow modelling methods from SHW are discussed further in Lukenbach et al., (2019).

Model Domain

The model domain is 990 m by 1180 m, discretized to a 10 m x 10 m grid horizontally and extends beyond the southern extent of the study site to encompass 318 Berm; the most laterally extensive upland feature in the tailings deposit and an interpreted major source of groundwater recharge to the watershed (Figure H-2). Areas extending beyond the northern, eastern and western boundaries of the watershed were defined as inactive (*i.e.*, beyond the perimeter of the watershed; Figure H-2). The surface of the model corresponds to the topographic surface defined by the LiDAR (Figure H-2; D. Heisler, SCL, pers. com.), and the entire base of the model was set to 304 m ASL, the approximate elevation of the interface between the composite tailings and the hydraulically-placed tailings sand cap. This interface is approximately 10 m thick below the lowlands and up to 18 m thick below the upland hummocks. Three hydrostratigraphic units were defined vertically downwards from ground surface: topsoil (layer 1 = 0.50 m thick) and subsoil (layer 2 = 0.5 m thick) overly the tailings sand that was equally discretized into three sublayers between the subsoil and base of the model (layers 3 to 5; Figure H-3). All layers were defined as variably confined/unconfined layers.

Hydrogeological Parameters

The topsoil and subsoil hydraulic properties observed in the watershed were incorporated into the upper two layers of the groundwater model based on the observed areal coverage of each soil type (Figure H-3; Appendix A). The entirety of the remaining layers is comprised of tailings sand. These parameters were calibrated through trial and error based on field data (Appendix G) or literature values (Table H-1).

Table H-1: Hydrostratigraphic parameters in base case model compared to literature values

Hydro-stratigrapic Zone	**Depth Range (m BGS)**	**Material**	**Calibrated Parameters**			**Literature K (m/s)**	**Literature Source**
			Kx (m/s)	**Ky (m/s)**	**Kz (m/s)**		
Topsoil	0.0-0.5	PMM[1]	0.01	0.01	0.004	2.8E-04	Lukenbach et al., (2019)
		PMM[2]	4.0E-6	4.0E-6	4.0E-6	1.5E-05	Benyon (2014)
		LFH-A/B	0.02	0.02	0.0002	6.1E-05	Lukenbach et al., (2019)
		LFH-D	4.3E-6	4.3E-6	4.3E-6	1.3E-05	Lukenbach et al., (2019)
Subsoil	0.5-1.0	Clay Till[1]	4.0E-6	4.0E-6	4.0E-6	1.0E-07	Lukenbach et al., (2019)
		Clay Till[2]	1.0E-6	1.0E-6	1.0E-6	1.5E-05	Lukenbach et al., (2019)
		PMM[2]	4.0E-6	4.0E-6	4.0E-6	1.5E-05	Benyon (2014)
		Pf Sand	1.0E-4	1.0E-4	1.0E-4	5.1E-05	Benyon (2014)
		Tailings Sand	1.3E-5	1.3E-5	1.3E-5	2.6E-05	Benyon (2014), Appendix F
Tailings Sand	>1.0	Tailings Sand	1.3E-5	1.3E-5	1.3E-5	2.6E-05	Benyon (2014), Appendix F

[1] Lowlands: regularly experiences standing water and permanently saturated soils in some areas. Subsoil was compacted during initial placement.

[2] Uplands: topsoil and subsoils do not experience lowland saturated hydrologic conditions.

Boundary Conditions & Initial Conditions

The inflows and outflows of the groundwater model are represented by specified flux (net-recharge and no-flow) boundary conditions (BC), and head-dependent flux (general head) BCs. No specified head BCs were used in the model.

- Recharge BC

A net-recharge flux was applied to the uppermost active layer, lumping evapotranspiration (AET) and groundwater recharge (Figure H-4). Net-recharge zones were defined by the hydraulic properties of the soil (topsoil and subsoil transmissivity) and vegetation, which were independently simulated by Lukenbach et al., (2019) to provide recharge rates for reclamation materials in SHW (Table H-2). Negative net-recharge rates in the lowlands reflect excess AET losses to the atmosphere due to vegetation and permanent surface water in the wetland. It also accounts for annual average 'managed' outflows that occurred from the lowlands, calculated from the three years of detailed study.

- Watershed Perimeter

The perimeter of the active cells in the model represents the interface between the tailings sand and surrounding geology (Clearwater Formation; K_h = 1E-8 m/s, K_v = 1E-10 m/s, n = 0.20; BGC, 2015). Because of the low hydraulic conductivity of these surrounding materials, this interface was represented as a no-flow boundary condition (Figure H-4).

Table H-2: Recharge Parameters/Zones in base case model

Recharge Zone	Areal Coverage (m^2)	Rate (mm/y)	Ponding Depth (m AGS)
LFH-A/B	81,293	88	0
LFH-D	115,179	40	0
PMM - Lowlands	162,309	-50	1.5
PMM - Uplands	160,144	41	1
PMM[1] - 318 Berm	331,932	88	1

[1] 318 Berm did not have PMM placed until winter 2016-2017, or vegetation until summer 2017; less soil moisture storage and ET demand meant more recharge available.

- Base of Model

The base of the model was assigned a no-flow boundary condition due to differences in hydraulic conductivity between the overlying sand cap and underling composite tailings (K_h = 1.7E-7 m/s, K_v = 1.7E-8 m/s; Thompson et al., 2011). Groundwater would preferentially flow through the sand cap due to differences in hydraulic conductivity of approximately three orders of magnitude.

- General Head BC

Two general head boundary conditions (GHB), to the east and to the north, were used represent lateral outflows from the watershed (Figure H-4). The eastern GHB was split into two GHBs, one to represent seepage under Hummock 6 to the north, through the Sandhill Berm eastward (East GHB-1), and the other to represent seepage through Sandhill Berm, spanning the topographic low between the easternmost hummocks (East GHB-2). For the eastern GHBs, hydraulic heads were assigned to 311 m ASL, the approximate elevation of standing water in the down gradient Kingfisher Watershed. Eastward flow appeared to be constrained by the topography and hydraulic conductivity of the materials in Sandhill, adjacent to the berm. Specifically, standing water is often observed in the lowlands adjacent to the berm. Therefore, these differences were modelled through using different conductance values (C) in the East GHB-1 and East GHB-2 boundaries (C = 0.03 m^2/d, and 1.4 m^2/d, respectively).

The northern GHB was constructed to represent groundwater that is diverted from the primary flow path, flowing north likely through buried gravel channels beyond the northern extent of SHW boundary. No standing water was observed within the area 200 m north of the watershed during the summer of 2017; therefore, the hydraulic head for that boundary was interpreted as 310.85 m ASL, below the drainage ditch adjacent to the highway located approximately 70 m north of the watershed's northern boundary. The boundary spanned from the western wetland to hummock 4 (C = 0.33 m^2/d).

III. Calibration

Annual recharge fluxes were determined for each soil type (LFH-A/B, LFH-D, and upland PMM) in SHW independently by Lukenbach et al., (2019). The values specified in this model were for the annual recharge values from 2015 (M. Lukenbach, unpublished data). The values for cumulative recharge from 2015 were below (LFH-A/B, PMM) or identical (LFH-D) to the average annual recharge values simulated in Lukenbach et al., (2019).

Calibration involved individually adjusting hydraulic parameters (hydraulic conductivity, and GHB conductance) by performing multiple simulations through trial and error until the simulated hydraulic heads adequately represented the water table configurations observed during summer months of 2017. Calibrated hydraulic parameters were compared to values obtained from the field (*e.g.,* tailings sand and peat-mineral-mix hydraulic conductivities; Appendix G) or the literature where field data were unavailable (Lukenbach et al., 2019). Calibrated hydraulic parameters were maintained within half an order of magnitude of previously estimated values.

Calculated hydraulic heads were compared to observed average water levels from the 22 piezometers across SHW (calibration points; Figure H-5). The goodness of fit between calculated and observed hydraulic heads were quantified using the software's performance indicators which indicated the model achieved a statistically acceptable representation of the groundwater flow system in SHW (summarized in Table H-3). The Normalized Root Mean-Square error for the calibrated parameters was 5.05% (obtained from data in Figure H-5). Given that a) the calibrated hydraulic conductivity values fall within an acceptable range of the literature values (Table H-1), b) the simulated water table resembles the water table configuration observed during summer field seasons (Figure 15; Appendix B) and c) the calibration statistics indicate calculated heads adequately represent field conditions (Table H-3), the model provides a reasonable representation of the groundwater system in SHW. The largest residuals were observed at calibration points along the southern boundary of the watershed, where the simulated water table was slightly lower than observed in the field (-0.4 m). The heads in the wetland were most sensitive to small adjustments in the GHBs during calibration; hydraulic heads in the uplands were the least responsive. Raising hydraulic heads in the uplands to observed values required raising recharge values beyond an acceptable range and led to large water level rises elsewhere in the model.

The water table mounded below 318 Berm, extending into the study watershed below the southern hummocks (Figure 15). As the topography flattens to the lowland, the hydraulic gradient also flattens as flow is diverted through the wetland to the north and east GHBs. Maintaining realistic volumetric flows into and out of the model required adjusting the areal extent of 318 Berm by gradually deactivating cells, since the area of 318 Berm contributing recharge is poorly constrained and the watershed's range of recharge are limited (M. Lukenbach, University of Alberta, personal communication). Given that SHW loses an unknown amount of groundwater through the northern boundary and Sandhill Berm was constructed to permit

Table H-3: Calibration statistics from base case model

Calibration Statistics	**Base Case Results**
Min. Residual	-0.0045 m (SH-GW-39)
Max. Residual	-0.4 m (SH-GW-05)
Residual Mean	-0.013 m
Abs Residual Mean	0.13 m
Standard Error of the Estimate	0.035 m
Root Mean Squared	0.16 m
Normalized Root Mean Square	5.05 %
Correlation Coefficient	0.99

Determined from data in Figure H-5

groundwater flow, the rate of flows out the GHBs were constrained by modifying the conductance terms (a model parameter used to represent resistance to flow) within reasonable limits to ensure flow was predominantly through the eastern boundary (Table H-4).

While evaluating the elevation of the modelled water table relative to topographic surface was considered, the LiDAR that was used to produce the digital elevation model (DEM) did not account for standing bodies of water in the lowlands; therefore, the DEM over-estimates the topographic elevation in some areas. This made it impossible to produce accurate soil wetness maps within the model, as the water table is near and above ground surface throughout the lowlands.

Table H-4: Base case water budget

Model Output	**Base Case Results**
Cumulative Input (m^3/d)	108
Net-Recharge	(108)
SHW	(28)
318 Berm	(80)
Cumulative Output (m^3/d)	-108
North GHB	(-39)
East GHB (1&2)	(-47)
Net-Recharge	(-22)
Percent Discrepancy	4E-02
Convergence Residual	2E-003

Inflows are positive, outflows are negative; breakdown of input/outputs are in brackets.

IV. Scenario Analyses

As vegetation grows and becomes established, the water available for recharge will likely decline due to decreases in soil moisture (increased rooting depth and above ground interception) and increased AET (increased leaf area index; Lukenbach et al., 2019). Furthermore, while boreal wetlands can naturally self-regulate water resources in a moisture-limited climate (Waddington et al., 2015), the province's climate will likely become drier overall in the coming decades (Keshta et al., 2011; Schneider, 2013). In northern Alberta, the distribution of precipitation throughout the year is expected to decrease during the growing season and increase during the winter months (Schneider, 2013). There is also expected to be an increase in mean annual temperatures, which will result in longer growing seasons, thereby increasing mean annual AET and reducing groundwater recharge.

Forecasting the availability of groundwater for possible future scenarios helps to elucidate the trajectory of reconstructed landscapes. Therefore, the calibrated steady-state model was used to test potential changes in recharge (including ET) that the watershed might encounter. Specifically, scenario testing was conducted by reducing the base case recharge values in the upland areas by 5%, 10% and 25%, and by increasing the base case recharge by 5% (Table H-2). Comparisons were made by evaluating the differences from the water levels predicted for the base case at observation points along Transect 1 and Transect 2 (Figure H-1).

In general, the water table elevation decreases as recharge decreases and increases as recharge increases (Figure H-7). Overall, areas in the watershed that have previously been described as having shallow water tables (*i.e.*, upland areas adjacent to and transitioning into lowlands), also have the greatest capacity to buffer the water level changes through different recharge scenarios (Figure H-7). The hydraulic heads in these areas consistently have the least fluctuations (*e.g.,* nests 23, 24, 26, 27, 75, 76). Upland areas adjacent to and including 318 Berm have some of the largest changes in water levels through different recharge scenarios. This follows from the steady-state calibration; the groundwater mound below 318 Berm is sensitive to changes in recharge. Large changes in hydraulic heads are also observed in lowland areas across different recharge scenarios (*e.g.*, nests 66 and 69; Figure H-7).

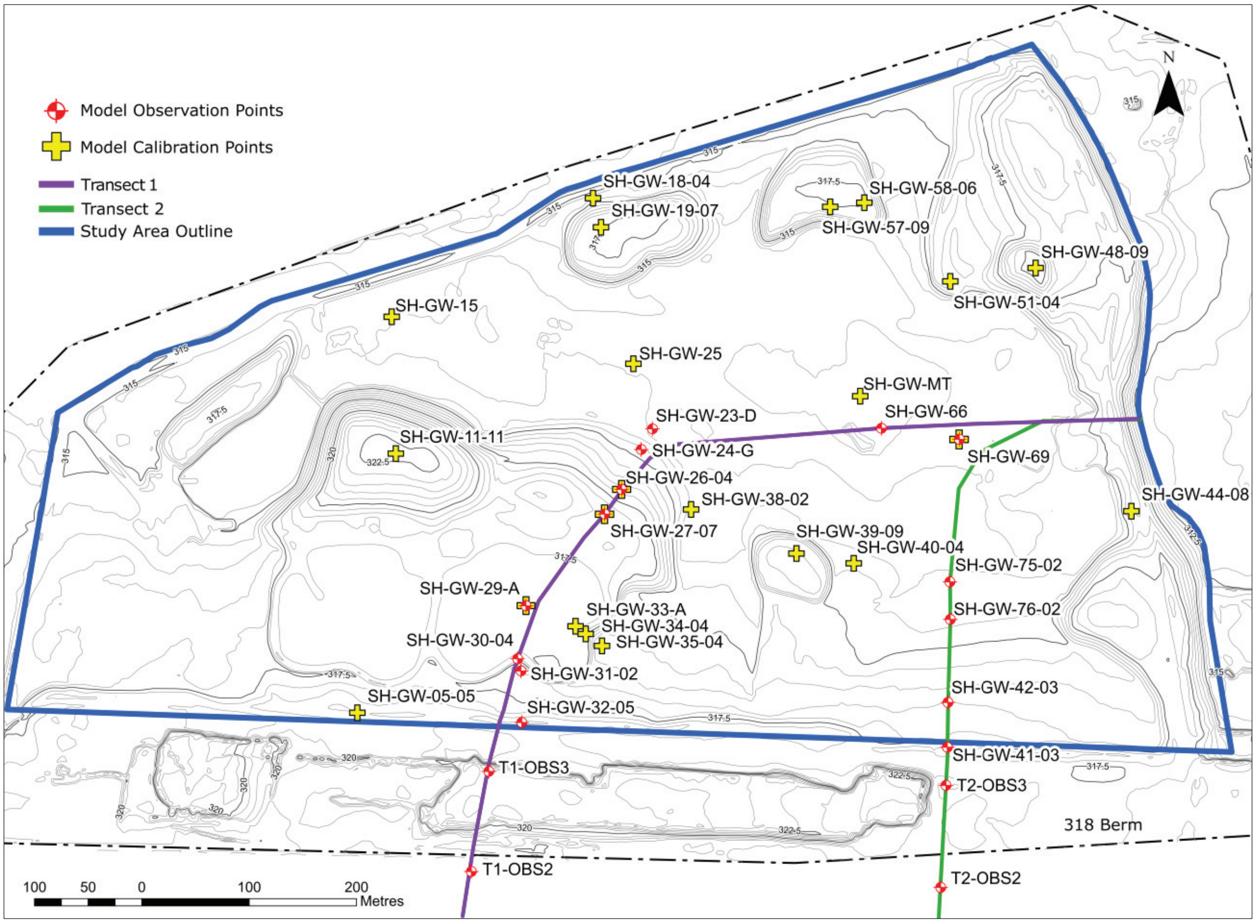

Figure H-1: Topographic map of SHW piezometers used to calibrate the groundwater model (calibration points), and observation points along Transects 1 and 2 used to record waterlevels from the model. Note: symbols overlap at certain locations.

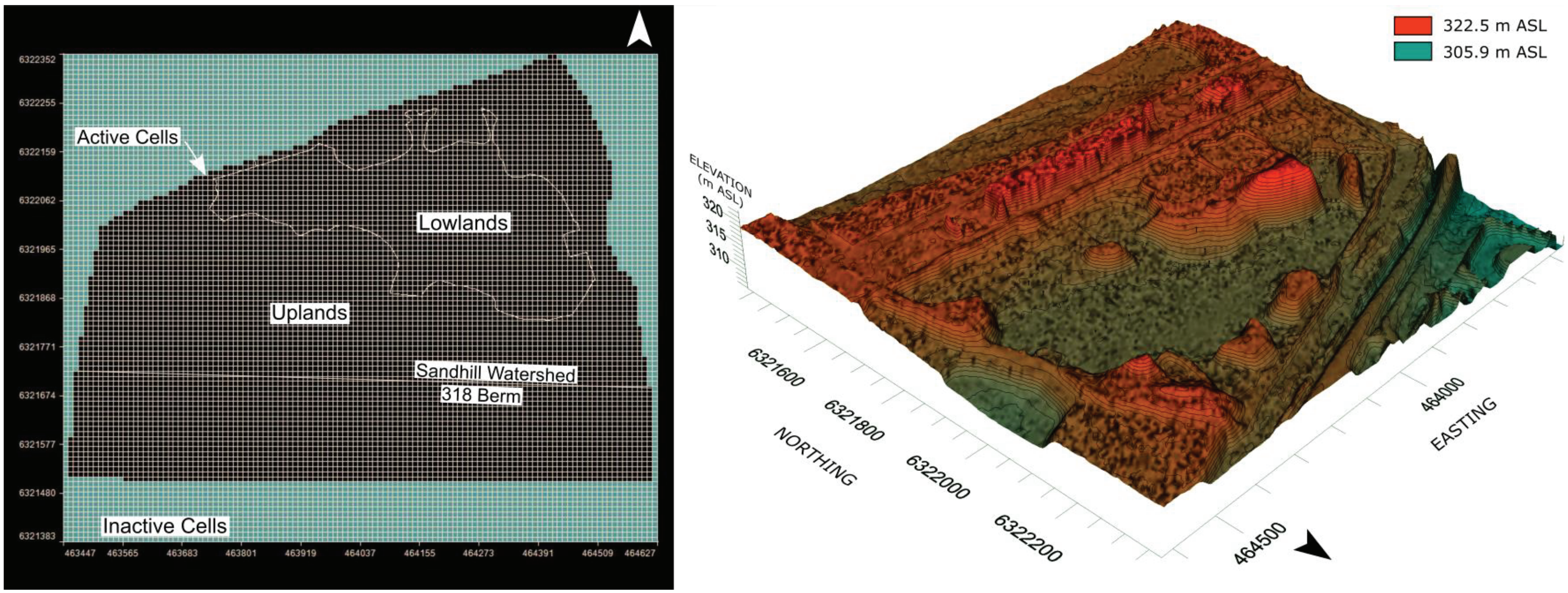

Figure H-2: Model domain and grid (left; active cells black, inactive teal) and domain's topography defined by LiDAR (right; 10xVE). Uplands and lowlands are outlined, arrowhead indicates north.

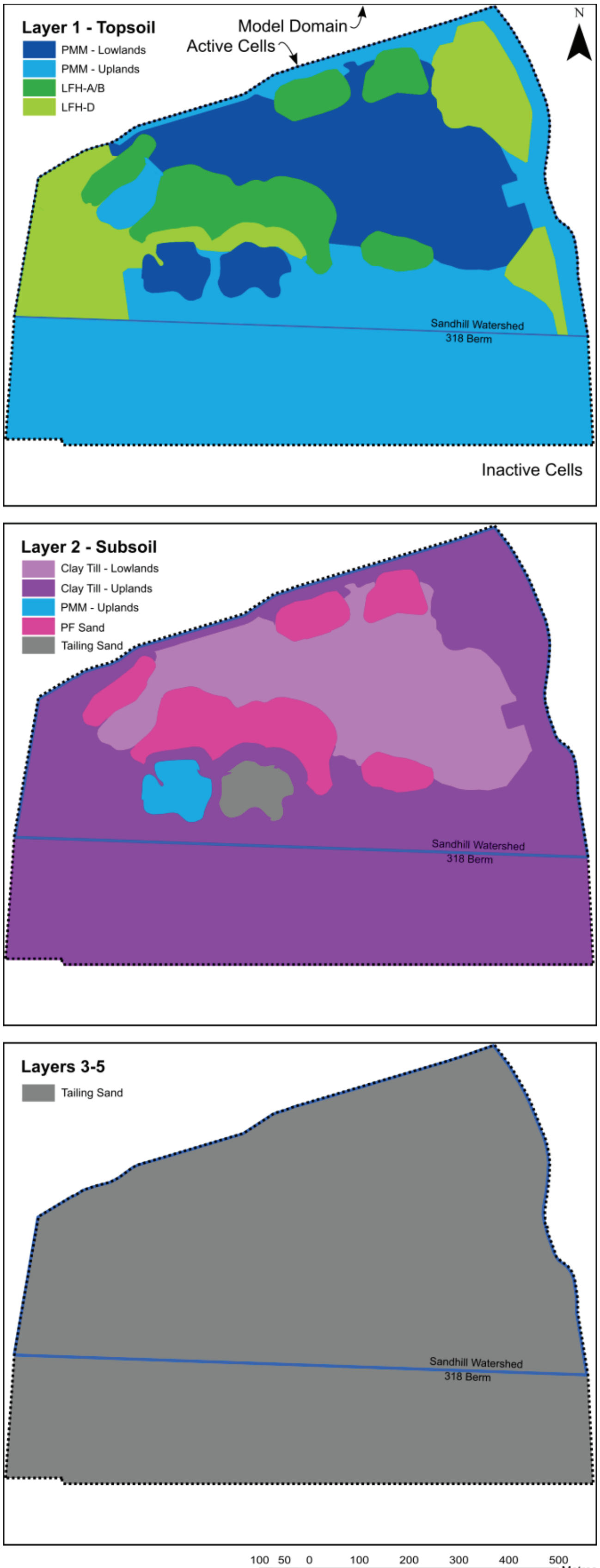

Figure H-3: Base case hydrostratigraphic layers and zones, in descending order: layer 1 (topsoil), layer 2, (subsoil), and layers 3-5 (tailing sand), respectively. Sandhill Watershed (study site) outlined in blue. Active cells outlined in dashed black line. White area are inactive cells in the domain.

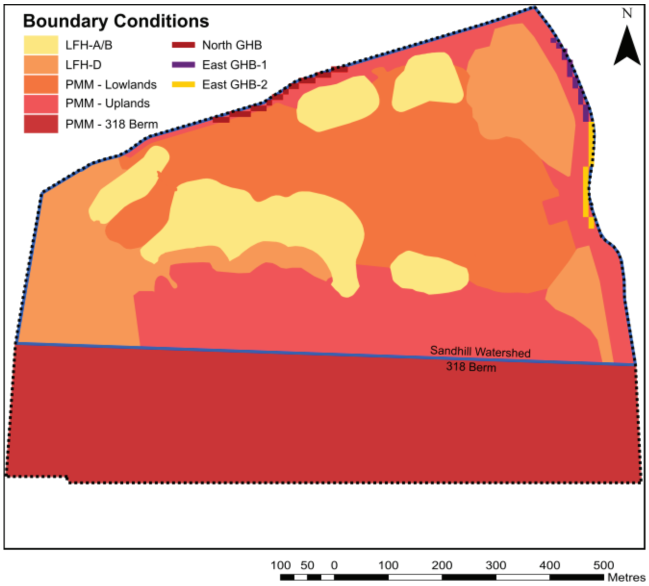

Figure H-4: Areal extent of recharge zones (polygons) and General Head (GHB; lines) boundary conditions. GHBs fall along the active/inactive cell boundary. All other cells along this boundary are no-flow boundary conditions. The base of the model (not shown) is also a no-flow boundary condition.

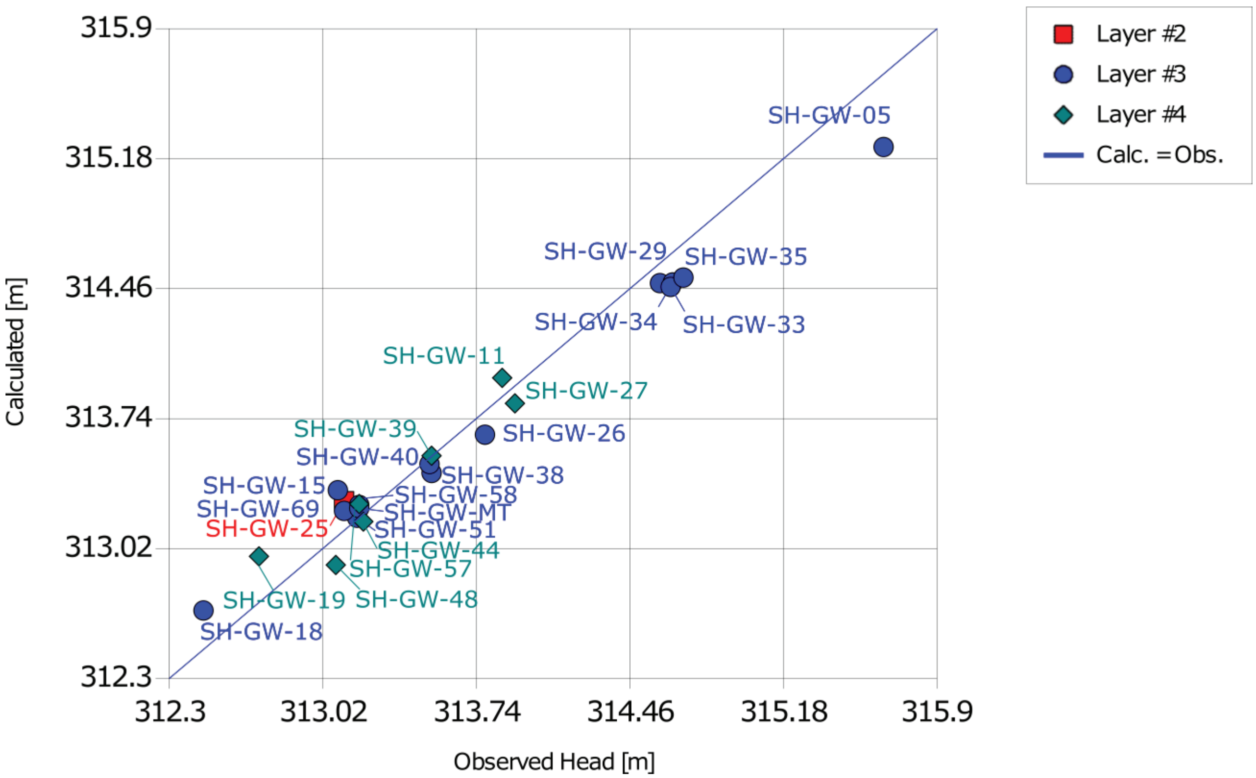

Figure H-5: Calculated versus Observed hydraulic heads (m) from the base case model calibration. Labels correspond to calibration points in Figure H-1.

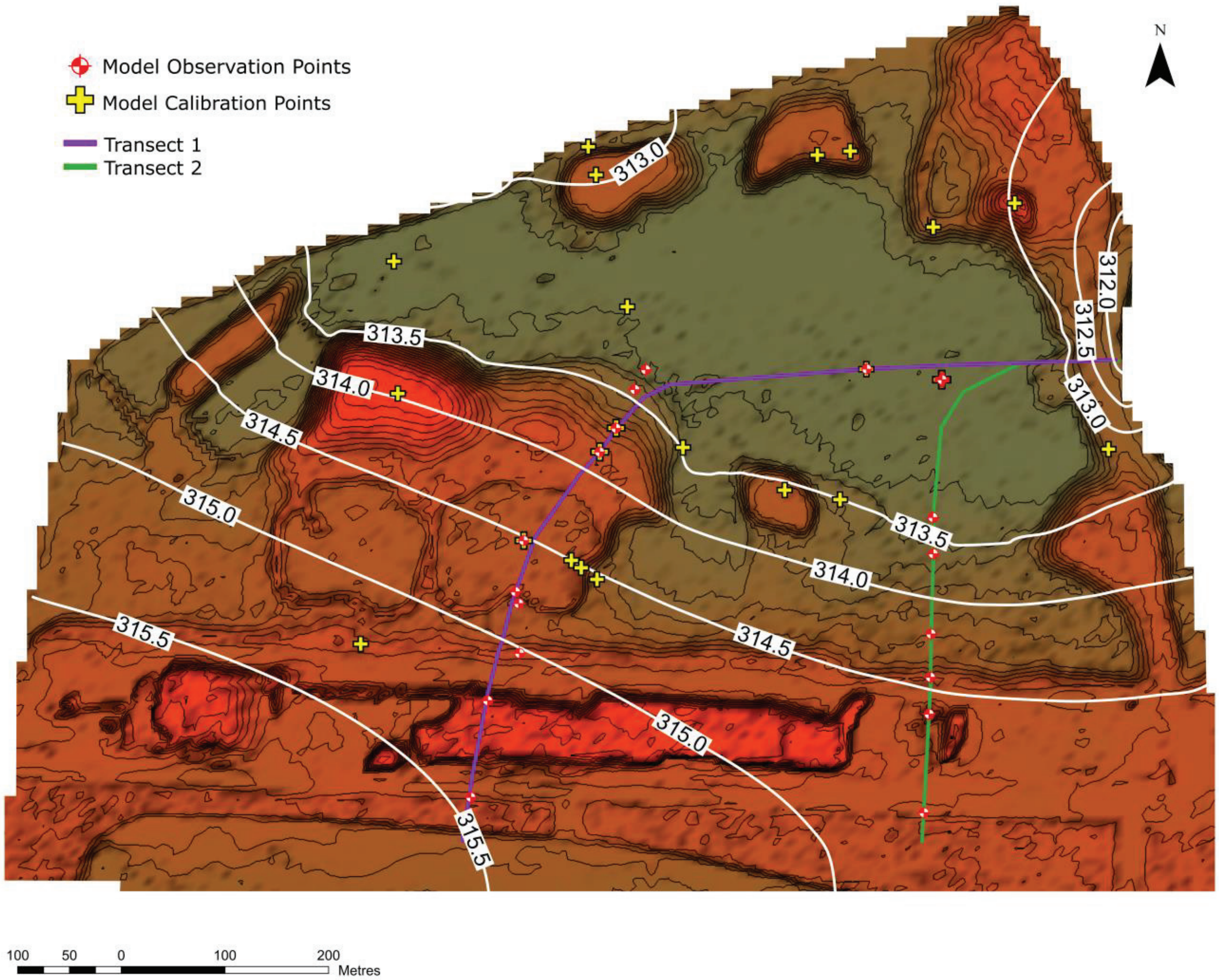

Figure H-6: Water table map of SHW steady state model (hydraulic heads in white; m ASL), observation piezometers located along Transect 1 and Transect 2 (as in Figure H-1).

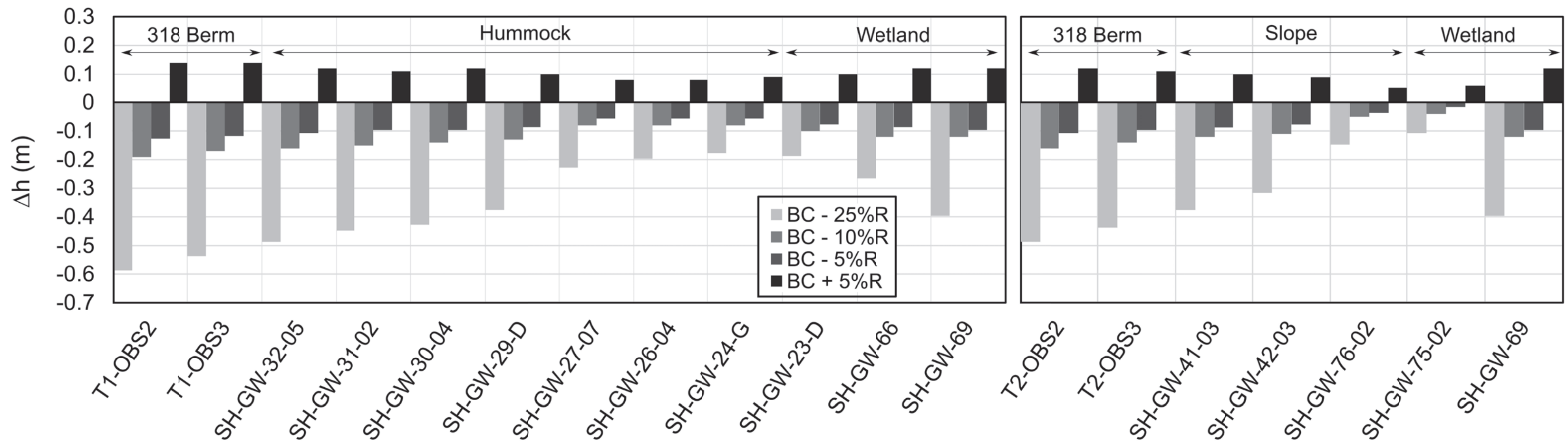

Figure H-7: Residual data at observation points along Transect 1 (left) and Transect 2 (right) for four scenario tests: base case (BC) recharge (R) was reduced (-) by 25%, 10% and 5%, and increased (+) by 5%, respectively.